STRUCTURE-FUNCTION ANALYSIS OF MAMMALIAN ORTHOREOVIRUS ATTACHMENT PROTEIN σ1

By

Kristen Marie Guglielmi

Dissertation

Submitted to the Faculty of the

Graduate School of Vanderbilt University

in partial fulfillment of the requirements

for the degree of

DOCTOR OF PHILOSOPHY

in

Microbiology and Immunology

May, 2008

Nashville, Tennessee

Approved:

Dr. Christopher R. Aiken, Ph.D.

Dr. Timothy L. Cover, M.D.

Dr. Mark R. Denison, M.D.

Dr. Terence S. Dermody, M.D.

Dr. Phoebe L. Stewart, Ph.D.

To my mother, whose inspiration endures

ACKNOWLEDGEMENTS

This work was financially supported by the Cellular, Biochemical and Molecular Sciences Training Program (Public Health Service award T32 GM08554), the Molecular Basis of Reovirus Pathogenesis (Public Health Service award R37 AI38296), the Structural Analysis of Reovirus Attachment Mechanisms (Public Health Service award R01 GM67853), and a Vanderbilt University Research Council Dissertation Enhancement Grant. Additional support was provided by the Vanderbilt-Ingram Cancer Center (Public Health Service award P30 CA68485), the Vanderbilt Diabetes Research and Training Center (Public Health Service award P60 DK20593), the Nashville Veterans Affairs Hospital, and the Elizabeth B. Lamb Center for Pediatric Research.

First and foremost, I thank Dr. Terence Dermody for serving as my mentor during the past five years. Terry's guidance has been patient, enthusiastic, and consistent. He has provided an environment and opportunities that have fostered my development as a scientist and permitted me to attain important skills, including critical thinking, public speaking, and scientific writing. Terry's dedication to teaching and genuine desire to see those he mentors succeed are inspiring. In short, he is an exemplary mentor. The Dermody laboratory has been a wonderful training environment. I could not have chosen a kinder, funnier, more insightful, and dedicated group of scientists to work with. Each lab member has contributed positively to my research experience, and I thank them all for their support and company. I would also like to acknowledge the contributions of the bright rotation students who have worked with me in the Dermody lab, Hannah Fish, Kenneth Drake, and Magdalena Bokiej.

I would like to thank Dr. Thilo Stehle, who has served, in effect, as a second mentor to me, and members of the Stehle laboratory, especially Eva Kirchner, Pierre Schelling, and Dirk Reiter. Thilo's experimental suggestions and assistance with data interpretation have been invaluable. Thilo leads a wonderful and talented group of scientists. I thank them for their hard work, beautiful protein structures and models, good humor, and graciousness as hosts.

I thank all of the members of my thesis committee for their intellectual and personal contributions to my graduate career. I thank Dr. Timothy Cover, who has been an ideal chair, interested, organized, and diplomatic. I thank Dr. Chris Aiken for consistently asking challenging questions. He has pushed me to become a more careful and critical scientist. I thank Dr. Phoebe Stewart for her insight as a talented structural biologist. Her perspective and advice have been immeasurably useful. From the time when I first rotated in his laboratory, Dr. Mark Denison has taken a genuine interest in my graduate education. I thank him for his dedication to teaching and training.

There are many other individuals and groups at Vanderbilt University who have made my research both possible and pleasurable. I thank the administrators of BRET and the IGP for offering me the opportunity to join a wonderful graduate program. I thank the faculty members who organized and taught the graduate courses I attended. They have helped me build a solid foundation of knowledge in the biomedical sciences. I thank my colleagues in the Department of Microbiology and Immunology, all of whom have played an active role in my training by attending seminars, asking insightful questions, providing experimental and career advice, and being a lighthearted and fun group of people to socialize with. I thank the administrators, doctors, and researchers in

the Division of Pediatric Infectious Diseases for providing a fantastic work environment and sharing advice, equipment, and reagents. I thank Dr. James Thomas and members of his laboratory for letting me visit several times a week for months at a time to perform experiments in a reovirus-free environment. I thank Catherine Alford at the Veteran's Affairs Medical Center Flow Cytometry Special Resource and the staff at the Vanderbilt Molecular Recognition and Screening Facility and the Vanderbilt DNA Sequencing Core for expert assistance.

The majority of the credit for my successes in life must go to my family and friends. My parents are my primary role models. They have given me sound advice, enthusiastic encouragement, unconditional love, and all of my best qualities. Thank you, Mom and Dad, for all the sacrifices you've made for me and for the example you set with your strength, integrity, and faith. Mom, you are still an inspiration, even though you are no longer with us. I thank Jennie for being the best big sister I could want. For countless phone calls, listening patiently, always being in my corner, and making me laugh when I really need it, I thank you, Jennie. My grandfather, Freddy Lutfy, has shown me that hard work, dedication to family, and living honorably are the things that make us truly rich. I thank him and the rest of my family, my brother-in-law, Andrew, aunts, Laurel and Jan, uncle, Bobby, and cousins, John, Beth, and Kate, for their continued love and support and for being fantastic individuals. The encouragement of my friends has been more valuable to me than I can say. I thank all of them, especially Jeannelle Kantz, Rachel Henry, Matt and Keelie Stambaugh, Brian Yaspan, Lisa Weiss, Chris McKee, Mike McEachern, Ben Hoffmeyer, and Katy Swanson, for counsel and unwavering support. Seth Ogden has been a source of comfort and encouragement over the past

several years. Thank you, Seth, for enthusiastically sharing my joys and triumphs and patiently sharing my sorrows and stresses with me.

TABLE OF CONTENTS

LIST OF TABLES

LIST OF FIGURES

LIST OF ABBREVIATIONS

βME	beta-mercaptoethanol
σ1H	σ1 head domain, residues 293-455 of T3D σ1
Buffer 1	50 mM Tris pH 7.5, 3 mM EDTA
Buffer 2	20 mM $MgSO_4$ and 10 mM ATP in Buffer 1
Buffer 3	1 M NaCl in Buffer 1
CAR	coxsackievirus and adenovirus receptor
CD	circular dichroism
CFG	Center for Functional Glycomics
CHES	N-cyclohexyl-2-aminoethanesulfonic acid
CHO	Chinese hamster ovary
CNS	central nervous system
ds	double-stranded
EM	electron microscope
fJAM-A	feline JAM-A
GST	glutathione S-transferase
GST-JAM-A	N-terminal GST fusion with the extracellular region of JAM-A
HBS	HEPES-buffered saline
HEPES	4-(2-hydroxyethyl)-1-piperazineethanesulfonic acid
HIV	human immunodeficiency virus
hJAM-A	human JAM-A
Ig	immunoglobulin

IgSF	immunoglobulin superfamily
IPTG	isopropyl-β-D-thiogalactoside
JAM-A	junctional adhesion molecule-A (F11R, JAM, JAM1)
JAM-A D1	membrane-distal Ig-like domain of JAM-A
JAM-A D2	membrane-proximal Ig-like domain of JAM-A
JAM-A D1D2	extracellular domain of JAM-A
L cell	murine L929 cell
LFA-1	leukocyte function-associated antigen-1, integrin αLβ2
M cell	microfold cell
MEL	murine erythroleukemia
mJAM-A	murine JAM-A
PBS	phosphate-buffered saline
PBS/BSA	PBS plus 0.1% bovine serum albumin
PBST	PBS plus 1% Tween 20
PMSF	phenylmethylsulfonyl fluoride
reovirus	mammalian orthoreovirus
SPR	surface plasmon resonance
T1L	type 1 Lang
T2J	type 2 Jones
T3D	type 3 Dearing
TX-100	Triton X-100
VSV	vesicular stomatitis virus

CHAPTER I

BACKGROUND

Introduction

To efficiently initiate infection of target cells, viruses must become tethered to the plasma membrane by engaging cellular receptors. As the first step in the viral replication cycle, attachment is a key determinant of viral tropism and pathogenesis. The adhesion process is often mediated by a viral attachment protein and can involve binding to multiple receptors at the cell surface. For a given virus, the attachment protein has evolved to be ideally-suited for its functional requirements, which may include receptor binding, conformational rearrangement, multi-step adhesion, and triggering signaling events that lead to viral internalization and uncoating. A detailed understanding of the structure and function of a viral attachment protein and the specific mechanisms by which it engages cellular receptors can aid the development of antivirals aimed at blocking the attachment step, the engineering of viral vectors with enhanced cellular targeting capabilities, and an improved understanding of viral disease outcomes.

Mammalian orthoreoviruses (reoviruses) are nonenveloped, double-stranded (ds) RNA viruses that bind to multiple cell-surface molecules and serve as tractable models for studies of virus-receptor interactions and viral pathogenesis. The reovirus attachment protein, σ1, is a filamentous, trimeric molecule that extends from the icosahedral vertices of reovirus virions. Reovirus σ1 of some serotypes binds α-linked sialic acid, a carbohydrate, and σ1 of all serotypes binds junctional adhesion molecule-A (JAM-A), a

dimeric protein involved in cell-cell adhesion and tight junction formation. X-ray crystal structures of a JAM-A-binding fragment of σ1 and the extracellular domain of JAM-A have been solved. The structures have revealed interesting features of the two molecules and provided clues about their structure-function relationships. Yet they also have generated many new questions.

When this work was initiated, structural features of σ1 important for mediating attachment functions were not known. An unusual cluster of six aspartic acid residues in close proximity at the subunit interface of the σ1 trimer had been identified. However, the precise nature of atomic interactions at this interface and the function of this motif in mediating conformational changes in the σ1 head region had not been explored. The C-terminal half of σ1 was known to bind JAM-A with high affinity. However, sequences involved in binding and the nature and stoichiometry of σ1-JAM-A interactions had not been determined. While evidence suggested that when locked in a dimeric form JAM-A was unable to efficiently bind σ1, it was unclear whether σ1 binds directly to sequences within the dimer interface and, if so, how it might access this surface. In addition, it was not known whether differences in the nature or mechanism of JAM-A engagement among the reovirus serotypes exist.

In my dissertation research, I have attempted to elucidate details of the mechanism of σ1-JAM-A engagement and understand features of σ1 that confer functionality. This research has been accomplished using a combination of structural, genetic, biochemical, biophysical, and biological approaches. In Chapter II, I report the characterization of a novel trimerization motif, the aspartic acid sandwich, which might be important for structural rearrangements in σ1. In Chapter III, I present a systematic

analysis of the contributions of individual residues in the JAM-A dimer interface to reovirus binding and JAM-A homodimer stability. In Chapter IV, I report the structure of a complex between σ1 and JAM-A and identify sequences in σ1 required for efficient JAM-A binding and reovirus infectivity. These studies will enhance an understanding of σ1 structure-function relationships. More specifically, a detailed understanding of σ1-JAM-A interactions will yield insight into the role of JAM-A in reovirus pathogenesis and provide a basis for vector retargeting as we explore the potential of reovirus for vaccine delivery and oncolysis.

Reovirus pathogenesis

There are three reovirus serotypes, which can be differentiated by the capacity of anti-reovirus antisera to neutralize viral infectivity and inhibit hemagglutination (126, 129). The three serotypes are each represented by a prototype strain isolated from a human host: type 1 Lang (T1L), type 2 Jones (T2J), and type 3 Dearing (T3D). Reoviruses have a wide geographic distribution, and virtually all mammals, including humans, serve as hosts for infection (154). However, reovirus is rarely associated with disease, except in the very young (97, 147).

Newborn mice are exquisitely sensitive to reovirus infection and have been used as the preferred experimental system for studies of reovirus pathogenesis (160). Following oral or intramuscular inoculation of newborn mice, strains of serotype 1 and serotype 3 reoviruses invade the central nervous system (CNS), yet by different routes and with distinct pathologic consequences. Serotype 1 reovirus spreads to the CNS hematogenously and infects ependymal cells (155, 165), resulting in hydrocephalus

(164). In contrast, serotype 3 reovirus spreads to the CNS by neural routes and infects neurons (103, 155, 165), causing lethal encephalitis (147, 164). Studies using T1L x T3D reassortant viruses have shown that the pathways of viral spread (155) and tropism for neural tissues (41, 165) segregate with the viral S1 gene, which encodes attachment protein σ1 (86, 163). T1L x T3D reassortant viruses also were used to demonstrate that serotype-specific differences in virus binding to primary cultures of ependymal cells and neurons are determined by the S1 gene (41, 148). These studies suggest that σ1 dictates the CNS cell types that serve as targets for reovirus infection, presumably by its capacity to bind receptors expressed by specific CNS cells.

Structure and function of reovirus attachment protein σ1

Reovirus particles are approximately 850 Å in diameter (109). The ten segments of dsRNA that compose the reovirus genome are encapsidated within two concentric protein shells, the outer capsid and inner core. Together, the outer capsid and core are composed of eight structural proteins. The bulk of the outer capsid consists of the tightly-associated μ1 and σ3 proteins (91). There are turrets at each of the twelve icosahedral vertices of the virion formed by the pentameric λ2 protein, from which the viral attachment protein, σ1, extends (6, 28, 42, 54, 55) (Figure I-1).

The σ1 protein is a filamentous, trimeric molecule about 480 Å in length with distinct head-and-tail morphology (54, 55) (Figure I-2A). Discrete regions of the molecule mediate binding to cell-surface receptors. Sequences in the N-terminal σ1 tail bind to carbohydrate, which is known to be sialic acid in either α2,3 or α2,6 linkages for serotype 3 reoviruses (28, 29, 40, 58, 120). The C-terminal σ1 head binds to junctional

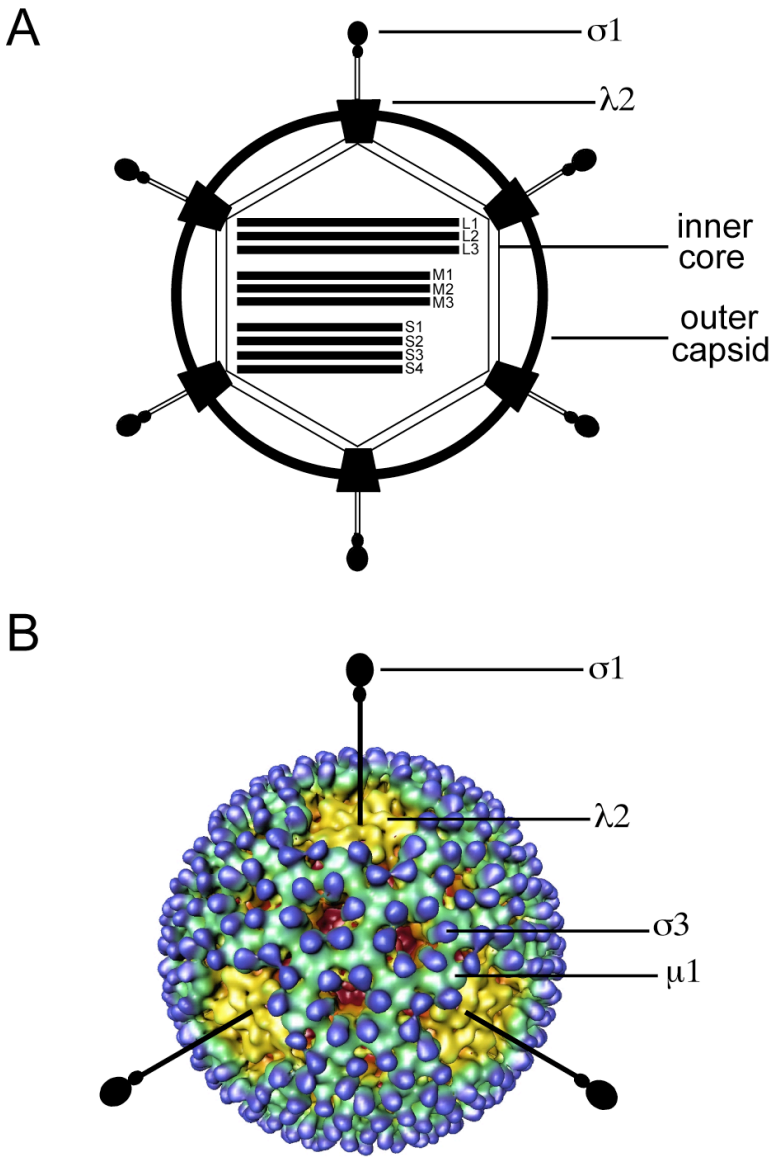

FIGURE I-1. Organization and structure of a reovirus virion. (A) Schematic representation of a reovirus virion. Outer capsid, inner core, viral attachment protein σ1, the λ2 base into which σ1 inserts, and ten viral dsRNA genome segments are indicated. (B) Cryo-electron microscopic image reconstruction of a reovirus virion. Major outer capsid proteins are pseudocolored and indicated. σ1 molecules are represented schematically. Image adapted from Nason et al. (105).

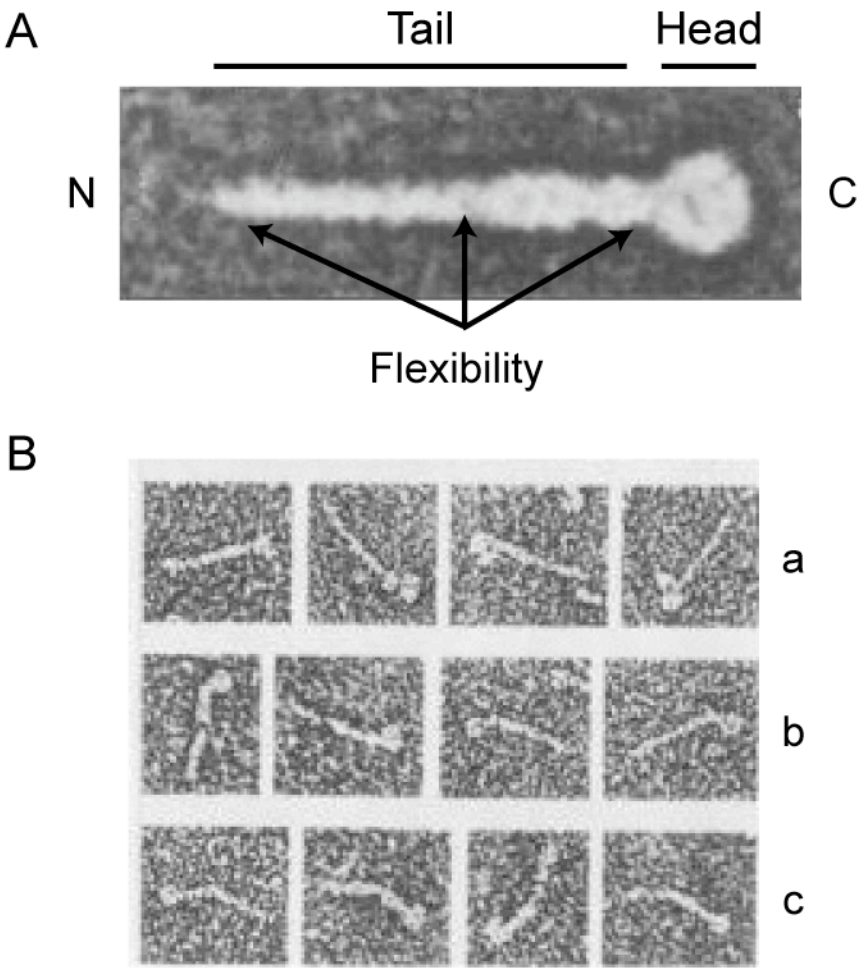

FIGURE I-2. Computer-processed negative-stain electron micrographs of σ1. (A) Composite electron micrograph of σ1. N and C termini, head and tail domains, and regions of observed flexibility of the molecule are indicated. (B) Individual electron micrographs of σl molecules, highlighting distinct morphologies: (a) the head appears multi-lobed; (b) the tail is kinked immediately adjacent to the head; (c) the tail is kinked near its midpoint. Images adapted from Fraser et al. (54).

adhesion molecule-A (JAM-A, previously called F11R, JAM, or JAM1) (6, 46). The σ1 tail partially inserts into the virion, while the head projects away from the virion surface (43, 55) (Figure I-1). Insertion of the trimeric σ1 protein into a pentameric λ2 base results in an unusual symmetry mismatch. Such symmetry mismatches often produce

interactions of limited strength or specificity and indicate a strong potential to undergo structural rearrangement.

Structural analysis of the C-terminal half of T3D σ1 (residues 246-455) has revealed a trimeric structure, in which each monomer is composed of a slender tail and a compact head (30) (Figure I-3A). The C-terminal residues that form the head domain (310-455) consist of two Greek-key motifs that fold into a β-barrel. Loops connecting the individual strands of the β-barrel are short with the exception of the loop that connects β-strands D and E, which contains a 3_{10} helix (Figure I-3B, C). N-terminal residues in the crystallized fragment form a portion of the tail, residues 246-309, which consists of three β-spiral repeats (Figure I-3A). Each repeat is composed of two short β-strands connected by a four-residue β-turn that has either a proline or a glycine residue at its third position (30). A surface-exposed, variable loop links successive repeats, and trimerization generates a triple β-spiral motif that has been observed in the tail domains of the attachment proteins of avian reovirus, σC (63), and adenovirus, fiber (158), and in the spike protein P5 of bacteriophage PRD1 (101). The σ1 trimer features a distinct bend between the three-fold axes of the head and tail domains. Although this bend is most likely introduced by crystal packing forces, it indicates that the σ1 trimer possesses a high degree of flexibility. The region of flexibility is located between the second and third β-spiral repeats in the tail and corresponds to a 4-residue insertion, amino acids 291-294 (30) (Figure I-3A).

Sequence analysis has facilitated the development of a model of full-length σ1 (30). The σ1 tail is thought to contain an N-terminal α-helical coiled-coil followed by eight β-spiral repeats (Figure I-4). Sequences predicted to form the α-helical coiled coil

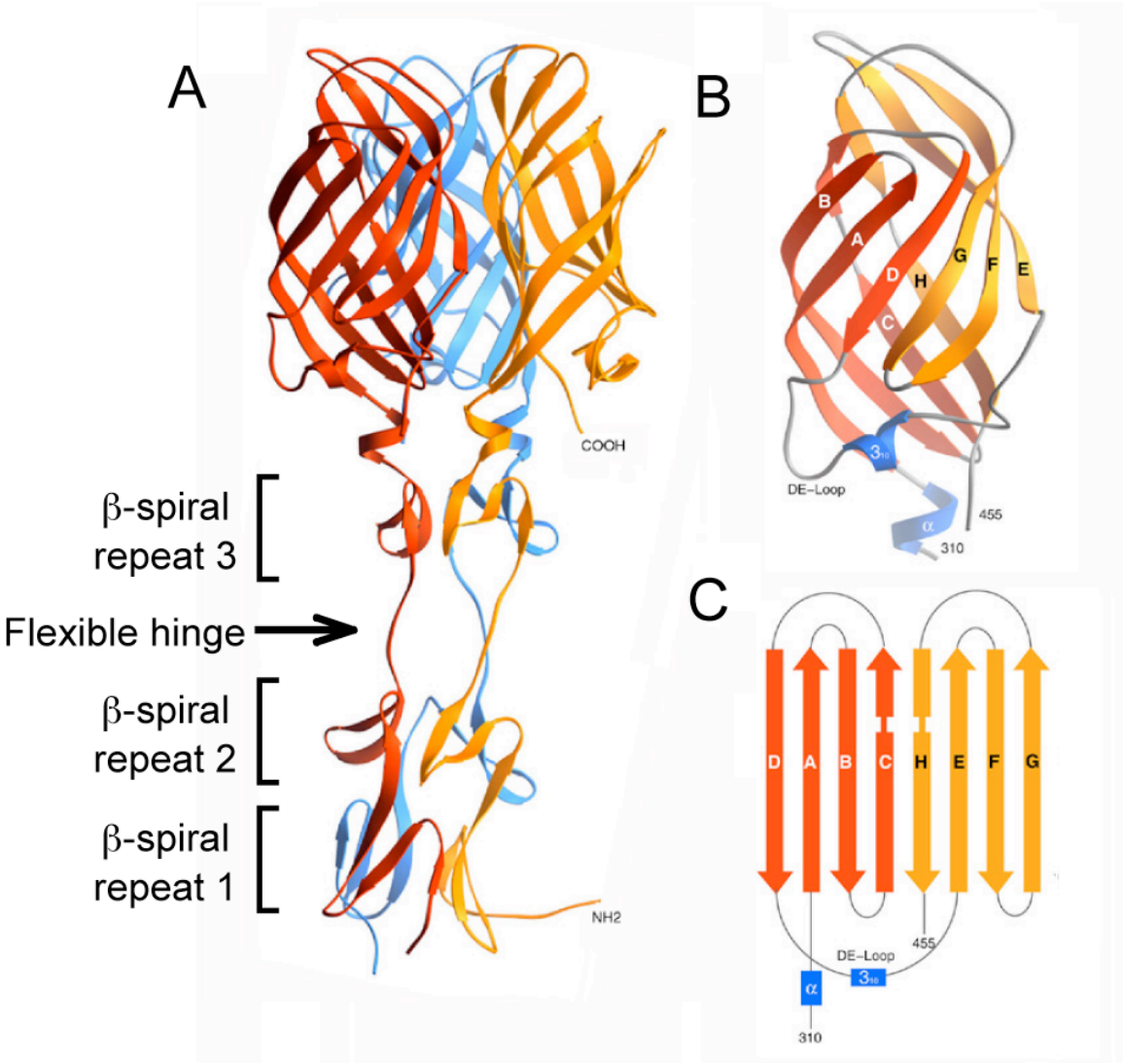

FIGURE I-3. Crystal structure of reovirus σ1. (A) Ribbon drawing of the σ1 trimer with σ1 monomers shown in red, orange, and blue. Each monomer consists of a head domain formed by a compact β-barrel and a slender tail with three β-spiral repeats. (B) Enlarged view of the σ1 head domain. The two Greek-key motifs, shown in red and orange, form a compact, cylindrical β-sheet that contains eight β-strands (A–H). The head domain also contains two short helices, shown in blue: one 3_{10} and one α-helix. (C) Schematic view of the β-strand arrangement in the σ1 head domain. Colors are as in (B). Image adapted from Chappell et. al (30).

are required for trimer stability (28, 87, 145, 170). Electron microscope (EM) images of full-length σ1 have shown flexibility at three regions of the molecule, a region near the N-terminus, a region that correlates with the transition from the predicted α-helical coiled coil to the triple β-spiral, and a region that corresponds to the insertion between β-spiral repeats 2 and 3 of the crystallized portion of T3D σ1 (30, 54) (Figures I-2 and I-4). These regions of flexibility could facilitate interactions with receptors or enable structural rearrangements during viral assembly or disassembly.

Interactions of σ1 with sialic acid

Reoviruses exhibit the capacity to agglutinate erythrocytes of several mammalian species (88). For serotype 3 reoviruses, hemagglutination is mediated by interactions of the σ1 protein with terminal α-linked sialic acid residues on several glycosylated erythrocyte proteins such as glycophorin A (57, 121). The carbohydrate receptors for other serotypes of reovirus have not been well characterized. Sialic acid binding is required for reovirus attachment and infection of certain cell types including murine erythroleukemia (MEL) cells (29, 128). Although not all serotype 3 strains are capable of binding to sialic acid, the majority bind to this carbohydrate and produce hemagglutination. Sequence polymorphism within the σ1 tail determines the capacity of field-isolate reovirus strains to bind to sialic acid and infect MEL cells (39, 128). Furthermore, non-sialic acid-binding serotype 3 variants have been adapted to growth in MEL cells during serial passage. These variants have gained the capacity to bind to sialic acid and contain sequence changes within a discrete region of the σ1 tail (residues 198-204) predicted to form a β-spiral (29). Residues in this vicinity may form part of a sialic

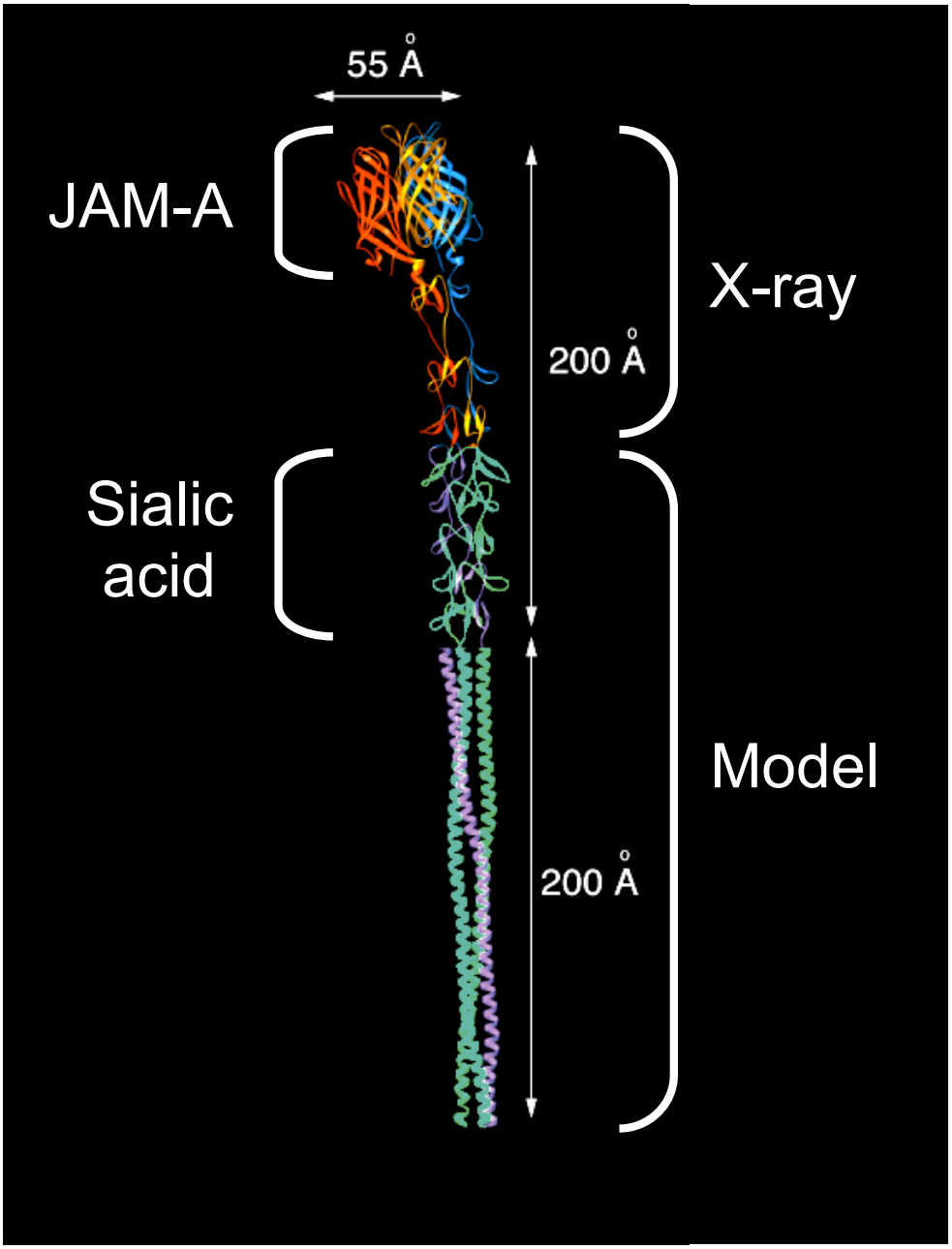

FIGURE I-4. Full-length model of reovirus σ1. The model was generated by adding five β-spiral repeats, followed by a trimeric coiled coil formed by elongating an existing coiled-coil structure (166), to the N terminus of the crystallized fragment of σ1 (30). Regions of the molecule that interact with JAM-A and sialic acid, and approximate molecular dimensions, are indicated.

acid-binding site (30, 140). Experiments using expressed σ1 truncation mutants and chimeric molecules derived from T1L and T3D σ1 proteins have confirmed that the sialic acid-binding domain of serotype 3 σ1 is contained within this predicted β-spiral region of the σ1 tail (28) (Figure I-4).

Serotype 1 reoviruses also appear to bind sialic acid in some contexts. T1L, but not T3D, has been shown to bind to the apical surface of microfold (M) cells, but not to enterocytes, in tissue sections of rabbit Peyer's patches (67). In this model, binding was inhibited by pre-incubation of the tissue sections with neuraminidase or with lectins that specifically recognize α2-3-linked sialic acid. The capacity of T1L to bind to the apical surface of M cells was shown to segregate with the S1 gene using reassortant genetics and with reovirus particles recoated with recombinant σ1 protein. The interaction between T1L σ1 and sialic acid is especially intriguing as serotype 1 reoviruses are incapable of infecting MEL cells, a property dependent on sialic acid binding that segregates with the S1 gene (128), and are insensitive to the growth-inhibitory effects of neuraminidase treatment of murine L929 (L) cells (107).

Interactions of σ1 with JAM-A

Substantial evidence has accumulated to suggest that the σ1 head also binds to receptors on the cell surface (8, 44, 107, 152). Neutralization-resistant variants of T3D selected using σ1-specific monoclonal antibody 9BG5 contain mutations in the σ1 head that segregate genetically with alterations in neural tropism (8, 76, 137, 138). This finding suggests a role for the σ1 head in receptor binding. Truncated forms of σ1 containing only the head domain are capable of specific interactions with cells (44, 45).

Concordantly, proteolysis of T3D virions leads to release of a C-terminal receptor-binding fragment of σ1 and a resultant loss in infectivity (107). These findings indicate that the σ1 head promotes receptor interactions that are distinct from interactions with sialic acid mediated by the σ1 tail.

A flow cytometry-based expression-cloning approach was employed to identify a receptor bound by the σ1 head (6). A non-sialic acid-binding strain of reovirus that contains a serotype 3 σ1 protein was used as an affinity ligand to avoid the potential complication of isolating heavily glycosylated molecules that might not interact specifically with σ1. A neural precursor cell (NT2) cDNA library was selectively enriched for cDNAs that confer binding of fluoresceinated virions to transfected cells. Four clones were identified that conferred virus binding. Each encoded JAM-A, a member of the immunoglobulin superfamily (IgSF) postulated to regulate formation of intercellular tight junctions (93, 98, 169). Three lines of evidence support the contention that JAM-A is a functional receptor for reovirus (6). First, JAM-A-specific monoclonal antibodies inhibit reovirus binding and infection. Second, expression of JAM-A in nonpermissive cells allows reovirus growth. Third and most convincingly, the T3D σ1 protein binds directly to JAM-A with an apparent K_D of ~ 6 x 10^{-8} M. Together, these findings indicate that JAM-A serves as a receptor for the σ1 head. Surprisingly, JAM-A serves as a receptor for both prototype and field-isolate strains of all three reovirus serotypes (6, 20). Therefore, JAM-A does not appear to explain the serotype-dependent differences in reovirus tropism observed in the murine CNS. These observations suggest that receptors other than JAM-A, possibly including carbohydrate-based coreceptors, influence reovirus pathogenesis. However, it is unclear whether differences in the

mechanism of attachment or affinity for JAM-A, which could contribute to differences in tropism, exist among the reovirus serotypes.

Structure and function of JAM-A

Reovirus receptor JAM-A is a type I transmembrane protein with two extracellular Ig-like domains, a transmembrane domain, and a short cytoplasmic tail possessing a PDZ-domain-binding motif (93, 98, 118). JAM-A is an important component of barriers known as the zonula occludens or tight junctions that form between endothelial and epithelial cells (93, 98, 118). JAM-A is expressed in diverse tissues including the lungs, liver, kidney, pancreas, heart, brain, intestine, and lymph nodes (2, 37, 90, 93), all of which are tissues capable of supporting reovirus infection in newborn mice (80). In addition, JAM-A is expressed in monocytes, neutrophils, lymphocytes, erythrocytes, and platelets (2, 93, 98, 117, 136, 169). Several cellular proteins are known to interact with JAM-A. The extracellular domain of JAM-A interacts with the leukocyte function-associated antigen-1 (LFA-1, integrin $\alpha L\beta 2$) (115). Cytosolic proteins including zonula occludens-1 (10, 47), AF-6 (47), multi-PDZ-domain protein 1 (66, 156), and partitioning-defective protein-3 (48, 70), interact with the JAM-A cytoplasmic tail in a PDZ-domain-dependent manner. Interactions between JAM-A and LFA-1 are thought in part to mediate the migration of leukocytes across endothelial and epithelial barriers during the course of an inflammatory response (37, 85, 115, 162), although precise mechanisms by which JAM-A regulates transendothelial migration are not known.

The crystal structure of the extracellular region of human (h) JAM-A (79, 122)

consists of two concatenated Ig-like domains (D1 and D2) (Figure I-5A, B). Two monomers form a symmetrical homodimer in which the monomers engage in an "arm-wrestling grip" via a large interface between the D1 domains. The JAM-A dimer interface is concave and composed of four β-strands (C', C, F, and G) (Figure I-5C). The dimeric structure is maintained by an unusual interface that is rich in charged residues (122) (Figure I-5C). The principal means of association between JAM-A monomers involves four salt bridges at the center of the interface. These interactions are mediated by the side chains of Arg59, Glu61, Lys63, and Glu121, all of which are buried and solvent-inaccessible (122). Protein-protein contacts are often mediated by hydrophobic or polar residues, whereas charged amino acids are more typically found in solvent-exposed areas. Although formation of salt bridges is generally viewed as energetically favorable, the stability of these interactions depends very much on the nature of the surrounding environment. Apolar surroundings increase the energy gained by salt bridge formation, whereas highly polar surroundings or low pH values decrease the stability of these contacts. Of note, JAM-A dimers can dissociate into monomers under conditions of moderately high ionic strength or when exposed to low pH (9). This dynamic nature of the JAM-A interface may facilitate efficient binding of the viral attachment protein at the cell surface or dissociation of the virus in the low pH environment of the endosome.

JAM-A belongs to a structurally related family of cell-adhesion molecules. The most closely related of these proteins to JAM-A are JAM-B and JAM-C (1, 35, 49), neither of which serves as a receptor for reovirus (20, 122). Although structural information is not available for JAM-B and JAM-C, sequence analysis suggests that homophilic contacts are conserved between JAM-family members (122). The

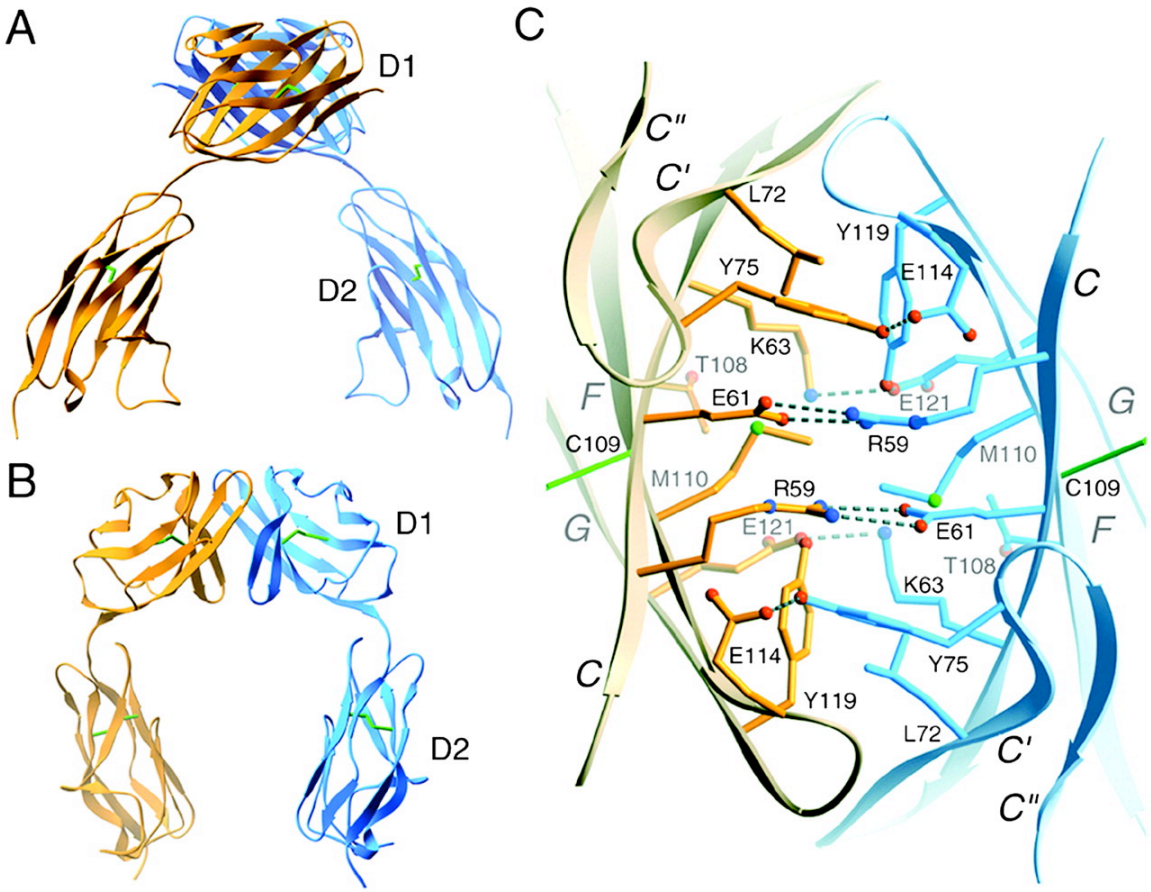

FIGURE I-5. Crystal structure of the hJAM-A extracellular domain. (A and B) Ribbon drawings of the hJAM-A dimer, with one monomer shown in orange and the other in blue. Two orthogonal views are displayed. Disulfide bonds are shown in green. (C) View of the interface between two hJAM-A monomers. The interface is formed by residues on the GFCC' faces of two membrane-distal (D1) domains. The view is along a crystallographic dyad. Hydrogen bonds and salt bridges are represented by broken cylinders. Amino acids are labeled in single-letter code. Image from Prota et. al (122).

coxsackievirus and adenovirus receptor (CAR) also contains two extracellular Ig-like domains that form similar dimers via the GFCC' interface. However, intermolecular interactions in CAR are more hydrophobic in nature than those in JAM-A (157).

Model of σ1-JAM-A interactions

Although structural data for a σ1-JAM-A complex previously were not available, experimental results have provided clues about the location of a reovirus-binding site in JAM-A. Expression in nonpermissive cells of JAM-A constructs in which individual domains had been substituted with structurally homologous domains of CAR identified the membrane-distal D1 Ig-like domain of JAM-A as necessary for reovirus binding (52). Chemical crosslinking of the JAM-A dimer diminishes the capacity of T1L reovirus to bind JAM-A *in vitro* and on cells and negates the competitive effects of soluble JAM-A on reovirus attachment (52). These observations suggest that the virus cannot interact with a covalently linked JAM-A dimer and, thus, might engage the D1 domain via residues that are buried in the dimer interface. In an attempt to identify residues that are required for efficient reovirus binding, several solvent-accessible residues as well as a few solvent-inaccessible residues in JAM-A were altered. Residues selected for this analysis are conserved in human and murine homologues of JAM-A, which both serve as reovirus receptors (6, 122). Assaying the mutant constructs for the capacity to bind T1L reovirus in solid-phase studies identified residues Ser57 and Tyr75 as important for efficient reovirus attachment (52). Tyr75 is located near the "top" of the JAM-A dimer interface on β-strand C' and forms a hydrogen bond with Glu114 (122) (Figure I-5C). Thus, Tyr75 would not be accessible to ligand in the context of fully dimeric JAM-A.

Ser57 is located close to Tyr75, at the edge of the JAM-A dimer interface. Together, these results provide support for a binding model in which reovirus engages forms of JAM-A that are at least partially dissociated via residues near the "top" and within the dimer interface. However, the extent of the binding site, the nature of interactions, and how σ1 might gain access to residues within the dimer interface of JAM-A remain unclear.

Sequence analysis has suggested a potential JAM-A-binding site in σ1. Alignment of σ1 sequences from prototype and field-isolate strains of the three reovirus serotypes, which each use JAM-A as a receptor (20), identified a cluster of conserved, solvent-exposed residues at the lower edge of the BADG sheet of the β-barrel head of σ1, including several residues that form the loop connecting β-strands D and E (Figure I-3B) (20, 30). As the largest cluster of conserved residues in the σ1 head, this region represents a candidate JAM-A-binding site. However, we have not identified a prototype or field-isolate strain of reovirus incapable of utilizing JAM-A as a receptor (20), and selection of JAM-A-resistant variants using soluble JAM-A constructs has been unsuccessful to date (K. M. Guglielmi, J. A. Campbell, and T. S. Dermody, unpublished observations). Thus, the location of the JAM-A-binding site in σ1 and the nature of interactions between the virus and receptor remain unknown.

Adhesion-strengthening mechanism of reovirus attachment to cells

Monoreassortant viruses containing the σ1-encoding S1 gene of either non-sialic acid-binding strain T3C44 (T3SA-) or sialic acid-binding strain T3C44-MA (T3SA+) in a T1L background have been used to study the contribution of sialic acid to stable reovirus

attachment to cells (5). T3SA- and T3SA+ vary by a single amino acid residue at position 204 (leucine for T3SA- and proline for T3SA+), which correlates with the capacity to bind sialic acid (29). T3SA+ binds sialic acid with an apparent K_D of ~ 5 x 10^{-9} M, while T3SA- displays no specific interaction with this carbohydrate (5). While the steady-state avidity of these strains for L cells, as determined by competition binding assays, is nearly equivalent (K_D ~ 3 x 10^{-11} M), the avidity of T3SA+ for HeLa cells is fivefold higher than that of T3SA- (5). Kinetic assessments of binding indicate that the capacity to engage sialic acid functions primarily to increase the k_{on} value of virus attachment to HeLa cells.

The enhanced infectivity of T3SA+ is mediated by the interaction of σ1 with cell-surface sialic acid, since preincubation of virus with sialyllactose dramatically reduces the efficiency of T3SA+ infection, yet has no effect on T3SA- infectivity (5). However, sialic acid-mediated enhancement of T3SA+ infection occurs only during the initial phases of virus-cell interaction, since sialyllactose does not inhibit productive binding of T3SA+ after the first 30 minutes of virus adsorption. In contrast, Fab fragments of a monoclonal antibody directed to the JAM-A-binding σ1 head (9BG5) neutralize T3SA+ infection efficiently, even when added at late times during adsorption (5).

Results of the binding studies performed using T3SA+ and T3SA- suggest that reovirus attaches to cells using an adhesion-strengthening mechanism, in which initial low-affinity binding to sialic acid facilitates secondary higher-affinity binding to JAM-A. For sialic acid-binding reovirus strains, the initial interaction between virus and cell is likely mediated by sialic acid due to the high surface concentration of this carbohydrate. By virtue of its rapid association rate, virus binding to sialic acid would adhere the virion

to the cell surface, thereby enabling it to diffuse laterally until it encounters JAM-A. Such lateral diffusion has been reported for influenza virus (130) and phage T4 (171).

Reovirus entry

Once stably tethered to the target cell membrane, reovirus must be internalized to initiate its infectious cycle. The JAM-A cytoplasmic tail is dispensable to confer reovirus infectivity in nonpermissive cells, suggesting that signaling events mediated by molecules other than JAM-A mediate virus internalization (95). Several lines of evidence support a model of reovirus entry in which β1 integrins serve as reovirus internalization receptors. First, a β1-specific antibody, but not antibodies against several other α and β integrin subunits, inhibits reovirus infection of HeLa cells (95). Second, co-expression of β1 and JAM-A in nonpermissive chicken embryo fibroblast cells confers reovirus infectivity, whereas expression of JAM-A alone confers only binding to these cells. Third, mouse embryo stem cells lacking β1 show reduced reovirus infectivity, but not binding, in comparison to wild-type cells. The pentameric λ2 protein, into which σ1 inserts, contains integrin-binding motifs (RGD and KGE), at least one of which is likely to be accessible in virions (43, 95, 105). Thus, analogous to the adenovirus penton base, which binds integrins αvβ3 and αvβ5 (33), λ2 may recognize integrins that mediate viral internalization into host cells.

Viral internalization occurs by receptor-mediated endocytosis that is likely clathrin-dependent (4, 50, 127, 146). Within endosomes, reovirus virions undergo acid-dependent, proteolytic disassembly to form infectious subvirion particles (ISVPs) (3, 26, 146) (Figure I-6). ISVPs are characterized by the loss of outer-capsid protein σ3, a

conformational change in attachment protein σ1, and cleavage of outer-capsid protein μ1 to form particle-associated fragments, δ and φ. ISVPs penetrate endosomal membranes and release transcriptionally active cores into the cytoplasm (25, 26, 113). Thus, reovirus disassembly consists of a highly coordinated series of events that requires exposure to the low-pH environment encountered in an endosome.

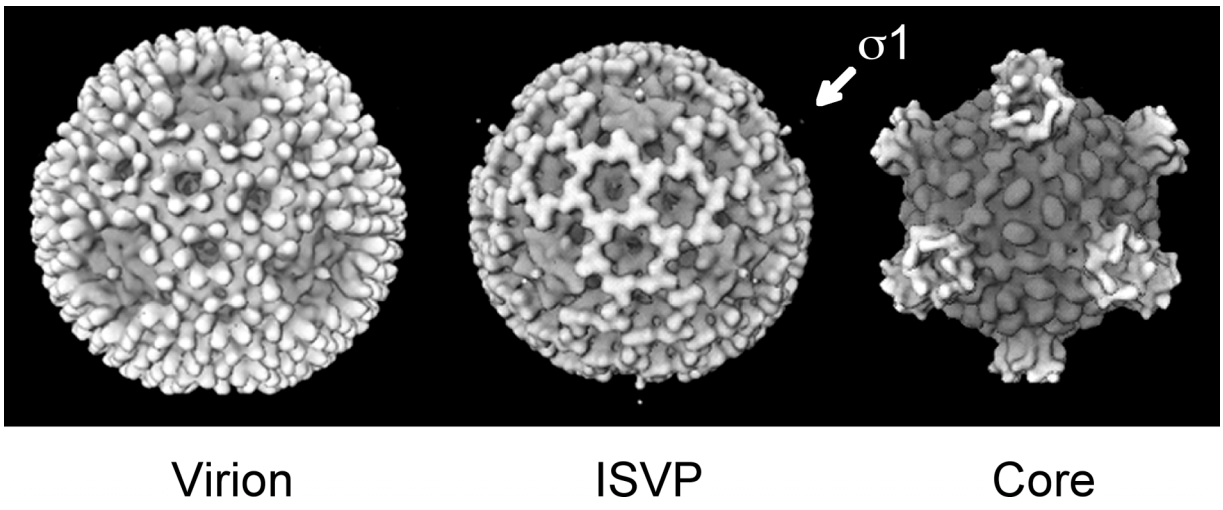

FIGURE I-6. Structure of reovirus virions, ISVPs, and cores. Surface-shaded representations of cryo-electron microscopic image reconstructions of reovirus are shown, as viewed along a twofold axis of symmetry. Density representing σ1 can be seen extending from turrets of λ2 at the icosahedral axes of virions and ISVPs. Cores lack σ1. Image adapted from Dryden et. al (43).

Conformational changes in σ1

Accumulating evidence suggests that σ1 undergoes dramatic conformational changes during viral disassembly and that these changes facilitate key steps in the cell entry process (43, 55, 107). EM images of negatively stained reovirus virions and ISVPs reveal filamentous projections extending up to 400 Å from the surface of ISVPs but not

virions (55). These images suggest that σ1 adopts a compact form in the virion and a more extended one in the ISVP. Cryo-EM image reconstructions of virions of reovirus prototype strains and cores of T1L each lack a discernable density corresponding to σ1 at the icosahedral vertices (43, 102) (Figure I-6). However, in cryo-EM image reconstructions of T1L ISVPs, discontinuous density is observed for σ1 extending ~100 Å from each vertex. Presumably, the full length of σ1 is not visible in reovirus particles because icosahedral averaging was employed for the cryo-EM image reconstructions. The trimeric σ1 protein is positioned at an icosahedral five-fold axis; therefore, it does not obey icosahedral symmetry. Moreover, σ1 possesses structural flexibility, which also may preclude its visualization by this technique.

The flexibility of σ1 has been observed in EM images of negatively stained σ1 molecules isolated from virions, which show bending in individual fibers at specific regions within the tail (54) (Figure I-2B), and in the crystal structure of the C-terminal half of T3D σ1 (30) (Figure I-3A). In addition to flexibility within the tail domain, some EM images of individual σ1 molecules reveal a head domain that appears multi-lobed, suggesting that head might adopt a more open conformation than the one observed in the crystal structure (Figures I-2B and I-3). A highly unusual cluster of conserved aspartic acid residues is found at the trimer interface at the base of the σ1 head (30) (Figure I-7). These residues may be important for triggering conformational changes in the low-pH environment of the endocytic pathway. Acid-dependent conformational changes in the attachment proteins of enveloped viruses, such as influenza virus and tick-borne encephalitis virus, are well-documented (19, 144). Despite the importance of σ1 in mediating attachment to host cells, the conformational changes that occur in σ1 during

the viral entry and uncoating steps and their significance are, at present, poorly understood.

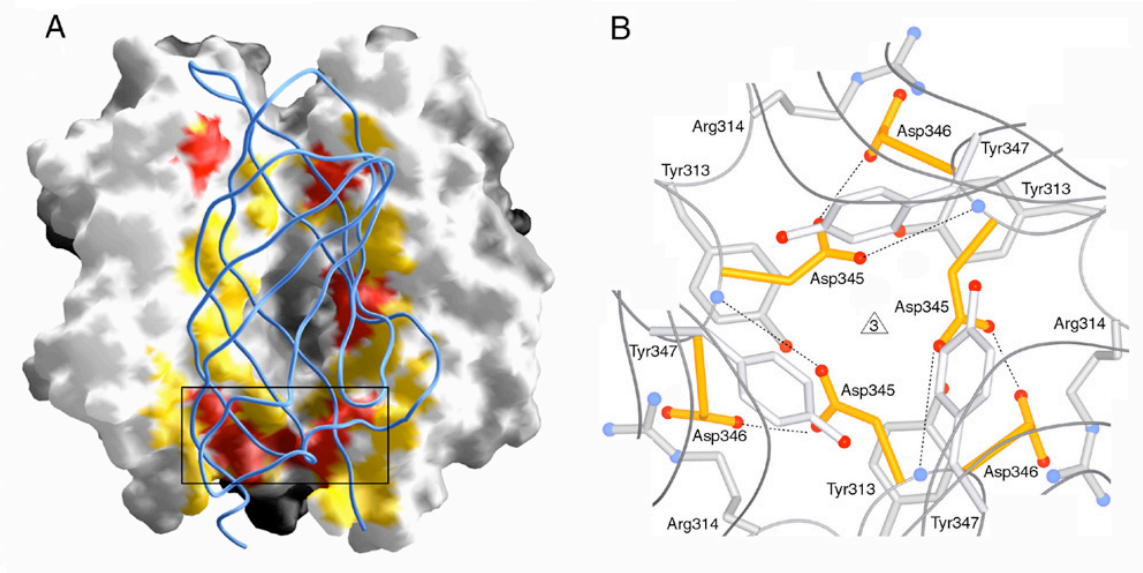

FIGURE I-7. The σ1 head trimer interface. (A) View into the head trimer interface. Two monomers are shown as surface representations and the third monomer is shown as a blue ribbon. Surface residues that are within 4 Å of residues in the third monomer are shown in red (residues conserved in T1L, T2J, and T3D σ1) and yellow (residues unique to T3D σ1). The contact area involving conserved residues Val344, Asp345, and Asp346 is boxed, and this region is shown in more detail in (B). (B) View along the trimer axis, centered at conserved residues Asp345 and Asp346 (yellow) located at the base of the σ1 head. Residues Tyr313, Arg314, and Tyr347 engage in contacts with the two aspartic acids. The side chains of Asp345 are likely to be protonated to avoid an accumulation of negative charge at the interface. Hydrogen bonds involving protonated Asp345 are indicated. Oxygen and nitrogen atoms of side chains are shown as red and blue spheres, respectively. The Asp346 main chain amides also are shown as blue spheres. Image from Chappell et. al (30).

Significance of the research

Reoviruses provide a tractable model system for studies of viral attachment and pathogenesis. Since σ1 is the primary determinant of viral tropism (41, 155, 165), studies of its interactions with receptors are critical to understanding mechanisms of reovirus

disease. Yet much remains unknown about how reovirus targets specific cells within the host for infection. Understanding how σ1 engages cellular receptors and contributes to early steps in the viral life cycle will permit an enhanced understanding of how viral protein structure and function relate to viral disease outcomes. Many viruses utilize attachment and entry strategies that are similar to reovirus, including binding to multiple receptors at the cell surface and internalization into the endocytic pathway. Furthermore, many viruses specifically engage IgSF members to achieve attachment to host cells (6, 12, 36, 59, 61, 94, 139, 149-151, 161). Thus, mechanisms of attachment elucidated for reovirus might contribute to a broader understanding of interactions of other viruses with cellular receptors. In addition, reovirus shows promise as an oncolytic therapeutic (153) and is currently being employed in Phase I clinical trials to treat malignant gliomas (53). A precise understanding of viral attachment protein structure and function and virus-receptor interactions might contribute to improved design of viral vectors for oncolytic and vaccine delivery purposes. My research has focused on structure-function relationships of reovirus attachment protein σ1 and JAM-A. This work has led to the discovery of a novel protein homotrimerization motif, the aspartic acid sandwich, which includes several charged residues in close proximity and might contribute to σ1 structural rearrangements. These studies also have revealed the basis of σ1-JAM-A interactions on a near-atomic level and enhanced an understanding of the forces that stabilize the σ1-JAM-A complex and JAM-A homodimers. Collectively, my dissertation research has enhanced an understanding of the molecular framework that guides reovirus to its cellular targets.

CHAPTER II

THE REOVIRUS σ1 ASPARTIC ACID SANDWICH: A TRIMERIZATION MOTIF POISED FOR CONFORMATIONAL CHANGE

Introduction

One of the most remarkable features of the previously-determined structure of the C-terminal half of σ1, is a cluster of aspartic acid residues at the base of the head domain (30) (Figure I-7). Molecular dynamics studies suggest that these residues are likely to play a role in mediating conformational changes in σ1 (22). However, at a resolution of 2.6 Å, the structure did not allow precise placement of water molecules and visualization of contacts between amino acids with sufficient accuracy to explain how such a unique arrangement of amino acids is compatible with a higher-order structure.

In this study, we determined a high-resolution structure of a fragment of T3D σ1 that comprises the head domain and a single β-spiral repeat of the tail. The structure has been refined to a resolution of 1.75 Å allowing us to discern with high clarity details of the subunit interface in the vicinity of the aspartic acid cluster. Furthermore, we have analyzed two σ1 mutants with alterations in the vicinity of the subunit interface to determine the effects on receptor-binding capacity and trimer stability. Our studies suggest that the aspartic acid cluster serves as a molecular switch that, depending on the microenvironment, can stabilize or destabilize the formation of a trimeric structure.

The research described in this chapter was performed in collaboration with past and present members of the Thilo Stehle laboratory (Universitat Tübingen). Dr. Pierre Schelling (Millipore) purified, crystallized, and solved the structure of the wild-type T3D

σ1 head domain. I generated and initially purified and characterized the two σ1 head domain mutants, σ1H-D345N and σ1H-Y313A, using gel filtration chromatography. I also performed all surface plasmon resonance experiments. Eva Kirchner (Universitat Tübingen) crystallized, determined the structure, and performed gel filtration studies of σ1H-D345N. Eva also prepared the structural figures shown in this chapter. Bernhard Paetzold (Universitat Tübingen) performed crosslinking, gel filtration, and circular dichroism (CD) spectroscopy studies of σ1H-Y313A.

Results

Purification of σ1H - The previously crystallized T3D σ1 protein (30) contains a flexible linker between the C-terminal two β-spiral repeats of the tail. This flexibility likely contributed to the observed diffraction limit of 2.6 Å for these crystals. To obtain better-diffracting crystals of T3D σ1, we designed a modified construct containing the entire head domain and only the C-terminal β-spiral repeat of the tail (σ1H; residues 293-455). We also tested an additional construct comprising only the head domain (residues 309-455), but it did not yield soluble and trimeric protein, suggesting that the C-terminal β-spiral contributes to trimer formation. The protein was produced with a cleavable N-terminal GST tag and purified via sequential glutathione-affinity chromatography and anion exchange chromatography. Subsequent gel filtration showed that the protein elutes at an apparent molecular weight of ~ 45 kDa, consistent with a trimer (data not shown). N-terminal sequencing confirmed that the product released following protease treatment was the σ1 head domain with two additional amino acids from the protease recognition sequence (data not shown).

Binding of σ1H to JAM-A - To determine whether the purified protein folds natively, we quantitatively assessed the capacity of σ1H to bind to JAM-A using SPR. The JAM-A ectodomain, expressed and purified as a GST fusion protein (122), was captured on a biosensor surface with a GST-specific antibody. When injected across the biosensor surface, purified σ1H bound saturably and reversibly to the GST-JAM-A ectodomain but not to GST alone (Figure II-1A). Kinetic analysis of the σ1-GST-JAM-A interaction using BIAevaluation 3.0 software indicated a K_D of ~7 x 10^{-9} M, a value that approximates the K_D determined for a larger fragment of σ1 (6). These results indicate that purified σ1H is functional and that the JAM-A-binding domain of σ1 lies within residues 293-455.

Overall structure of σ1H at 1.75 Å resolution - Diffraction data were collected at the National Synchrotron Light Source (Brookhaven National Laboratory) using crystals of purified σ1H. The structure was solved by molecular replacement using the previously determined lower-resolution structure of a C-terminal fragment of σ1 (30) and refined to 1.75 Å (Table II-1). A simulated-annealing omit map for the refined structure calculated without model bias demonstrates that the model is accurate (data not shown). Concordantly, both working and free R-factors are very low (Table II-1), indicating that the structure is well refined and of high quality. A total of six monomers, arranged into two almost identical trimers, are present in the asymmetric unit of the crystals. A ribbon tracing of one trimer is shown in Figure II-1B. Each σ1 monomer is composed of an eight-stranded β-barrel. The overall conformation of the monomers is very similar, with

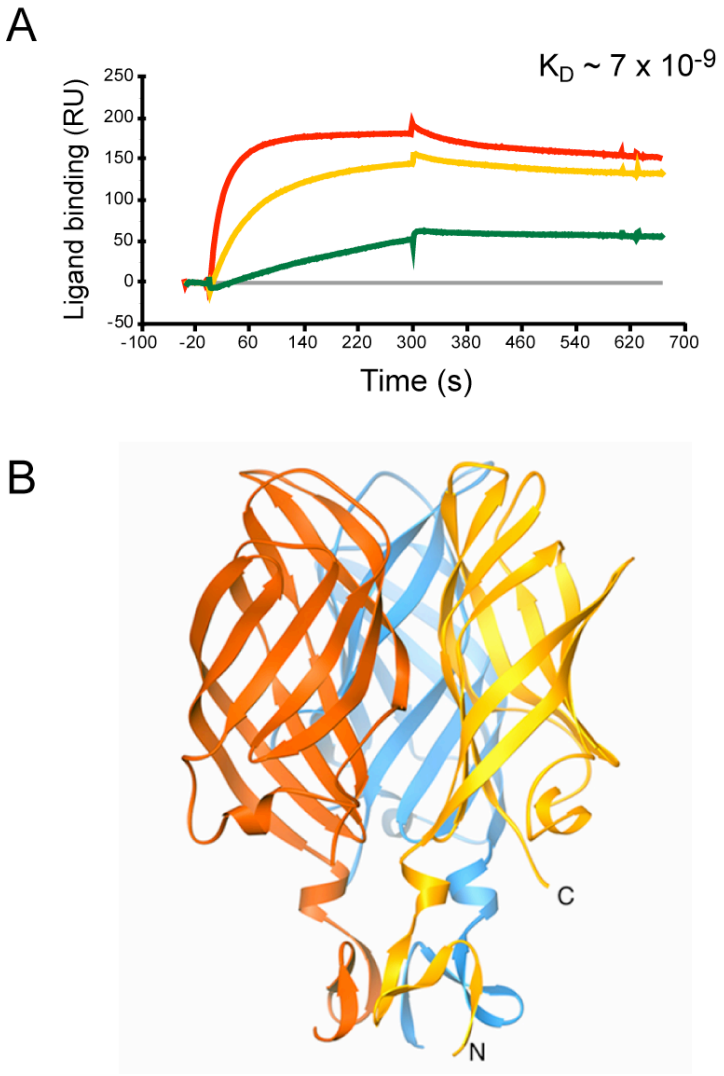

FIGURE II-1. Functional and structural characterization of the σ1 head domain. (A) T3D σ1H binding to the JAM-A ectodomain. Purified σ1H at a concentration of 300 nM (red), 30 nM (yellow), and 3 nM (green) was injected across a biosensor surface coated with either GST or GST-JAM-A. Binding of σ1H to GST was set as the baseline (grey). The calculated affinity for binding to GST-JAM-A, expressed as apparent K_D, is approximately 7 x 10^{-9} M. (B) High-resolution structure of σ1H. Shown is a ribbon tracing of the trimer, with the three monomers drawn in red, orange, and blue. Termini are labeled in one monomer with N (N terminus) and C (C terminus).

TABLE II-1. Data collection and refinement statistics for σ1H and σ1H-D345N crystal structures.

Data set	σ1H	σ1H-D345N
Diffraction data*		
Space group	$P2_1$	$P2_1$
Unit cell dimensions (Å)	a=83.9	a=84.0
	b=51.4	b=51.6
	c=108.9	c=108.9
Angles (°)	β=95.7	β=95.6
Resolution range (Å)	30 – 1.75	30 – 1.85
Completeness (%)	96.7 (86.7)	98.7 (97.9)
Total reflections	300,167	347,405
Redundancy (%)	3.3 (2.6)	4.4 (4.0)
R_{merge} [#] (%)	9.3 (42.7)	9.6 (41.6)
I/σI	15.71 (2.26)	6.5 (1.4)
Refinement statistics		
R_{cryst} (%); work set[†]	22.4 (30.1)	17.5 (23.1)
R_{cryst} (%); free set[†]	27.4 (38.5)	22.5 (27.3)
Overall B-factor (Å^2)	16.0	17.3
R.m.s.d. bond lengths (Å)	0.008	0.012
R.m.s.d. bond angles (°)	0.962	1.234
Number of water molecules	1220	994
Ramachandran plot: [‡]		
most favorable regions	88.5%	87.9%
additional allowed regions	10.0%	10.5%
generously allowed regions	1.0%	1.5%
Disallowed regions	0.5%	0.0%

* Data sets were collected at 100 K and a wavelength of 1.1 Å (σ1H) and 1.54 Å (σ1H-D345N). Values in parentheses refer to the outermost resolution shell (1.75-1.81 Å for σ1H and 1.92-1.85 Å for σ1H-D345N).

[#] $R_{merge} = \Sigma_{hkl}|I - \langle I\rangle| / \Sigma_{hkl} I$, where I is the intensity of a reflection hkl, and $\langle I\rangle$ is the average over symmetry-related observations of hkl.

[†] $R_{cryst} = \Sigma_{hkl}| F_{obs} - F_{calc} | / \Sigma_{hkl} F_{obs}$, where F_{obs} and F_{calc} are observed and calculated structure factors, respectively. Free set (17) contains 10% of the data.

[‡] Calculated with PROCHECK (23).

the exception of two longer and presumably flexible loops: the G-H loop at the top of each monomer and the D-E loop at its base. With the exception of His388, all σ1 residues occupy allowed regions in the Ramachandran diagram (23). However, since the density corresponding to His388 is unambiguous, it appears that a salt bridge to Glu348

fixes its side chain in the observed conformation. Asp345 is located in the generously allowed region of the Ramachandran diagram; it forms, together with Asp346, a β-hairpin between β-strands B and C. The dihedral angles classify this region as a type II' β-hairpin (134).

Contacts in the σ1 trimer - Trimer formation buries from solvent an area of 2292 $Å^2$ per monomer. Residues in the tail account for about 25% of this area, primarily through hydrophobic interactions between the strands of the β-spiral. The three β-barrel domains that form the head engage in a more complex pattern of interactions. Multiple contacts between the subunits at the outer edges of each monomer result in binding surfaces that extend from the base of the head to its top (Figure II-2A). However, a large cavity exists at the center of the trimer, and this cavity is surrounded by smaller regions that lack intersubunit contacts (Figure II-2A). The central cavity measures ~ 15 Å in height and ~ 10 Å in width and contains a large number of ordered water molecules that are connected to the exterior surface through channels at the top of the trimer (Figure II-2B). The cavity probably also contains many less-well ordered water molecules, which are not visible in our electron density maps. Dimensions of the channels leading toward the cavity suggest that water molecules can flow freely to the top of the trimer. In contrast, the bottom of the cavity is sealed by the three Tyr347 side chains (Figure II-2A).

The aspartic acid sandwich - An unusual cluster of aspartic acid residues lies just below the water-filled cavity. Each monomer contributes two aspartic acid residues, Asp345 and Asp346, to this cluster, giving rise to a total of six aspartic acid side chains that are

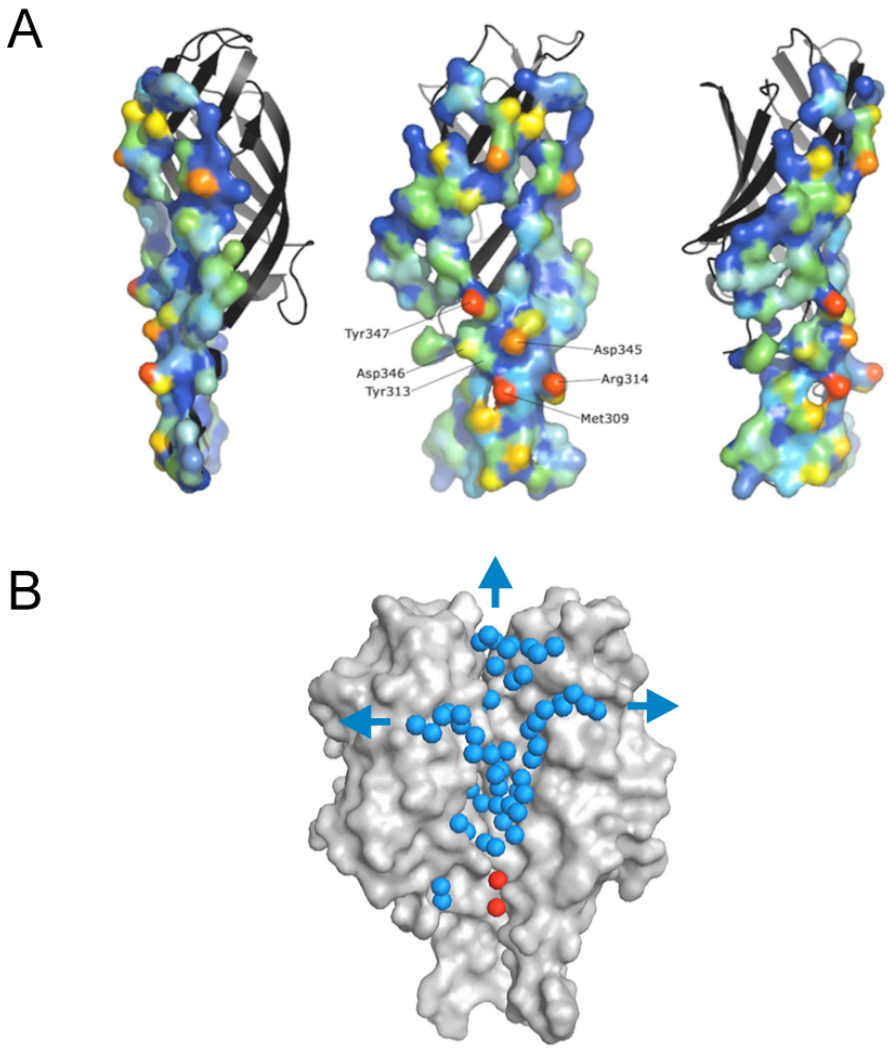

FIGURE II-2. Architecture of the σ1 head subunit interface. (A) Contacts between subunits in the T3D σ1 trimer. Three views, each differing by 90°, are shown. One monomer is shown as a black ribbon, and its contact area with the other two monomers is represented as a molecular surface. Residues discussed in the text are labeled. The contact area was calculated using AREAIMOL (23) as the solvent accessible area difference between the trimeric and monomeric forms of the molecule. The difference values range from 1 $Å^2$ (dark blue) to 52 $Å^2$ (red). Regions with a high area difference have low solvent accessibility in the trimer and thus represent areas with high-affinity intersubunit contacts. Surfaces with an area difference of less than 1 $Å^2$ are not shown. Calculations were performed using a point density/$Å^2$ of 1 and a solvent molecule radius of 1.4 Å. (B) Solvent structure at the σ1 head interface. Two monomers are shown as a surface representation. The third monomer has been removed to allow a view into the trimer interface. Ordered water molecules at the interface are represented with spheres. The water molecules shown in blue fill most of the central cavity between the monomers and can leave the cavity via channels leading to the top and the sides of the trimer (arrows). The two water molecules shown in red are located near the Asp345 side chains. These water molecules are solvent-inaccessible.

arranged in close proximity. Asp345 and Asp346 are located at the very tip of a β-hairpin between β-strands B and C (Figure II-3A). β-hairpins are small structural motifs stabilized by a defined backbone hydrogen bond pattern (15). The hairpins of the three monomers face each other, with the side chains of Asp345 making key contacts. The aspartic acids are partitioned between two layers that each contain three tyrosine residues, Tyr347 at the top and Tyr313 at the bottom (Figure II-3C and D).

Each Asp346 side chain forms a salt bridge with Arg314 from a neighboring monomer, but the Asp345 side chains are not engaged in any ionic interactions (with other residues or with cations) that would negate their negative charges. The accumulation of three negative charges in such a hydrophobic environment would be highly unfavorable. Although hydrogen atoms cannot be seen in our electron density maps even at the high resolution obtained (1.75 Å), the location and orientation of the carboxyl groups strongly suggests that they are protonated. A protonated state of Asp345 is also suggested by molecular dynamics studies of σ1 (22). Each protonated carboxylate forms two hydrogen bonds. One of these involves the hydrogen atom of the Asp345 carboxyl group and the carbonyl oxygen of a neighboring Asp346 residue; a second is formed between the carbonyl oxygen and the backbone amide group of Asp346 in a neighboring monomer (Figure II-3C). Since these two hydrogen bonds occur three times, and since there are few other hydrogen bonds involved in head trimerization, the aspartic acid sandwich likely makes a major contribution to trimer stability.

The cluster of aspartic acids is sandwiched between hydrophobic residues that block access of solvent molecules to the carboxylate groups. One side of this sandwich (the "top" in Figure II-3D) is formed by Val344 and Tyr347; the other (the "bottom" in

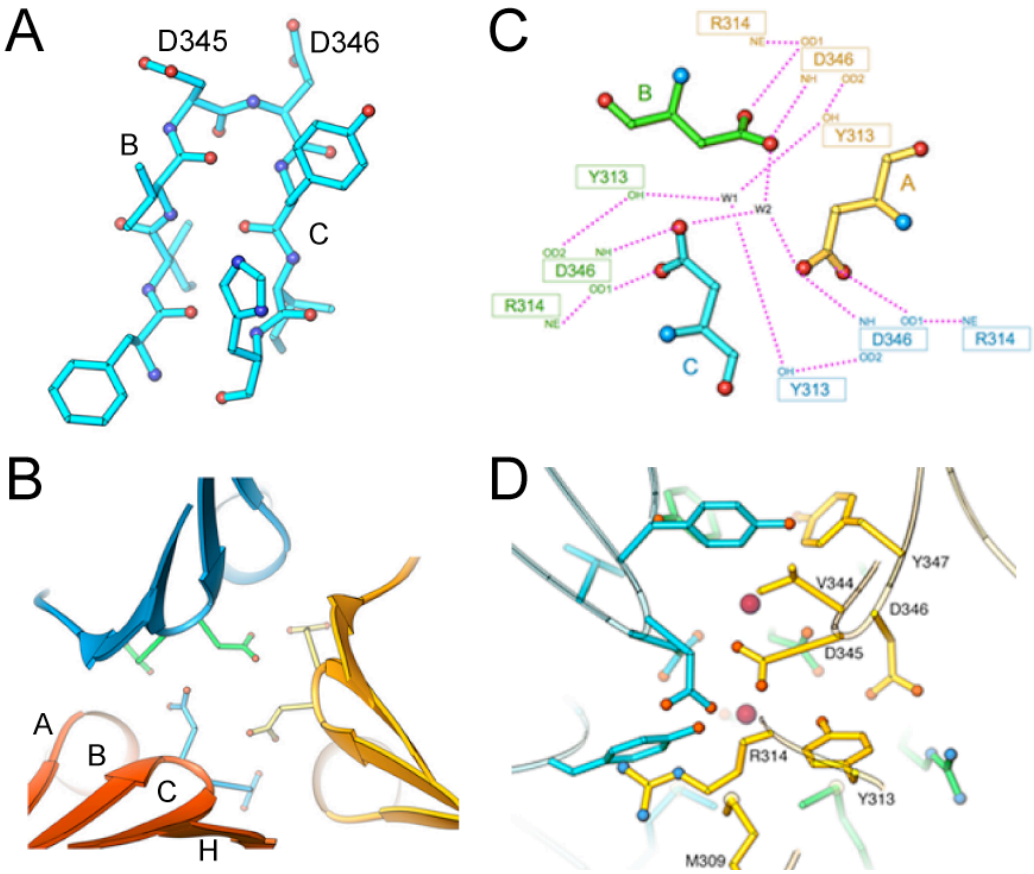

FIGURE II-3. An aspartic acid sandwich at the σ1 head trimer interface. (A) Ball-and-stick view of the type II' β-hairpin on which Asp345 is located. Residues 342 to 349 are shown. Oxygen atoms are shown in red, and nitrogen atoms are shown in blue. Main-chain hydrogen bonds are represented with black dotted lines. Letters B and C refer to β-strands in σ1H. (B) Arrangement of β-hairpins and the aspartic acid cluster as seen from the top of the molecule. The view is along the three-fold axis. The β-strands are depicted as arrows, and β-strands of one monomer are labeled. Side chains of Asp345 and Asp346 are shown in ball-and-stick representation. (C) Schematic view of the aspartic acid cluster, shown in the same orientation as that in panel B. Residues that interact with Asp345 are shown in orange (monomer A), green (monomer B), and blue (monomer C). Hydrogen bonds are shown as dotted lines. W1 and W2 represent the two water molecules trapped inside the cluster. (D) Ball-and-stick representation of the aspartic acid cluster and surrounding residues. The view is perpendicular to the three-fold axis. Residues discussed in the text are labeled in one monomer. The two trapped water molecules are represented with red spheres. The color code is the same as that used in panel C.

Figure II-3D) is formed by Tyr313 and Met309. Two well-ordered water molecules located directly on the three-fold axis are also present in this arrangement of amino acids (Figure II-2B). These water molecules interact with Tyr313 and Asp345, respectively, and they are held in place by an extensive hydrogen bond network (Figure II-3C and D). Buried water molecules can sometimes be exchanged without major unfolding. However, residues in the immediate vicinity of the two water molecules have temperature factors that are among the lowest of the entire structure (data not shown), suggesting that thermal mobility is low in this area. Thus, it is unlikely that the water molecules can be exchanged.

Purification and characterization of σ1H-Y313A - To explore potential conformational changes of σ1, we generated substitutions of two key residues of the cluster, Tyr313 (Y313A) and Asp345 (D345N). The mutant proteins were analyzed for receptor-binding properties and the capacity to form trimers. We reasoned that substitution of Tyr313 with a smaller amino acid might allow influx of water molecules to the aspartic acid cluster, thereby causing the trimer to undergo structural changes triggered by charged Asp345 side chains. The σ1H-Y313A mutant protein was expressed as a GST fusion in bacteria, purified by glutathione affinity, proteolytically cleaved from the GST tag on-column, and further purified using gel filtration. Purified σ1H-Y313A is soluble and elutes as a monomer by gel filtration chromatography (Figure II-4). Treatment of σ1H-Y313A with each of three different crosslinking reagents of various lengths (11.4 to 16.1 Å) failed to alter the chromatographic mobility of the mutant protein (data not shown). σ1H-Y313A was incapable of binding to JAM-A by either gel filtration (data not shown) or SPR

(Figure II-5), indicating that a trimeric form of σ1 is required for JAM-A engagement. CD spectra of σ1H-Y313A show a secondary structure content of the protein similar to that of wild-type σ1H, suggesting that σ1H-Y313A monomers are folded properly (data not shown). Thus, our results indicate that residue Tyr313 is required for trimerization and that the trimeric form of σ1 is essential for receptor binding

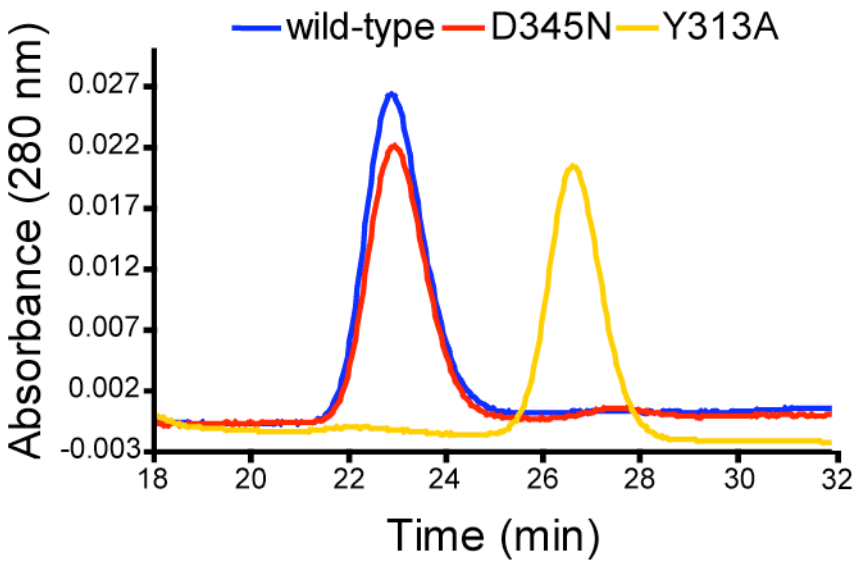

FIGURE II-4. Gel filtration of T3D σ1 head mutants. Purified σ1H (blue), σ1H-D345N (red), and σ1H-Y313A (yellow) constructs were applied to a Superdex 75 gel filtration column in 20 mM Tris pH 7.5, 100 mM NaCl. The D345N mutant elutes at the same time as the wild-type protein, indicating that it forms a trimer, whereas the Y313A mutant shows a significantly smaller molecular weight that corresponds to monomeric protein.

Characterization and structure analysis of σ1H-D345N - To determine whether structural and functional changes occur upon replacement of Asp345 with asparagine, we engineered a D345N mutation in the wild-type T3D σ1H construct. We anticipated that hydrogen bonds might form between the asparagine residues, stabilizing the trimer

interface in much the same manner as accomplished by the protonated Asp345 side chains. The mutant protein was purified using the strategy employed for purification of wild-type T3D σ1H. The σ1H-D345N mutant forms trimers at neutral pH (Figure II-4) and binds to JAM-A with an affinity similar to that of wild-type σ1H (Figure II-5). Thus, σ1H-D345N is biochemically and functionally indistinguishable from the wild-type protein.

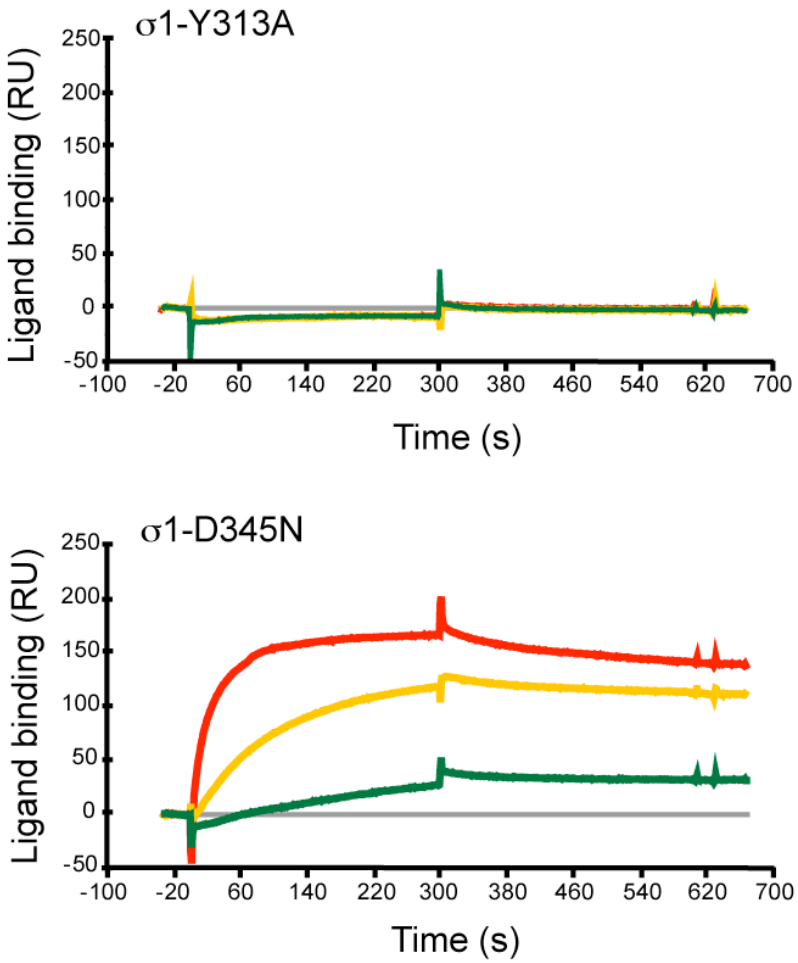

FIGURE II-5. Binding of T3D σ1 head mutants to the JAM-A ectodomain. Purified point mutants of σ1H at 300 nM (red), 30 nM (yellow), and 3 nM (green) concentrations were injected across a biosensor surface coated with either GST or GST-JAM-A. Binding of σ1H point mutants to GST was set as the baseline (grey line). The identity of the mutants is indicated. The calculated affinity for binding of σ1H-D345N to GST-JAM-A, expressed as apparent K_D, is approximately 1 x 10^{-8} M.

To test whether the D345N mutation in T3D σ1H alters the conformation of the aspartic acid sandwich, we determined the structure of σ1H-D345N. The mutant protein was crystallized using conditions similar to those employed to crystallize the wild-type protein. We collected a complete data set from the σ1H-D345N crystals to 1.85 Å and solved the structure by molecular replacement using the wild-type protein structure as a model (Table II-1). The σ1H-D345N mutant crystallized as a trimer with a structure that is nearly identical to that of wild-type σ1H (Figure II-1B). At the subunit interface, the two water molecules observed just above and below residues 345 are at almost exactly the same position in σ1H-D345N (Figure II-6). The amino groups of Asn345 form the same hydrogen-bond pattern as the hydroxyl group of protonated Asp345. Thus, the mutant structure provides evidence that in trimeric, wild-type σ1 all Asp345 residues are protonated.

Discussion

Formation of σ1 trimers - Although a C-terminal fragment of σ1 has been crystallized (30), further characterization at an atomic level of resolution has enhanced an understanding of its trimeric nature. Interactions that form the trimer are highly complex. The base of the trimer is held firmly together by hydrophobic interactions, a standard means of inducing the formation of oligomeric structures. In contrast, contacts at the center and top of the trimer involve interrupted surfaces, cavities filled with water molecules, trapped individual water molecules, very few hydrophobic contacts, and protonated side chains that form hydrogen bonds. These types of interactions are unusual

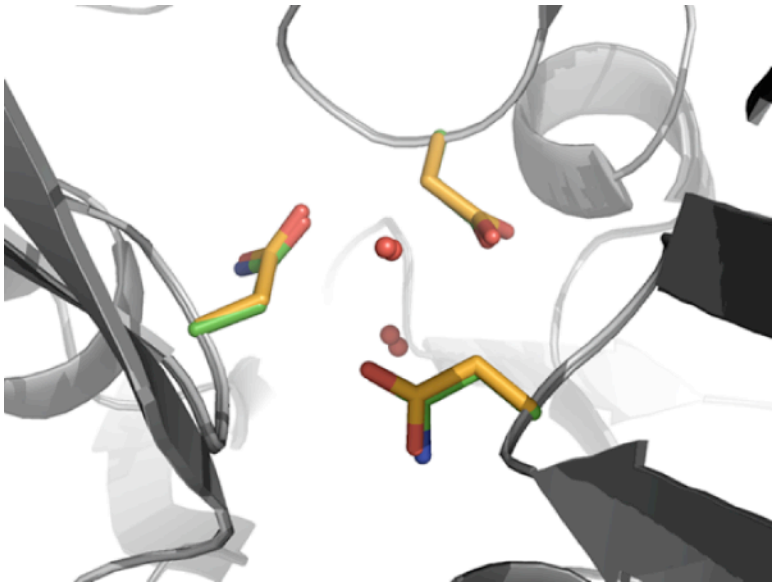

FIGURE II-6. Structure of σ1H-D345N. Superposition of wild-type T3D σ1H and σ1H-D345N at the aspartic acid cluster. Ribbon drawings of the σ1H and σ1H-D345N backbones are shown in grey, oxygen atoms are shown in red, and nitrogen atoms are shown in blue. The Asn345 side chains of σ1H-D345N (green) show the same conformation as those of wild-type σ1H (yellow). The water molecules above and below the cluster also occupy virtually identical positions in both molecules.

for protein-protein contacts. We think that the σ1 head is designed to exist as both monomeric and trimeric species. In fact, the mutation of only one residue, Tyr313, results in soluble, folded protein that is entirely monomeric. A single substitution at the base of the trimer therefore suffices to completely abolish trimer formation, indicating that the lower-affinity contacts at the center and top of the σ1 head are not sufficient for stabilization of the trimer.

Comparison of deduced amino acid sequences of σ1 proteins from prototype and field-isolate reovirus strains reveals that Asp345 and Asp346 are highly conserved (20, 30). Additionally, hydrophobic residues that form the "top" and "bottom" of the aspartic

acid sandwich show a high degree of conservation. Phenyl ring-containing side chains are found at positions 313 and 347 in a σ1 sequence alignment (30). For example, strain T1L contains phenylalanine and tryptophan residues and strain T2J contains tyrosine and tryptophan residues at positions corresponding to Tyr313 and Tyr347 in T3D σ1. Furthermore, a hydrophobic residue (isoleucine, leucine, methionine, or valine) is found at position 309, and a valine is absolutely conserved at position 344. The striking level of sequence conservation at these positions suggests that the aspartic acid sandwich serves an essential function in reovirus replication.

Engagement of JAM-A - Our analysis shows that the σ1H-Y313A mutant is soluble and monomeric. Furthermore, since its CD spectrum is similar to that of wild-type σ1H, σ1H-Y313A appears to be properly folded. However, the mutant protein does not bind JAM-A. The most likely interpretation of these findings is that a trimeric form of σ1 is required for JAM-A engagement. We envision two possible explanations for these results. First, the JAM-A-binding site may extend across more than one monomer. Second, the surface structure of the JAM-A-binding region may be stable only in the context of a trimer. We think it unlikely that JAM-A makes a direct contact with Tyr313 or with residues in close proximity. Tyr313 is not exposed to solvent in the trimeric wild-type protein and would be unlikely to encounter JAM-A at its position in the head trimer interior.

The structure of σ1 is closely related to that of the adenovirus attachment protein, fiber (30). Moreover, the receptors for reovirus and adenovirus, JAM-A and CAR, respectively, also share significant structural and functional homology and may engage

their viral ligands in a similar manner (141). We note that the adenovirus fiber knob binds to its receptor CAR via contacts between two knob subunits and a single receptor molecule. If this mode of binding is conserved in σ1, it would be affected by alterations at the trimer interface.

We observed a single magnesium ion adjacent to residues Asp365 and Glu419 at the center of the concave surface of σ1H (data not shown). This surface of σ1 has been proposed to participate in interactions with JAM-A (52, 141). The side chains of Asp365 and Glu419 are exposed to solvent and exist in close spatial proximity to side chains of Arg427 and Arg429. These residues would be positioned to engage in salt-bridge interactions with charged residues in the receptor. In support of this idea, analysis of point mutants of JAM-A suggests that acidic and basic residues in the JAM-A dimer interface are required for high-affinity interactions with σ1 ([65]; discussed in Chapter III).

An unusual cluster of aspartic acid residues at the trimer interface – The structure of σ1 reveals an unusual cluster of solvent-inaccessible, conserved aspartic acid residues at the head trimer interface. A key aspect of these residues is that they are located at the very tip of a β-hairpin. As judged by its temperature factors (data not shown), the β-hairpin is rigid and possesses limited mobility. Three lines of evidence support the conclusion that the side chains of Asp345 must be protonated to allow formation of the trimer. First, molecular dynamics studies show that the introduction of negative charges at the Asp345 side chains destabilizes the trimer, causing partial separation of the three chains at the base of the σ1 head (22). Second, the mutant σ1H-D345N protein assembles into a

trimeric structure that is indistinguishable from that of wild-type protein. Remarkably, the arrangement of water molecules in the vicinity of residue 345 in both the wild-type and mutant structures is identical. Since the asparagine side chain is an excellent mimic for a protonated aspartic acid but not for a charged aspartate, the structural similarities between the two proteins argue strongly that the wild-type protein contains protonated Asp345 residues. Third, alanine substitution of a residue that shields Asp345 from solvent, Tyr313, results in monomeric protein. It is likely that mutation of Tyr313 renders Asp345 solvent-accessible, causing it to lose its proton at neutral pH.

The hypothesis that Asp345 in σ1 is protonated is also supported by the finding of a similar cluster of aspartic acids in the G protein of vesicular stomatitis virus (VSV) (124). Although the global architecture of VSV G differs substantially from reovirus σ1, VSV G also forms a trimer that features three aspartic acids that face each other at the trimer interface. The location and orientation of the aspartic acid clusters in VSV G and σ1 are in fact surprisingly similar (Figure II-7). In both cases, hydrogen bonds are thought to mediate interactions between protonated aspartic acid side chains. These hydrogen bonds lie in a plane that is perpendicular to the trimer axes, and deprotonation would lead to destabilization of the trimer. In both molecules, the aspartic acids emanate from well-ordered backbone structures with low mobility (an α-helix in VSV G and a β-hairpin in σ1). Most interestingly, both clusters contain trapped water molecules that form hydrogen bonds with the protonated carboxylate groups.

Implications for viral attachment and entry - What are the implications of the aspartic acid cluster for σ1 function in viral attachment and cell entry? Both VSV and reovirus

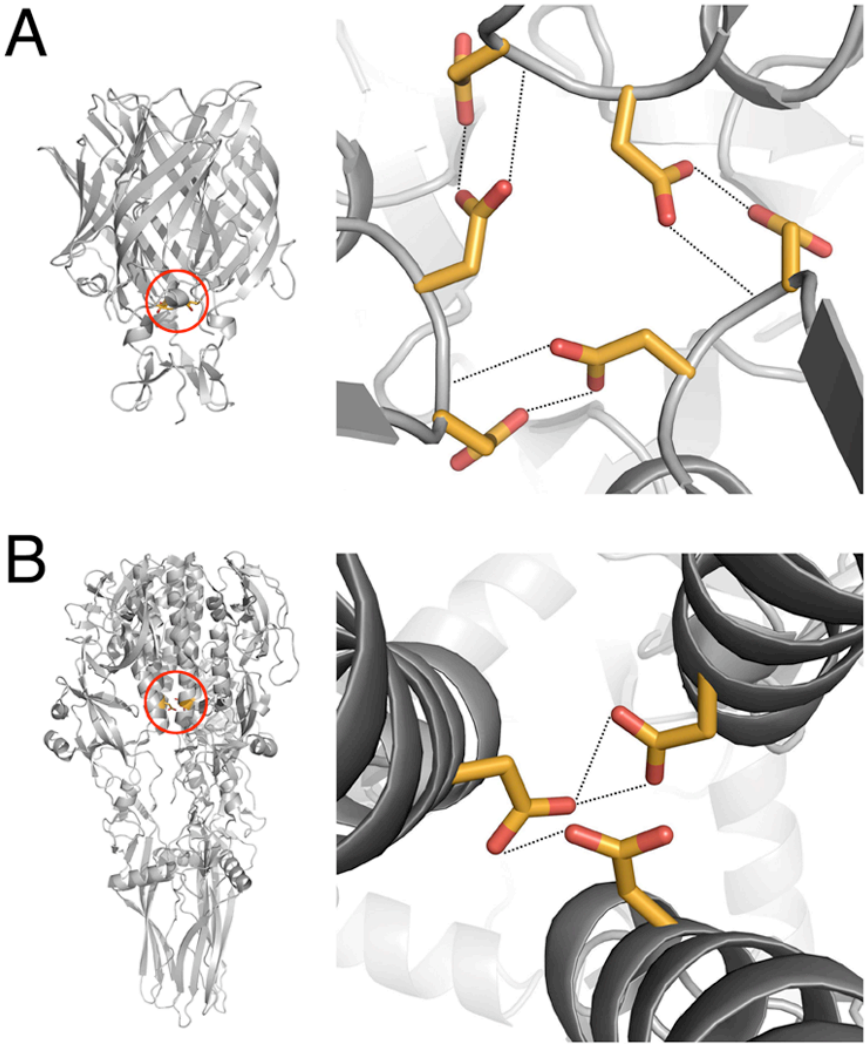

FIGURE II-7. Comparison of aspartic acid clusters in reovirus σ1 (A) and VSV G (B). In both cases, the view is along the threefold axis. Ribbon drawings of the complete trimers are shown on the left in each case to depict the location of the clusters (red circles). Ribbon tracings of the backbones are shown in grey, carbon atoms of aspartic acid residues Asp268 (VSV G) and Asp345 and Asp346 (σ1) are shown in orange, and oxygen atoms are shown in red. Hydrogen bonds are represented with dotted lines.

enter cells via the endosomal pathway and thus encounter a low-pH environment during the entry process. The VSV G structure has been interpreted as a low-pH conformer of the molecule (124). In keeping with this conclusion, it is possible that the σ1 structure reported here also represents a form of the protein found at low pH. Both VSV G and reovirus σ1 were crystallized at close-to-neutral pH, but the conditions used for crystallization are far from physiologic in both cases and may easily create an environment that favors protonated aspartic acids. Thus, the aspartic acid cluster may act as a molecular switch that disfavors trimerization when charged but favors trimerization when the protein encounters a low-pH environment that allows it to be protonated. Because the aspartic acids project from rigid structural motifs, they may prevent trimerization in environments that favor deprotonation.

Conformational changes of viral proteins in response to ligand binding or exposure to acidic pH are well established (19, 31, 81). These changes allow viruses to expose previously hidden epitopes for ligand binding and membrane penetration. For example, the influenza virus hemagglutinin undergoes a massive rearrangement upon exposure to acidic pH. This conformational change is enabled by prior proteolytic cleavage and leads to the formation of α-helical coiled-coil structures that expose a hydrophobic fusion peptide. Importantly, the hemagglutinin structure at neutral pH represents a metastable form of the protein, as the low pH conformer, once formed, is stable even at neutral pH (32). The conspicuous location of Asp345 at the σ1 trimer interface suggests that the aspartic acid cluster serves a similar function to mediate a structural transition between a form of the protein that is at least partially detrimerized in the head region and a fully trimerized molecule (as seen in the crystal structure here).

Evidence for the existence of a partially detrimerized σ1 head domain comes from EM images of individual σ1 molecules, in which the head domain appears bi- or multi-lobed ([54] and Figure I-2). Based on our current data, it appears that the fully trimerized protein is the energetically favored form. Placed in the context of the entire virion, such a conformational change might facilitate events during reovirus entry subsequent to viral attachment, such as internalization into the endocytic pathway and proteolytic disassembly to form infectious subvirion particles.

CHAPTER III

REOVIRUS BINDING DETERMINANTS IN JUNCTIONAL ADHESION MOLECULE-A

Introduction

Previous research findings identified JAM-A as a serotype-independent reovirus receptor (6, 20) and showed that the σ1 head domain binds to JAM-A with high affinity (6, 131). Studies in which CHO cells were transfected with plasmids encoding chimeric CAR-JAM-A receptor constructs or JAM-A domain-deletion mutants provided evidence that the N-terminal D1 domain of JAM-A (Figure III-1A) is required for reovirus attachment and infection (52). Chemical cross-linking of JAM-A diminishes the capacity of reovirus to bind JAM-A *in vitro* and on cells and negates the competitive effects of soluble JAM-A on reovirus attachment (52), suggesting that reovirus binds a surface of JAM-A that is at lest partially obscured in the dimer. However, the precise nature of σ1-JAM-A interactions is not understood. While virus binding to the GFCC'C" surface of the D1 domain of an IgSF member would not be unexpected, the highly charged nature of the residues that compose the GFCC'C" surface of JAM-A D1 (Figure III-1B), coupled with the observation that this surface is buried in JAM-A homodimers, make it an unusual target for reovirus binding. Moreover, it is not apparent how JAM-A-binding contributes to serotype-dependent differences in reovirus tropism in the murine CNS.

In this study, I engineered point mutations in the dimer-contributing surface of the D1 domain of JAM-A, purified the resultant mutants, and characterized effects of the

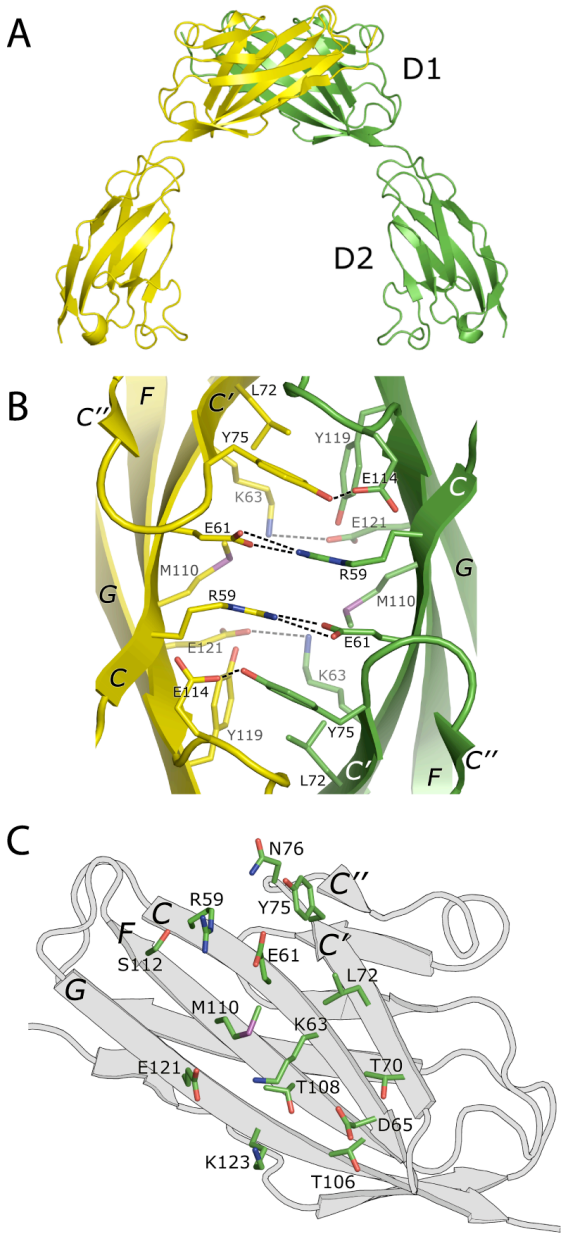

FIGURE III-1. Structure and location of residues in the JAM-A D1 domain. (A) Ribbon drawing of the hJAM-A dimer, with one monomer shown in yellow and the other in green. (B) View of the interface between two hJAM-A monomers. The interface is formed by residues on the GFCC' faces of two D1 domains. The view is along a crystallographic dyad. Oxygen atoms are shown in red, nitrogen in blue, and sulfur in purple. Hydrogen bonds and salt bridges are represented by dashed lines. Amino acids are labeled in single-letter code. (C) View of the GFCC' β-sheet that composes the dimer interface of one JAM-A monomer, labeled as in panel B. Side chains are shown for residues that were altered in this study.

mutations on JAM-A homodimerization and binding to σ1H or intact reovirus virions. In complementary experiments, I tested the capacity of CHO cells expressing full-length JAM-A point mutants to support binding and infection by prototype strains from each of the three reovirus serotypes. My results indicate that binding of reovirus T3D σ1 to JAM-A requires residues in β-strands C and C' within the dimer interface and that JAM-A binding requirements differ among the reovirus serotypes. These findings enhance an understanding of reovirus-receptor interactions and suggest that the nature of JAM-A contacts might contribute to differences in pathogenesis among reovirus serotypes.

I would like to acknowledge Eva Kirchner (Universitat Tübingen) for performing the gel filtration experiments shown in Figure III-5 and for generating Figures III-1 and III-10, which show the X-ray crystal structure of JAM-A, location of residues in the D1 domain, and a model of the σ1 binding site in JAM-A. I would also like to acknowledge Dr. Geoffrey Holm (Vanderbilt University) for generation of the GST-D2 construct used in this study.

Results

Analysis of σ1H binding to GST-JAM-A - For studies of σ1-JAM-A interactions, I purified an N-terminal GST fusion with the extracellular region of JAM-A (122). Bacteria were transfected with plasmids encoding GST-JAM-A, harvested by centrifugation, and lysed by sonication. GST-JAM-A constructs were purified from bacterial lysates using glutathione-affinity chromatography (52). To determine whether GST-JAM-A is capable of binding σ1, I captured GST-JAM-A on the surface of a

biosensor chip via a covalently linked GST-specific antibody. I then injected purified T3D σ1H (131) at three different concentrations and detected association with GST-JAM-A by SPR (Figure III-2A). σ1H did not show any specific binding to the GST-specific antibody or to GST captured on the biosensor surface (data not shown). However, σ1H bound GST-JAM-A with an affinity of ~ 2.4 x 10^{-9} M, which approximates previous calculations of σ1 affinity for JAM-A (6, 131). To determine whether the isolated D1 Ig-like domain of JAM-A is capable of σ1 engagement, I expressed and purified N-terminal GST fusions with only the D1 or D2 Ig-like domains of JAM-A. Protease treatment of the purified proteins removed the GST tag, but did not degrade either Ig-like domain, which suggests that the proteins are properly folded (data not shown). I assessed the capacity of the fusion proteins to bind σ1H using the SPR strategy employed for GST-JAM-A. While σ1H bound GST-D1 with a similar affinity to GST-JAM-A, GST-D2 was incapable of capturing σ1H (Figure III-2B). Together with data obtained using chimeric receptor molecules (52), these results indicate that the membrane distal D1 domain of JAM-A is sufficient for high-affinity interactions with σ1.

Generation and characterization of JAM-A point mutants - To identify specific residues in the D1 domain required for σ1 binding, I generated individual alanine substitutions of residues with surface-exposed side chains in the JAM-A dimer interface (Figure III-1C and Table III-1). Two groups of residues were targeted for mutagenesis: (i) those that form intersubunit contacts-Arg59, Glu61, Lys63, Leu72, Tyr75, Met110, and Glu121, and (ii) those that do not-Asp65, Thr70, Asn76, Thr106, Thr108, Ser112, and Lys123. GST-JAM-A point mutants were purified by glutathione affinity chromatography and

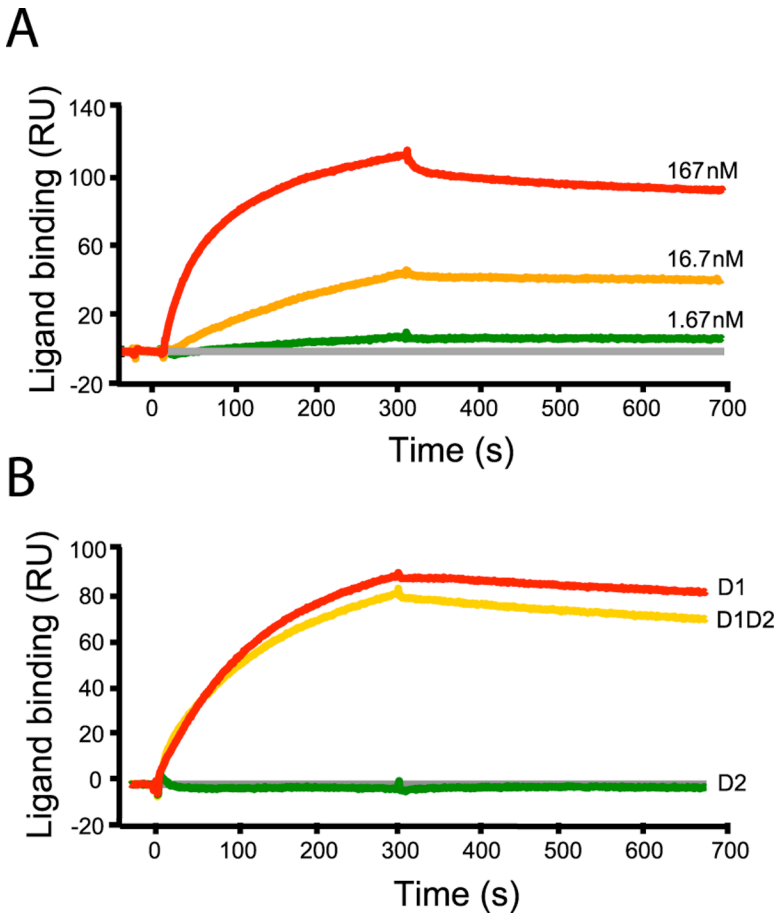

FIGURE III-2. Characterization of σ1H binding to GST-JAM-A. (A) Binding of σ1H to GST-JAM-A. Purified σ1H, at a concentration of 167 nM (red), 16.7 nM (yellow), or 1.67 nM (green) was injected for 5 min across a biosensor surface on which GST fused to the JAM-A ectodomain previously had been captured. Buffer alone was injected for 6.7 min. The baseline is 167 nM σ1H binding to GST (grey). The K_D of σ1H binding to GST-JAM-A is approximately 2.4 x 10^{-9} M. (B) Binding of σ1H to GST-JAM-A Ig-like domains. Purified σ1H, at a concentration of 167 nM, was injected for 5 min across a biosensor surface on which GST-JAM-A fusion proteins previously had been captured. Buffer alone was injected for 6.7 min. The resultant traces show binding to GST-JAM-A (yellow), GST-D1 (red), and GST-D2 (green). The baseline is 167 nM σ1H binding to GST (grey). Binding is expressed in resonance units (RU).

TABLE III-1. Primer pairs used to engineer point mutations in JAM-A [a]

JAM-A Mutation	*Forward primer*	*Reverse primer*
R59A[b]	5' GGCTTTTCTTCTCCCGCGGTGGAGTGG AAGTTTG	5' CAAACTTCCACTCCACCGCGGGAGAA GAAAAGCC
E61A[b]	5' CTTCTCCCCGTGTGGCGTGGAAGTTTG ACC	5' GGTCAAACTTCCACGCCACACGGGGA GAAG
K63A[b]	5' CCCGTGTGGAGTGGGCATTTGACCAAG GAGAC	5' GTCTCCTTGGTCAAATGCCCACTCCAC ACGGG
D65A	5' GAGTGGAAGTTTGCCCAAGGAGACACC	5' GGTGTCTCCTTGGGCAAACTTCCACTC
T70A	5' CAAGGAGACACCGCCAGACTCGTTTG	5' CAAACGAGTCTGGCGGTGTCTCCTTG
L72A	5' CAAGGAGACACCACCAGAGCCGTTTGC TATAATAACAAG	5' CTTGTTATTATAGCAAACGGCTCTGGT GGTGTCTCCTTG
Y75A	5'CCACCAGACTCGTTTGCGCCAATAACA AGATCACAGCTTCC	5' GGAAGCTGTGATCTTGTTATTGGCGCA AACGAGTCTGGTGG
N76A	5' CCAGACTCGTTTGCTATGCCAACAAGA TCACAGCTTC	5' GAAGCTGTGATCTTGTTGGCATAGCAA ACGAGTCTGG
T106A	5' CGGGAAGACACTGGGGCGTACACTTG TATGGTC	5' GACCATACAAGTGTACGCCCCAGTGTC TTCCCG
T108A	5' GACACTGGGACATACGCGTGTATGGTC TCTGAGG	CCTCAGAGACCATACACGCGTATGTCCCA GTGTC
M110A	5' GGACATACACTTGTGCGGTCTCTGAGG AAGG	5' CCTTCCTCAGAGACCGCACAAGTGTAT GTCC
S112A	5' CATACACTTGTATGGTCGCGGAGGAAG GCGGCAACAG	5' CTGTTGCCGCCTTCCTCCGCGACCATA CAAGTGTATG
E121A[b]	5' CAACAGCTATGGGGCGGTCAAGGTCAAG	5' CTTGACCTTGACCGCCCCATAGCTGTTG
K123A	5' CAACAGCTATGGGGAGGTCGCGGTCA AGCTCATCGTGCTTG	5' CAAGCACGATGAGCTTGACCGCGACC TCCCCATAGCTGTTG
E61A[b]	5' CTCCCCGTGTGGACTGGAAGTTTGAC	5' GTCAAACTTCCAGTCCACACGGGGAG
K63R[b]	5' CGTGTGGAGTGGAGGTTTGACCAAGG	5' CCTTGGTCAAACCTCCACTCCACACG
R59A/E61A[b]	5' GCTTTTCTTCTCCCGCTGTGGCGTGGA AGTTTG	5' CAAACTTCCACGCCACAGCGGGAGAA GAAAAGC
E61A/K63A[b]	5' CGTGTGGCGTGGGCATTTGACCAAGG AGACACCAC	5' GTGGTGTCTCCTTGGTCAAATGCCCAC GCCACACG

[a] Primer pairs were used to engineer point mutations in the JAM-A extracellular domain in pGEX 4T-3. Underlined nucleotides denote changes from the wild-type sequence.

[b] Primer pairs also were used to engineer point mutations in full-length JAM-A in pcDNA 3.1+.

used in GST precipitation assays to identify mutations that ablate σ1 binding. In these experiments, glutathione coated beads were used to capture GST fusion proteins, which in turn were used to capture purified σ1H. As anticipated, σ1H was captured efficiently by GST-JAM-A and GST-D1 but not detectably by beads alone, GST, or GST-D2 (Figure III-3). The majority of the JAM-A dimer interface point mutants were capable of binding σ1H. However, mutants E61A, K63A, L72A, and N76A were incapable of binding σ1H as detected by Coomassie blue staining or immunoblotting, despite similar capture of the mutants on the beads (Figure III-3 and data not shown). Residues Leu72 and Asn76 are located at the top of the dimer interface in β-strand C' and the C'C'' loop, respectively (Figure III-2). Leu72 participates in a hydrophobic interaction with Tyr119 on an apposing JAM-A monomer. Residues Glu61 and Lys63 are located in β-strand C and participate in salt-bridge interactions that stabilize JAM-A dimers (6, 131). These data suggest that σ1 engages JAM-A via residues at the top of and within the dimer interface.

Kinetics of σ1H binding to GST-JAM-A point mutants - To quantitatively assess the effects of mutations in the JAM-A dimer interface on interactions with σ1, GST-JAM-A point mutants were captured on a biosensor surface and tested for σ1H binding by SPR. Based on the kinetics and affinity of the interaction with σ1H, the majority of the JAM-A mutants clustered into one of four groups. The first group (I) includes point mutants that display binding kinetics similar to wild-type JAM-A (Figure III-4A and Table III-2). Group I includes mutants with alterations of residues Thr70 in β-strand C' and nearby residue Thr106 in β-strand F, which do not contribute to intersubunit interactions at the

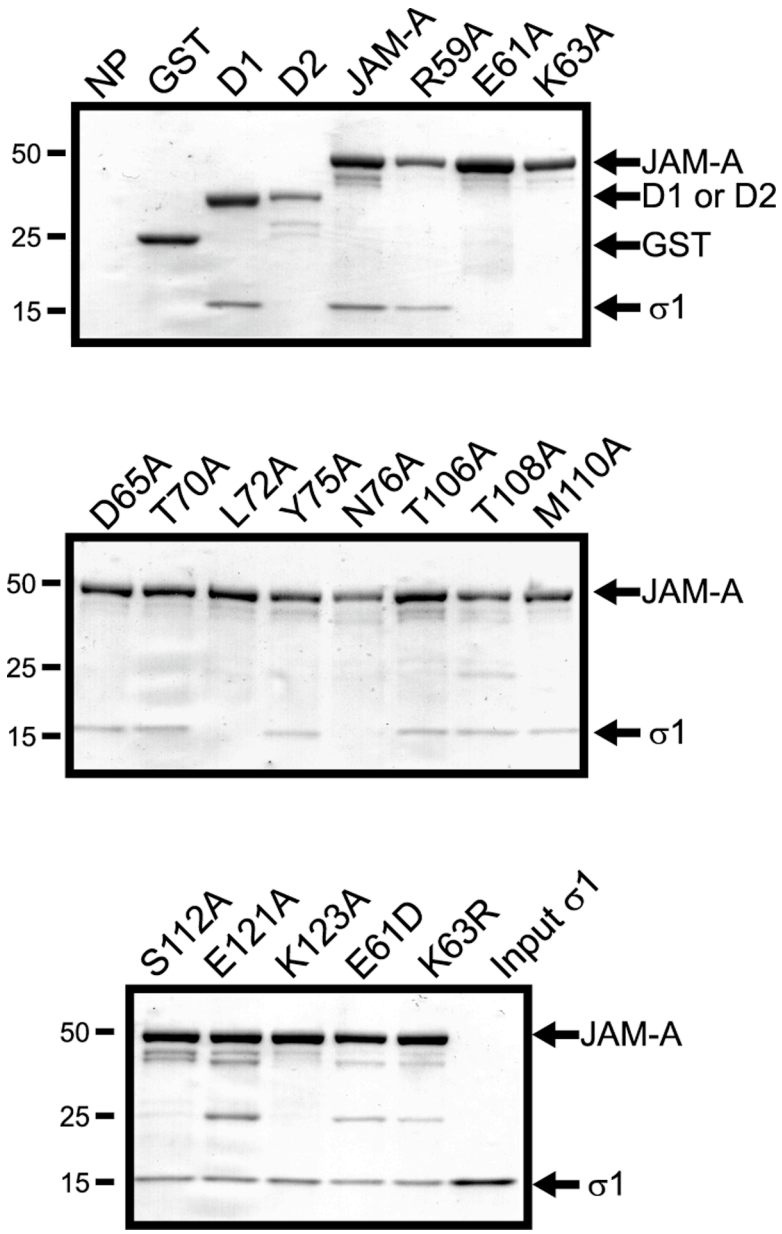

FIGURE III-3. Precipitation of σ1H with purified GST-JAM-A point mutants. Glutathione agarose was incubated with buffer alone (NP), GST, or GST fused to the JAM-A D1, D2, entire extracellular domain (JAM-A), or point mutants shown at 4°C for 1 h. The glutathione agarose was pelleted, washed, and incubated with purified T3D σ1H at 4°C for an additional 1 h. The glutathione agarose was washed, pelleted, resuspended in SDS sample buffer, and boiled. Samples were resolved by SDS-PAGE and stained with Coomassie brilliant blue to visualize captured proteins. Input T3D σ1H also was resolved following boiling in SDS sample buffer. Molecular weights of protein standards in kDa are indicated on the left. Proteins are labeled on the right

JAM-A dimer interface. The second group of GST-JAM-A mutants (II) exhibited faster association kinetics than wild-type JAM-A by ~ 5-10 fold, resulting in higher calculated affinities for σ1 than wild-type JAM-A (Figure III-4B and Table III-2). Upon injection of wash buffer, much of the σ1H was removed from these mutants. However, specifically bound σ1H protein exhibited a similar off-rate to wild-type GST-JAM-A. Group II includes mutants T108A, M110A, and E121A. Thr108, Met110, and Glu121 are located within the dimer interface in proximity to one another on β-strands F and G (Figure III-1C). Glu121 participates in salt-bridge interactions that stabilize the dimer interface. Met110 participates in hydrophobic interactions with an apposing JAM-A monomer. The third group (III) includes GST-JAM-A mutants R59A, Y75A, and N76A (Figure III-4C and Table III-2), which exhibited a faster σ1H on-rate than wild-type JAM-A but also a faster off-rate, resulting in affinities similar to wild-type. The N76A mutant exhibited a slower on-rate and a lower level of σ1 binding, relative to the other mutants in this group, and binding returned to baseline levels after several minutes of wash buffer injection. This result agrees with results obtained in the GST precipitation assay, in which the N76A mutant of JAM-A was incapable of capturing σ1H domain (Figure III-3). Arg59, Tyr75, and Asn76 are located near the "top" of the dimer interface, in proximity to residues Glu61, Lys63, and Leu72 (Fig. III-1C). The final group of JAM-A point mutants includes E61A, K63A, and L72A (Figure III-4D), which showed very low levels of σ1H binding above background. Upon injection of wash buffer, the binding signal returned to baseline level immediately, indicating that the observed binding was not specific for any of the mutants. I also was unable to find suitable binding models for the interaction of these mutants with σ1H using

BIAevaluation software (data not shown). These results are in accord with results obtained using GST precipitation assays, in which no σ1H was bound detectably by the E61A, K63A, or L72A GST-JAM-A point mutants. These data reinforce the importance of Glu61, Lys63, and Leu72 as mediators of σ1-JAM-A interactions and suggest that these residues serve as contact points for the σ1 head.

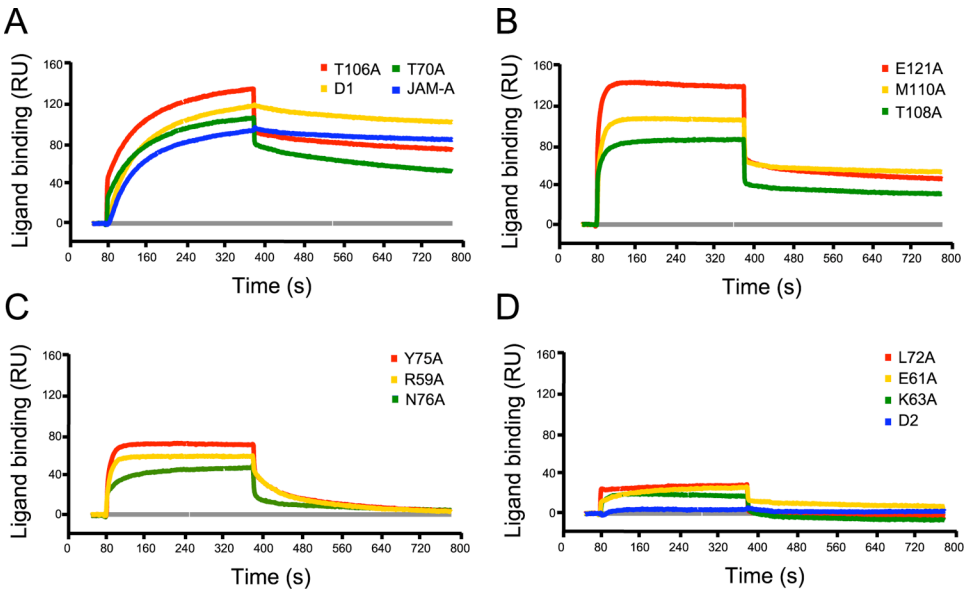

FIGURE III-4. Binding of σ1H to GST-JAM-A point mutants. Purified σ1H, at a concentration of 167 nM, was injected for 5 min across a biosensor surface on which GST-JAM-A fusion proteins, as indicated, had been captured. Buffer alone was injected for 6.7 min. The resultant traces show binding to GST-JAM-A and GST-JAM-A point mutants, as indicated. The resultant sensograms are grouped based on binding kinetics: (A) k_{on} and k_{off} similar to wild-type JAM-A, (B) faster k_{on} than wild-type JAM-A, (C) faster k_{on} and k_{off} than wild-type, and (D) no specific binding. The baseline is 167 nM σ1H binding to GST (grey). Binding is expressed in resonance units (RU).

Oligomeric state of JAM-A point mutants - Since two residues that participate in salt-bridge interactions at the JAM-A dimer interface are required for efficient σ1 binding, I questioned whether mutation of these residues or other residues in the dimer interface alters the capacity of JAM-A to form dimers. To answer this question, the extracellular

TABLE III-2. Kinetics of σ1H binding to GST-JAM-A point mutants [a]

Group	*JAM-A Mutant*	*Association rate (1/Ms)*	*Dissociation rate (1/s)*	*Dissociation constant (M)*
I	Wild-type	8.9×10^{4}	2.5×10^{-4}	2.8×10^{-9}
	D1	8.9×10^{4}	3.1×10^{-4}	3.5×10^{-9}
	T70A	7.1×10^{4}	9.9×10^{-4}	1.4×10^{-8}
	T106A	7.8×10^{4}	4.5×10^{-4}	5.8×10^{-9}
II	T108A	4.1×10^{5}	6.1×10^{-4}	1.5×10^{-9}
	M110A	6.5×10^{5}	3.5×10^{-4}	5.4×10^{-10}
	E121A	5.7×10^{5}	8.5×10^{-4}	1.5×10^{-9}
III	R59A	3.8×10^{5}	8.4×10^{-3}	2.2×10^{-8}
	Y75A	5.0×10^{5}	7.0×10^{-3}	1.4×10^{-8}
	N76A	7.3×10^{4}	3.5×10^{-3}	4.7×10^{-8}

[a] Association and dissociation rates and dissociation constants were calculated using BIAevaluation 3.0 software. Mutants are grouped as in Figure III-4. Group IV mutants did not display specific binding.

domains of wild-type JAM-A and selected JAM-A point mutants were released from the GST tag by thrombin cleavage and resolved using gel-filtration chromatography. The extracellular domain of wild-type JAM-A eluted as a single peak, with an apparent molecular weight of ~ 48 kDa, indicating that it forms a dimer (Table III-3 and data not shown) (122). Likewise, alanine substitutions of Ser112 and Lys123, which do not participate in intersubunit contacts, do not alter the apparent oligomeric state of JAM-A (Table III-3). In sharp contrast, JAM-A extracellular domains with alanine substitutions of Arg59, Glu61, Lys63, or Glu121, which form salt bridges across the dimer interface, or Tyr75, which forms a hydrogen bond with Glu114 from an apposing monomer, eluted from the column as a single species with an apparent molecular weight of ~ 30 kDa. This elution peak likely represents solely monomeric JAM-A, with a slightly exaggerated

apparent molecular weight due to its elongated shape. These data indicate that each salt-bridge pair and Tyr75 individually is required for stability of JAM-A dimers.

TABLE III-3. Characterization of JAM-A point mutants by gel filtration [a]

JAM-A Mutant	*Apparent MW (kDa)*	*Apparent Oligomeric State*	*σ1 Binding*
Wild-type	46.1	dimeric	+
R59A	32.5	monomeric	+
E61A	32.5	monomeric	-
K63A	33.8	monomeric	-
Y75A	27.8	monomeric	+
S112A	49.8	dimeric	+
E121A	30.0	monomeric	+
K123A	46.1	dimeric	+

[a] Apparent molecular weights were calculated by graphing V_e-V_o against the $\log_{10}$ MW of protein standards, performing linear regression, and back-calculating, based on elution time.

To determine whether σ1 engages monomeric or dimeric forms of the JAM-A extracellular domain, we assessed binding of σ1H to the JAM-A extracellular domain in solution using gel filtration chromatography. Incubation of purified wild-type JAM-A and σ1H in a 3:1 molar ratio (three JAM-A monomers to one σ1 trimer), results in formation of a higher molecular weight complex that contains both JAM-A and σ1H (Figure III-5A and data not shown). Similar findings were made following incubation of the extracellular domain of dimeric JAM-A mutant S112A or the monomeric mutant E121A with σ1H (Figure III-5). In both cases, a complex was formed that eluted from the size-exclusion column at the same time as the complex observed following incubation of wild-type JAM-A with σ1H. As expected, monomeric JAM-A point mutant E61A does not form a detectable complex when incubated with σ1H (Figure III-5D). Since

mutant forms of JAM-A that are incapable of forming dimers retain the capacity to interact with σ1H, we conclude that σ1 engages monomeric forms of JAM-A.

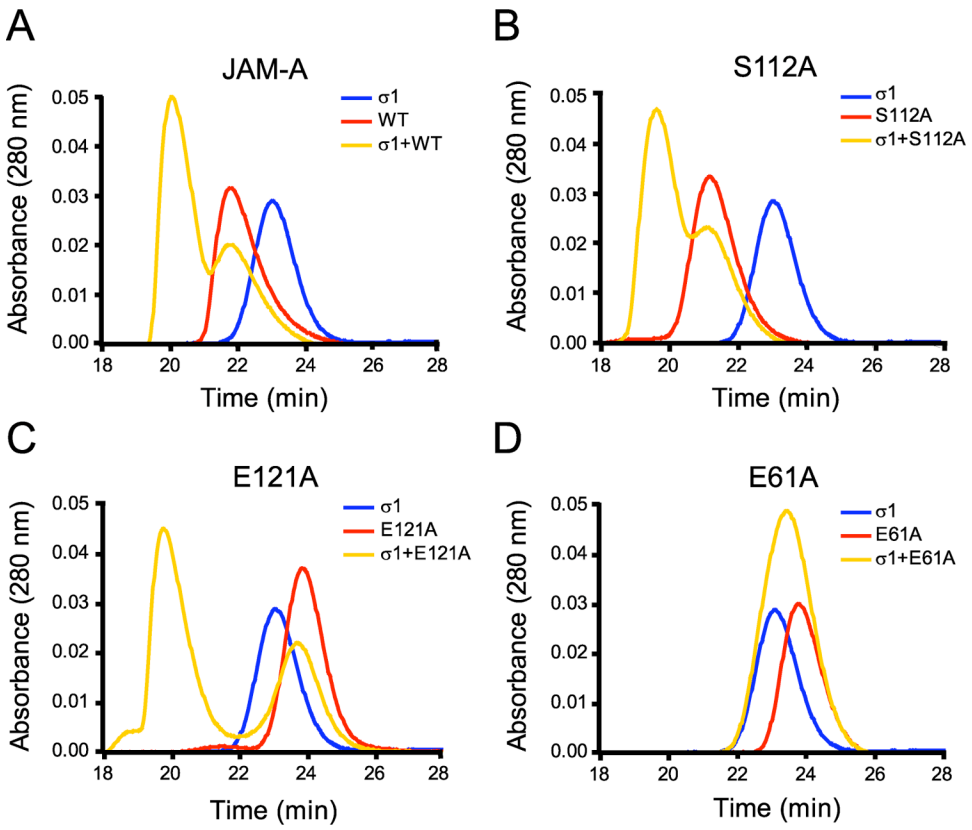

FIGURE III-5. Characterization of σ1H-JAM-A extracellular domain mixtures using gel filtration chromatography. Purified T3D σ1H and wild-type JAM-A (A) or JAM-A point mutants S112A (B), E121A (C), and E61A (D) were mixed in a 3:1 molar ratio and incubated on ice for 40 min. The mixtures (yellow) or individual purified proteins (red and blue) were applied to a Superdex 75 gel-filtration column, and proteins in the column fractions were detected by A_{280}. Dimeric forms of wild-type JAM-A and S112A elute earlier than monomeric forms E121A and E61A. Wild-type JAM-A, S112A, and E121A each form a complex with σ1 that elutes from the column at approximately the same time, thus with similar apparent molecular weight, for each protein mixture.

Reovirus binding and infectivity of CHO cells expressing mutant forms of JAM-A - In the context of a virion, multiple copies of σ1 likely engage JAM-A simultaneously. Thus, at the cell surface, viral avidity might alter the capacity of reoviruses to bind JAM-A or

JAM-A mutants. To assess the capacity of reovirus to bind JAM-A mutants in cell culture, I transiently transfected CHO cells, which are poorly permissive for reovirus infection (20, 52), with plasmids encoding wild-type (122) or mutant forms of full-length JAM-A. Transfected cells were incubated for 24 h to allow receptor expression and adsorbed with reovirus virions. Surface expression of JAM-A and reovirus binding were assessed by flow cytometry (Figure III-6). Wild-type JAM-A and each of the JAM-A mutants were expressed at the surface of transfected cells to approximately equivalent levels, providing confidence that the mutant constructs are properly folded. In agreement with previous studies (20, 52), JAM-A is not detectably expressed on the surface of CHO cells transfected with empty vector. Virions of T3SA-, a non-sialic acid-binding reovirus strain with a serotype 3 σ1 identical in sequence to T3D in the σ1 head domain (5), bound poorly to vector-transfected CHO cells. However, I observed specific binding to CHO cells expressing wild-type JAM-A. T3SA- binding approximated JAM-A expression at the surface of CHO cells expressing the majority of the point mutants. However, T3SA- binding to cells expressing the K63A or L72A mutants was diminished, and no binding above background was observed to cells expressing the E61A mutant form of JAM-A. These results closely mimic the binding of T3D σ1H to JAM-A mutants in the GST precipitation and SPR assays (Figures III-3 and III-4). Interestingly, mutation of Glu61 to aspartate or Lys63 to arginine was not associated with the binding defects observed for the E61A and K63A mutants (Figure III-6), indicating that the acidic or basic properties of these residues are important for reovirus engagement.

To compare JAM-A binding determinants for reoviruses of the three serotypes, I used flow cytometry to assess binding of virions of strains T1L and T2J to CHO cells

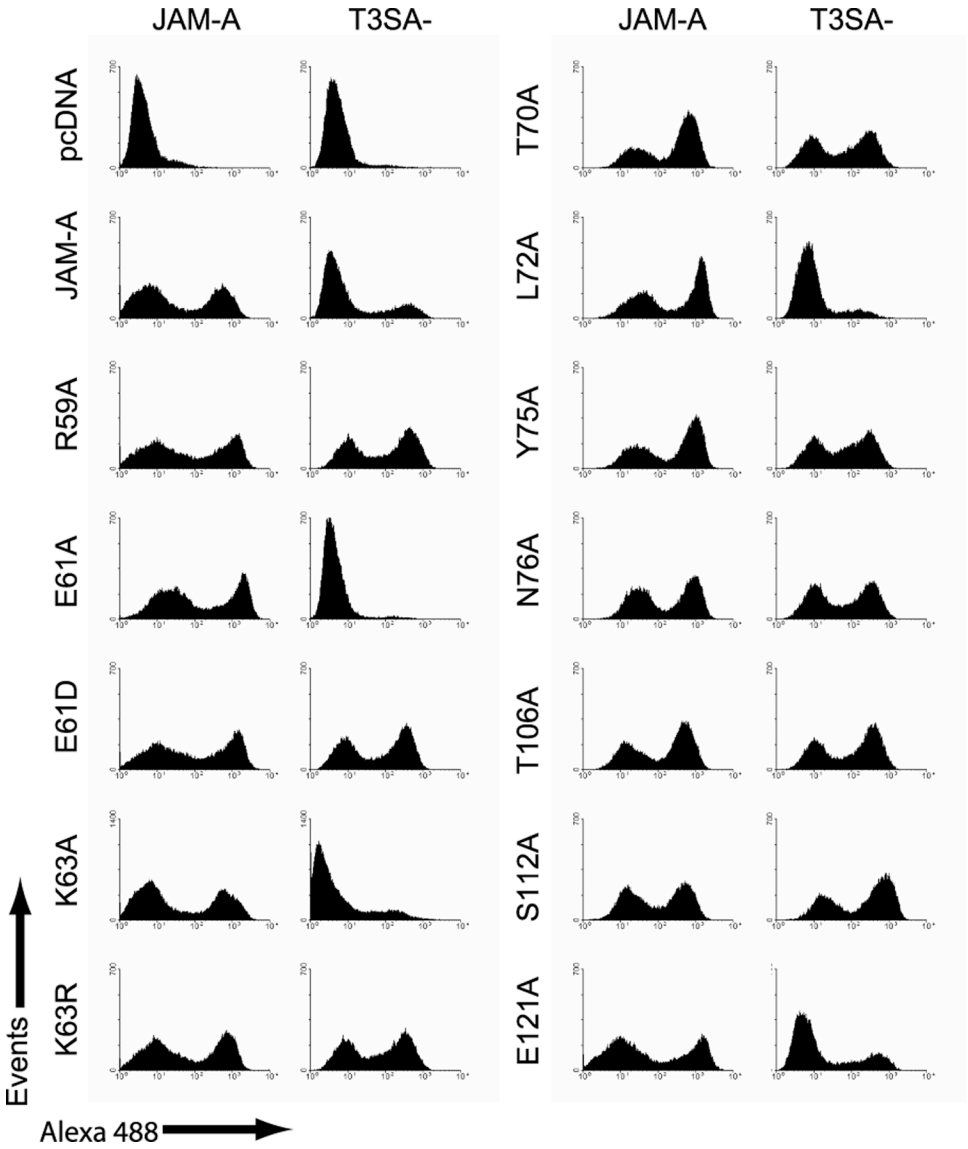

FIGURE III-6. Reovirus T3SA- binding to CHO cells expressing JAM-A mutants. CHO cells (10^6) were transiently transfected with plasmids encoding the indicated receptor constructs. Following incubation for 24 h to permit receptor expression, cells were lifted from plates using EDTA and stained with hJAM-A-specific mAb J10.4 or adsorbed with reovirus T3SA- (10^5 particles/cell). Cell-surface expression of receptor constructs and virus binding was assessed by flow cytometry.

expressing wild-type and mutant forms of JAM-A. Similar to T3SA-, each virus bound poorly to vector-transfected cells, whereas T1L and T2J binding to cells expressing wild-type JAM-A approximated levels of JAM-A expression (Figure III-7). Interestingly, more events were observed for T1L and T2J binding to CHO cells expressing JAM-A than for T3SA-, although the same number of reovirus particles was used in each case. In contrast to T3SA-, T1L and T2J bound equivalently to CHO cells expressing wild-type and mutant forms of JAM-A (data not shown). To determine whether T1L and T2J might share similar binding determinants with T3D and T3SA- but with less stringency, I constructed double point mutants R59A/E61A and E61A/K63A. As anticipated, T3SA- showed no specific binding to CHO cells expressing either of the JAM-A double point mutants (Figure III-7). Although not with the same magnitude as T3SA-, both T1L and T2J showed diminished binding to CHO cells expressing the double point mutants, with T1L exhibiting highly impaired binding to CHO cells expressing the R59A/E61A JAM-A mutant.

To assess the functional significance of mutations in JAM-A that alter reovirus binding, I quantified infectivity of T1L, T2J, and T3SA- following adsorption to CHO cells expressing full-length wild-type or mutant forms of JAM-A by indirect immunofluorescence (5). Infectivity of T3SA- was significantly decreased (~ 50%) following infection of CHO cells expressing the E61A and K63A mutants in comparison to cells expressing wild-type JAM-A (Figure III-8). Consistent with the flow cytometry experiments, conservation of charge at residues Glu61 and Lys63 by substituting aspartate and arginine, respectively, rescued the infectivity defect. T3SA- infectivity was decreased almost to the level of background following adsorption to CHO cells

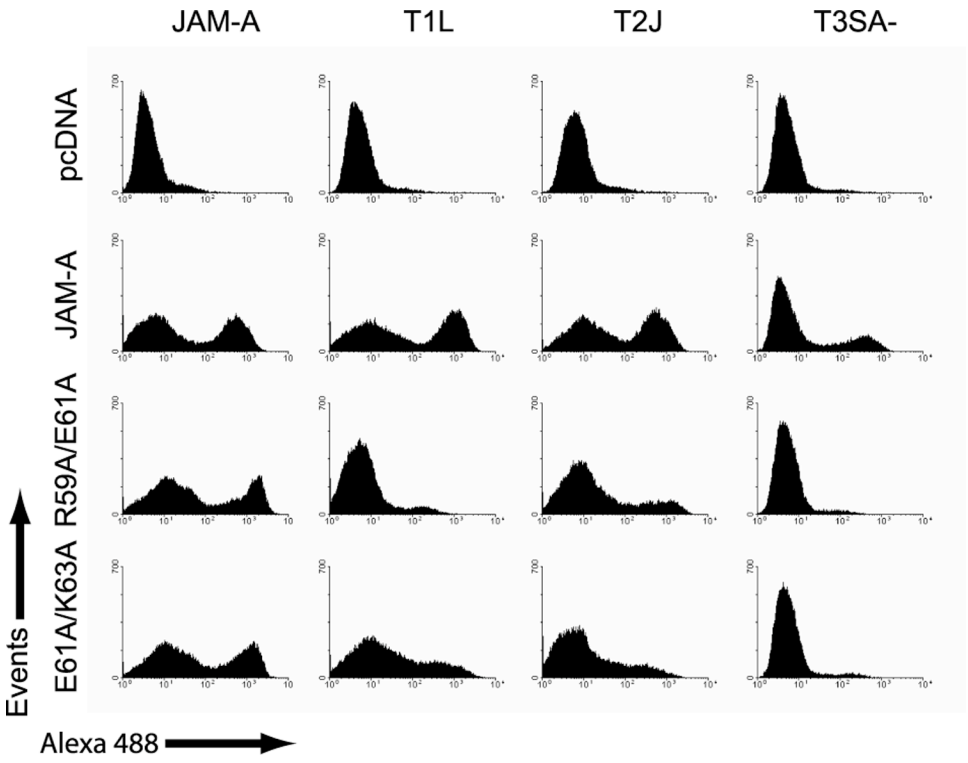

FIGURE III-7. Reovirus T1L, T2J, and T3SA- binding to CHO cells expressing JAM-A mutants. CHO cells (10^6) were transiently transfected with plasmids encoding the indicated receptor constructs. Following incubation for 24 h to permit receptor expression, cells were lifted from plates using EDTA and stained with hJAM-A-specific mAb J10.4 or adsorbed with reovirus T1L, T2J, or T3SA- (10^5 particles/cell). Cell-surface expression of receptor constructs and virus binding was assessed by flow cytometry.

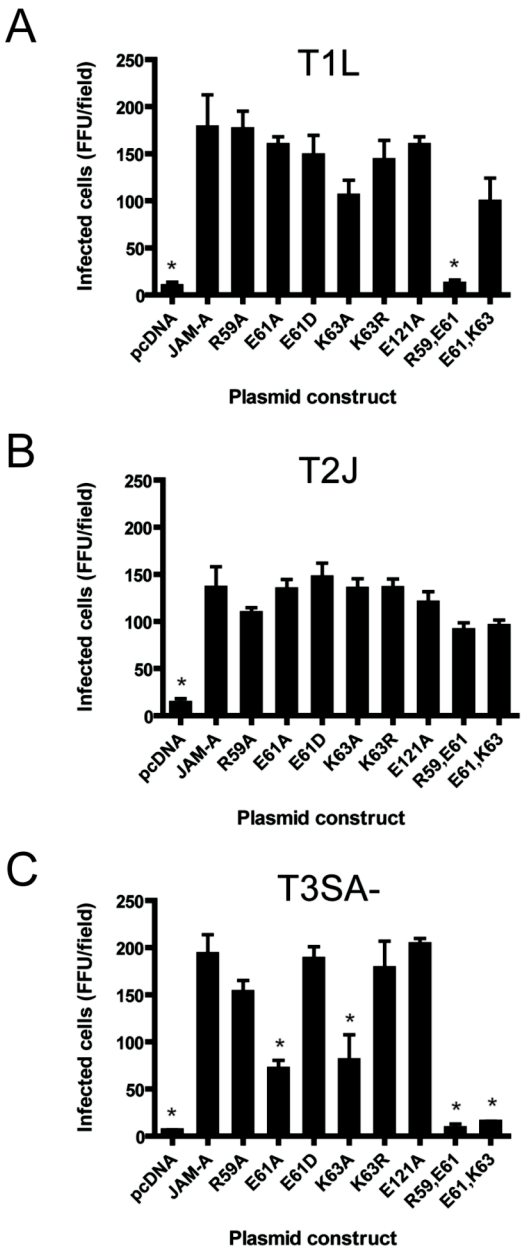

FIGURE III-8. Reovirus infection of CHO cells expressing JAM-A mutants. CHO cells (2 x 10^5) were transiently transfected with empty vector (pcDNA) or plasmids encoding wild-type or mutant forms of JAM-A. Following incubation for 24 h to permit receptor expression, cells were adsorbed with reovirus at a multiplicity of infection of (A) 1 (T1L), (B) 5 (T2J), or (C) 10 (T3SA-) pfu/cell at room temperature for 1 h. Cells were washed with PBS, incubated in complete medium at 37°C for 20 h, and stained for reovirus antigen. Infected cells were identified by indirect immunofluorescence and quantified by counting cells exhibiting cytoplasmic staining in three confluent fields of view per experiment. The results are expressed as the mean fluorescent focus units (FFU) per field of view for triplicate experiments. Error bars indicate S. D. *, $P < 0.05$ in comparison to cells expressing wild-type JAM-A.

expressing the double point mutants R59A/E61A and E61A/K63A. As predicted by the binding results, T1L also showed a striking loss of infectivity in cells expressing the R59A/E61A JAM-A mutant and a slight decrease in infectivity in cells expressing the K63A or E61A/K63A mutant. T2J showed only a very modest decrease in infectivity, less than 25%, in CHO cells expressing the R59A mutant or either of the double point mutants, in accordance with the flow cytometry results. Taken together, these data confirm results obtained from binding assays using the T3D σ1 head domain and suggest that T1L, T2J, and T3SA- engage JAM-A using different residues or at distinct sites.

Reovirus virions binding to GST-JAM-A point mutants - The tethering of reovirus to the CHO cell surface might involve interactions with molecules other than JAM-A, such as carbohydrates or integrins. To assess interactions of virions of the three reovirus serotypes with JAM-A in a more simplified system, I captured GST-JAM-A or select GST-JAM-A salt-bridge mutants on a biosensor surface and measured the binding of purified T1L, T2J, and T3SA- virions using SPR. Virions of all three serotypes demonstrated specific binding to JAM-A but not GST (Figure III-9 and data not shown), with T1L and T2J showing greater maximal binding than T3SA-. Interestingly, all three viruses showed enhanced binding to the E121A mutant in comparison to wild-type JAM-A (Figure III-9). While none of the viruses bound the GST-JAM-A E61A or K63A mutants, only T2J bound the R59A mutant. These SPR results were surprising, given that neither T1L nor T2J demonstrated impaired binding or infectivity in CHO cells expressing any single point mutant of JAM-A and that the T3D σ1 head showed a moderate affinity for R59A in multiple assays. Taken together, these finding suggest that

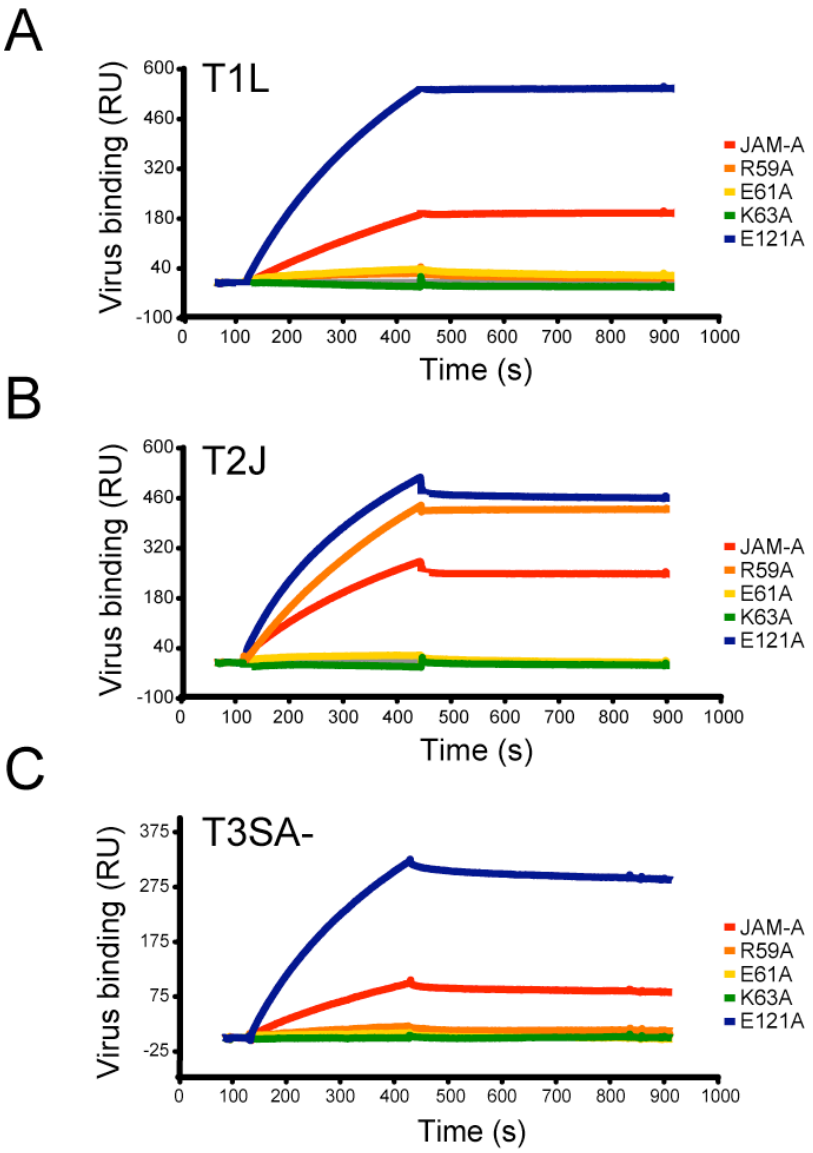

FIGURE III-9. Binding of reovirus virions to GST-JAM-A point mutants. Purified reovirus virions of (A) T1L, (B) T2J, or (C) T3SA-, at a concentration of 5 x 10^{12}/ml, were injected for 5 min across a biosensor surface on which GST-JAM-A fusion proteins had been captured. Buffer alone was injected for 10 min. The resultant traces show binding to GST-JAM-A and GST-JAM-A point mutants, as indicated. The baseline is virus binding to GST (grey). Binding is expressed in resonance units (RU).

serotype 1, 2, and 3 reoviruses engage JAM-A via an overlapping, but not necessarily identical, binding site and that interactions with JAM-A are not the sole determinants of reovirus binding and infectivity of CHO cells.

Discussion

T3D σ1H binding determinants in JAM-A - Recognition of cellular receptors by viruses is a key determinant of target cell selection and disease pathogenesis in infected host organisms. Reoviruses of different serotypes display distinct tropism and illness outcomes in newborn mice. These viruses bind to several receptors on the target cell surface, including sialic acid for serotype 3 reoviruses (40) and JAM-A for all serotypes (6). However, the contributions of individual receptors to end-organ disease are incompletely understood. The goal of experiments performed in this study was to identify reovirus binding determinants in JAM-A. Using a combination of GST precipitation, SPR, gel filtration, flow cytometry, and fluorescent focus assays, I identified three residues in JAM-A that are strictly required and three additional residues that contribute to serotype 3 reovirus binding and infectivity. These residues are located at the top of and within the JAM-A dimer interface in β-strands C, C', and the C'- C" loop, suggesting that reovirus attachment protein σ1 engages monomeric forms of JAM-A.

I generated alanine substitutions of residues with solvent-exposed side chains in the JAM-A dimer interface in the context of a GST-JAM-A fusion protein. Analysis of the point mutants using GST precipitation assays led to the identification of Glu61, Lys63, Leu72, and Asn76 that individually are required for efficient binding of T3D

σ1H. Glu61 and Lys63 have charged side chains and participate in salt-bridge contacts that stabilize the JAM-A dimer interface. Leu72 and Asn76 are located in proximity to Glu61 and Lys63, and Leu72 participates in hydrophobic interactions with Tyr119 from an apposing JAM-A monomer. SPR findings were concordant with GST precipitation results and indicate that mutation of specific residues in the JAM-A dimer interface can enhance or diminish the rate of association and dissociation of T3D σ1H. Specifically, M110A, T108A, and E121A mutations enhanced association of σ1, leading to higher calculated binding affinities in comparison to wild-type JAM-A. On the other hand, R59A and Y75A displayed faster association with σ1H, but also faster dissociation, resulting in an affinity similar to wild-type. Charged residues required for JAM-A-σ1 interactions in biochemical assays, Glu61 and Lys63, also are required for the binding of intact serotype 3 reovirus virions to JAM-A in cultured cells and on a biosensor surface.

Model of reovirus-JAM-A interactions - Gel filtration chromatography of purified, mutant JAM-A extracellular domains revealed that mutation to alanine of any residue in the JAM-A dimer interface that contributes to salt-bridge interactions as well as one residue, Tyr75, which makes a hydrogen-bond contact with Glu114, abolishes the capacity of JAM-A to form dimers in solution at neutral pH. These data indicate that each salt-bridge interaction and the Tyr75-Glu114 hydrogen-bond interaction are essential mediators of JAM-A dimer formation. Both monomeric and dimeric point mutants of JAM-A are capable of binding σ1H, suggesting that a monomeric form of JAM-A is the relevant σ1 binding partner. Based on elution profiles, it is formally possible that the σ1-JAM-A complex contains dimeric JAM-A and monomeric σ1. However, we think it

unlikely that dimeric JAM-A is in the complexes, since the monomeric E121A mutant of JAM-A forms complexes with σ1 that are indistinguishable by gel filtration from wild-type complexes. It also is unlikely that monomeric σ1 interacts with JAM-A, given that a σ1 point mutant that is incapable of trimer formation, σ1H-Y313A, is incapable of JAM-A binding (131).

Our data support a model of reovirus-JAM-A interactions in which the T3D σ1 head domain interacts with residues near the top of the dimer interface, such as Arg59, Tyr75, and Asn76, followed by higher-affinity interactions with residues within the dimer interface of JAM-A monomers, primarily Glu61 and Lys63 in β-strand C and Leu72 in β-strand C' (Figure III-10). In this model, σ1 is anticipated to bind with high affinity only to JAM-A monomers. How might σ1 access monomeric forms of JAM-A? Comparisons of the hJAM-A and murine (m)JAM-A crystal structures suggest that small movements of one JAM-A monomer with respect to the apposing monomer occur in a physiologic context (122). Such movements might provide σ1 the opportunity to interact with residues closer to the solvent-exposed regions of the JAM-A dimer interface, such as Arg59, Tyr75, and Asn76, as the dimer shifts slightly to a more open conformation. This interaction could potentially orient σ1 to access the dimer interface, where interactions that lead to high-affinity binding occur. In support of this model, mutation of Arg59, Tyr75, or Asn76 to alanine leads to reduced levels of binding and faster association and dissociation kinetics between JAM-A and the σ1H, whereas mutation of Glu61, Lys63, or Leu72 to alanine ablates binding altogether.

It is possible that the variably impaired binding observed for mutants with alterations of residues Arg59, Tyr75, or Asn76 is simply a result of the proximity of these

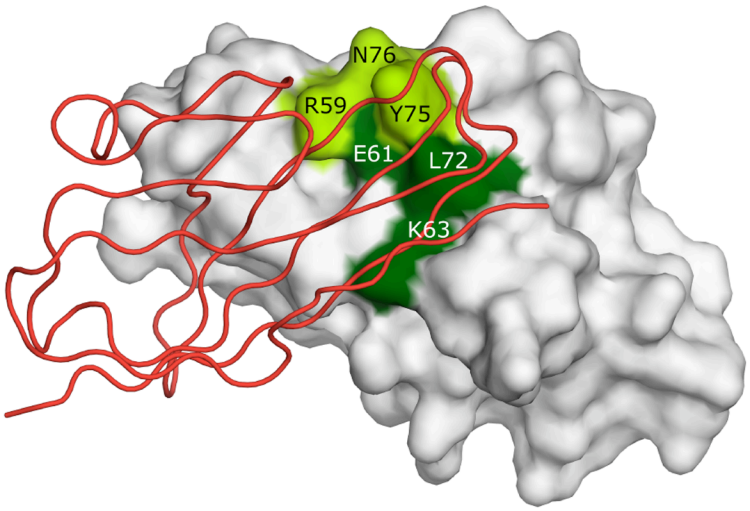

FIGURE III-10. Predicted serotype 3 binding region in JAM-A. View of the JAM-A D1 domain dimer. One monomer is oriented as in Figure III-1C and is shown as a space-filling representation. The apposing monomer is shown as a red ribbon drawing. Residues Glu61, Lys63, and Leu72 (dark green) are required for efficient serotype 3 reovirus engagement of JAM-A and are proposed to serve as critical contacts for T3D σ1. Residues Arg59, Tyr75, and Asn76 (light green) are proposed to serve as additional contacts.

amino acids to critical contact residues Glu61, Lys63, and Leu72. However, mutation of residues Thr108, Met110, and Glu121, which also are located in proximity to the proposed high-affinity contact residues, leads to faster association without diminishment of dissociation, resulting in overall higher affinity of σ1 for JAM-A. Mutation of Arg59, Tyr75, or Glu121 disrupts dimer formation. Based on these data, I predict that mutation of Thr108 or Met110 also would alter JAM-A dimer contacts to some degree, permitting σ1 to access the dimer interface more quickly. Faster access to the dimer interface might explain the enhanced σ1H association rates observed for all JAM-A mutants of residues with side chains proximal to required residues Glu61, Lys63, and Leu72. However, enhanced access to the dimer interface fails to explain the faster σ1H off-rate observed with the R59A, Y75A, and N76A mutants. Rather, the enhanced dissociation kinetics

observed for these mutants suggest a more direct, role in reovirus binding for Arg59, Tyr75, and Asn76. The incapacity of T3SA- virions to bind the R59A mutant lends further support to the contention that Arg59 serves as a direct contact point for serotype 3 σ1.

Reovirus specificity among JAM family members - It is noteworthy that the four salt-bridge-forming residues in the JAM-A dimer interface, Arg59, Glu61, Lys63, and Glu121, are conserved among mJAM-A and hJAM-A, hJAM-B, and hJAM-C. However, of these proteins, only hJAM-A and mJAM-A mediate reovirus infection of non-permissive cells (6, 20). This observation suggests that charged residues Glu61 and Lys63 are necessary, but not sufficient, for efficient serotype 3 reovirus binding. The molecular context of these residues also must contribute to efficient σ1 binding. In support of this idea, Leu72 and Asn76 are conserved between mJAM-A and hJAM-A but not hJAM-B and hJAM-C.

Serotype-specific differences - Our binding and infectivity data from CHO cells transfected with JAM-A mutants and SPR data using virions highlight differences in attachment among the reovirus serotypes. All of the viruses exhibited enhanced binding to the E121A mutant in comparison to wild-type JAM-A, likely because Glu121 lies outside of the binding site for all of the viruses and its mutation enhances access to the dimer interface by ablating dimer formation. In SPR studies of T1L and T3SA-, residues Arg59, Glu61, and Lys63 individually are required for reovirus binding. Thus, it appears that T1L utilizes a binding site that is similar to the serotype 3 binding site. However, for

JAM-A expressed on CHO cells, a requirement for residues Arg59 and Glu61 for efficient T1L binding and infectivity is apparent only when both residues are mutated simultaneously, while a small infectivity diminishment is observed when Lys63 is altered. In contrast, binding and infectivity of JAM-A-expressing CHO cells by reovirus strain T3SA- individually requires residues Glu61 or Lys63, with some additional contribution from Arg59. Based on results from studies using CHO cells expressing JAM-A mutants, it does not appear that T2J shares contact points with serotype 1 or 3 reoviruses. T2J shows a slight decrease in binding to CHO cells transfected with JAM-A double point mutants R59A/E61A and E61A/K63A, but infectivity was not significantly diminished in these cells. Yet in SPR experiments, T2J virions demonstrated a clear requirement for Glu61 and Lys63, but not Arg59, suggesting that the serotype 2 binding site in JAM-A overlaps, but is not identical, with the serotype 1 and 3 binding sites. These findings constitute the first evidence that different serotypes of reovirus engage JAM-A via different contact residues.

Why are individual point mutations sufficient to render virions of all serotypes incapable of binding to JAM-A on a biosensor surface but not to strongly affect interactions of T1L and T2J with JAM-A at the surface of a CHO cell? I envision three potential contributing factors. First, interactions with molecules other than JAM-A on CHO cells might mask JAM-A binding deficiencies. Reoviruses, including T1L and T2J, are capable of agglutinating human erythrocytes (88), suggesting that they bind carbohydrates. While T3SA- σ1 encodes a polymorphism that ablates sialic acid binding, T1L and T2J retain native carbohydrate-binding capacity. Since reoviruses employ an adhesion-strengthening mechanism of cell attachment (5), initial engagement of

carbohydrate prior to adhering tightly to JAM-A may confer an attachment advantage to T1L and T2J over T3SA-. Carbohydrate binding could tether T1L and T2J virions to the CHO cell surface, enabling them to diffuse laterally to bind JAM-A or JAM-A point mutants and integrins. If a single point mutation in JAM-A only modestly diminished the binding affinity of σ1, which would be expected if the binding surface is sufficiently large, then avidity effects might still permit stable cell attachment. However, in the case of T3SA-, the virus would not be tethered to the cell and therefore must have a high affinity for JAM-A to achieve stable cell attachment. Thus, engagement of carbohydrates or other unidentified low-affinity receptors on the CHO cell surface might mask defects in reovirus-JAM-A interactions in binding and infectivity studies. Second, binding defects may be exaggerated in SPR experiments, in which conditions at the biosensor surface may diminish avidity effects. For example, the rigidity of the surface may prevent virions from simultaneously engaging as many JAM-A molecules as might be bound in the fluid membrane of a CHO cell. Furthermore, for my experiments, JAM-A was captured on the biosensor surface via an N-terminal GST tag. The physical positioning of the D1 domain between an N-terminal GST tag and the C-terminal D2 domain might sterically hinder virus access to the binding surface, thereby diminishing virus binding to JAM-A on the biosensor chip versus properly-oriented, untagged JAM-A molecules expressed on CHO cells. Third, serotype 1 and 2 σ1 might bind to JAM-A with higher affinity than serotype 3 σ1. This idea is supported by my SPR data with virions, in which additional receptors play no role, yet binding to JAM-A by T1L and T2J is enhanced in comparison to T3SA-. On the CHO cell surface, enhanced avidity for JAM-A might compensate for individual point mutations, leading to smaller changes in

binding and infectivity in our assays. Of note, differences in affinity for the primary cellular receptor α-dystroglycan have been shown to mediate strain-specific differences in tropism for lymphocytic choriomeningitis virus (135). It is possible that a similar mechanism plays a role in serotype-dependent differences in reovirus pathogenesis.

In this study, I identified reovirus binding determinants in the most membrane-distal Ig-like domain of JAM-A and provided evidence that σ1 engages monomeric forms of JAM-A. I also provided the first evidence that reoviruses of different serotypes engage JAM-A via non-identical binding sites or with different affinities. Thus, although all serotypes of reovirus can utilize JAM-A as a receptor, JAM-A binding may still contribute to differential pathogenesis outcomes *in vivo* among the serotypes. This work has established a foundation for future studies aimed at understanding the roles of reovirus-receptor interactions in pathogenesis.

CHAPTER IV

CRYSTAL STRUCTURE OF THE HEAD DOMAIN OF MAMMALIAN REOVIRUS σ1 BOUND TO JUNCTIONAL ADHESION MOLECULE-A

Introduction

Our studies have indicated that the D1 domain of JAM-A is both necessary and sufficient to mediate interactions with reovirus (52, 65) and identified residues in the surface of JAM-A D1 that mediates dimer formation required for these interactions (52, 65, 122). However, the precise nature of σ1-JAM-A interactions and the mechanism by which σ1 gains access to this surface are unknown. To define the structural basis of σ1-JAM-A interactions, we crystallized a complex of the head domain of T3D σ1 and the D1 Ig-like domain of human JAM-A and determined its structure at 3.2 Å resolution. We used plasmid-based reverse genetics to engineer reoviruses expressing mutant forms of σ1 to determine the contributions of specific residues that contact JAM-A. These studies reveal the biochemical basis of σ1-JAM-A interactions and provide clues about how σ1 successfully engages the JAM-A dimer interface.

This study was peformed in collaboration with Eva Kirchner in Dr. Thilo Stehle's laboratory (Universitat Tübingen). I would like to acknowledge Eva for the purification and crystallization of complexes between the reovirus σ1 head and the JAM-A D1 domain and cryopreservation of the crystals. I assisted Eva in the collection of diffraction data and the earliest stages of structure determination. Eva completed the structure determination and refinement steps, performed gel filtration experiments, and prepared the figures showing structures of σ1 and JAM-A presented in this chapter. I

generated, purified, and characterized all reoviruses containing mutations in the JAM-A binding region of σ1 using assays of viral binding, including SPR and flow cytometry, and infectivity, including time courses of infection and plaque assays.

Results

Complex formation and crystallization – The T3D σ1 head domain (σ1H; residues 293-455) and the D1 domain of human JAM-A (D1; residues 28-129) were purified using GST-affinity purification (65, 131). In each case, domain boundaries were chosen to eliminate regions of known flexibility (30, 122) and retain binding capacity (65, 122, 131). After removal of GST, the sequence of each protein was identical to the native sequence with the exception of two amino acids at the N-terminus: Gly291 and Ser292 for σ1H and Gly26 and Ser27 for D1. None of these amino acids contribute to complex formation. As gel filtration studies indicated that one σ1H trimer binds up to three D1 monomers (data not shown), purified proteins were mixed with an excess of D1. Following incubation, σ1H-D1 complexes were separated from excess D1 by gel filtration.

During screening and optimization of crystallization conditions, only a single crystal form was obtained. SDS-PAGE analysis indicated that the crystals contained both σ1H and D1 (data not shown). Diffraction data were collected at the Swiss Light Source (Villigen, Switzerland) using several crystals. The structure was determined by molecular replacement using the previously determined structures of σ1H (131) and the D1 domain of JAM-A (122) and refined to 3.2 Å resolution (Table IV-1). Two residues of σ1H, Asp345 and His388, are found in the generously allowed and disallowed regions

of the Ramachandran plot, respectively. Both residues have similar conformations in the high-resolution crystal structure of unliganded σ1H (131). The crystallographic asymmetric unit consists of two σ1H trimers, each bound to three D1 monomers. The presence of six independent copies enabled us to carry out non-crystallographic averaging and refinement using non-crystallographic symmetry restraints, both of which helped to establish a high-quality model.

TABLE IV-1. Data collection and refinement statistics for the σ1H-JAM-A complex

Diffraction data[a]	
Space group	$P2_12_12$
Unit cell dimensions (Å)	a = 105.7, b = 123.8, c = 131.0
Resolution range (Å)	30 - 3.2
Completeness (%)	85.4 (59.4)
Total reflections	84,231
Unique reflections	24,856
Redundancy	3.4 (1.6)
R_{merge} (%)[b]	16.5 (21.0)
I/σI	5.6 (1.7)
Refinement statistics	
R_{cryst} (%); work set[c]	23.0 (32.9)
R_{cryst} (%); test set[c]	26.7 (34.9)
Overall B-factor (Å^2)	62.7
Root mean square deviation, bond lengths (Å)	0.011
Root mean square deviation, bond angles (°)	1.560
Ramachandran plot:[d]	
Most favorable regions (%)	80.8
Additional allowed regions (%)	18.3
Generously allowed regions (%)	0.5
Disallowed regions (%)	0.5

[a] Data were collected at 100 K and a wavelength of 0.92 Å. Values in parentheses refer to the outermost resolution shell (3.20-3.31 Å).
[b] $R_{merge} = \sum_{hkl} |I-\langle I\rangle| / \sum_{hkl} I$, where I is the intensity of a reflection hkl, and $\langle I\rangle$ the average over symmetry-related observations of hkl.
[c] $R_{cryst} = \sum_{hkl} |F_{obs} - F_{calc}| / \sum_{hkl} F_{obs}$, where F_{obs} and F_{calc} are observed and calculated structure factors, respectively. Free set (17) contains 10% of the data.
[d] Calculated with PROCHECK (83).

Overall structure of the complex - The complex consists of a σ1H trimer ligated by three D1 domains. When viewed along the three-fold non-crystallographic symmetry axis, its overall structure resembles a three-bladed propeller, with σ1H forming the hub and D1 forming the blades (Figure IV-1A). Each D1 monomer interacts with one σ1H monomer, making extensive contacts that shield a combined area of 1622 $Å^2$ from solvent. Crystal packing results in additional contacts between the molecules. However, the interactions we describe are common to all σ1H-D1 pairs. D1 residues involved in contact formation are located at the most membrane-distal part (top) of the domain and on the face of JAM-A that mediates homodimer formation. These regions in D1 pack tightly into a recessed region of σ1H just below the β-barrel (Figure IV-1B, C). Residues at the D1 dimer interface form extensive contacts with the D-E loop and 3_{10} helix of σ1H at the upper boundary of this recessed region, whereas the top of D1 contacts residues in the C-terminal β-spiral repeat of the σ1 tail at the lower boundary of the recessed region. In comparison to structures of isolated σ1 (30, 131) and JAM-A (122), the architectures of both σ1H and D1 in the complex are largely preserved. Differences are observed primarily in side-chain orientations at the interfaces between σ1H and D1.

Four of the six σ1H-D1 pairs present in the asymmetric unit have similar structures and feature identical interactions. The analysis of the complex presented here is based on these pairs. The remaining two σ1H-D1 pairs exhibit larger intermolecular distances of up to 1.2 Å, resulting in fewer contacts and higher crystallographic temperature factors. Moreover, the total buried surface areas for these two interacting pairs are about 60 $Å^2$ smaller. The crystal packing is extremely tight for a protein complex of this size, with only 50% solvent content (99). The only gaps in the packing

occur directly beneath those D1 chains that exhibit larger intermolecular distances to σ1. Flash-cooling of crystals prior to data collection, as was done here, may have partially dislodged D1 from its binding site (125).

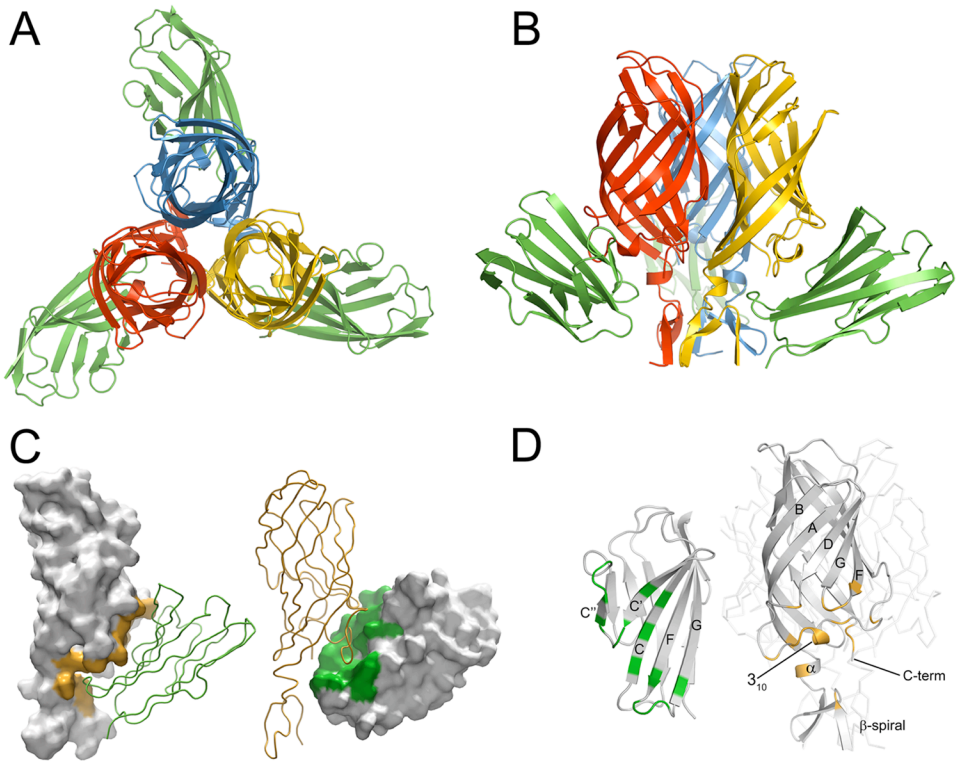

FIGURE IV-1. Structure of the σ1H-D1 complex. (A, B) Ribbon drawings of the complex between trimeric σ1H and monomeric D1, viewed along the three-fold symmetry axis (A) and from the side (B). σ1H monomers are shown in blue, yellow, and red; D1 is shown in green. (C) Surface representation of the contact area of reovirus σ1H (left, orange) and D1 (right, green). Interacting partners are shown as ribbon traces. (D) Ribbon drawings of D1 (left) and σ1H (right). Secondary structure elements are labeled. Contact residues (distance cutoff 4 Å) in the σ1H-D1 interface are colored green (D1) or orange (σ1H).

Interaction of reovirus σ1H with JAM-A D1 - Reovirus σ1H latches onto JAM-A D1 using two main contact areas: a larger region centered at the D-E loop and its 3_{10} helix, just below the β-barrel, and a second, smaller region formed by the top of the β-spiral and

the α-helix (Figure IV-1D). These two regions resemble "jaws" that engage the D1 domain at its interdomain interface and at its top (Figure IV-2A). Although exact placement of individual atoms is not possible at 3.2 Å resolution, there is unambiguous electron density in a composite annealed omit map for all side chains in the interface (data not shown), allowing for assignment of contacts.

The upper, larger σ1H jaw contacts the D1 interdomain interface. Contacts are largely of a polar nature, featuring numerous hydrogen bonds and two salt bridges. These interactions are centered around the σ1H 3_{10} helix, in which residues Thr380, Gly381, and Asp382 interact with D1 residues Glu61, Asn76, and Arg59, respectively (Figure IV-2B). These contacts are augmented by interactions between σ1H D-E loop residues Val371 and Glu384 and D1 residues Asn76, Lys78, and Lys63, and by contacts between Asp423 in the F-G loop of σ1H and main-chain nitrogen atom of Ala81 in D1 (Figure IV-2C). In addition to these polar interactions, D1 residues Leu72 and Tyr75 are engaged in extensive hydrophobic contacts with D-E loop residues and the terminal part of β-strand F in σ1H (Figure IV-2C). Of note, my previous point mutagenesis study (Chapter III) showed that D1 residues Arg59, Glu61, Lys63, Leu72, Tyr75, and Asn76 contribute to σ1 binding (65). An interesting characteristic of the contacts involving the D1 interface is that most of the residues engaged in interactions with σ1H form contacts of a similar nature in the D1-D1 homodimer. For example, D1 residue Arg59 forms a salt bridge with Asp382 in the complex and a salt bridge with D1 residue Glu61 in the D1-D1 dimer. Similarly, Leu72 and Tyr75, which mediate hydrophobic contacts in the complex, also do so in the D1-D1 dimer.

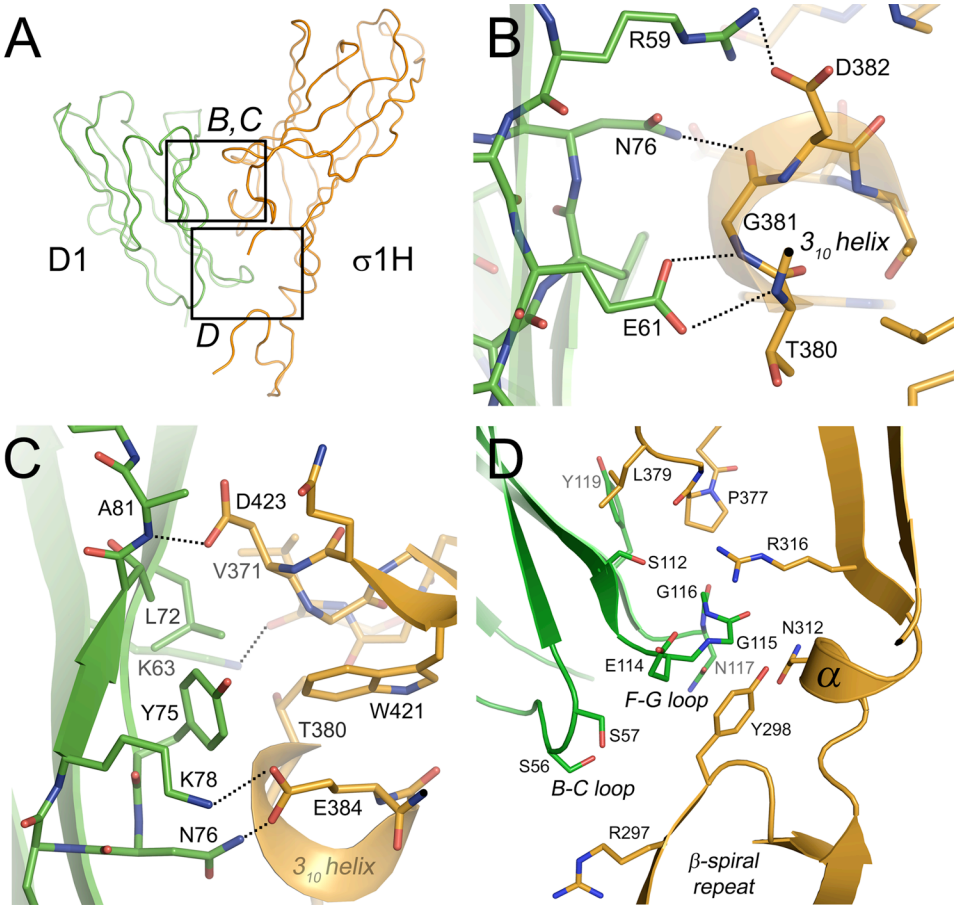

FIGURE IV-2. Contacts at the σ1H-D1 interface. (A) Overview displaying the location of residues in the σ1H-D1 complex shown in panels B-D. D1 and σ1H are colored green and orange, respectively. (B) Interactions between D1 and residues in the 3_{10} helix in the D-E loop of σ1H. Secondary-structure elements are depicted in lighter shading. (C) Additional interactions between D1 and σ1H in the same region. The view is rotated laterally 180° relative to panel B. (D) Interactions at the F-G and B-C loops of D1 with σ1H. (B-D) Carbon atoms are shown in green (D1) or orange (σ1H), oxygen atoms in red, and nitrogen atoms in blue. Dotted lines represent hydrogen bonds and salt bridges. For clarity, some non-interacting residues are not shown. Amino acids are labeled in single-letter code.

Contacts mediated by the lower, smaller jaw of σ1H lack hydrogen bonds and salt bridges. Instead, extensive hydrophobic interactions with substantial surface complementarity are found, indicating that this contact area also plays an important role in defining specificity and providing high affinity. In σ1H, interactions involve β-spiral residue Tyr298, a mostly hydrophobic surface of the α-helix connecting the β-spiral with the β-barrel, the non-polar portion of the Arg316 side chain, and Pro377 in the D-E loop (Figure IV-2D). These residues essentially surround the D1 F-G loop, which contains several partially hydrophobic residues. The nearby B-C loop of D1 also faces towards the σ1H β-spiral. Its closest contact, at about 4.7 Å, is between the hydroxyl group of D1 residue Ser57 and the hydrophobic portion of Arg297 in σ1H. Ser57 also has been implicated in σ1 binding (52).

Rescue of reoviruses with engineered mutations in σ1 - To identify contributions of individual residues in σ1 to JAM-A engagement, I employed plasmid-based reverse genetics (78) to engineer mutations into the σ1 protein of T3D. Mutant viruses were isolated following cotransfection of murine L cells with nine RNA-encoding plasmids corresponding to wild-type T3D genes and a tenth plasmid corresponding to the σ1-encoding S1 gene incorporating site-specific mutations. Thus, each resultant virus is isogenic, with the exception of the S1 gene and its protein product, viral attachment protein σ1. Guided by the structure of the σ1H-D1 complex, I engineered individual substitution mutations in several residues in the JAM-A-binding region of σ1, including Asn369, Val371, Thr380, Gly381, Asp382, and Glu384 in the D-E loop and Trp421 and Asp 423 in β-strand F and the F-G loop. Although the efficiency of rescue varied, all of

the mutant viruses were recovered, with the exception of D382A and W421V (Table IV-2). However, upon cotransfection of a plasmid encoding wild-type σ1, I was able to rescue W421V by pseudotyping for the first round of replication. Although a D382A mutant virus was not recovered, a T380A/D382A double-point mutant was isolated. However, this virus reverted to the parental sequence at position 382, as indicated by an equal nucleotide signal for both Asp and Ala codons in RNA extracted from purified virions (data not shown). With the exception of V371A and W421V, each of the mutant viruses produced sufficiently high titers to permit viral purification. For the purified wild-type and mutant viruses, I employed plaque assays to determine particle to plaque-forming unit (pfu) ratios using L cells (Figure IV-3). Alanine substitutions at positions T380 and G381 increased the particle to pfu ratio by approximately three-fold and two-fold over wild-type, respectively, suggesting that residues Thr380 and Gly381 play a role in the efficiency of viral infectivity, possibly because of the importance of their interactions with JAM-A. The most inefficient mutant reovirus was the T380/D382A double point mutant, with a particle to pfu ratio that was nearly seven-fold greater than the parental virus, despite some portion of the viral population already having reverted to the parental sequence at position 382.

Contribution of individual σ1 residues to JAM-A engagement - To determine the JAM-A-binding capacity of the sequence-verified mutant viruses, I captured GST alone or GST-JAM-A on a biosensor chip and employed SPR to assess viral binding (65). Purified reovirus particles (5×10^{12}/ml) were injected across the biosensor surface, and association and dissociation with GST-JAM-A were measured over time. In each case,

TABLE IV-2. Engineered mutant reoviruses

Virus name	Location of σ1 mutation	Interaction of residue with JAM-A	Rescue titer[a]
WT	---	---	~ 3 x 10^5 pfu/ml
N369A	Terminus of β-strand D	---	~ 2 x 10^4 pfu/ml
V371A	D-E loop	H-bond with K63	~ 3 x 10^3 pfu/ml
T380A	3_{10} helix in D-E loop	H-bond with E61	~ 1 x 10^5 pfu/ml
G381A	3_{10} helix in D-E loop	H-bonds with E61 and N76	~ 3 x 10^4 pfu/ml
D382A	3_{10} helix in D-E loop	Salt bridge with R59	Unable to rescue after five attempts
E384A	D-E loop	H-bond with N76, salt-bridge with K78	~ 5 x 10^2 pfu/ml
W421V	Terminus of β-strand F	Hydrophobic packing against Y75 and L72	~ 40 pfu/ml
D423A	F-G loop	H-bond with A81	~ 5 x 10^5 pfu/ml
T380A/D382A	3_{10} helix in D-E loop	H-bond with E61, salt-bridge with R59	~ 20 pfu/ml

[a] Rescue titer is the viral titer assessed using L cell monolayers 6 d post-transfection.

an immediate association of reovirus particles with GST was detected (Figure IV-4). However, the particles dissociated immediately upon injection of wash buffer, indicating that the interaction was not specific. In the case of the wild-type virus and several of the mutants, association with GST-JAM-A exceeded the background levels of binding to GST, indicating a specific binding interaction. Like the wild-type strain, N369A, D423A, and E384A bound specifically to GST-JAM-A. N369A and D423A exhibited slightly lower maximal binding signals, whereas E384A displayed enhanced binding to GST-JAM-A. In sharp contrast, T380A and G381A showed no specific binding to GST-JAM-A, suggesting that Thr380 and Gly381 contribute importantly to the interaction with JAM-A. These results are in accord with the larger particle to pfu ratios exhibited by

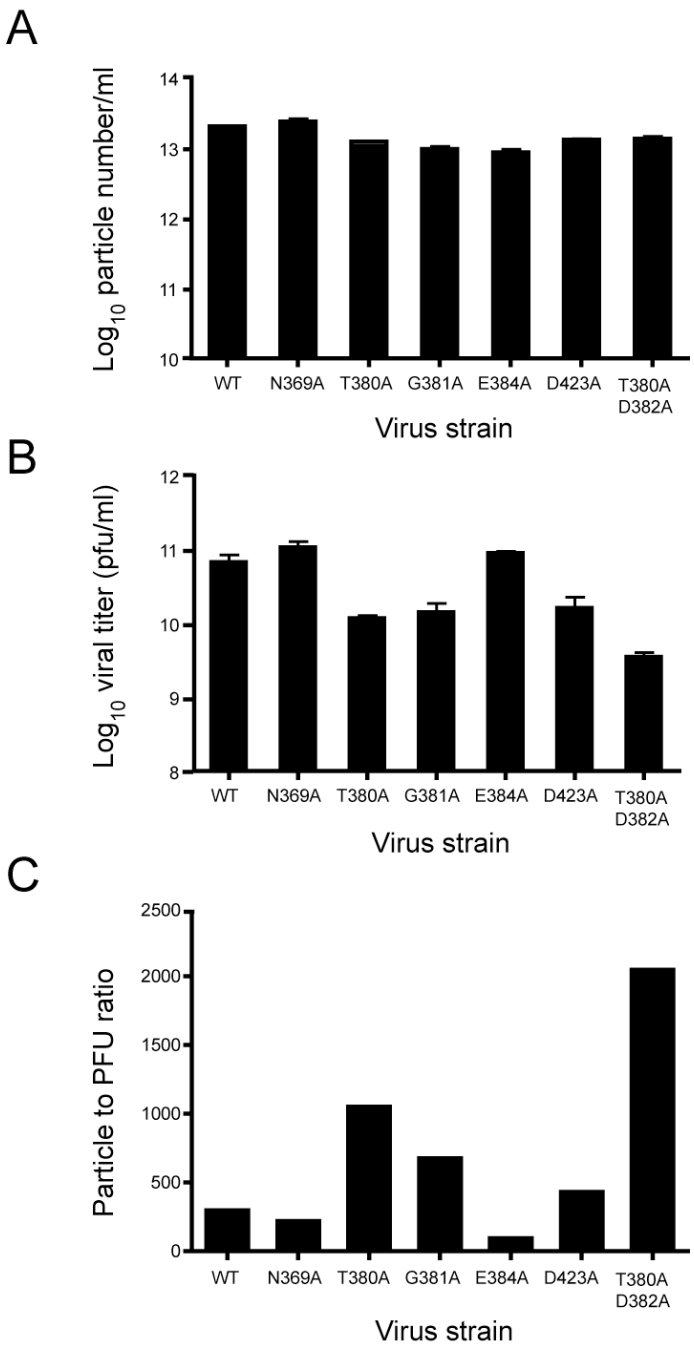

FIGURE IV-3. Particle to plaque forming unit ratios for reovirus mutants. (A) Particle numbers of purified wild-type and mutant reoviruses, determined in triplicate using a conversion factor of 1 OD_{260} = 2.1 x 10^{12} particles/ml. Error bars indicate S. D. (B) Titers of purified wild type and mutant reoviruses, determined in quadruplicate by plaque assay. Titers are graphed on a $\log_{10}$ scale. Error bars indicate S. D. (C) Particle to PFU ratios for wild-type and mutant reoviruses. The mean particle number was divided by the mean titer for each purified virus to obtain the values shown. WT, wild-type virus.

these viruses (Figure IV-3). Thr380 and Gly381 are located in the 3_{10} helix of the σ1 D-E loop, Asn369 and Glu384 are located in the D-E loop on either side of the 3_{10} helix, and Asp423 is located at the terminus of β-strand D (Figure IV-2).

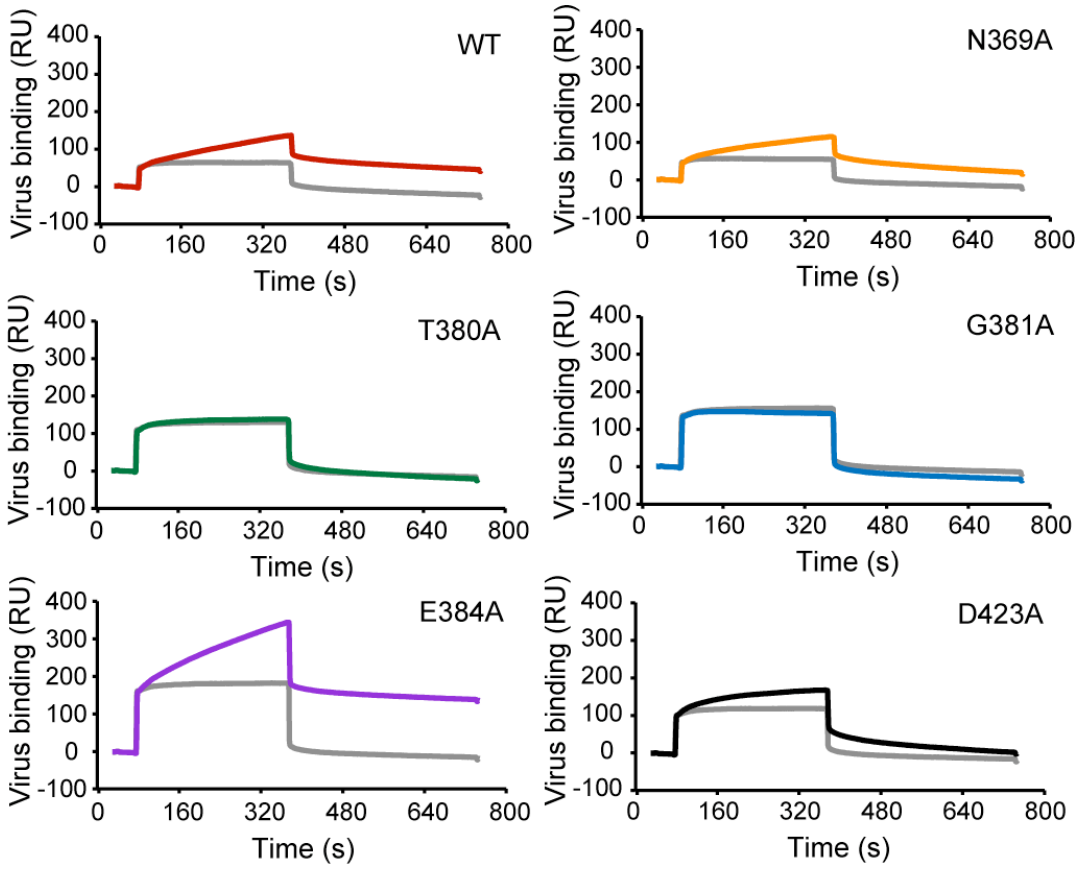

FIGURE IV-4. SPR analysis of reovirus mutants binding to JAM-A. Purified reovirus (5×10^{12} particles/ml) was injected for 5 min across a biosensor surface on which GST fused to the JAM-A ectodomain previously had been captured. Following injection of virus, buffer alone was injected across the biosensor surface. Traces show binding and dissociation from GST (grey) and GST-JAM-A (color or black). Binding is expressed in resonance units (RU).

To determine effects of substitution mutations in the JAM-A-binding region of σ1 using a more physiologic system, we employed flow cytometry to assess the binding of wild-type and mutant viruses to CHO cells transfected with hJAM-A. Approximately 100% of CHO cells expressing JAM-A were bound by wild-type virus (Figure IV-5). However, both T380A and G381A demonstrated a statistically significant reduction in binding to JAM-A-expressing CHO cells, although much less than the reduction in

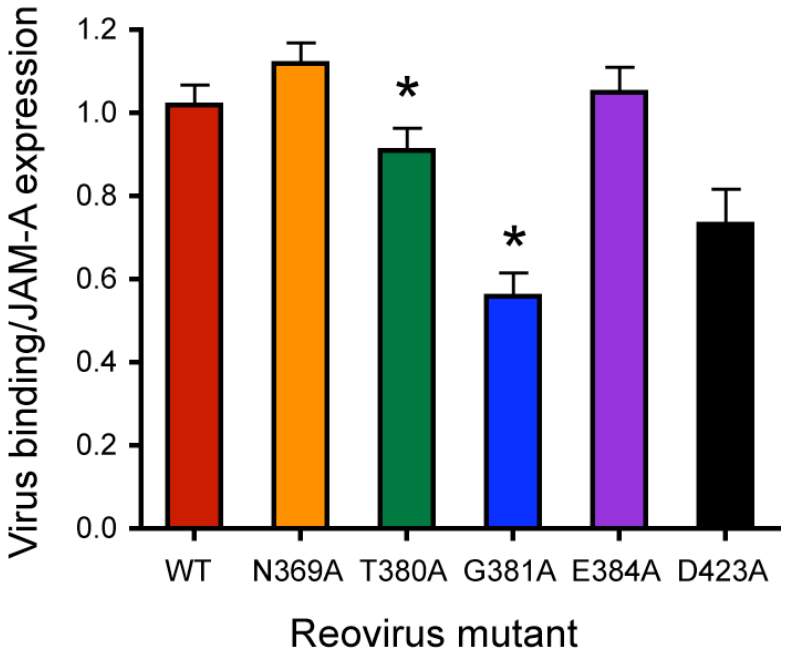

FIGURE IV-5. Flow-cytometric analysis of reovirus binding to cells. CHO cells (10^6) were transiently transfected with plasmids encoding the indicated full-length JAM-A. Following incubation for 24 h to permit receptor expression, cells were lifted from plates using EDTA and stained with hJAM-A-specific mAb J10.4 or adsorbed with the indicated reovirus (10^5 particles/cell). Cell-surface expression of receptor JAM-A and virus binding was assessed by flow cytometry. Results are expressed as a ratio of the percentage of cells with bound reovirus divided by the percentage of cells expressing JAM-A. WT, wild-type virus. Data were collected from three independent experiments. Error bars indicate S. D. *, $P < 0.05$ in comparison to wild-type virus.

binding to GST-JAM-A detected by SPR (Figure IV-4). The difference in binding to cells versus GST-JAM-A observed for these viruses is likely due to carbohydrate binding and increased capacity to engage JAM-A anchored in a membrane rather than immobilized on a rigid biosensor surface.

Growth of mutant reoviruses in cultured cells - To test whether differences in JAM-A binding capacity displayed by the mutant viruses influence viral yield, I adsorbed L cells with the wild-type or mutant viruses at an MOI of 0.01 pfu/cell and quantified viral titer following 0, 24, 48, 72, or 96 h of incubation (Figure IV-6). Infecting at a lower MOI enabled me to use the poorly-growing mutant viruses that produced insufficient titer for binding analyses. Based on growth kinetics and peak titers, the mutant viruses clustered into three groups. The first contains E384A and D423A, which exhibited growth kinetics and peak titers indistinguishable from wild-type virus. The second contains N369A, T380A, and G381A, which showed slower growth kinetics than wild-type virus, with titers approximately 10- to 15-fold lower on day four post-infection. The third contains V371A and W421V, which demonstrated the most severely impaired replication at all time points, with yields 100- to 300-fold less than wild-type virus after four days of growth. Thus, targeted mutations in the JAM-A binding surface of σ1 influence viral replication kinetics.

Stability of the σ1H-D1 complex - In contrast to many other protein-protein complexes, in which the interfaces are hydrophobic in nature (71, 72), interactions between σ1H and D1 feature numerous salt bridges and polar interactions. Moreover, many of the

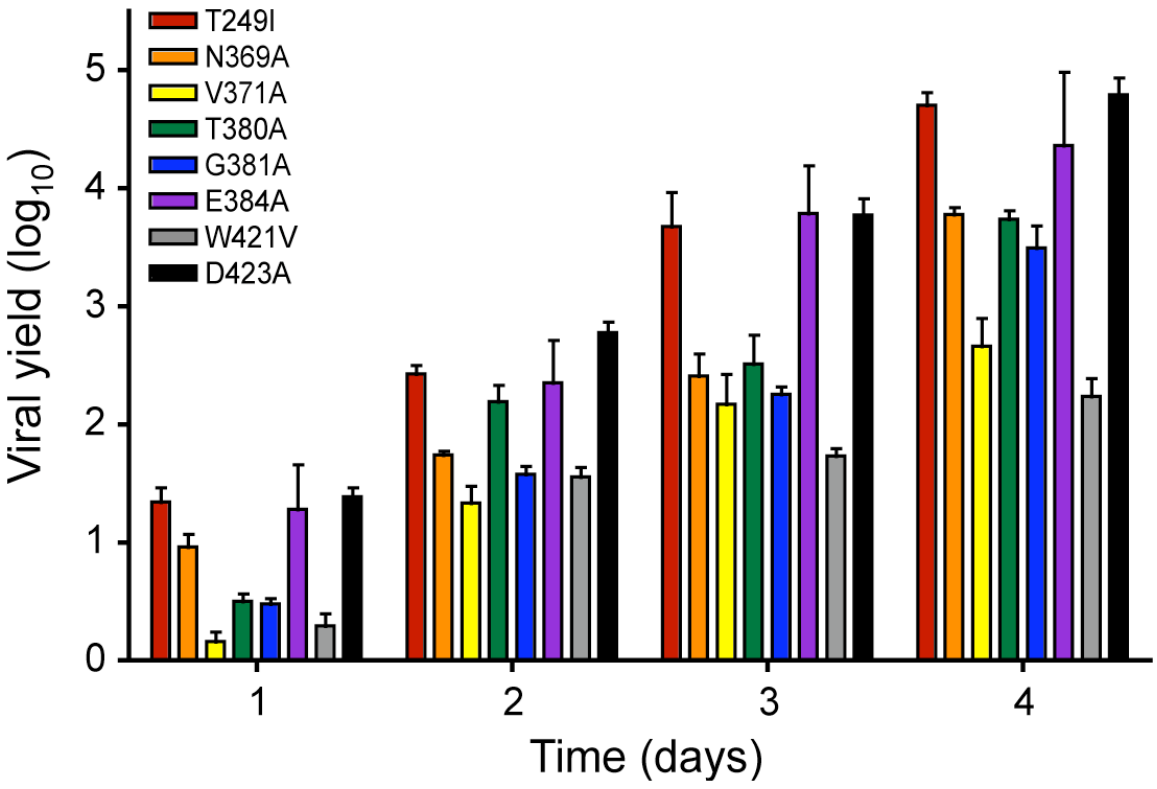

FIGURE IV-6. Growth of mutant reoviruses in L cells. L cells were adsorbed with virus at an MOI of 0.01 PFU/cell. Following incubation at room temperature for 1 h, complete medium was added, and cells were incubated at 37°C for 0, 24, 48, 72, or 96 h. Viral titers were determined by plaque assay. Data were collected from three independent experiments per time point per virus. Error bars indicate S. D. WT, wild-type virus.

observed interactions involve charged residues. Three charged σ1H residues (Asp382, Glu384, and Asp423) participate directly in polar interactions with D1, and two others (Arg297 and Arg316) do so indirectly. In D1, four direct contacts are mediated by charged residues (Arg59, Glu61, Lys63, and Lys78). As a result, the interacting surfaces of both σ1H and D1 display strong electrostatic potentials (Figure IV-7A). When comparing the two, the interacting surface of σ1H has a dominant electronegative potential in the upper jaw, whereas the lower jaw is electropositive. The interacting

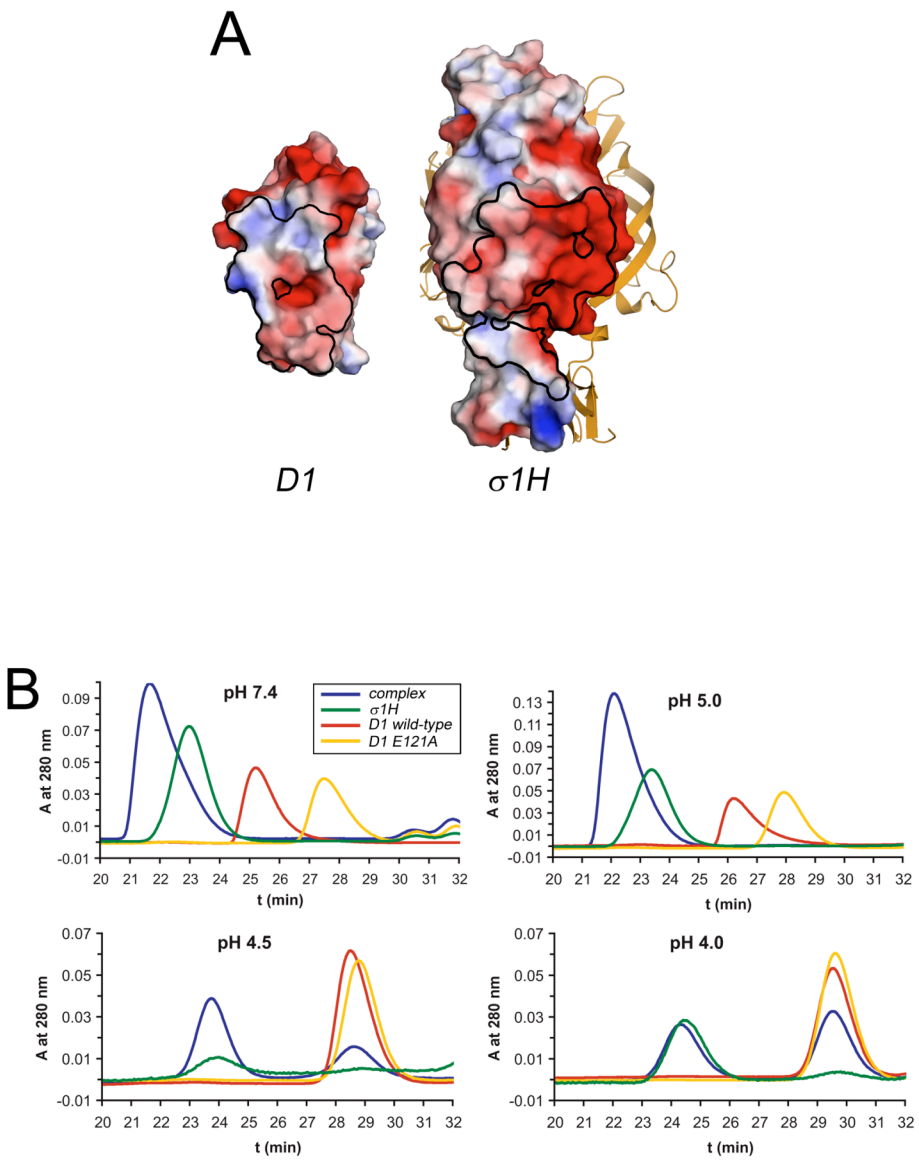

FIGURE IV-7. Stability of the σ1H-D1 complex. (A) Electrostatic potential of the surfaces of D1 (left) and a single σ1H subunit (right) calculated with APBS tools (89). The scale ranges from -3 (red) to +3 (blue) in units of k_BT/e_c. Boundaries of the contact areas are outlined in black. The other two σ1H monomers are shown as yellow ribbons. (B) Gel filtration elution profiles of the σ1H-D1 complex using conditions of varied pH. The σ1H, wild-type D1, and monomeric D1 E121A proteins were used as controls. At pH 4.5 and 4.0, the A_{280} of σ1H was multiplied by 10 to compensate for the lower concentration due to precipitation.

surface of D1 is complementary to that of σ1H, featuring an electropositive potential at the dimer interface and a more electronegative potential at the most membrane-distal part of the domain.

The dominance of charge on the interacting surfaces of σ1H and D1 suggests that complex formation is at least partially dependent on pH or ionic strength. To test this hypothesis, we used gel filtration chromatography to assess the stability of preformed complex following equilibration with buffered solutions of progressively lower pH. Purified σ1H, wild-type D1, and monomeric D1 mutant E121A (65) were used as controls. Glu121 in the D1 dimer interface does not participate in complex formation with σ1H. Thus, its alteration affects JAM-A dimerization but not σ1H ligation (65). In accordance with our prediction, the σ1H-D1 complex was stable at pH 5.0 but disassembled into its components at pH 4.5 or 4.0, which approximates the pK value for acidic side chains (Figure IV-7B). Similarly, wild-type D1 dissociated under conditions of low pH, similar to results obtained in previous studies of the murine JAM-A dimer (9).

Stability of the JAM-A homodimer - The σ1H-D1 complex is readily produced in solution by mixing the two components. Although JAM-A dissociates under high salt or low pH conditions (9), we were not able to detect monomeric species of JAM-A in the neutral pH, low-salt environment used for complex formation (data not shown). However, it is possible that some monomeric JAM-A is present transiently in these conditions. If so, σ1 could trap monomeric JAM-A in a complex, which is a reasonable possibility since σ1-JAM-A binding occurs with faster kinetics than JAM-A homophilic association in solid-phase binding assays (52). To test this hypothesis, we incubated dimeric JAM-A D1 and

JAM-A D1D2 (the entire extracellular domain of JAM-A) (122) in an equimolar ratio and performed gel filtration experiments. Since D1 and D1D2 dimers have molecular weights of 22 and 46 kDa, respectively, they can be distinguished by elution volume. If JAM-A transiently dissociates into monomers, one would expect the formation of a dimeric species with one monomer contributed by D1 and the other by D1D2. Such a species should produce a peak with an elution volume between the two observed for the D1 and D1D2 dimers. No such species was observed, even after 60 min incubation, indicating that JAM-A does not dissociate into monomers under these conditions (Figure IV-8A). Although not fully separated, the two peaks of the protein mixtures do not change between 5 and 60 min of incubation, indicating that the differences compared to the unmixed proteins are due to the limits of column resolution. Thus, we conclude that, at least in solution, σ1 forcibly displaces a JAM-A monomer to gain access to the JAM-A dimer interface.

Discussion

Implications for σ1-JAM-A complex formation - Reovirus attachment to host cells is mediated by interactions between σ1 protein and JAM-A. While some reovirus strains utilize additional co-receptors, all strains tested to date engage JAM-A (20). JAM-A exists as a dimer in solution and most likely also at the cell surface, but only a monomer is bound by σ1 in our crystal structure. Since the σ1-JAM-A complex can be produced readily in solution by mixing the two components, its formation must be thermodynamically favored to that of the JAM-A dimer. The molecular basis for this preference is not obvious on initial inspection of the structure. In fact, comparison of the

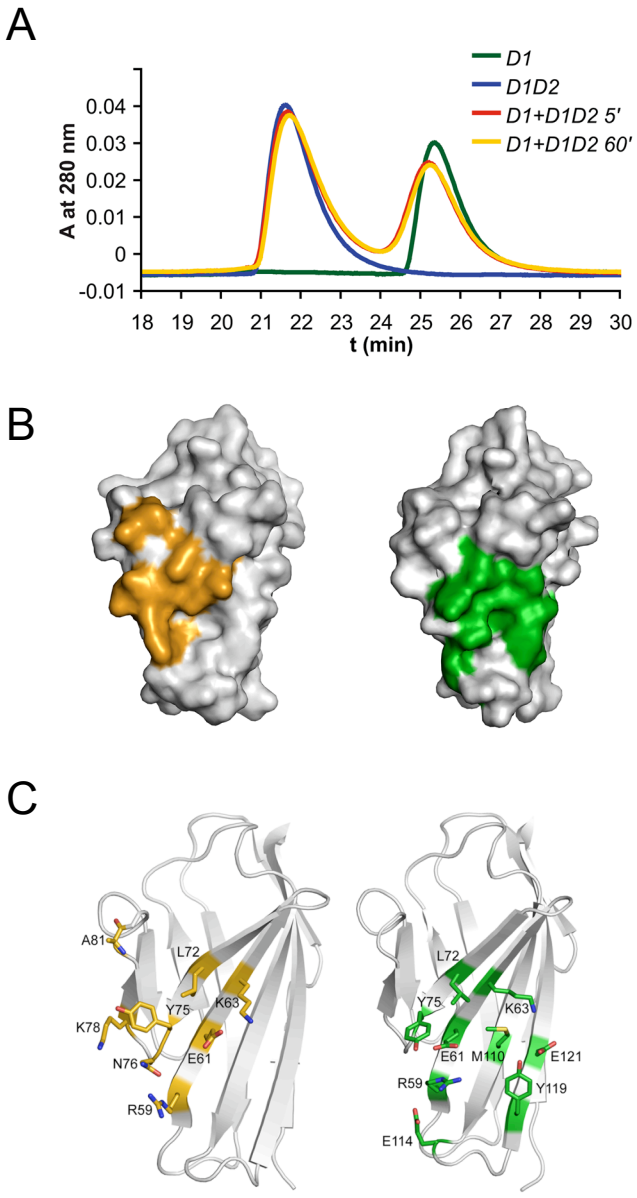

FIGURE IV-8. Comparison of the D1 dimer and the σ1H-D1 complex. (A) Gel filtration chromatograms of JAM-A D1 (green), D1D2 (blue), and equimolar mixtures of both proteins after 5 (red) and 60 (yellow) min of incubation at 4°C. (B) Surface representations of D1, with key amino acids (residues forming hydrogen bonds, salt bridges, or close hydrophobic contacts) highlighted in orange (σ1H-D1 complex, left) or green (D1 dimer, right). (C) Ribbon drawings of D1, showing stick representations of key contact residue side chains. Main-chain atoms of Ala81 are also depicted in stick representation. Carbon atoms are shown in orange (σ1H-D1 complex, left) or green (JAM-A dimer, right), oxygen atoms in red, nitrogen atoms in blue, and sulfur atoms in yellow. Amino acids are labeled in single-letter code.

surfaces buried in the two complexes reveals striking similarities. Both surfaces are almost identical in size, with buried surface area values for one JAM-A molecule of 804 $Å^2$ and 808 $Å^2$ for JAM-A and σ1, respectively. Moreover, JAM-A contact surfaces for opposing JAM-A monomers and σ1 substantially overlap and share many residues. Arg59, Glu61, Lys63, Leu72, and Tyr75 serve as a footprint on β-strands C and C' that is recognized by both JAM-A and σ1 (Figure IV-8B, C). In both complexes, these residues form critical contacts of a similar nature (Figure IV-2 and I-5 [122]). The JAM-A homodimer has additional contacts with residues on β-strands F and G on one side of this footprint, whereas σ1 also recognizes residues on the other side, in the adjacent C'-C" and C"-E loops.

Despite these similarities, our gel filtration experiments show that σ1 disrupts the JAM-A dimer and engages monomeric JAM-A. What then leads to formation of σ1-JAM-A complexes versus JAM-A dimers? Analysis of the electrostatic potential of the interacting surfaces reveals that the JAM-A binding surface of σ1 exhibits a strong electronegative potential (Figure IV-7A), which largely covers the loop between β-strand D and the 3_{10} helix and the short F-G loop and its adjacent residues. An accumulation of solvent-exposed acidic residues (Asp382, Glu384, Asp390, Glu419, and Asp423) is largely responsible for this potential. In the σ1-JAM-A complex, the negatively-charged face of σ1 binds to an electropositive area that is not buried in the D1-D1 dimer interface (Figures IV-7A). Since electrostatic interactions can be established over a larger distance, it is likely that the negatively-charged surface of σ1 is first attracted by JAM-A and makes the initial contact. JAM-A dimer stability depends critically on salt bridges involving Arg59 (65, 122). This residue might be reoriented during the initial contact of

σ1 with JAM-A to allow interactions with acidic σ1 residues. This arrangement could then lead to destabilization and opening of the JAM-A dimer. We note that in the σ1-JAM-A complex, Arg59 forms a salt bridge with σ1 residue Asp382, which protrudes from the 3_{10} helix in the D-E loop, at the edge of the negatively-charged face. The Asp382 side chain could easily offer an alternative contact point for Arg59. Our findings, including the central location of Asp382 in the σ1H-D1 binding interface, the lack of recovery of a D382A mutant, and reversion of the T380/D382A mutant to the wild-type sequence at position 382, reinforce the importance of Asp382 in viral attachment.

The σ1 D-E loop is central in the binding interface, and our results suggest that several residues in this region in addition to Asp382 are important for efficient JAM-A engagement. Mutation of either Thr380 or Gly381 to alanine leads to impaired JAM-A binding both on a biosensor surface and on CHO cells (Figures IV-4 and IV-5). Furthermore, mutation of any of the residues we chose in the σ1 D-E loop result in defective viral growth following infection at low MOI (Figure IV-6). Both findings can be easily explained by the structure. Mutation of Gly381 would directly affect interactions with JAM-A, as any side chain at this position would lead to steric clashes with D1 residue Tyr75. Thr380 likely shields hydrophobic interactions from solvent (Figure IV-2C), a function abolished by the T380A mutation. Moreover, the Thr380 side chain makes extensive contacts with other σ1H residues (Phe370, Val371, Gly424), helping to fasten the 3_{10} helix to the D-E and F-G loops of σ1H. Truncation of its side chain would likely perturb the structural integrity of the 3_{10} helix. Since this helix mediates several contacts to D1 (Figure IV-2B, C), alteration of its structure would

diminish JAM-A binding. Changes in local structure also might explain the impaired replication kinetics observed for the N369A mutant. Although Asn369 does not directly contact D1, its location at the N-terminus of the D-E loop is strictly conserved among reovirus serotypes (20) and may stabilize the 3_{10} helix.

While complementary electrostatic forces may facilitate engagement of JAM-A by σ1, dependence on charge also may mediate σ1 disengagement from JAM-A once the virus reaches the low-pH environment of the endosome. Our data demonstrate that the complex dissociates when exposed to pH 4, most likely due to protonation of acidic residues at the interface (Figure IV-7B).

Charged residues are not the sole contributors to σ1-JAM-A interactions. Val371 and Trp421 participate in hydrophobic interactions with D1. As the poor growth of the V371A and W421V viruses prohibited direct assessment of JAM-A binding capabilities, it was not possible to quantify the contribution of these residues to JAM-A engagement. However, altering the opposing residues of JAM-A, Leu72 and Tyr75, abolishes (L72A) or diminishes (Y75A) binding to σ1H (65), suggesting an important role for interactions at these positions. Thus, the dramatic effects on viral replication observed for the V371A and W421V mutants are likely due to deficiencies in JAM-A binding, although it is possible that these mutations diminish JAM-A engagement indirectly by altering σ1 structure.

Biological context of the σ1-JAM-A interaction - To envision how σ1 interacts with JAM-A at the cell surface, we combined the structures of the σ1H-D1 complex, the JAM-A extracellular domain (122), and the C-terminus of σ1 (30) with a model of the N-

terminus of σ1 (30, 64) (Figure IV-9). This model demonstrates that JAM-A must reach beyond the approaching head to access residues in the neck, which links the σ1 head and tail segments. Since the sites for JAM-A are distant from each other on the σ1 trimer, it is conceivable that each σ1 trimer engages more than one JAM-A monomer. This scenario appears plausible as σ1 binding leads to separation of JAM-A dimers into monomers, both of which likely remain in close proximity. Thus, several molecules of JAM-A could form a clamp that engages σ1 by its neck and tightly adheres the virus to the cell, as depicted in our model (Figure IV-9).

Since the binding JAM-A binding site in σ1 resides within the base of the head, flexibility within σ1 or JAM-A would appear essential to facilitate complex formation. The linker connecting the D1 and D2 domains of JAM-A possesses some flexibility (122), and residues linking D2 to the transmembrane region also may allow for some movement. However, as reovirus is capable of efficiently infecting CHO cells expressing a JAM-A construct that lacks the D2 domain (52), it is likely that flexibility of σ1 is even more critical than JAM-A flexibility. Electron microscopic images of full-length σ1 combined with structural studies and molecular modeling indicate that σ1 has at least three major regions of flexibility: (i) near the N-terminus, (ii) at the midpoint of the molecule, where the predicted α-helical coiled-coil transitions to a triple β-spiral, and (iii) just below the neck of σ1, between the C-terminal two β-spiral repeats of the crystallized portion of T3D σ1 (30, 54, 64). Similar to the adenovirus fiber (173), σ1 length and flexibility might contribute importantly to the capacity of reovirus to interact with JAM-A, carbohydrate, and additional receptors at the cell surface.

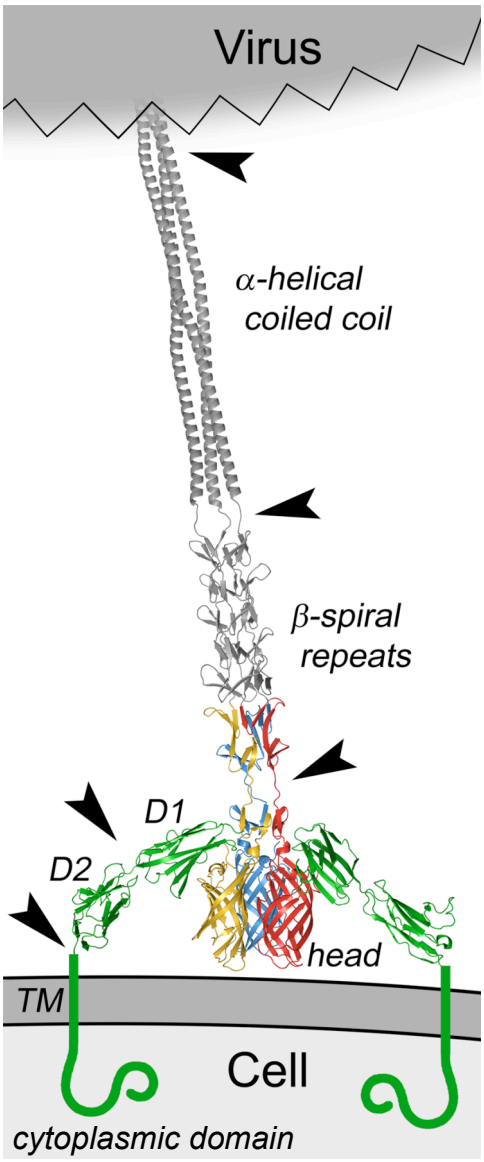

FIGURE IV-9. Full-length model of the complex between reovirus σ1 and JAM-A. A model of full-length σ1 extending from a schematic representation of a virion is shown as a ribbon drawing, with the known structure of the C-terminus (30) in tricolor and the predicted structure of the N-terminus in grey. A model of full-length JAM-A is shown in green as a ribbon drawing of the known structure of the extracellular domain (122) and a schematic representation of the transmembrane (TM) and intracellular domains. The model was produced by superimposing JAM-A (122) and the full-length model of σ1 (30) onto the σ1H-D1 complex structure. Arrowheads indicate regions of possible flexibility. For clarity, only two JAM-A monomers are shown bound to σ1.

Serotype-specific differences - Although the σ1 sequence is the most divergent among the reovirus proteins, prototype and field-isolate strains from the three most prevalent reovirus serotypes use JAM-A as a receptor (20). Based on sequence alignment, the highest degree of conservation is observed among residues in the D-E loop, which previously prompted us to propose that this region forms part of the JAM-A-binding site (20, 30). In keeping with this prediction, residues in T3D σ1 that comprise the D-E loop form the upper jaw contacting JAM-A. Val371 also is conserved and likely plays an important role in the interaction. However, several T3D σ1 residues that interact with JAM-A are not conserved in prototype strains T1L and T2J σ1 (30). For example, in the T3D σ1H-D1 complex, the carbonyl oxygen atoms of the Asp423 side chain form hydrogen bonds with the main-chain nitrogen atom of Ala81 in JAM-A. In T2J σ1, Asp423 is replaced by alanine, which would not be capable of forming a similar bond. In addition, several of the residues in the lower jaw of T3D σ1 differ among reovirus serotypes. In some cases, these polymorphisms are unlikely to have profound effects on the largely hydrophobic interactions with JAM-A that occur in this region. However, the absence of a bulky proline side chain at position 377 in T1L and T2J σ1, which each have glycine residues at that position, could potentially alter the means by which σ1 interacts with JAM-A. These observations suggest that, while the binding sites may be similar, σ1-JAM-A interactions may differ at an atomic level among the reovirus serotypes. Such serotype-specific differences may in turn alter the affinity of the various σ1 proteins for JAM-A and thus influence reovirus tropism.

CHAPTER V

SUMMARY AND FUTURE DIRECTIONS

Introduction

Initiation of viral infection requires specific interactions of a virus with receptors on the host-cell surface. A viral attachment protein often mediates the adhesion process. Although much progress has been made in understanding the relationships between the structures of viral proteins and cellular components with which they interact, much remains unknown about the precise nature and mechanisms of virus-receptor interactions. A detailed understanding of virus structure-function relationships and attachment strategies can direct the design of efficacious antivirals and viral vectors for therapeutic purposes. The goals of my dissertation research were to elucidate features of reovirus attachment protein σ1 that confer functionality and define the molecular basis σ1 interactions with JAM-A. I characterized a novel trimerization motif, the aspartic acid sandwich, consisting of an unusual cluster of six aspartic acid residues located between residues with aromatic and hydrophobic side chains at the subunit interface of the σ1 (Chapter II). This motif might be important in mediating structural rearrangements in σ1. I systematically defined the contributions of individual residues in the JAM-A dimer interface to reovirus binding and JAM-A homodimer stability (Chapter III). Residues with charged side chains play critical roles in stabilizing both interactions. In addition, I reported the structure of a complex between σ1 and JAM-A and identified sequences in σ1 required for efficient JAM-A binding and reovirus infectivity (Chapter IV). In this

chapter, I will discuss the broader implications of this body of work and future directions for this research.

The aspartic acid sandwich motif

Studies reported in Chapter II describe structural and mutational analysis of the aspartic acid sandwich, a novel trimerization motif that might mediate structural changes in σ1 during reovirus entry into target cells. A likely scenario is that the aspartic acid residues act as a switch that allows full trimerization of the σ1 head only at low pH (131). There is evidence to suggest that σ1 exists in a partially detrimerized state ([54] and Figure I-2). While JAM-A is incapable of binding monomeric mutant σ1H-Y313A (Chapter II), it is possible that JAM-A still can bind partially detrimerized σ1. The β-barrel fold of a σ1 monomer appears to be stable, since monomeric mutant σ1H-Y313A has similar structural character as wild-type σ1H when assessed by CD spectroscopy (Chapter II). In the crystal structure of the σ1-JAM-A complex, each JAM-A monomer contacts only a single σ1 monomer (Chapter IV). Thus, if the σ1 tail is structurally intact and properly spaced from the head, JAM-A is likely capable of binding σ1. Furthermore, partial detrimerization of the head may actually result in a higher-affinity interaction due to tighter packing of hydrophobic side chains in the σ1 tail against JAM-A D1 (Chapter IV). Thus, it is possible that a version of σ1 that is partially detrimerized in the head region mediates attachment functions at the cell surface and that exposure to low pH in the endocytic compartment results in full trimerization of σ1. Such a conformational change might permit σ1 to mediate additional functions, perhaps in viral uncoating steps or penetration of endosomal membranes by the viral core.

Clearly, we do not yet fully understand the significance of the aspartic acid sandwich motif in reovirus biology. To investigate the roles of individual residues in the aspartic acid sandwich in reovirus attachment and entry, future studies should be directed toward engineering mutant viruses containing each of the eight individual σ1 point mutations shown in Table V-1. Based on studies reported in Chapter II, most of these mutations (Y313A, Y313F, D346A, D346N, Y347A, and Y347L) are expected to decrease the stability of σ1 trimers, thus altering the efficiency of attachment and entry into target cells. Mutations D345A and D345N could facilitate or even trigger premature σ1 trimer formation at neutral pH. If the Asp345 sandwich is indeed a molecular switch, these two mutations will likely have severe consequences for viral attachment and cell entry. In addition, D345A would render an already-formed trimer less stable. However, as much remains unknown regarding the function of the aspartic acid sandwich motif, the viruses should be used in discovery-based research (i. e., what are the specific alterations in viral replication associated with aspartic acid sandwich mutations?) as well as for testing specific hypotheses.

Mutant viruses should be recovered using plasmid-based reverse genetics (78). If mutant viruses are unable to be rescued easily, the pseudotyping approach described in Chapter IV should be employed. So far, I have recovered Y313A, Y313F, D345A, D345L, D345N, and D345R mutant viruses for use in the proposed studies. Following recovery of the mutant viruses, SPR should be used to assess binding to the extracellular domain of JAM-A (131) and sialoglycophorin (5) following incubation at high, neutral, and low pH. These studies will determine whether pH-mediated conformational

TABLE V-1. Planned mutations at the head trimer interface and their anticipated effects.

Mutation	Name	Anticipated result
Tyr313→Ala	Y313A	Increase solvent access to Asp345, destabilize the σ1 trimer, decrease virus binding to JAM-A and growth in target cells
Tyr313→Phe	Y313F	Slightly destabilize the trimer, but retain all hydrophobic interactions and likely the local structure, which might permit JAM-A binding
Asp345→Asn	D345N	Allow for hydrogen bond formation between Asn345 residues, stabilize the interface independent of pH, permit binding but possibly alter growth or disassembly
Asp345→Ala	D345A	Remove most of the side chain at position 345, also stabilize interface, but less so than D345N
Asp346→Ala	D346A	Remove most of the side chain at position 346, prevent salt bridge interaction with Arg314, destabilize the trimer, decrease growth
Asp346→Asn	D346N	Prevent hydrogen bond interaction with Arg314, destabilize the trimer, but less so than D346A
Tyr347→Ala	Y347A	Increase solvent access to Asp345, destabilize the σ1 trimer, decrease virus binding to JAM-A and growth in target cells
Tyr347→Leu	Y347L	Destabilize the σ1 trimer, but less so than Y347A, might permit JAM-A binding

rearrangements enhance or inhibit receptor binding. To assess the biological relevance of σ1 mutations that alter the architecture at the subunit interface, the capacity of mutant reoviruses to bind the cell surface, internalize, undergo disassembly in the endocytic compartment, and replicate in cultured cells should be determined. Virus binding to HeLa cells should be assessed using flow cytometry (52). To demonstrate specificity for JAM-A and sialic acid, virus binding should be assessed following incubation of cells with JAM-A-specific mAb J10.4 (93), *A. ureafaciens* neuraminidase (Sigma), or both (100). To determine the capacity of mutant reoviruses to be internalized, HeLa cells should be adsorbed with virus particles at 4°C, warmed over a time course, stained with fluor-conjugated reovirus-specific antibodies, and imaged using laser-scanning confocal microscopy (95). To determine the capacity of mutant reoviruses to undergo disassembly in the endocytic compartment, HeLa cells should be adsorbed with ^{35}S-labeled virions at 4°C, warmed over a time course, and lysed in the presence of protease inhibitors. Virions

should be purified from cell lysates by freon extraction and resolved by SDS-PAGE and autoradiography to visualize viral disassembly intermediates (4). Reovirus growth should be quantified by plaque assay (159). These studies may reveal a role for the aspartic acid sandwich motif and provide evidence that σ1 structural rearrangements occur during reovirus entry.

Implications for serotype-specific differences in pathogenesis

Despite the accumulated knowledge about reovirus attachment to cell-surface receptors and internalization into host cells, a precise understanding of the mechanisms underlying the serotype-dependent differences in tropism exhibited by reovirus in the murine CNS remains elusive. Since prototype and field-isolate strains of all three serotypes of reovirus utilize JAM-A as a receptor (6, 20), we previously thought that binding to JAM-A was unlikely to explain serotype-specific differences in reovirus pathogenesis (64). Studies reported in Chapters III and IV defined the nature of T3D σ1-JAM-A interactions and provide clues about JAM-A interactions with T1L and T2J reoviruses. These findings permit proposal of an expanded list of σ1-dependent mechanisms that may contribute to serotype-specific differences in reovirus tropism and disease outcomes. I envision three possibilities. First, it is possible that differences in the interaction kinetics or affinity of σ1 of a particular serotype for JAM-A contribute to differences in tropism. Second, the carbohydrate specificity of a particular strain of reovirus directs infection to specific cells or tissues. A third possibility is that JAM-A may serve as a serotype-independent reovirus receptor at some sites within the host, and other as yet unidentified receptors may confer serotype-dependent tropism in the CNS.

To understand the precise contributions of σ1 to reovirus pathogenesis, these possibilities must be explored.

On a cell in which little JAM-A is expressed, differences in interaction kinetics or affinity might determine whether or not reovirus can infect. While some residues in JAM-A required for T3D reovirus binding appear also to be required for binding by T1L and T2J reoviruses, my studies have provided evidence that the binding sites in JAM-A for these viruses likely differ (Chapter III). Furthermore, sequence analysis reveals that the residues in T3D σ1 that contact JAM-A in the structure of the complex reported in Chapter IV are mostly, but not entirely, conserved among reoviruses of all serotypes (20, 30). Thus, my studies suggest that there are differences in the interacting residues of T1L, T2J, and T3D σ1 and JAM-A (Chapters III and IV), which may alter their interactions. To test the hypothesis that σ1 of each serotype binds JAM-A with different kinetics or affinity, future work should be aimed at expression and purification of the head domains of T1L and T2J σ1 for SPR studies. Sequence alignments suggest that the domain organization and topology are similar for the σ1 proteins of prototype strains (20, 30, 108). Thus, it is likely that expression of sequences of T1L and T2J σ1 analogous to T3D σ1H and using a similar strategy will result in folded, functional protein. However, expression of constructs including longer fragments of the σ1 tail or expression in mammalian cells are reasonable alternatives, should this strategy fail. Interaction kinetics and affinities for JAM-A should be determined for each protein using SPR. Crystallization of the T1L and T2J σ1 head domains alone and in complex with JAM-A D1 should be pursued concurrently to define the structural basis of serotype-specific differences in interactions with JAM-A.

Differential carbohydrate coreceptor utilization also may contribute to serotype-specific differences in reovirus tropism and pathogenesis. In support of this idea, reovirus strains that vary in sialic acid utilization also vary in disease pathogenesis in the hepatobiliary system (7). While there is some evidence that T1L binds sialic acid in intestinal loops (67), the exact nature of the carbohydrate coreceptors used by T1L and T2J remains largely undefined. To identify carbohydrate ligands for these viruses, future studies should be directed toward glycan array screening of prototype strains of reovirus. Glycan arrays have been used to identify carbohydrates bound by influenza virus (16) and minute virus of mice (104) and to differentiate carbohydrates bound by influenza virus hemagglutinins (142, 143). I have initiated studies with Core H of the Center for Functional Glycomics (CFG) at Emory University to define carbohydrate-binding specificities of reovirus prototype strains, T1L, T2J, and T3D (CFG_Request_1305). Virions will be sent to the CFG and tested for binding to printed glycan arrays that include 377 glycan targets. We currently are in the process of optimizing screening conditions using T3D, before collecting data for T1L and T2J. If successful in identifying new carbohydrate coreceptors, these studies will open a new area of research in the reovirus field.

It is possible that high-affinity receptors other than JAM-A exist and contribute to the observed serotype-specific differences in reovirus tropism and pathogenesis. Studies using JAM-A-null mice (24) are currently underway (A. A. R. Antar and T. S. Dermody, unpublished observations). These studies should permit assessment of the role of JAM-A in reovirus pathogenesis and may serve to highlight the existence of additional receptors. However, these animals exhibit alterations in inflammatory and other biological

processes, including dendritic cell trafficking to lymph nodes, neutrophil diapedesis in response to injury, colonic inflammation, and mucosal permeability (24, 34, 84, 172). These altered phenotypes might interfere with assessment of serotype-specific differences in reovirus tropism and pathogenesis conferred solely by σ1. Thus, future studies should be directed towards engineering JAM-A-blind reoviruses that express σ1 from prototype reovirus strains T1L, T2J, and T3D for studies using wild-type mice. Since the D-E loop is central to the interaction of T3D σ1 with JAM-A (Chapter IV), and this region of σ1 is highly conserved among reoviruses of all serotypes (20, 30), the D-E loop should be the initial target in studies to engineer non-JAM-A-binding reoviruses. Plasmids encoding T1L, T2J, and T3D σ1 for reverse genetics have been generated ([78] and T. Kobayashi and T. S. D., unpublished observations). The majority of the D-E loop, including the 3_{10} helix, should be deleted in each construct. This region may be replaced with alternating glycine and serine residues to maintain spacing between β-strands D and E. Mutant viruses should be recovered using plasmid-based reverse genetics (78). If mutant viruses are unable to be rescued easily, the pseudotyping approach described in Chapter IV should be employed. Following verification of loss of JAM-A-binding capacity by SPR and flow cytometry, the recovered viruses should be used to infect newborn mice perorally. Survival studies should be performed, and titers of JAM-A-blind viruses in specific organs should be assessed along with any associated histopathology in comparison to mice infected with viruses expressing wild-type parental σ1. Should these viruses fail to replicate or spread from the primary site of infection, direct inoculation at sites of secondary replication, such as the brain, and binding and infectivity studies using cultures of primary cells from secondary sites of replication (112, 123, 148) should be

pursued. These experiments will define the role of JAM-A in serotype-specific differences in reovirus pathogenesis. If the results provide evidence for the existence of additional receptors, the identity of the receptors should be sought using an expression-cloning approach (6) or by passing lysates of an appropriate cell type over columns using purified JAM-A-blind reoviruses as affinity ligands.

Immunoglobulin superfamily members as virus receptors

Despite an impressive variety in the structures of viral attachment proteins, many viruses use IgSF members as receptors (6, 12, 36, 59, 61, 94, 139, 149-151, 161). In all cases described to date, the virus binds the most membrane-distal, or D1, Ig-like domain of the receptor. Although the residues in the D1 domain required for engagement of individual viruses vary, some viruses, including adenovirus and HIV are known to make contacts in the same region of the D1 domain of an IgSF receptor as the σ1-binding site in the JAM-A D1 domain. Thus, viruses from different families appear to share similar attachment strategies.

Structural analyses have revealed striking similarities between reovirus σ1 and adenovirus fiber (141). Moreover, the receptors for reovirus and adenovirus, JAM-A and CAR, respectively, also share many structural and functional properties. Collectively, these similarities point to an evolutionary relationship in the attachment strategies used by these viruses (140). A comparison of the σ1-JAM-A complex with that of the Ad12 fiber knob in complex with the N-terminal D1 domain of human CAR reveals conserved features, providing additional support for common ancestry between the two viruses ([13] and Chapter IV) (Figure V-1). The overall structures of both complexes are similar.

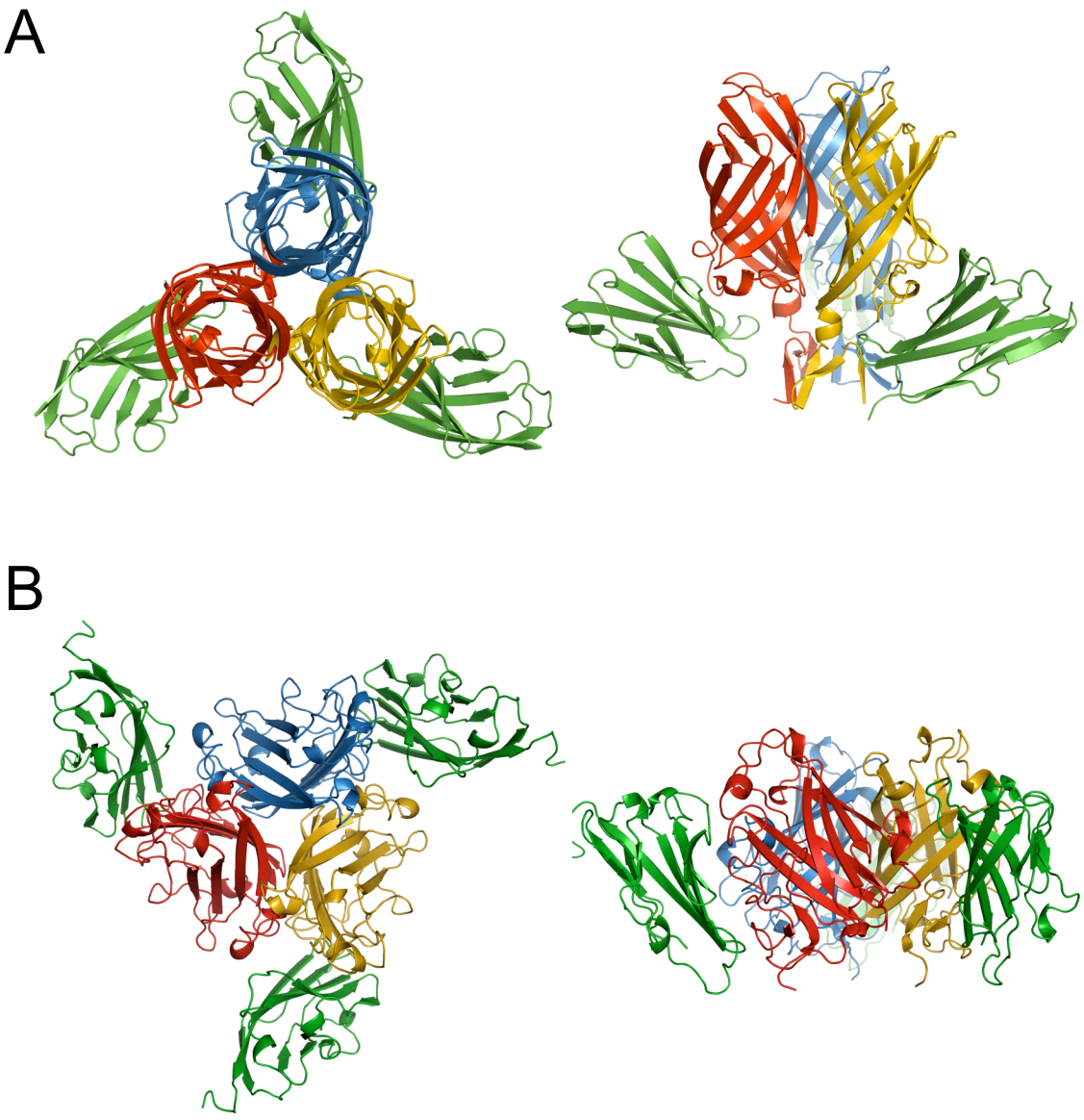

FIGURE V-1. Comparison of reovirus σ1H-JAM-A D1 and adenovirus fiber knob-CAR D1 complexes. (A) Ribbon drawings of the complex between trimeric σ1H and monomeric JAM-A D1, viewed along the three-fold symmetry axis (left) and from the side (right). σ1H monomers are shown in blue, yellow, and red; D1 is shown in green. (B) Ribbon drawings of the complex between trimeric Ad12 knob and monomeric CAR D1, viewed along the three-fold symmetry axis (left) and from the side (right). Knob monomers are shown in blue, yellow, and red; D1 is shown in green. Modified from (13).

Both attachment proteins form trimers that bind three copies of the D1 domain of the receptor. The combined contact area of the σ1-JAM-A complex (1622 $Å^2$) is only slightly larger than the combined area of the CAR-Ad12 fiber complex of 1493 $Å^2$. Similar to the D-E loop in σ1, the A-B loop, which contains several highly conserved contact residues, is thought to "anchor" the virus-receptor complex. Like JAM-A, CAR uses the dimer interface and its top (B-C and F-G loops) to contact its viral ligand. Also like JAM-A, the fiber-contacting residues of CAR are mainly located on and adjacent to β-strands C, C', C'', F and G. However, compared to reovirus σ1, which uses sequences in its head and tail to bind JAM-A, the CAR-binding area in Ad12 fiber is located entirely on the knob and does not include parts of the shaft. In contrast to the σ1-JAM-A complex, in which one JAM-A D1 domain exclusively contacts one σ1 monomer, CAR also has some contacts with a second subunit in the fiber knob. Thus, the two virus-receptor complexes share high similarity in the contact areas formed by the receptors, but the viral attachment proteins engage the receptors using different binding sites.

Structures of the knob domains of Ad37 and canine adenovirus serotype 2 (CAV-2) in complex with CAR D1 also have been solved (133). The overall topology of the interactions is generally conserved among the complex structures, but the number and identity of specific interacting residues at the interfaces differ. Interestingly, contacts between the F-G loop of Ad12 and Ad37 with the C-C' loop of CAR are not observed in the CAV-2-CAR D1 complex structure. Thus, like JAM-A D1, each monomer of CAR D1 contacts a single monomer of CAV-2 knob, rather than interacting with two adjacent monomers in the knob trimer. Furthermore, the affinities of Ad37 and CAV-2 for CAR, as assessed by SPR, also differ, with CAV-2 showing higher affinity for the receptor.

These observations provide further support for the idea that reovirus σ1 may exhibit serotype-specific differences in JAM-A engagement, which may in turn alter interaction kinetics or affinities.

While structurally quite different from σ1, HIV attachment protein gp120 contains β-strands and loops that are involved in receptor engagement (81). HIV gp120 binds the D1 domain of CD4, an IgSF member with four extracellular Ig-like domains (82). Binding buries a combined area of 1544 $Å^2$ (81), which is similar to the buried surface area in the σ1-JAM-A complex (Chapter IV). However, the true contact area is much smaller, due to an unusual symmetry mismatch that results in occlusion of large cavities in the interface (81). Binding of gp120 occurs via residues in β-strands C, C', C'', D, and the DE loop of CD4, a region that overlaps closely with the σ1-binding site in JAM-A ([81] and Chapter IV). However, binding of CD4 appears to induce a conformational change in gp120, whereas binding to JAM-A by σ1 does not. Similar to JAM-A contacts with highly conserved residues in the D-E loop of σ1, key residues in CD4 contact residues in loops of gp120 that are highly conserved among primate immunodeficiency viruses. Contacts between CD4 and gp120 consist primarily of van der Waals interactions and H-bonds, whereas interactions of JAM-A with σ1 are largely polar and involve two salt-bridges in the "upper jaw" and hydrophobic in character in the "lower jaw" ([81] and Chapter IV). Therefore, HIV binds a similar region of CD4 as reovirus does in JAM-A. However, the general topology and side chain contacts that mediate attachment protein-receptor interactions differ in nature from those of reovirus.

Like reovirus, feline calicivirus uses JAM-A as a receptor (96). The D1 domain of feline (f) JAM-A is necessary but not sufficient for virus attachment to cells (114).

Unlike reovirus, calicivirus requires a D2 domain for binding. However, the requirement appears to be steric rather than specific, as the D2 domain of hJAM-A or CAR can substitute for fJAM-A D2 with only a moderate decrease in binding efficiency. Experiments using fJAM-A D1 point mutants indicate that residues residing in loops outside the dimer interface in the D1 domain of fJAM-A are required for calicivirus binding (114). These findings suggest that the calicivirus binding site in fJAM-A is distinct from the reovirus binding site in hJAM-A. However, it is noteworthy that the two fJAM-A residues required for calicivirus attachment, Asp42 and Lys43, possess charged side chains. Thus, similar to reovirus, charge may play an important role in calicivirus binding to fJAM-A.

Contributions of σ1 length and flexibility to viral attachment

The model of σ1-JAM-A interactions at the cell surface presented in Chapter IV (Figure IV-7) suggests that flexibility of the attachment molecule might facilitate receptor engagement. JAM-A- and sialic acid-binding sites are located in the σ1 head (6, 65, 131) and tail (28, 107), respectively. A four-residue linker that connects two β-spiral repeats N-terminal to the σ1 head imparts flexibility between head and tail regions of the molecule (30). Interdomain flexibility might facilitate receptor engagement by permitting structural rearrangements of σ1 that change the relative orientations of the receptor-binding sites, permitting concurrent interaction of the tail with sialic acid and the head with JAM-A. Furthermore, the length of σ1 may contribute to receptor-binding capacity by appropriately spacing the receptor-binding sites to gain access to both JAM-A and carbohydrate coreceptors on the cell surface without steric hindrance from the bulk

of the virus particle. In support of these hypotheses, both flexibility and length of the adenovirus fiber are important mediators of efficient receptor engagement (173). To test these hypotheses, future studies should be directed toward engineering reoviruses that contain insertions or deletions in σ1.

Two reovirus mutants proposed to alter σ1 flexibility, F1 and F2, already have been engineered (Figure V-2). These mutants contain a deletion or tandem duplication of flexible hinge residues Ser291-Pro294 in the β-spiral region of σ1, which is anticipated to decrease or increase flexibility, respectively, between the JAM-A- and SA-binding regions of the molecule. Mutants that affect the length of σ1 also should be generated by altering the predicted α-helical and β-spiral regions of the molecule. I propose the generation of 4 such mutants (Figure V-2). In L1, the N-terminal 7 predicted β-spiral repeats should be deleted. This deletion should decrease the overall length of σ1 and remove the predicted SA-binding site, while maintaining flexibility N-terminal to the C-terminal β-spiral repeat of the molecule. In L2, the central 10 heptad repeats of the tail should be removed. This deletion is expected to decrease the length of σ1 by removing 20 α-helical turns, which are predicted to account for about one-third of the length of the protein. Importantly, this deletion will maintain the integrity of the receptor-binding sites, the N-terminal virion-insertion domain, and the region of the molecule that links the predicted α-helix to the predicted β-spiral region. In L3, the majority of the predicted α-helix and β-spiral regions of the molecule should be deleted. This deletion will shorten σ1 by more than two-thirds and remove the sialic acid-binding region. The L1, L2, and L3 deletions might decrease the capacity of σ1 to bind JAM-A due to steric hindrance from the bulk of the virion as it encounters other cell-surface structures. In L4, the

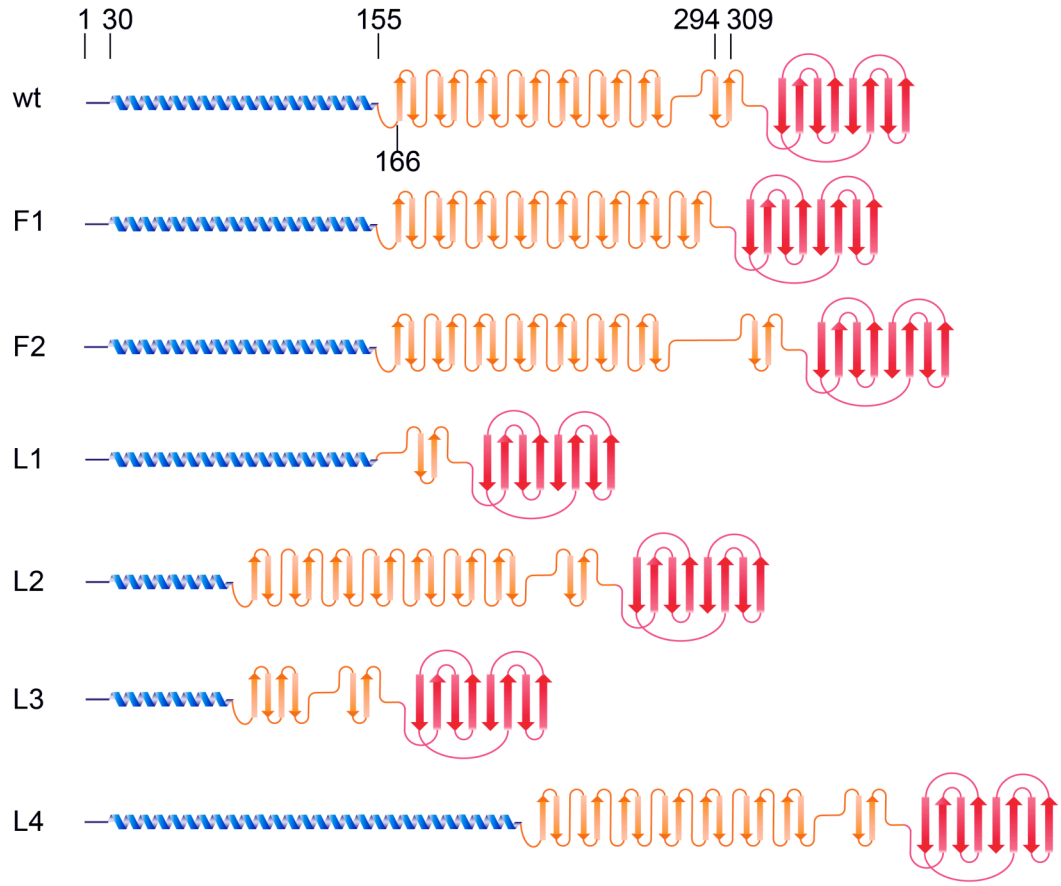

FIGURE V-2. Design of σ1 constructs differing in length and flexibility. The σ1 head is shown in red; the 8 β-spiral repeats are shown in orange; and the α-helical coiled coil is shown in blue. Amino acid positions refer to wild-type T3D σ1.

predicted α-helical region of the protein should be extended by tandemly duplicating 10 heptad repeats. This insertion is expected to increase the length of the molecule by about 40% without directly altering its flexibility. It is possible that such an alteration will increase the capacity of the attachment protein to access receptors on the cell surface and thus enhance viral avidity.

Deletion mutations should be introduced into full-length σ1 using site-directed mutagenesis (131), whereas insertion mutations should be engineered using SOE PCR

(28). Mutant reoviruses should be recovered by reverse genetics (78). If mutant viruses are unable to be easily rescued, a pseudotyping approach should be employed or full-length wild-type and mutant σ1 proteins, along with outer-capsid proteins σ3 and μ1, should be expressed in insect cells using recombinant baculovirus and recoated onto reovirus core particles (27).

To quantify interactions of mutant forms of σ1 with JAM-A and sialic acid, SPR should be used to assess mutant reovirus binding to the JAM-A extracellular domain (131) and sialoglycophorin (5). These experiments will provide an assessment of the interaction kinetics and avidity of reoviruses with wild-type and mutant forms of σ1 for the receptors JAM-A and sialic acid individually. To assess the biological relevance of mutations that alter the flexibility and length of σ1, the capacity of mutant reoviruses to attach, internalize, and infect cultured cells should be determined, as described for reovirus mutants in the aspartic acid sandwich. These studies will enhance an understanding of the structural features in σ1 that contribute to attachment and entry steps and provide a platform for engineering reoviruses with altered attachment properties for oncolytic and vaccine delivery purposes.

Reovirus vector retargeting

Significant efforts are being made to exploit viruses for medical applications, such as gene delivery, oncolysis, and vaccination (92, 119). The capacity to redirect viral vectors to specific target cells through modification of receptor-binding capacity provides a powerful approach for delivery of an engineered viral payload to the appropriate target site. For example, retargeting adenovirus from cells expressing CAR to cells expressing

JAM-A has been accomplished using a chimeric adenovirus that expresses reovirus σ1 in place of adenovirus fiber (100). Replacement of the CAR-binding adenovirus fiber knob with a single-chain TCR molecule specific for a melanoma-associated antigen results in efficient killing of target tumor cells *in vitro* (132). Development of a plasmid-based reverse genetics system for reovirus (78), coupled with the oncolytic potential of this virus (53, 153), underscores the importance of a precise understanding of the basis of σ1 interactions with cellular receptors. In Chapter IV, I reported the recovery and characterization of reoviruses with mutations in the JAM-A-binding site. These studies provide proof-of-principle that reovirus mutants with structure-guided alterations in receptor-binding capacity can be engineered. This achievement represents a first step towards designing viruses containing modified σ1 proteins to target specific sites in the host based on receptor utilization.

My findings also highlight limitations of our current reverse genetics system. Based on the low rescue titers of the T380A/D382A and W421V viruses, which likely bind poorly to JAM-A (Table IV-2), sialic acid binding alone does not appear to permit efficient rescue. Optimization of expression of the enzymes that mediate transcription of reovirus cDNAs, a reduction in the number of plasmids, or enhancement of plasmid uptake in L cells might serve to increase the efficiency of rescue for all reovirus mutants. In the case of mutants with alterations in tropism, a pseudotyping approach using transient or stable expression of wild-type σ1 protein in L cells should be employed to enhance recovery of viruses that have been engineered to be receptor-blind or to bind alternative receptors. Rescue of the W421V mutant reovirus using this strategy, described in Chapter IV, indicates a potential for success.

Future studies should be directed toward recovery of reoviruses with altered tropism. A logical first step would be to substitute the reovirus σ1 head domain with the adenovirus fiber knob. Reovirus σ1 and adenovirus fiber are both filamentous trimeric molecules that extend from icosahedral virion vertices. The slender tail of each attachment molecule contains triple β-spiral repeats, while the head is composed of eight β-strands arranged in an identical topological order (30, 158). These structural similarities suggest that substitution of the σ1 head domain with fiber knob is likely to result in a folded, functional, chimeric attachment molecule. Reovirus and adenovirus receptors, JAM-A and CAR, respectively, each localize to tight junctions in epithelial and endothelial cells, contain two extracellular Ig-like domains, and form similar dimers (141). Furthermore, both viruses use integrins as internalization receptors (95, 168) and traffic to the endocytic compartment for disassembly (60, 146). However, the integrins required for efficient internalization differ between the two viruses. Binding to cellular moieties may serve solely to tether the viruses to the cell surface, to initiate intracellular signaling required to recruit the internalization machinery, or both properties. Reovirus currently is being employed in Phase I clinical trials to treat malignant gliomas (53). The capacity to retarget reovirus to specific receptors that are highly expressed on tumor cells may enhance its efficacy as an oncolytic agent. While CAR expression is down-regulated in some tumors, high levels of CAR are observed in many osteosarcomas (62, 75). Substitution of the σ1 head with fiber knob will concurrently permit us to distinguish between the attachment and signaling functions of JAM-A in reovirus infectivity, provide clues about whether the attachment receptor used by a virus dictates

its internalization receptor, and determine whether reovirus can be retargeted to alternate receptors to enhance its therapeutic potential.

Sequences encoding the Ad5 knob domain should be amplified by PCR and ligated into a plasmid encoding a reovirus S1 transcript using SOE PCR. Recombinant viruses should be recovered using plasmid-based reverse genetics in the context of rsT3D/S4-GFP, an assembly-defective virus that encodes GFP in place of reovirus major outer-capsid protein σ3 (78), and amplified in σ3-expressing L cells prior to use in binding or single-cycle infectivity assays. This approach diminishes biosafety concerns. Thus, following attachment and entry via a productive pathway, the viral core particle will generate transcripts, and GFP will be expressed as an indicator of viral infection. Infectious progeny containing chimeric attachment proteins will not assemble and thus not propagate. If recovery of chimeric viruses is difficult, a pseudotyping strategy should be employed or additional constructs encompassing progressively longer portions of the fiber tail, up to but not including the virion-insertion domain should be generated.

Binding and infectivity studies using the recovered chimeric viruses initially should be performed using CHO cells that express full-length JAM-A or CAR. CHO cells are poorly permissive for binding and infection by both reovirus and adenovirus but are rendered permissive following expression of JAM-A or CAR, respectively (12, 52). Similar studies also may be performed using HeLa cells, which are permissive for both reovirus and adenovirus, following treatment with mAbs J10.4 (93) and RmcB (68), which block reovirus binding to JAM-A and adenovirus binding to CAR, respectively. Expression of GFP will indicate that the virus has been internalized via a productive pathway. If viruses expressing σ1/knob chimeras are able to bind cells expressing CAR,

but do not express GFP following adsorption, the step in the virus life cycle that is blocked should be identified. These experiments will test the exciting possibility that reovirus has evolved to use JAM-A both as an attachment receptor and to exploit a specific function of the receptor for viral replication. The capacity of viruses expressing wild-type σ1 and σ1/knob chimeras to bind and infect osteosarcoma cell lines U2OS and SaOS2, which express high levels of CAR (75), also should be assessed, to determine whether knob-expressing reoviruses have the potential to be employed as highly specific oncolytics.

Conclusions

My dissertation research has enhanced an understanding of features of reovirus attachment protein σ1 that confer functionality, defined the molecular basis σ1 interactions with JAM-A, and provided a platform for engineering reoviruses with altered tropism. This work raises several important questions that will collectively contribute to a general understanding of virus-receptor interactions. First, analysis of the aspartic acid sandwich motif may provide new insights into the relevance of metastable multimerization domains and pH in nonenveloped virus attachment and entry. Second, studies of JAM-A engagement by related, yet distinct ligands (the head domains of the three σ1 serotypes) will clarify common features of protein-protein interactions involving the Ig superfamily of adhesion molecules. Third, identification of novel carbohydrate coreceptors and defining infection outcomes *in vivo* using JAM-A-blind reoviruses will improve an understanding of the roles of receptor specificity in viral pathogenesis. Finally, analysis of mutant reoviruses with alterations in topological placement, number,

and type of receptor-binding domains will lend general insights into the biomechanics of cell-surface engagement by multi-valent ligands. Thus, knowledge gained from ongoing research on mechanisms of reovirus attachment should inform a more thorough understanding of the initial steps in viral infection, contribute new insights into the function of virus-receptor interactions in viral disease, and move the field towards targeting reovirus for oncolytic therapy and vaccine applications.

CHAPTER VI

DETAILED METHODS OF ANALYSIS

Cells, viruses, and antibodies

Spinner-adapted murine L cells were maintained in Joklik's minimal essential medium supplemented to contain 5 % fetal bovine serum, 2 mM L-glutamine, 100 units/ml penicillin, and 100 μg/ml streptomycin. CHO cells were maintained in Ham's F-12 medium supplemented to contain 10 % fetal bovine serum, 2 mM L-glutamine, 100 units/ml penicillin, and 100 μg/ml streptomycin.

Reovirus strains T1L, T2J, and T3D are laboratory stocks originally obtained from Dr. Bernard Fields. Strain T3SA- is a reassortant strain containing the *S1* gene of T3C44, which does not bind sialic acid (29, 39), and the remaining nine genes of T1L (5). Reovirus strain rsT3D-σ1T249I was engineered using plasmid-based reverse genetics (78). Titers of all virus stocks were determined by plaque assay using L-cell monolayers (159). Reoviruses were purified by cesium chloride-gradient centrifugation from infected L cells as described (55). Particle concentrations were determined by spectrophotometry at 260 nm using a conversion factor of 2.1×10^{12} particles/ml/A_{260}. Attenuated vaccinia virus strain rDIs-T7pol expressing T7 RNA polymerase was propagated in chick embryo fibroblasts (69).

The combined T1L/T3D antiserum (167) used for detection of reovirus particles and viral protein products in infected cells was clarified by pre-adsorption on CHO cells. Alexa Fluor 488-conjugated goat anti-rabbit or goat anti-mouse IgG were obtained from

Molecular Probes (Invitrogen). hJAM-A-specific monoclonal antibody J10.4 was provided by Dr. Charles Parkos (Emory University).

Expression and purification of T3D σ1H

Nucleotide sequences corresponding to residues 293-455 of T3D σ1 (σ1H) were amplified by PCR and ligated into pGEX4T-3 (GE Healthcare) for bacterial transformation. D345N and Y313A mutations were engineered in the plasmid using the QuikChange Site-Directed Mutagenesis Kit (Stratagene) according to the manufacturer's instructions. *Escherichia coli* strain BL21 (DE3) pLysS (Novagen) transformed with plasmids encoding GST-T3D σ1H constructs were cultured in Luria-Bertani broth, and protein expression was induced with 0.2 mM isopropyl-β-D-thiogalactoside (IPTG, GE Healthcare) at 25°C for 16 h. Bacteria were harvested by centrifugation, solubilized in 50 mM Tris, pH 7.8, 3 mM EDTA, 1% Triton X-100 (TX-100), 2 mM beta-mercaptoethanol (βME), 1 mM phenylmethylsulfonyl fluoride (PMSF), and 100 μg/ml lysozyme, and lysed by sonication. The clarified supernatant was passed over a 5 ml GSTrapFF column (GE Healthcare), which was washed with Buffer 1 (50 mM Tris pH 7.5, 3 mM EDTA), Buffer 2 (20 mM $MgSO_4$ and 10 mM ATP in Buffer 1), and Buffer 3 (1 M NaCl in Buffer 1). Soluble wild-type or mutant σ1H domain was liberated from the glutathione resin by controlled tryptic protease treatment at 4ºC overnight and purified using MonoQ anion-exchange chromatography (GE Healthcare) with an increasing gradient of NaCl in 20 mM 4-(2-hydroxyethyl)-1-piperazineethanesulfonic acid (HEPES), pH 7.1.

T3D σ1H protein crystallization and data collection

Purified wild-type or mutant T3D σ1H was subjected to size-exclusion chromatography in 20 mM Tris, pH 7.5, 100 mM NaCl, and 0.01 % sodium azide and concentrated using Millipore 5 MWCO filters to 13.6 mg/ml, as assessed by direct measurement of absorbance at 260 and 280 nm using the relationship: concentration [mg/ml] = $(1.55 \times A_{280nm}) - (0.76 \times A_{260nm})$, since the T3D σ1H does not react linearly with either Bradford or Lowry dyes (data not shown). Crystals of native σ1 protein were grown from 10-12% PEG 8K, 0.2 M magnesium sulfate, and 0.1 M sodium cacodylate, pH 6.9 by mixing an equal amount of protein and precipitant solution. σ1H-D345N was concentrated to 8 mg/ml, and crystals were grown using the same conditions used to cultivate crystals of the wild-type protein, but with 20% PEG 8K. Crystals were flash-frozen using glycerol as cryoprotectant. Data from native crystals were collected at the Brookhaven National Laboratory Synchrotron (beamline X29 features high-flux radiation and ADSC Quantum-315 CCD detector). Data for σ1H-D345N crystals were collected at the X6S beamline of the Swiss Light Source (Villigen, Switzerland) using a MarCCD detector. Both data sets were collected from single crystals and processed with HKL2000 (116).

T3D σ1H structure determination

Crystals of wild-type σ1H belong to space group $P2_1$ (a= 83.93 Å, b= 51.38 Å, c= 108.87 Å, β= 95.66º) and contain six molecules, forming two complete trimers, in the asymmetric unit. The structure was determined by molecular replacement using the trimeric σ1 head domain (30) as a search model in AMORE (106). Alternating rounds of

model building and refinement were performed initially using O (73) and CNS (18), respectively. The programs Coot (51) and Refmac5 (23) were used to refine the model. σ1H-D345N also formed crystals that belong to space group $P2_1$, with very similar unit cell dimensions (Table II-1). The structure of this protein was solved and refined to 1.85 Å using Coot and Refmac5. Atomic coordinates and structure factors have been deposited with the ProteinDataBank with the accession codes 2OJ5 and 2OJ6.

Expression and purification of soluble JAM-A constructs

Soluble ectodomains of wild-type and point-mutant hJAM-A constructs were fused to an amino-terminal GST affinity tag via a thrombin cleavage site and expressed and purified as described (122). Nucleotide sequences corresponding to residues 27-233 of wild-type hJAM-A (D1D2) were cloned by PCR, digested with Bam HI and Xho I, and ligated into pGEX-4T-3 (GE Healthcare) for bacterial transformation. Point mutants of hJAM-A were engineered using the QuikChange Site-Directed Mutagenesis Kit. Sequences of primers used to engineer point mutations in hJAM-A are listed in Table III-1. A GST fusion with the D1 domain of hJAM-A was engineered by inserting a Xho I or Bam HI restriction site into the D1/D2 linker of hJAM-A in pGEX-4T-3 using site-directed PCR mutagenesis. Digestion with Xho I or Bam HI followed by ligation eliminated the D2 domain (residues 131-233) or D1 domain (residues 27-131), respectively, and fused the remaining domain to GST. *Escherichia coli* strain BL21 (DE3) (Novagen) transformed with plasmids encoding GST-JAM-A constructs were cultured in 1 L Luria-Bertani broth at 37°C with shaking. Protein expression was induced with 0.2 mM IPTG (GE Healthcare) for 4-6 h. Bacteria were harvested by centrifugation,

solubilized in phosphate-buffered saline (PBS) plus 1% TX-100, 2 mM βME, 1 mM PMSF, and 100 μg/ml lysozyme, and lysed by sonication. The clarified supernatant was passed over a 5 ml GSTrapFF column (GE Healthcare), which was washed with PBS, PBS + 150 mM NaCl, and PBS + 0.1 % TX-100 + 100 mM NaCl . GST-hJAM-A fusion proteins were liberated from the glutathione resin using 10 mM reduced glutathione in PBS, pH 8.0. Soluble wild-type and point-mutant hJAM-A ectodomains were liberated from the glutathione resin by incubation with 100 U/ml thrombin (Sigma) at room temperature overnight.

Expression and purification of a σ1H-D1 complex

Sequences corresponding to residues 28-129 of wild-type human JAM-A (D1) were amplified from a plasmid encoding full-length JAM-A (122) and cloned into pGEX-4T-3 (GE Healthcare) using the BamHI and XhoI restriction sites. The D1 E121A mutation was engineered from this construct using the QuikChange Site-Directed Mutagenesis Kit. Expression of GST-D1 fusion proteins was induced in 1 L Luria Broth (Sigma-Aldrich) with 0.2 mM IPTG in *Escherichia coli* strain BL21 (DE3) pLysS (Novagen) at 25°C for 16 h. Bacteria were harvested by centrifugation, resuspended in 50 mM Tris pH 7.5, 50 mM NaCl, 3 mM EDTA, 1% Triton X-100, 2 mM βME, 1 mM PMSF, and 100 μg/ml lysozyme, sonicated with 50% duty-cycle using a Branson Digital Sonifier 250, and centrifuged at 15,000 x *g*. The clarified supernatant was passed over a 5 ml GSTrapFF column (GE Healthcare), which was washed with Buffer 1, Buffer 2, and Buffer 3. D1 was cleaved from GST by overnight incubation with 150 units of thrombin (GE Healthcare) in 20 mM Tris pH 7.8, 2.5 mM $CaCl_2$, 150 mM NaCl. Pure

protein was obtained after elution with buffer. T3D σ1H was expressed and purified as described (131), except that induction was achieved using 0.4 mM IPTG, and bacteria were lysed using a high-pressure homogenizer (Avestin EmulsiFlex). Purified σ1H and D1 were mixed at a ratio of 1:1.2 and incubated at 4°C for 30 min. Complexes were separated from excess D1 by gel filtration in 20 mM Tris pH 7.5, 100 mM NaCl with a Superdex 75 column (GE Healthcare).

σ1H-D1 complex crystallization and data collection

The σ1H-D1 complex was concentrated to 4 mg/ml according to direct measurement of A_{280} and A_{260} (concentration [mg/ml] = 1.55 x A_{280} – 0.76 x A_{260}). Crystals were initially obtained by mixing equal volumes of protein and 0.1 M N-cyclohexyl-2-aminoethanesulfonic acid (CHES), pH 9.5, 30% polyethylene glycol 3000 (Wizard I Screen, Emerald BioSystems) at 20°C. Larger crystals were grown upon replacement of polyethylene glycol 3000 with polyethylene glycol 3350 and with streak seeding using cat whiskers. Crystals were flash-frozen with glycerol as cryoprotectant. Data were collected at the X06SA beamline of the Swiss Light Source (Villigen, Switzerland) using a MarCCD detector. The crystals were extremely thin; they had to be exposed for 10 seconds to an unattenuated beam to yield any diffraction beyond 3.5 Å and suffered severe radiation damage after only a few images were taken. We therefore collected data from several dozen crystals to obtain a complete data set. A total of 286 images were collected, and 85 of these were used to assemble the final data set. Data were integrated and reduced with HKL (116).

Since the radiation damage led to dramatic decreases in spot intensity for many reflections at higher resolution, we evaluated all processed data files with an in-house program, calculating the signal-to-noise ratio (I/σI) according to resolution bins for each frame. We then applied individual resolution cut-offs to each frame at the resolution bin in which I/σI dropped below 1.4. This procedure significantly improved the overall quality of the data set.

σ1H-D1 complex structure determination and refinement

Crystals belong to the orthorhombic space group $P2_12_12$ (a = 105.74 Å, b = 123.78 Å, c = 131.02 Å). The asymmetric unit consists of two σ1H trimers, each complexed with three D1 monomers. The structure of the complex was determined by molecular replacement with PHASER in CCP4 (23) using the trimeric T3D σ1 head structure (131) and the monomeric D1 domain of the hJAM-A structure (122) as search models. Molecular replacement solutions for two σ1H trimers in the asymmetric unit were readily obtained and resulted in an overall R-factor of 40.1% (30-3.2 Å). Attempts to locate the D1 domains by molecular replacement yielded ambiguous results. However, $2F_{obs}$-F_{calc} and F_{obs}-F_{calc} electron-density maps, calculated using phases obtained from the two σ1H trimers, which account for 61% of the protein atoms present in the crystal, clearly revealed the position and location of the six D1 domains. Adding the D1 domains to the structure reduced the overall R-factor to 34.7% (30-3.2 Å).

The structure was refined using CNS (18) and Coot (51). Electron-density maps were improved using non-crystallographic symmetry averaging (77) and data sharpening (56) by adding an overall B-factor of -70 $Å^2$ to the observed structure factors with CAD

in CCP4 (23). Progress of the refinement was periodically evaluated by calculation of composite annealed omit maps (14) to confirm the electron density for several protein side chains. Contact areas were calculated with AREAIMOL (23) as buried surface areas upon complex formation using a point density/$Å^2$ of 10 and a solvent molecule radius of 1.4 Å.

Gel filtration chromatography

For studies of purified hJAM-A extracellular domains (Chapter III), gel filtration was performed by loading approximately 0.5 mg of each protein onto a Superdex 75 column mounted on a BioLogic HR Workstation (BIO-RAD). Proteins were resolved in 20 mM Tris, pH 7.5, 100 mM NaCl, 0.01% sodium azide. Additional gel filtration studies of the hJAM-A extracellular domain and σ1H were performed using a Superdex 75 column mounted on a SMART system (GE Healthcare). σ1H (10 μg) in 20 mM HEPES, pH 7.1 and wild-type or mutant forms of the hJAM-A extracellular domain (12.74 μg) in PBS were mixed and incubated at 0°C for 40 min prior to gel filtration. Mixtures of proteins or individual proteins were resolved in 20 mM Tris, pH 7.5, 100 mM NaCl.

For studies of the σ1H-D1 complex (Chapter IV), analytical-scale gel filtration was performed using a SMART system (GE Healthcare) with a Superdex 75 column. Stability of the JAM-A homodimer was determined by incubating purified JAM-A D1 and D1D2 (122) in a molar ratio of 1:1 in 20 mM HEPES, 100 mM NaCl, pH 7.4 at 4°C or 22°C for 5 or 60 min. Effects of pH on complex stability were investigated by concentrating purified σ1H, wild-type D1, monomeric D1 E121A (65), and the σ1H-D1

complex to 10% of the original volume using Millipore 5,000 MWCO filters. Samples were diluted in 20 mM citrate buffers adjusted pH 4.0, 4.5, or 5.0 or 20 mM HEPES, pH 7.4 and re-concentrated. This procedure was repeated five times. Gel filtration was performed using the respective buffer, containing 100 mM NaCl, for each sample.

GST capture assays

Swelled, washed, glutathione-coated beads (Sigma) were incubated with 20 μg of purified GST or GST-hJAM-A fusion proteins and diluted in 200 μl PBS plus 1% Tween 20 (PBST) at 4°C for 1 h. Glutathione beads with captured GST fusion proteins were washed twice with PBST and incubated with 10 μg purified T3D σ1 head domain in 200 μl PBST at 4°C for 1 h. Following two additional washes, buffer was aspirated carefully, and beads with bound proteins were resuspended in 30 μl sample buffer (313 mM Tris, pH 6.8, 4% SDS, 10% βME, 20% glycerol, 0.01% bromophenol blue). Samples (15 μl/lane) were loaded into wells of a SDS 4-20% continuous gradient polyacrylamide gel and electrophoresed at 120 V until the dye front reached the bottom of the gel. Proteins were visualized by staining with Coomassie brilliant blue.

Assessment of reovirus-JAM-A interactions using SPR

A BIAcore CM5 chip (Biacore/GE Healthcare) was coated with mouse ascites containing monoclonal GST-specific antibody (Sigma) to ~ 1800-2000 RU of IgG by amine coupling. Purified GST or wild-type or mutant GST-hJAM-A ectodomain fusion proteins at a concentration of 2 μM in HEPES-buffered saline (HBS), pH 7.0 were captured by injection across individual flow cells of an antibody-coated chip for 3 min at

30 μl/min using a BIAcore 2000 (Biacore/GE Healthcare). Purified σ1H or purified reovirus (5×10^{12} particles/ml) was injected across the conjugated chip surface at 30 μl/min. Following σ1 binding, chip surfaces were regenerated with a 20 μl pulse of 10 mM glycine, pH 2.5. Affinity constants for σ1H binding to hJAM-A were determined using separate k_{on} and k_{off} nonlinear regression with BIAevaluation 3.0 software (Biacore/GE Healthcare), assuming a 1:1 Langmuir binding model (74). Molar concentrations of σ1 constructs were calculated based on σ1 forming a homotrimer (30, 131).

Flow cytometric analyses of receptor expression and virus binding

CHO cells (10^6) were transiently transfected with receptor-encoding plasmids using Lipofectamine and PLUS reagent (Invitrogen) according to the manufacturer's instructions and incubated for 24 h to allow receptor expression. Cells were detached from plates by incubation with 20 mM EDTA in PBS and incubated with hJAM-A-specific monoclonal antibody J10.4 at 10 μg/ml or adsorbed with reovirus (10^5 particles/cell) on ice for 1 hr. Virus-adsorbed cells were washed with PBS containing 0.1% bovine serum albumin (PBS/BSA) and incubated with clarified, combined T1L/T3D antiserum (11) at 1:1000 dilution on ice for 1 h. Samples were washed with PBS/BSA and incubated with Alexa Fluor 488-conjugated goat anti-rabbit or goat anti-mouse IgG (Invitrogen) at a 1:1000 dilution on ice for 1 hr. Cells were washed twice with PBS/BSA and fixed with 4% paraformaldehyde in PBS. Cells were analyzed for antibody or virus binding using a FACSCalibur (BD Biosciences) or FACSCanto II Flow Cytometry System (BD Biosciences). For quantification, data were collected from three

independent experiments per virus and analyzed for JAM-A expression and reovirus binding using WinMDI ver2.8 (Scripps Research Institute).

Transient transfection and infection of CHO cells

Point mutations were engineered into full-length hJAM-A in pcDNA3.1 (122) using the QuikChange Site-Directed Mutagenesis Kit and the same primers used to engineer mutations in the hJAM-A extracellular domain in pGEX-4T-3 (Table III-1). CHO cells (2×10^5) were transiently transfected with receptor-encoding plasmids using Lipofectamine and PLUS reagent (Invitrogen) as described (122) and incubated for 24 h to allow receptor expression. Cells were infected with reovirus at multiplicities of infection of 1 (T1L), 5 (T2J), and 10 (T3SA-) plaque forming units/cell and incubated at 37ºC for 18-20 h. Infected cells were processed for indirect immunofluorescence as described (5). Images were captured at 200X magnification using a Zeiss Axiovert 200 microscope. For each experiment, three fields of view were scored from three independently transfected wells. Data were collected from three independent experiments.

Plasmid-based reovirus reverse genetics

The parental *S1* gene used for studies of reovirus interactions with JAM-A encodes a σ1 molecule that is identical to T3D σ1 with the exception of a threonine-to-isoleucine substitution at position 249, which renders the σ1 protein resistant to proteolytic cleavage (78). Substitution mutations were engineered in pBacT7-S1T3D T249I (78) using the QuickChange site-directed mutagenesis kit (Stratagene).

Reoviruses were rescued as described (78). L cells were infected with an assembly-defective vaccinia virus (DIs-T7 RNA pol) that hyperexpresses T7 polymerase 1 h prior to transfection with ten plasmids encoding RNA molecules identical to each of the reovirus transcripts. Rescued viruses were recovered from cell-culture supernatants 5-6 d post-transfection by plaque assay. Viruses were amplified using L-cell monolayers. Confirmation of mutations in the *S1* gene of recombinant viruses was performed using the OneStep RT-PCR kit (Qiagen), gene-specific primer sets, and viral dsRNA extracted from infected L cells as template. Purified PCR products were directly subjected to sequence analysis. T3D σ1 protein was expressed for pseudotyping purposes by co-transfecting 2 mg of pCAG-S1T3D during rescue. The pCAG-S1T3D construct was generated by subcloning the T3D *S1* open reading frame from pBacT7-S1T3D (78) into the EcoRI-KpnI site of pCAGMCS, which was derived by modifying the multiple-cloning site of pCAGGS (111).

Viral growth in L929 cells

L cells were adsorbed with virus at an MOI of 0.01 PFU/cell. Following incubation at room temperature for 1 hr, complete medium was added, and cells were incubated at 37°C for 0, 24, 48, 72, or 96 h. Cells were frozen (-80°C) and thawed twice, and viral titers were determined by plaque assay (159). Data were collected from three independent experiments per time point per virus.

Statistical analysis

Mean values were compared from at least three independent experiments using the unpaired Student's *t* test as applied using Microsoft Excel. *P* values of less than 0.05 were considered statistically significant.

Preparation of figures

Structural figures were prepared using PyMOL (38), RIBBONS (21), and GRASP (110).

APPENDIX A

ATTACHMENT AND CELL ENTRY OF MAMMALIAN ORTHOREOVIRUS

Kristen M. Guglielmi*, Elizabeth M. Johnson*, Thilo Stehle, and Terence S. Dermody

Current Topics in Microbiology and Immunology. 309:1-38;2006

*Authors contributed equally to this manuscript

CTMI (2006) 309:1–38

Attachment and Cell Entry of Mammalian Orthoreovirus

K. M. Guglielmi[1,3] · E. M. Johnson[1,3] · T. Stehle[2,3,4] · T. S. Dermody[1,3,4] (✉)

[1]Departments of Microbiology and Immunology, and Pediatrics[4], Vanderbilt University School of Medicine, Nashville, TN 37232, USA

[2]Interfakultäres Institut für Biochemie, Eberhard-Karls Universität Tübingen, 72076 Tübingen, Germany

[3]Lamb Center for Pediatric Research, D7235 MCN, Vanderbilt University School of Medicine, Nashville, TN 37232, USA
terry.dermody@vanderbilt.edu.

Abstract Mammalian orthoreoviruses (reoviruses) serve as a tractable model system for studies of viral pathogenesis. Reoviruses infect virtually all mammals, but cause disease only in the very young. Prototype strains of the three reovirus serotypes differ in pathogenesis following infection of newborn mice. Reoviruses are nonenveloped, icosahedral particles that consist of ten segments of double-stranded RNA encapsidated within two protein shells, the inner core and outer capsid. High-resolution structures of individual components of the reovirus outer capsid and a single viral receptor have been solved and provide insight into the functions of these molecules in viral attachment, entry, and pathogenesis. Attachment of reovirus to target cells is mediated by the reovirus σ1 protein, a filamentous trimer that projects from the outer capsid. Junctional adhesion molecule-A is a serotype-independent receptor for reovirus, and sialic acid is a coreceptor for serotype 3 strains. After binding to receptors on the cell surface, reovirus is internalized via receptor-mediated endocytosis. Internalization is followed by stepwise disassembly of the viral outer capsid in the endocytic compartment. Uncoating events, which require acidic pH and endocytic proteases, lead to removal of major outer-capsid protein σ3, resulting in exposure of membrane-penetration mediator μ1 and a conformational change in attachment protein σ1. After penetration of endosomes by uncoated particles, the transcriptionally active viral core is released into the cytoplasm, where replication proceeds. Despite major advances in defining reovirus attachment and entry mechanisms, many questions remain. Ongoing research is aimed at understanding serotype-dependent differences in reovirus tropism, viral cell-entry pathways, the individual and corporate roles of acidic pH and proteases in viral entry, and μ1 function in membrane penetration.

1 Introduction

Mammalian orthoreoviruses (called reoviruses here) serve as highly tractable models for studies of viral pathogenesis. Reoviruses are nonenveloped, icosahedral viruses that contain a genome of ten double-stranded (ds) RNA gene segments. There are three reovirus serotypes, which can be differentiated by the capacity of anti-reovirus antisera to neutralize viral infectivity and inhibit hemagglutination [120, 126]. The three serotypes are each represented by a prototype strain isolated from a human host: type 1 Lang (T1L), type 2 Jones (T2J), and type 3 Dearing (T3D). Reoviruses have a wide geographic distribution, and virtually all mammals, including humans, serve as hosts for infection [146]. However, reovirus is rarely associated with disease, except in the very young [89, 142].

Newborn mice are exquisitely sensitive to reovirus infection and have been used as the preferred experimental system for studies of reovirus pathogenesis [151]. Following oral or intramuscular inoculation of newborn mice, strains of serotype 1 and serotype 3 reoviruses invade the central nervous sys-

tem (CNS), yet by different routes and with distinct pathologic consequences. Serotype 1 reovirus spreads to the CNS hematogenously and infects ependymal cells [147, 155], resulting in hydrocephalus [153]. In contrast, serotype 3 reovirus spreads to the CNS by neural routes and infects neurons [99, 147, 155], causing lethal encephalitis [142, 153]. Studies using T1L x T3D reassortant viruses have shown that the pathways of viral spread [147] and tropism for neural tissues [45, 155] segregate with the viral S1 gene, which encodes attachment protein σ1 [83, 154]. T1L x T3D reassortant viruses also were used to demonstrate that serotype-specific differences in virus binding to primary cultures of ependymal cells and neurons are determined by the S1 gene [45, 141]. These studies suggest that σ1 dictates the CNS cell types that serve as targets for reovirus infection, presumably by its capacity to bind to receptors expressed by specific CNS cells.

In addition to conferring viral attachment, engagement of reovirus receptors also induces postbinding signaling events that may influence disease pathogenesis. Reovirus induces apoptosis in cultured cells [32, 36, 119, 148] and in vivo [38, 109]. Strain T3D induces apoptosis to a greater extent than strain T1L in murine L929 (L) cells [148], Madin-Darby canine kidney cells [119], and human HeLa cells [34]. Differences in the capacity of these strains to induce apoptosis are determined primarily by the S1 gene [34, 119, 148], suggesting a critical role for receptor-linked signaling in the apoptotic response elicited by reovirus. However, viral disassembly steps that occur following cell attachment are also required for the induction of apoptosis by reovirus [35].

Following attachment to host cells, reovirus particles must penetrate cell membranes and uncoat to activate the viral transcription machinery. Mechanisms underlying these events are dependent on receptor-mediated endocytosis, host-cell proteases resident in the endocytic pathway, and a novel membrane penetration process that requires stepwise disassembly of the viral outer capsid. The σ3 protein is the outermost capsid component and acts as a protective cap for the μ1 protein, which facilitates membrane penetration. Following removal of σ3 by endocytic proteases [50, 68], μ1 undergoes a conformational rearrangement to facilitate entry of the core particle into the cytoplasm [26].

Here we review mechanisms of reovirus attachment and cell entry. Studies of these reovirus replication steps have been significantly advanced by the availability of high-resolution structures of the viral outer-capsid proteins and at least one of the viral receptors. This work, coupled with biochemical and genetic analyses of the reovirus attachment and entry process, has allowed an enhanced understanding of how viral protein structure and function relate to viral disease.

2
Structure and Function of Reovirus Attachment Protein σ1

2.1
Structure of the σ1 Trimer

Reovirus particles are approximately 850 Å in diameter [104]. The ten segments of dsRNA that compose the reovirus genome are encapsidated within two concentric protein shells, the outer capsid and inner core. Together, the outer capsid and core are composed of eight structural proteins. The bulk of the outer capsid consists of the tightly associated μ1 and σ3 proteins [86]. In addition, there are turrets at each of the 12 icosahedral vertices of the virion formed by the pentameric λ2 protein, from which the viral attachment protein, σ1, extends [8, 29, 47, 60, 61].

The σ1 protein is a fibrous, trimeric molecule about 480 Å in length with distinct head-and-tail morphology [60, 61] (Fig. 1). Discrete regions of the molecule mediate binding to cell-surface receptors. Sequences in the N-terminal σ1 tail bind to carbohydrate, which is known to be sialic acid in either α2,3 or α2,6 linkages for serotype 3 reoviruses [29, 30, 43, 64, 116]. The C-terminal σ1 head binds to junctional adhesion molecule-A (JAM-A, previously called JAM1) [8]. The σ1 tail partially inserts into the virion, while the head projects away from the virion surface [46, 61]. Insertion of the trimeric σ1 protein into a pentameric λ2 base results in an unusual symmetry mismatch. Such symmetry mismatches often produce interactions of limited strength or specificity and indicate a strong potential to undergo structural rearrangement.

Structural analysis of the C-terminal half of T3D σ1 (residues 246–455) reveals a trimeric structure, in which each monomer is composed of a slender tail and a compact head [31] (Fig. 2). The C-terminal residues that form the head domain (310–455) consist of two Greek-key motifs that fold into a β-barrel. Loops connecting the individual strands of the β-barrel are short with the exception of the loop that connects β-strands D and E, which contains a 3_{10} helix (Fig. 2). N-terminal residues in the crystallized fragment form a portion of the tail, residues 246–309, which consists of three β-spiral repeats. Each repeat is composed of two short β-strands connected by a four-residue β-turn that has either a proline or a glycine residue at its third position [31]. A surface-exposed, variable loop links successive repeats, and trimerization generates an unusual triple β-spiral motif that has been observed in only one other molecule to date, the adenovirus attachment protein, fiber [150]. The σ1 trimer features a distinct bend between the three-fold axes of the head and tail domains. Although this bend is most likely introduced by crystal packing forces, it indicates that the σ1 trimer possesses a high degree of flexibility. The region

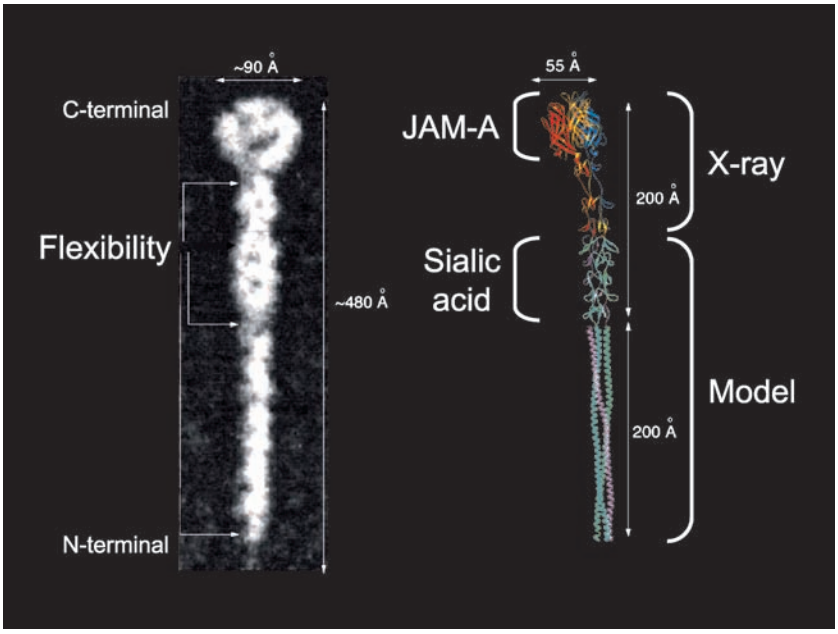

Fig. 1 Structure of reovirus σ1. *Left:* Computer-processed electron micrograph of σ1 showing regions of flexibility and approximate molecular dimensions. Image adapted from Fraser et al. [60]. *Right*: Full-length model of reovirus σ1 generated by adding five β-spiral repeats, followed by a trimeric coiled coil formed by elongating an existing coiled-coil structure [156], to the N-terminus of the crystallized fragment of σ1 [31]. Regions of the molecule that interact with JAM-A and sialic acid, and approximate molecular dimensions are indicated. This model was prepared using RIBBONS [22]

of flexibility is located between the second and third β-spiral repeats in the tail and corresponds to a four-residue insertion, amino acids 291–294 [31] (Fig. 2).

Sequence analysis has facilitated the development of a model of full-length σ1 [31]. The σ1 tail is thought to contain an N-terminal α-helical coiled-coil followed by eight β-spiral repeats (Fig. 1). Sequences predicted to form the α-helical coiled coil are required for trimer stability [29, 84, 138, 159]. Electron microscopic (EM) images of full-length σ1 show flexibility at three regions of the molecule, a region near the N-terminus, a region that correlates with the transition from the predicted α-helical coiled-coil to the triple β-spiral, and a region that corresponds to the insertion between β-spiral repeats 2 and 3 of the crystallized portion of T3D σ1 [31, 60] (Fig. 1). These regions of flexibility could facilitate interactions with receptors or enable structural rearrangements during viral assembly or disassembly (see also Sect. 1.9).

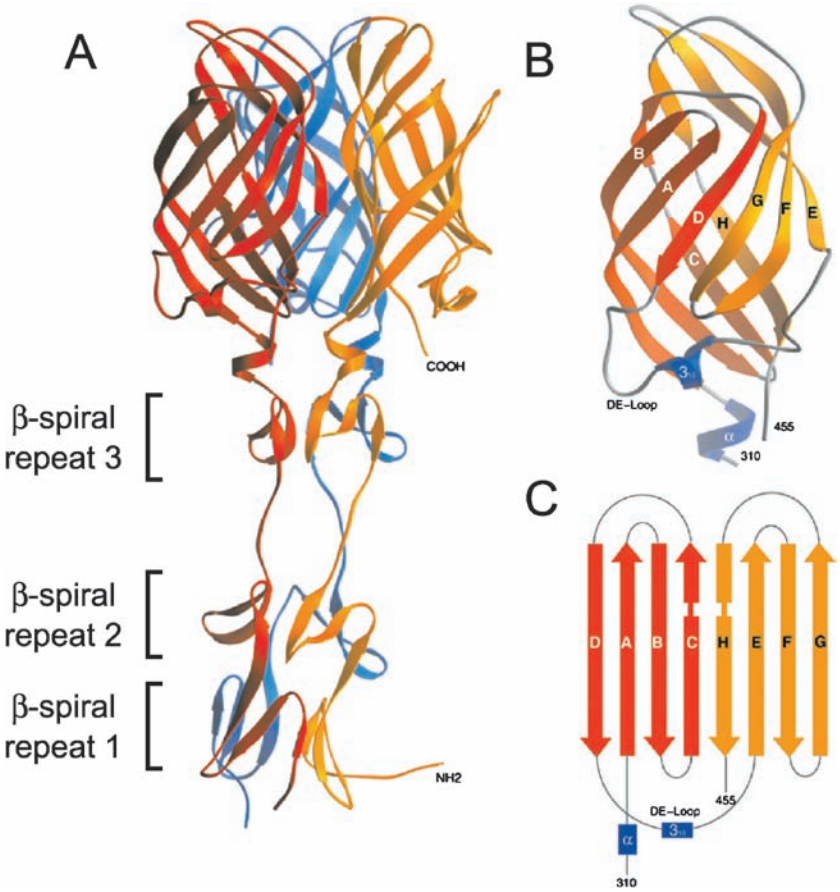

Fig. 2A–C Crystal structure of reovirus σ1. **A** Ribbon drawing of the σ1 trimer with σ1 monomers shown in *red*, *orange*, and *blue*. Each monomer consists of a head domain formed by a compact β-barrel and a fibrous tail with three β-spiral repeats. **B** Enlarged view of the σ1 head domain monomer. The two Greek-key motifs, shown in *red* and *orange*, form a compact, cylindrical β-sheet that contains eight β-strands (*A*–*H*). The head domain also contains two short helices, shown in *blue*: one 3_{10} and one α-helix. **C** Schematic view of the β-strand arrangement in the σ1 head domain. Colors are as in **B**. (Image adapted from Chappell et. al [31])

2.2 Interactions of σ1 with Sialic Acid

Reoviruses exhibit the capacity to agglutinate erythrocytes of several mammalian species [85]. For serotype 3 reoviruses, hemagglutination is mediated

by interactions of the σ1 protein with terminal α-linked sialic acid residues on several glycosylated erythrocyte proteins such as glycophorin A [65, 115]. The carbohydrate receptors for other serotypes of reovirus have not been well characterized. Sialic acid binding is required for reovirus attachment and infection of certain cell types, including murine erythroleukemia (MEL) cells [30, 122]. Although not all serotype 3 strains are capable of binding to sialic acid, the majority bind to this carbohydrate and produce hemagglutination. Sequence polymorphism within the σ1 tail determines the capacity of field-isolate reovirus strains to bind to sialic acid and infect MEL cells [42, 122]. Furthermore, non-sialic acid-binding serotype 3 variants can be adapted to growth in MEL cells during serial passage. These variants have gained the capacity to bind to sialic acid and contain sequence changes within a discrete region of the σ1 tail (residues 198–204) predicted to form a β-spiral [30]. Residues in this vicinity may form part of a sialic acid-binding site [31, 135]. Experiments using expressed σ1 truncation mutants and chimeric molecules derived from T1L and T3D σ1 proteins have confirmed that the sialic acid-binding domain of serotype 3 σ1 is contained within this predicted β-spiral region of the σ1 tail [29] (Fig. 1).

Serotype 1 reoviruses also appear to bind to sialic acid in some contexts. T1L, but not T3D, binds to the apical surface of microfold (M) cells, but not to enterocytes, in tissue sections of rabbit Peyer's patches [71]. Binding is inhibited by preincubation of the tissue sections with neuraminidase or with lectins that specifically recognize α2–3-linked sialic acid. The capacity of T1L to bind to the apical surface of M cells was shown to segregate with the S1 gene using reassortant genetics and with reovirus particles recoated with recombinant σ1 protein. The interaction between T1L σ1 and sialic acid is especially intriguing as serotype 1 reoviruses are incapable of infecting MEL cells, a property dependent on sialic acid binding that segregates with the S1 gene [123], and are insensitive to the growth-inhibitory effects of neuraminidase treatment of L cells [107].

2.3 Interactions of σ1 with JAM-A

Substantial evidence has accumulated to suggest that the σ1 head also binds to receptors on the cell surface [11, 49, 107, 145]. Neutralization-resistant variants of T3D selected using σ1-specific monoclonal antibody 9BG5 contain mutations in the σ1 head that segregate genetically with alterations in neural tropism [11, 75, 133, 134]. This finding suggests a role for the σ1 head in receptor binding. Truncated forms of σ1 containing only the head domain are capable of specific cell interactions [48, 49]. Concordantly, proteolysis of T3D

virions leads to release of a C-terminal receptor-binding fragment of σ1 and a resultant loss in infectivity [107]. These findings indicate that the σ1 head promotes receptor interactions that are distinct from interactions with sialic acid mediated by the σ1 tail.

A flow cytometry-based expression-cloning approach was employed to identify a receptor bound by the σ1 head [8]. A non-sialic acid-binding strain of reovirus that contains a serotype 3 σ1 was used as an affinity ligand to avoid the potential complication of isolating heavily glycosylated molecules that might not interact specifically with σ1. A neural precursor cell (NT2) cDNA library was selectively enriched for cDNAs that confer binding of fluoresceinated virions to transfected cells. Four clones were identified that conferred virus binding. Each encoded JAM-A, a member of the immunoglobulin superfamily postulated to regulate formation of intercellular tight junctions [87, 92, 158]. Three lines of evidence support the contention that JAM-A is a functional reovirus receptor [8]. First, JAM-A-specific monoclonal antibodies inhibit reovirus binding and infection. Second, expression of JAM-A in nonpermissive cells allows reovirus growth. Third and most convincingly, the σ1 protein binds directly to JAM-A with an apparent K_D of approximately 6×10^{-8} M. Together, these findings indicate that JAM-A serves as a receptor for the σ1 head. Surprisingly, JAM-A serves as a receptor for both prototype and field-isolate strains of all three reovirus serotypes [8, 165]. Therefore, utilization of JAM-A as a receptor does not appear to explain the serotype-dependent differences in reovirus tropism observed in the CNS. Variation in the affinity of σ1 for JAM-A among reoviruses or interactions with receptors other than JAM-A, possibly including carbohydrate-based coreceptors, may influence reovirus pathogenesis.

3
Structure of the JAM-A Ectodomain

Reovirus receptor JAM-A is an important component of barriers known as the zonula occludens or tight junctions that form between endothelial and epithelial cells [87, 92, 114]. Tight junctions constitute a semipermeable barrier to the transport of water and solutes between cells, help to establish distinct apical and basolateral regions in polarized epithelia, and serve as critical sites for vesicle targeting and signaling [5, 164]. Tight junctions are composed of complex networks of interacting fibrils that encircle the lateral portion of a polarized epithelial cell toward its apical end and seal the paracellular space. Occludin and members of the claudin family are concentrated in the fibrils and make important contributions to tight junction barrier func-

tion [144]. JAM-A interacts with several proteins. The extracellular domain of JAM-A interacts with the leukocyte function-associated antigen-1 (LFA-1, integrin αLβ2) [113]. Cytosolic proteins known to bind to tight junction components, including zonula occludens (ZO)-1 [13, 53], AF-6 [53], multi-PDZ-domain protein 1 (MUPP1) [70, 149], and partitioning-defective protein (PAR)-3 [54, 72], interact with the JAM-A cytoplasmic tail in a PDZ-domain-dependent manner. JAM-A appears to influence the migration of leukocytes across endothelial and epithelial barriers during the course of an inflammatory response [39, 82], although mechanisms by which JAM-A regulates transendothelial migration are not known.

The capacity of reovirus to interact with tight junctions via JAM-A may make important contributions to the pathogenesis of reovirus infection. Reovirus gains access to the basolateral surface of intestinal cells by transport through M cells [162], which would allow virus exposure to the area of highest JAM-A expression. It is also possible that transient disruptions of the tight junction barrier, such as those that occur during migration of immune and inflammatory cells, permit reovirus access to JAM-A from the intestinal lumen. In addition to reovirus, several other viruses bind to receptors expressed at regions of cell–cell contact [132]. Like JAM-A, the coxsackievirus and adenovirus receptor CAR [14] is expressed at tight junctions [33], and nectins, which serve as receptors for herpes simplex virus [67, 152], are expressed at adherens junctions [140, 163]. Interestingly, each of these viruses is capable of i (TJ)nfecting both epithelial surfaces and neurons in some types of hosts. Reovirus interactions with JAM-A may induce tight junction dysregulation, enhancing viral shedding and transmission. After spreading from the intestine, reovirus interactions with JAM-A may lead to a destabilization of tight junctions in CNS endothelium, which could promote breakdown of the blood–brain barrier and permit cerebral edema and neural inflammation, conditions evident in reovirus encephalitis [151].

JAM-A is a member of a family of related proteins. The proteins most closely related to JAM-A are JAM-B (JAM2) and JAM-C (JAM3), which share 44% and 32% amino acid identity with JAM-A, respectively [2, 37, 55]. Each protein consists of two extracellular immunoglobulin-like domains, a short transmembrane region, and a cytoplasmic tail containing a PDZ-domain-binding motif [14, 92, 131, 158]. Crystal structures are available for the extracellular regions of the human and murine homologues of JAM-A [80, 117] (Fig. 3), which both serve as reovirus receptors [8]. Unlike JAM-A, JAM-B and JAM-C do not serve as receptors for reovirus [117, 165].

JAM-A crystallizes as a homodimer in which monomers engage in an "arm-wrestling grip" via the membrane-distal, or D1, domain [80, 117] (Fig. 3A, B). This dimeric structure is maintained by a highly unusual interface that is

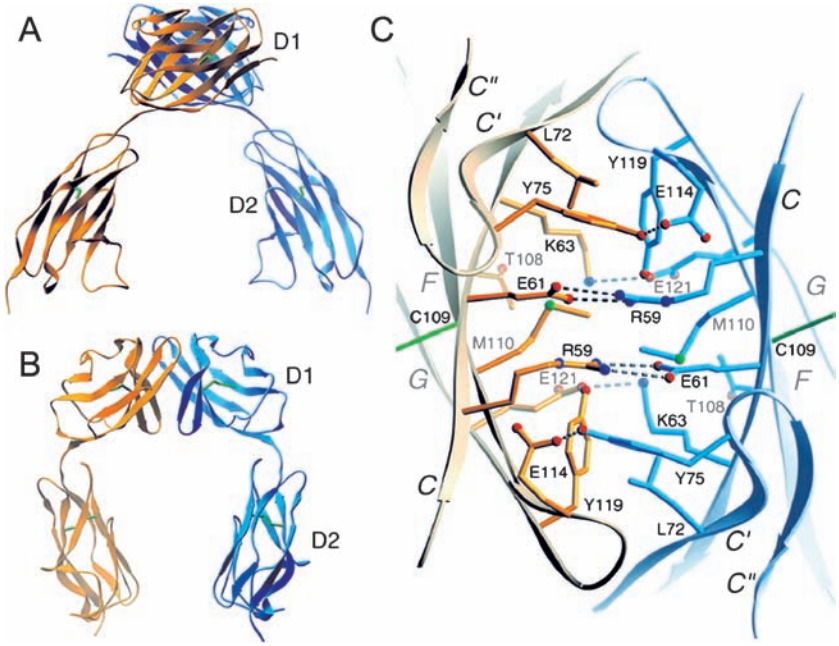

Fig. 3A–C Crystal structure of the hJAM-A extracellular domain. **A, B** Ribbon drawings of the hJAM-A dimer, with one monomer shown in *orange* and the other in *blue*. Two orthogonal views are displayed. Disulfide bonds are shown in *green*. **C** View of the interface between two hJAM-A monomers. The interface is formed by residues on the GFCC' faces of two membrane-distal (D1) domains. The view is along a crystallographic dyad. Hydrogen bonds and salt bridges are represented by broken cylinders. Amino acids are labeled in single-letter code. (Image from Prota et. al [117])

rich in charged residues [117] (Fig. 3C). The principal means of association between JAM-A monomers involves four salt bridges at the center of the interface. These interactions are mediated by the side chains of Arg59, Glu61, Lys63, and Glu121, all of which are buried and solvent-inaccessible [117]. Protein–protein contacts are often mediated by hydrophobic or polar residues, whereas charged amino acids are more typically found at solvent-exposed areas. Although formation of salt bridges is generally viewed as energetically favorable, the stability of these interactions depends very much on the nature of the surrounding environment. Apolar surroundings increase the energy gained by salt bridge formation, whereas highly polar surroundings or low pH values decrease the stability of these contacts. Of note, JAM-A dimers can dissociate into monomers under conditions of moderately high ionic strength or when exposed to low pH [12]. This dynamic nature of the JAM-A interface

may facilitate efficient binding of the viral attachment protein [59]. Sequence alignments show that most of the residues mediating dimer formation are conserved in JAM-B and JAM-C, which has led to the suggestion that these two molecules form similar dimeric structures [80, 117].

4 Model of σ1-JAM-A Interactions

Although structural data for a σ1-JAM-A complex are not yet available, experimental results suggest that σ1 engages monomeric JAM-A. Chemical cross-linking of the JAM-A dimer diminishes the capacity of reovirus to bind to JAM-A in vitro and on cells and negates the competitive effects of soluble JAM-A on reovirus attachment [59]. These observations suggest that the virus cannot interact with a covalently linked dimer, but can recognize a monomeric version of the receptor. Sequences required for reovirus binding have been defined in part by mutating several solvent-accessible residues covering most of the JAM-A D1 surface. Residues selected for this analysis are conserved in human and murine homologues of JAM-A, which both serve as reovirus receptors [8, 117]. Assaying the mutant constructs for the capacity to bind to reovirus in vitro identified residues Ser57 and Tyr75 as especially important for efficient reovirus attachment [59]. Tyr75 is located at the JAM-A dimer interface and forms a hydrogen bond with Glu114 [117] (Fig. 3C). Thus, Tyr75 would not be accessible to ligand in the context of dimeric JAM-A. Ser57 is located close to Tyr75, at the edge of the JAM-A dimer interface. Together, these results provide strong evidence that reovirus σ1 engages a monomeric form of JAM-A, most likely via residues located at or in the vicinity of the JAM-A dimer interface.

Structural observations and sequence analysis also support a model of the σ1-JAM-A interaction in which σ1 engages monomeric JAM-A via the dimer interface. The JAM-A dimer interface is concave and composed of four β-strands (C', C, F, and G). The structure of the monomeric reovirus σ1 head domain features a solvent-exposed surface that is similarly concave and also composed of four β-strands (B, A, D, and G). In fact, the concave β-sheets C'CFG of JAM-A and BADG of σ1 are so similar that they can be superimposed with low root mean square deviations [136]. Sequence analysis of prototype strains of the three reovirus serotypes, which each use JAM-A as a receptor [165], identifies a cluster of conserved residues at the lower edge of the BADG sheet of σ1, including several residues that form the loop connecting β-strands D and E (Fig. 2) [31]. Therefore, it is possible that the σ1 surface mimics features of the JAM-A dimer interface and engages JAM-A in

a manner similar to that used to form JAM-A dimers. Structural analysis of a σ1-JAM-A complex is ongoing to test this hypothesis.

5
Adhesion-Strengthening Mechanism of Stable Reovirus Attachment to Cells

Monoreassortant viruses containing the σ1-encoding S1 gene of either non-sialic acid-binding strain T3C44 ($T3SA^-$) or sialic acid-binding strain T3C44-MA ($T3SA^+$) in a T1L background have been used to study the contribution of sialic acid to stable reovirus attachment to cells [7]. $T3SA^-$ and $T3SA^+$ vary by a single amino acid residue at position 204 (leucine for $T3SA^-$ and proline for $T3SA^+$), which correlates with the capacity to bind to sialic acid [30]. $T3SA^+$ binds to sialic acid with an apparent K_D of approximately 5×10^{-9} M, while $T3SA^-$ displays no specific interaction with this carbohydrate [7]. While the steady-state avidity of these strains for L cells, as determined by competition binding assays, is nearly equivalent (K_D ~3×10^{-11} M), the avidity of $T3SA^+$ for HeLa cells is fivefold higher than that of $T3SA^-$ [7]. Kinetic assessments of binding indicate that the capacity to engage sialic acid functions primarily to increase the k_{on} value of virus attachment to HeLa cells.

The enhanced infectivity of $T3SA^+$ is mediated by the interaction of σ1 with cell-surface sialic acid, since preincubation of virus with sialyllactose (SLL) dramatically reduces the efficiency of $T3SA^+$ infection, yet has no effect on $T3SA^-$ infectivity [7]. However, sialic acid-mediated enhancement of $T3SA^+$ infection occurs only during the initial phases of virus–cell interaction, since SLL does not inhibit productive binding of $T3SA^+$ after the first 30 min of virus adsorption. In contrast, Fab fragments of a monoclonal antibody directed to the σ1 head (9BG5) neutralize $T3SA^+$ infection efficiently, even when added at late times during adsorption [7].

Results of the binding studies performed using $T3SA^+$ and $T3SA^-$ suggest that reovirus attaches to cells using an adhesion-strengthening mechanism, in which initial low-affinity binding to sialic acid facilitates secondary higher-affinity binding to JAM-A (Fig. 4A). For sialic acid-binding reovirus strains, the initial interaction between the virus and the host cell is likely mediated by sialic acid because of the high surface concentration of this carbohydrate. By virtue of its rapid association rate, virus binding to sialic acid would adhere the virion to the cell surface, thereby enabling it to diffuse laterally until it encounters JAM-A. Such lateral diffusion has been reported for influenza virus [127] and phage T4 [161]. After attachment, interactions between reovirus and additional proteins on the cell surface may be required for internalization.

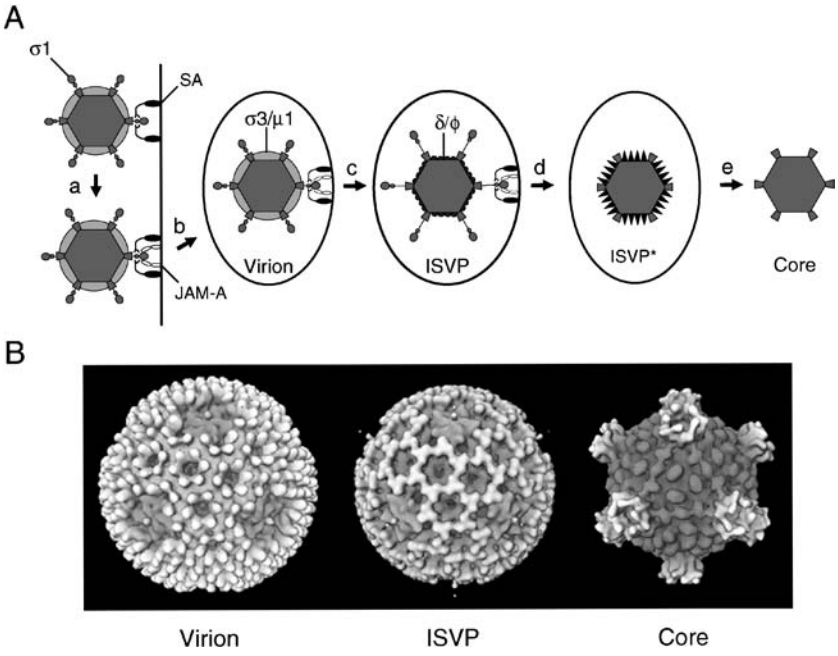

Fig. 4A, B Stepwise disassembly of reovirus. **A** Schematic of the reovirus disassembly steps. (*a*) Following attachment to cell-surface carbohydrate (α-linked sialic acid [SA] for type 3 reoviruses) and junctional adhesion molecule-A (JAM-A), reovirus virions enter cells by receptor-mediated endocytosis (*b*). Within an endocytic compartment, the viral outer-capsid undergoes acid-dependent proteolysis. (*c*) The first disassembly intermediate is the ISVP, which is characterized by loss of σ3 and cleavage of μ1C into particle-associated fragments δ and φ. (*d*) The ISVP then undergoes further conformational changes to form the ISVP*. The ISVP* is characterized by conformational rearrangements of the μ1 fragments to expose hydrophobic residues, release of μ1N, and loss of attachment protein σ1. (*e*) The μ1 cleavage fragments mediate penetration through the endosomal membrane releasing the transcriptionally active core into the cytoplasm. **B** Structure of reovirus virions, ISVPs, and cores. Surface-shaded representations of cryo-EM image reconstructions of reovirus are shown, as viewed along a twofold axis of symmetry. Density, representing σ1, can bee seen extending from turrets of λ2 at the icosahedral axes of virions and ISVPs. Cores lack σ1. (Image adapted from Dryden et. al [46])

6 Overview of Entry Steps

Following attachment to cell-surface receptors, reovirus virions are delivered into the endocytic pathway (Fig. 4A). Although conclusive evidence

for the mechanism of internalization is lacking, current data support a role for clathrin-dependent endocytosis in reovirus cell entry. Thin-section EM images show virions in structures that appear to be clathrin-coated pits on the cell surface and in clathrin-coated vesicles in the cytoplasm [17, 18, 122, 139], suggesting clathrin-dependent uptake. This finding was confirmed by using video fluorescence microscopy in which reovirus virions and clathrin were observed to colocalize during internalization [56]. While these results are interesting, the involvement of clathrin-dependent uptake in functional reovirus entry (i.e., leading to productive reovirus infection) has not been demonstrated.

Vesicles containing internalized reovirus virions are transported via microtubules [66] and accumulate in late endosomes [17, 18, 66, 122, 139]. In the endocytic compartment, reovirus virions undergo stepwise disassembly forming sequential disassembly intermediates, the first of which is the infectious subvirion particle (ISVP) (Fig. 4). ISVPs are characterized by the loss of outer-capsid protein σ3, a conformational change in attachment protein σ1, and cleavage of outer-capsid protein μ1 to form particle-associated fragments, δ and φ. Following further processing, ISVP-like particles (called ISVP*s) penetrate through the endosomal membrane, leading to release of transcriptionally active core particles, which lack μ1 and σ1, into the cytoplasm. Thus, the disassembly process consists of a highly coordinated series of events that are dependent on host cell functions that act upon discrete components of the viral outer capsid.

7
Cellular Factors That Facilitate Reovirus Disassembly

7.1
Reovirus Disassembly in Some Cell Types Requires Acidic pH and Endocytic Proteases

Treatment of murine L cells [21, 90, 139] or rat insulinoma cells [21, 90, 139] with the weak base ammonium chloride (AC), which raises the pH of endosomes and lysosomes [95, 111], blocks growth of reovirus when infection is initiated with virions. However, ISVPs generated in vitro by treatment of virions with chymotrypsin or trypsin can infect AC-treated cells [139]. This finding indicates that the block to reovirus growth mediated by AC occurs following internalization but prior to disassembly. Concordantly, treatment of L cells with inhibitors of vacuolar proton ATPase activity, such as bafilomycin A1 and concanamycin A, blocks infection by virions but not by ISVPs [91]. Thus, acidic pH is required for reovirus disassembly in some types of cells.

Pharmacologic treatments also have been used to demonstrate an important function for endocytic proteases in reovirus disassembly. Treatment of L cells with E64, an inhibitor of cysteine proteases [6], blocks growth of reovirus virions. Similar to findings made in studies using acidification inhibitors, ISVPs generated in vitro can infect E64-treated cells [3, 25, 52, 73], suggesting that one or more endocytic cysteine proteases can catalyze reovirus disassembly. However, pepstatin A, an inhibitor of aspartyl proteases, is incapable of blocking reovirus infection and uncoating in multiple cell types [81]. Moreover, in vitro treatment of reovirus virions with cathepsin D, an aspartyl protease, does not lead to generation of ISVPs [81]. Thus, aspartyl proteases appear to be incapable of mediating virion-to-ISVP conversion.

Proteolytic enzymes are required for reovirus infection when mice are infected by the peroral route [10, 15]. Virions are converted to ISVPs in the intestinal lumen by the resident proteases chymotrypsin and trypsin. ISVPs produced in this fashion infect intestinal M cells to gain entry into the host [1]. ISVPs generated by chymotrypsin or trypsin in vitro or in the gut lumen [10, 15] are similar to ISVPs generated in the endocytic compartment of cells [4, 51].

7.2 Studies of Persistent Reovirus Infections Provide Clues About the Identity of Proteases That Catalyze Disassembly

Support for a critical role of cysteine proteases in reovirus disassembly comes from studies of persistent reovirus infections in cultured cells. Although usually cytolytic, reoviruses are capable of establishing persistent infections in many types of cells in culture [41]. These cultures are maintained by horizontal transmission of virus from cell to cell and can be cured of persistent infection by passage in the presence of anti-reovirus serum. Cured (LX) cells and the viruses isolated from persistently infected L-cell cultures (PI viruses) harbor mutations that affect viral disassembly [41].

Parental L cells support growth of reovirus after infection by virions or in vitro generated ISVPs. In contrast, LX cells do not support growth of reovirus after infection by virions of wild-type virus but do so after infection by PI virus virions or wild-type ISVPs [4, 44] (Fig. 5A). Since LX cells allow growth of wild-type reovirus only when infection is initiated by ISVPs, these cells are altered in the capacity to support steps in viral replication leading to ISVP formation. L cells and LX cells do not differ in the capacity to bind or internalize virions or distribute them to a perinuclear compartment [4]. Intravesicular pH is equivalent in both cell types, and virions colocalize with an acid-sensitive fluorophore in both L cells and LX cells. However, LX cells

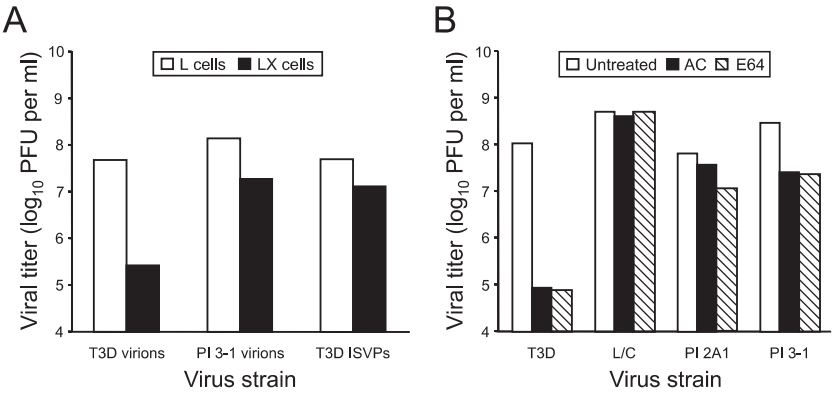

Fig. 5A, B Growth of wild-type and PI viruses in parental L cells and mutant LX cells in the presence and absence of inhibitors of reovirus disassembly. **A** Growth of T3D virions, PI 3–1 virions, and T3D ISVPs in L cells and LX cells. Monolayers of cells (5×10^5) were adsorbed with the viral particles shown at an MOI of 2 PFU per cell. After 1 h, the inoculum was removed, fresh medium was added, and cells were incubated at 37 °C for 24 h. Cells were frozen and thawed twice, and viral titers in cell lysates were determined by plaque assay. The results are presented as the mean viral titers for two independent experiments. (Figure adapted from Wilson et al. [160] and Dermody et al. [44]) **B** Growth of wild-type and PI viruses in the presence and absence of AC and E64. Monolayers of L cells (5×10^5) were adsorbed with T3D or the PI viruses shown at an MOI of 2 PFU per cell. After 1 h, the inoculum was removed, fresh medium was added (with or without 10 mM AC or 100 μM E64), and cells were incubated at 37 °C for either 0 or 24 h. Cells were frozen and thawed twice, and viral titers in cell lysates were determined by plaque assay. The results are presented as the mean viral yields (viral titer at 24 h divided by that at 0 h) for two independent experiments. (Figure adapted from Wetzel et al. [157] and Baer and Dermody [3])

do not support the proteolytic disassembly of the viral outer-capsid following internalization into the endocytic pathway [4, 51], suggesting a defect in proteolytic activity in LX cells.

The major cysteine proteases in the endocytic compartment of fibroblasts like L cells are cathepsins B, H, and L, with cathepsin L being the most abundant in several cell types [6, 16, 62, 69, 78]. These enzymes are first produced as inactive proenzyme precursors that are processed to yield single-chain intermediates that are subsequently cleaved in lysosomes to form two-chain mature forms consisting of heavy and light chains [63, 88, 93, 121, 125, 128]. In LX cells, only the precursor form of cathepsin L is found [4]. The mature, double-chain form of cathepsin B is found in these cells; however, the enzyme is inactive [51]. Neither cathepsin B nor cathepsin L is genetically altered in LX cells, indicating an extrinsic block to the function of these enzymes. Mixed

lysates of L cells and LX cells lack activity of both cathepsin B and cathepsin L [51], suggesting the presence of an inhibitor of cathepsin function in LX cells. These findings suggest that a mutation in LX cells selected during persistent reovirus infection alters the activity of cathepsin B and cathepsin L, suggesting a critical function for these enzymes in reovirus disassembly in fibroblasts. Consistent with a role for cysteine proteases in reovirus uncoating, treatment of virions with either cathepsin B or cathepsin L in vitro results in the formation of particles that have biochemical and growth properties similar to ISVPs generated by treatment of virions with chymotrypsin or trypsin [4, 50].

7.3
Proteases That Mediate Disassembly Vary Depending on Cell Type

The involvement of cathepsin B and cathepsin L in the disassembly of reovirus virions in fibroblasts was confirmed in studies using pharmacologic inhibitors (Fig. 6) and genetically deficient cell lines [50]. Infection of either L cells treated with the cathepsin L inhibitor A-Phe-Tyr(*t*-Bu)-diazomethyl ketone or cathepsin L-deficient mouse embryo fibroblasts results in inefficient proteolytic disassembly and decreased viral yields. In contrast, both L cells treated with the cathepsin B inhibitor CA-074Me and cathepsin B-deficient mouse embryo fibroblasts support reovirus disassembly and growth. However, removal of both cathepsin B and cathepsin L activity completely abrogates disassembly and growth of reovirus. Concordantly, cathepsin L mediates reovirus disassembly more efficiently than cathepsin B in vitro [50]. These results demonstrate that either cathepsin L or cathepsin B is required for reovirus entry into murine fibroblasts and indicate that cathepsin L is the primary mediator of reovirus disassembly in these cells.

Proteases other than cathepsin B and cathepsin L also are capable of ISVP formation. In P388D cells, a macrophage-like cell line, cathepsin S mediates uncoating of some strains of reovirus [68]. Like cathepsins B and L, cathepsin S is a cysteine protease required for processing internalized antigens by antigen-presenting cells [98, 101, 118]. The role of cathepsin S in reovirus disassembly is important because during enteric infection, primary replication is thought to occur in mononuclear cells of Peyer's patches [58, 99].

8
Outer-Capsid Protein σ3 Regulates Reovirus Disassembly

The fist step in the disassembly of reovirus virions is the proteolytic removal of outer-capsid protein σ3. The σ3 protein is a major outer-capsid component

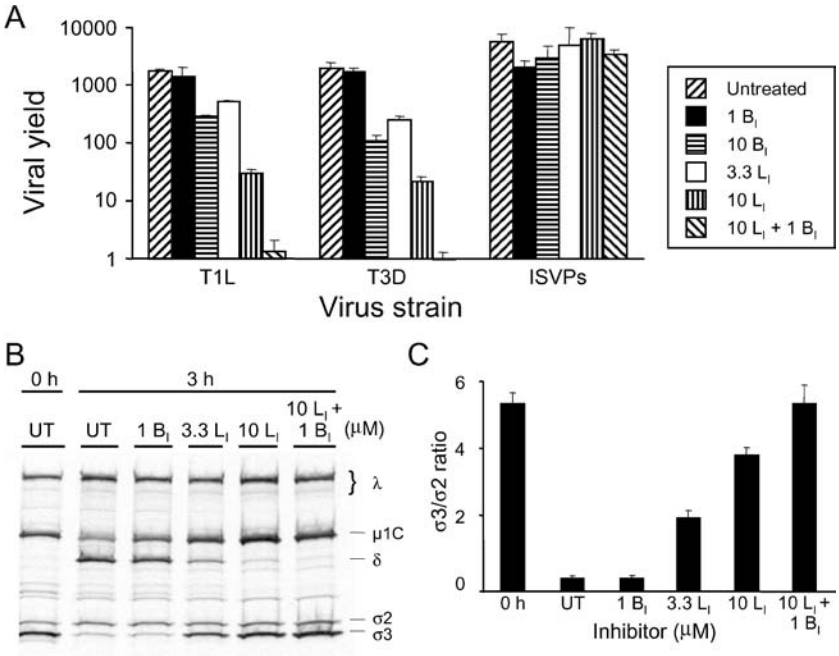

Fig. 6A–C Effect of cathepsin B inhibitor CA-074Me (B_I) and cathepsin L inhibitor Z-Phe-Tyr(*t*-Bu)-diazomethyl ketone (L_I) on growth and disassembly of reovirus strains T1L and T3D in L cells. **A** Monolayers of L cells (4×10^5) were preincubated for 1 h in medium supplemented with B_I, L_I, or both B_I and L_I at the concentrations shown in μM. The medium was removed, and cells were adsorbed with each virus strain at an MOI of 2 PFU per cell. After 1 h, the inoculum was removed, fresh medium with or without B_I and L_I was added, and cells were incubated for 24 h. Viral titers in cell lysates were determined by plaque assay. The results are presented as the mean viral yield, calculated by dividing titer at 24 h by that at 0 h, for three independent experiments. Error bars indicate standard deviations. *UT*, untreated. **B** Monolayers of L cells (1×10^7) were preincubated for 1 h in medium supplemented to contain 0–10 μM B_I or L_I. The medium was removed, and cells were adsorbed with purified ^{35}S-labeled T1L virions at 10,000 particles per cell. After incubation at 4°C for 1 h, the inoculum was removed, fresh medium with or without B_I or L_I was added, and cells were incubated at 37°C for either 0 or 3 h. Viral particles in cell lysates were subjected to SDS-PAGE. Concentrations of B_I and L_I (μM) are shown at the top. *UT*, untreated. Viral proteins are labeled on the right. **C** Quantitation of σ2 and σ3 band intensities. The densities of bands corresponding to the σ2 and σ3 proteins were determined, and the results are expressed as the mean σ3/σ2 ratios for three independent experiments. Error bars indicate standard deviations. (Figure and legend modified from Ebert et al. [50])

that protects the virion from degradation in the environment [105] and forms a protective cap for the μ1 protein [46]. The latter function is especially important during entry as μ1 is thought to be responsible for penetration of ISVPs into the cytoplasm. By capping the μ1 protein, σ3 controls the timing of penetration: if too early, the resulting particle may not be primed to initiate transcription; if too late, the particle may be proteolytically degraded in the lysosome before it gains access to the cytoplasm where transcription occurs.

The σ3 protein contains two large domains separated by a flexible hinge [46, 112] (Fig. 7). The N-terminus of σ3 is in the smaller, virion-proximal lobe, and the C-terminus is in the larger, virion-distal lobe. These domains are not discrete in primary sequence as the peptide chain passes back and forth between the two lobes. A σ3-specific monoclonal antibody that inhibits the σ1-mediated property of sialic acid binding engages the very tip of the virion-distal lobe [102].

Studies of PI viruses have shed light on mechanisms of σ3 cleavage during reovirus disassembly. In contrast to wild-type reoviruses, PI viruses can infect cells treated with either AC [4, 44, 157] or E64 [3] (Fig. 5B). In most cases, growth of PI viruses in the presence of AC or E64 segregates with the S4 gene segment [3, 157], which encodes σ3 [96, 100]. Moreover, passage of wild-type reovirus in the presence of E64 selects E64-resistant viruses (D-EA viruses) that contain mutations in the σ3-encoding S4 gene [52]. Therefore, mutations in σ3 protein confer the capacity of variant reoviruses to grow in the presence of pharmacologic inhibitors of reovirus disassembly.

All PI viruses analyzed to date have a mutation of Tyr354 to His near the C-terminus of σ3 [3, 157]. This mutation is also selected in D-EA viruses [52]. PI and D-EA viruses exhibit altered kinetics of disassembly with degradation of σ3 and cleavage of μ1 occurring much more rapidly both in vitro and in cells [52, 157]. Image reconstructions of cryo-EM images of virions of PI viruses indicate that the Tyr354 to His mutation confers an alteration in σ3 structure at the hinge region between the two lobes [160]. These findings suggest that the C-terminus of σ3 regulates susceptibility of the protein to cleavage.

The σ3 C-terminus also has been shown to dictate strain-specific differences in the susceptibility of σ3 to proteolytic attack [73, 74]. The σ3 protein of strain T1L is cleaved more rapidly than that of T3D. Analysis of ISVPs recoated with chimeric σ3 proteins generated from T1L and T3D revealed that the C-terminus is primarily responsible for the rate of σ3 proteolysis. Moreover, sequence polymorphisms at residues 344, 347, and 353 in σ3 contribute to this effect [74].

Treatment of reovirus virions in vitro with either cathepsin B or cathepsin L leads to an initial cleavage of σ3 at a terminus [50]. Given that sequence

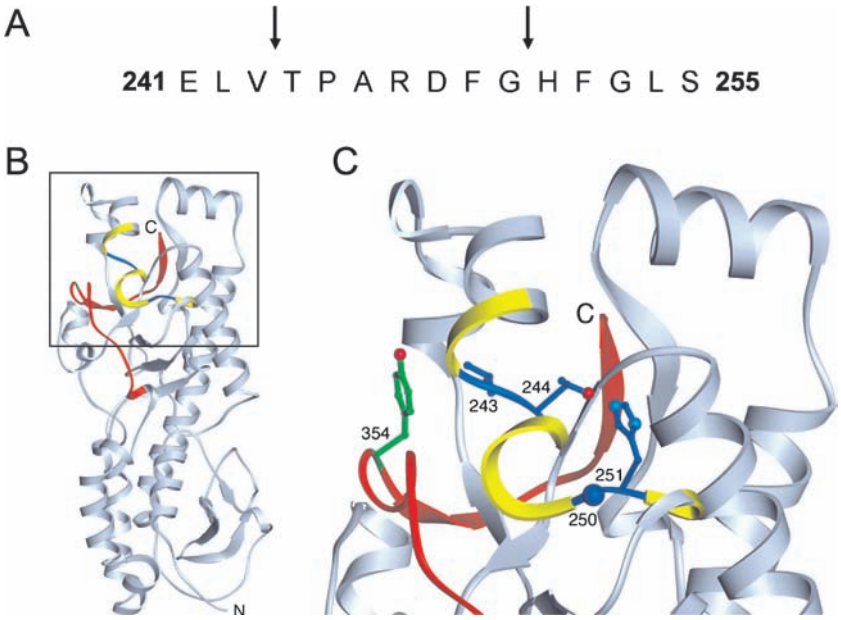

Fig. 7A–C Cathepsin L cleavage sites in T1L σ3. **A** The primary amino acid sequence of σ3 from amino acids 241 to 255 is shown. The *arrows* highlight cathepsin L cleavage sites identified by N-terminal sequencing of σ3 cleavage products following treatment of reovirus T1L with cathepsin L in vitro. **B** Cathepsin L cleavage sites are highlighted in the crystal structure of σ3. A ribbon diagram of the crystal structure of T3D σ3 [112] is displayed. The cathepsin L cleavage sites in T1L are depicted in *blue* between amino acids 243 and 244 and between 250 and 251. Surrounding residues, from amino acids 241 to 253, are shown in *yellow*. The C-terminal residues of σ3, from amino acids 340 to 365, are colored *red*. Amino acid 354, which is a site altered in PI and D-EA viruses, is colored *green*. The virion-distal end of σ3 is at the *top* of the figure, and the virion-proximal end and N-terminus are at the *bottom*. **C** An enlarged view of the boxed region of σ3 indicated in *panel B* is shown using the same color scheme. Amino acids 243, 244, 250, 251, and 354 are depicted in ball-and-stick representation. (Figure and legend modified from Ebert et al. [50])

polymorphisms in the C-terminus determine susceptibility to proteolysis, the initial cleavage of σ3 probably occurs in this region. During proteolysis by cathepsin L, subsequent cleavages occur between residues 243–244 and 250–251 [50] (Fig. 7A). These cleavage sites are physically located near the C-terminus in the σ3 crystal structure [112] (Fig. 7C). Because of this proximity, the small end fragment released following initial cathepsin L cleavage likely exposes the other two sites, rendering them sensitive to subsequent cleavage

events. The C-terminus therefore appears to act as a safety latch that controls access to internal, proteolytically sensitive sites in σ3. Because reovirus disassembly in some cell types is an acid-dependent process, the safety latch might be primed for movement at acidic pH. In viruses with mutations near the C-terminus, such as PI and D-EA viruses, the safety latch may be altered by structural rearrangements.

9 Conformational Changes in σ1

The disassembly of reovirus virions to ISVPs is accompanied by a dramatic conformational change in σ1. EM images of negatively stained reovirus virions and ISVPs reveal filamentous projections extending up to 400 Å from the surface of ISVPs but not virions [61]. These images suggest that σ1 adopts a compact form in the virion and a more extended one in the ISVP. Cryo-EM image reconstructions of virions of reovirus prototype strains and cores of T1L each lack a discernible density corresponding to σ1 at the icosahedral vertices [46, 97]. However, in cryo-EM image reconstructions of T1L ISVPs, discontinuous density is observed for σ1 extending approximately 100 Å from each vertex (Fig. 4B). Presumably, the full length of σ1 is not visible in reovirus particles because icosahedral averaging was employed for the cryo-EM image reconstructions. The trimeric σ1 protein is positioned at an icosahedral fivefold axis; therefore, it does not obey icosahedral symmetry. Moreover, σ1 possesses structural flexibility, which also may preclude its visualization by this technique.

The flexibility of σ1 has been observed in EM images of negatively stained σ1 isolated from virions, which show bending in individual fibers at specific regions within the molecule [60] (Fig. 1) and in the crystal structure of the C-terminal half of T3D σ1 [31] (Fig. 2). In addition, a highly unusual cluster of conserved aspartic acid residues is found at the trimer interface at the base of the σ1 head [31] (Fig. 8). These residues may be important for triggering conformational changes in the low pH environment of the endocytic pathway. Acid-dependent conformational changes in the attachment proteins of enveloped viruses, such as influenza virus and tick-borne encephalitis virus, are well-documented [20, 137]. A four-residue linker that connects β-spiral repeats 2 and 3 of the crystallized fragment of σ1, which are just N-terminal to the σ1 head, confers flexibility between the head and tail regions [31] (Fig. 2). Despite the importance of σ1 in mediating attachment to host cells, the conformational changes that occur in σ1 during the viral entry and uncoating steps and their significance at present are poorly understood.

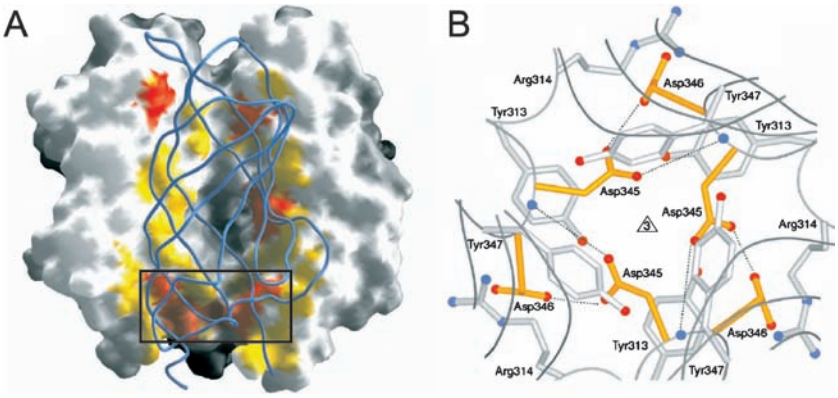

Fig. 8A, B The σ1 head trimer interface. **A** View into the head trimer interface. Two monomers are shown as surface representations and the third monomer is shown as a *blue ribbon*. Surface residues that are within 4 Å of residues in the third monomer are shown in *red* (residues conserved in T1L, T2J, and T3D σ1) and *yellow* (residues unique to T3D σ1). The contact area involving conserved residues Val344, Asp345, and Asp346 is boxed, and this region is shown in more detail in **B**. **B** View along the trimer axis, centered at conserved residues Asp345 and Asp346 (*yellow*) located at the base of the σ1 head. Residues Tyr313, Arg314, and Tyr347 engage in contacts with the two aspartic acids. The side chains of Asp345 are likely to be protonated to avoid an accumulation of negative charge at the interface. Hydrogen bonds involving protonated Asp345 are indicated. Oxygen and nitrogen atoms of side chains are shown as *red and blue spheres*, respectively. The Asp346 main chain amides also are shown as *blue spheres*. (Image from Chappell et al. [31])

Mutations found in PI viruses provide additional evidence of a role for σ1 in viral entry independent of its function in receptor binding. All mutations identified to date in PI virus σ1 protein are found in the tail region of σ1 and alter the stability of σ1 oligomers [159]. Several mutations also are found in the region of σ1 responsible for anchoring the protein into the virion surface. Thus, mutations selected during persistent infection suggest that oligomerization and σ1-capsid interactions are important for viral disassembly and growth.

10
Outer-Capsid Protein μ1 Mediates Membrane Penetration

Insight into mechanisms employed by reovirus to penetrate into the cytoplasm first came from studies of ISVPs generated in vitro. ISVPs, but not intact virions, release ^{51}Cr from preloaded L cells [17], lyse red blood cells in the

presence of cesium ions [25, 27, 73], and form ion-permeant channels in planar phospholipid bilayers [143]. ISVPs also facilitate entry into cells of the toxin alpha-sarcin in the presence of inhibitors of reovirus uncoating [26, 91, 110]. These observations suggest that ISVPs are the immediate precursor to the disassembly intermediate that facilitates delivery of the core particle into the cytoplasm.

Following formation of ISVPs in endosomes, transcriptionally active core particles, which lack both σ1 and μ1, are released into the cytoplasm. The mechanism of penetration and the shedding of these outer-capsid proteins has been the focus of recent work, which has led to the identification of an additional intermediate particle formed subsequent to the ISVP, the ISVP* [24, 26, 110] (Fig. 4A).

Most of the μ1 protein on mature virions is autocatalytically cleaved near the N-terminus to generate two fragments, μ1N and μ1C [106, 130] (Fig. 9). This cleavage is not required for virion assembly [110] and may occur physiologically during the transition from the ISVP to the ISVP* [108]. In ISVPs, μ1C is further cleaved by either endocytic [50, 139] or intestinal [15] proteases to form fragments δ and φ, which remain particle-associated [103]. However, the role of this cleavage in viral penetration is not understood, as core particles recoated with mutant forms of μ1 incapable of δ/φ cleavage can establish productive infection [27]. In addition, μ1 is not cleaved at the δ/φ junction in ISVPs generated in the presence of alkyl sulfate detergents (dpSVPs), yet dpSVPs are infectious [25].

Transformation from the ISVP to the ISVP* in vitro is triggered by differential cationic concentration or interactions with membranes [24, 26]. In contrast to ISVPs, ISVP*s lack σ1 and have an altered conformer of μ1 in which internal hydrophobic residues are exposed. ISVP*s are capable of membrane penetration and transcription initiation [24, 26]. The conformational change in μ1 may be the driving force for both the loss of σ1 and the initiation of transcription [86]. Mechanisms underlying these events are unknown, but it is possible that μ1 rearrangement induces a conformational change in λ2, the pentameric turret that anchors σ1, causing σ1 release. A μ1-induced conformational change in λ2 may also activate the transcriptional machinery through interactions with either or both of the core proteins λ1 and σ2.

Cleavage of intact μ1 to form μ1N and μ1C is required for the generation of the ISVP* [108, 110]. Particles recoated with mutant forms of μ1 incapable of μ1N/μ1C cleavage can facilitate each of the entry steps, including μ1 conformational changes and transcription initiation but are deficient in membrane penetration [110]. In addition to σ1, the N-terminal μ1 fragment μ1N is released from the ISVP* [26]. The function of the released μ1 fragment in membrane penetration is not understood. However, the presence of a myris-

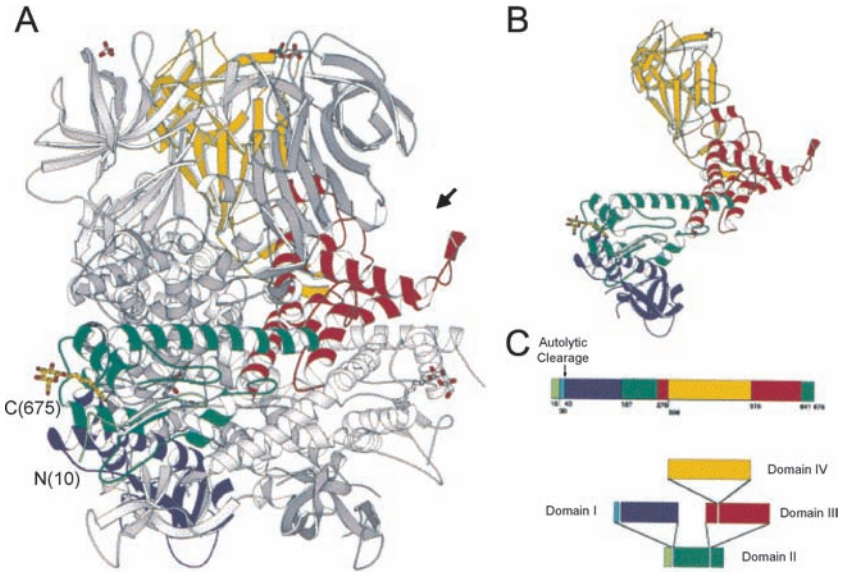

Fig. 9A–C The μ1 protein. **A** The μ1 trimer shown without bound σ3. One μ1 subunit is colored by domain (domain I, *light and dark blue* [μ1N, μ1C]; domain II, *light and dark green* [μ1N, μ1C]; domain III, *red*; domain IV, *yellow*); the other two μ1 subunits are shown in *gray*. The β-octyl glucoside in the colored subunit is in *yellow*; the sulfate ion is shown in *green* and *red*. The σ3 binding site is indicated by an *arrow*. **B** Ribbon diagram of an isolated μ1 subunit. Colors are as in **A**. **C** Domain segmentation of the amino acid sequence as determined from the three-dimensional structure. Domain color code as in **A**. The central domain II contains domains I and III as inserts, and domain III similarly contains domain IV. (Figure and legend modified from Liemann et al. [86])

toyl group at the N-terminus of μ1N suggests that this fragment interacts with membranes and that the released μ1N may form a membrane-penetration complex.

High-resolution structural analysis of μ1 has led to the development of a model for its role in membrane penetration (Figs. 9, 10). The protein consists of four domains: domains 1–3 are primarily α-helical while domain 4, which sits atop the molecule, is a jelly-roll β-barrel [86] (Fig. 9). Three μ1 subunits assemble into an oblong homotrimer, which is bound by the lower lobes of three σ3 subunits. This arrangement gives rise to a heterohexameric complex in which each σ3 subunit interacts intimately with two different μ1 subunits (Fig. 10). The μ1 proteins serve as the principal means of capsid association by mediating contacts between different heterohexamers [86]. The σ3 proteins

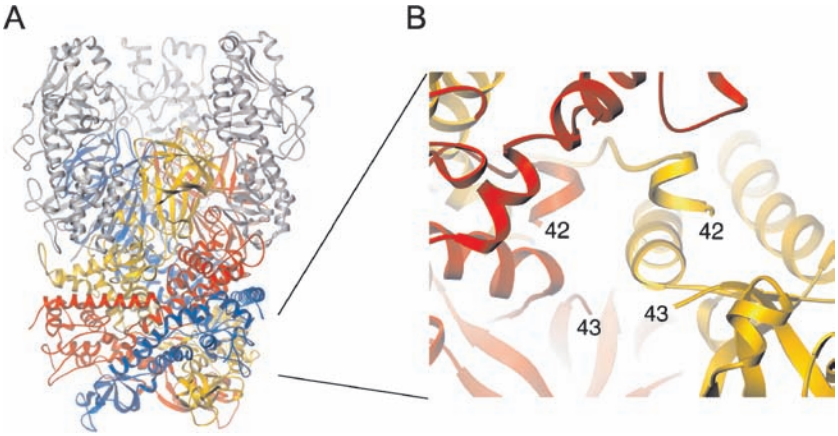

Fig. 10 Structure of the $\mu1_3\sigma3_3$ heterohexamer. **A** A $\mu1_3\sigma3_3$ complex, viewed from the side. The bottom of the complex would contact σ2 proteins on the surface of the reovirus core. Three σ3 proteins (shown in *gray*) bind to the upper part of the underlying trimer of μ1 (shown in *yellow*, *red*, and *blue*). The three μ1 chains are wound tightly around each other. Each σ3 contacts two μ1 proteins. **B** Enlarged view of the lower portion of the trimer, with the blue monomer removed for clarity. In this view, it is evident that the protein has undergone autocatalytic cleavage between residues 42 and 43. (Figure and legend modified from Liemann et al. [86])

do not contribute to the formation of this network but project outward, away from the virion surface. The C-terminal lobe of each σ3 protein is therefore easily accessible to proteases. The autocatalytic cleavage site that yields μ1N and μ1C is located between residues 42 and 43, at the center of the trimer near the base of the protein (Fig. 10). This site is buried in μ1 and distant from residues that interact with σ3. The crystallized protein has undergone cleavage at this position, resulting in separation of residues 42 and 43. The δ/φ cleavage site is located in domain 3.

There are amphipathic helices and other hydrophobic residues in the center of μ1, including the myristoylated Gly2 at the N-terminus [86]. Cleavage of μ1 to μ1N and μ1C does not appear to result in conformational rearrangements, but this cleavage, along with the loss of σ3, may render the μ1 trimer metastable. Since the μ1N/μ1C cleavage sites in the three monomers lie next to each other, cleavage may soften this area of the molecule by altering protein–protein contacts and allow an influx of solvent into an area at the center of the trimer structure. When the steric hindrance imposed by σ3 is released, μ1 may then undergo the conformational alterations necessary to allow membrane penetration.

The conformational changes in μ1 that accompany viral disassembly are thought to expose internal hydrophobic residues and release μ1N from the particle [24, 26, 110]. Massive rearrangements are necessary to expose the hydrophobic residues and myristoylated N-terminus [86]. The cleavage of μ1 to form μ1N and μ1C is necessary for productive infection [110]. However, it is not clear whether membrane penetration is accomplished by soluble or particle-associated μ1N, perhaps acting in concert with other regions of the molecule. For example, an anion-binding site in domain 4 lies on the outermost, solvent-exposed surface of the ISVP [86]. This site may bind to phospholipid head groups bringing the virus particle into proximity with the endosomal membrane. This association also might trigger rearrangements in μ1, revealing the myristoylated μ1N and the internal hydrophobic residues.

11 Conclusions and Future Directions

Despite the accumulated knowledge about reovirus attachment to cell-surface receptors and internalization into host cells, a precise understanding of the mechanisms underlying the serotype-dependent differences in tropism exhibited by reovirus in the murine CNS remains elusive. Since prototype and field-isolate strains of all three serotypes of reovirus utilize JAM-A as a receptor [8, 165], more work is required to determine the basis for serotype-dependent differences in reovirus disease. We envision four possibilities. First, JAM-A may serve as a serotype-independent reovirus receptor at some sites within the host, and other as yet unidentified receptors may confer serotype-dependent tropism in the CNS. Studies using JAM-A-null mice [23] should permit assessment of the role of JAM-A in reovirus pathogenesis and may serve to highlight the existence of additional receptors. Second, it is possible that the carbohydrate specificity of a particular strain of reovirus directs infection to specific cells or tissues. In support of this idea, reovirus strains that vary in sialic acid utilization have also been shown to vary in disease pathogenesis in the hepatobiliary system [9]. A third possibility is that reovirus requires independent receptors for attachment and internalization. It has not been definitively demonstrated that JAM-A alone can mediate internalization into host cells. Therefore, it is possible that virus is tethered to the cell surface through interactions with carbohydrate and JAM-A, but only the strains or serotypes that are capable of interactions with an internalization receptor, which may be expressed in a cell- or tissue-specific manner, achieve entry. Finally, differences in receptor utilization and internalization pathways might influence disease pathogenesis by virtue of activating different types

of signaling networks. Reovirus strains T1L and T3D differ in the capacity to induce apoptosis [36, 119, 148], a property that has been linked to receptor binding and disassembly [8, 34, 35]. Studies of reovirus-induced myocarditis provide support for the hypothesis that postattachment signaling plays a role in disease production. Treatment of reovirus-infected mice with a calpain inhibitor dramatically reduces myocardial injury and apoptotic myocardial cell death [38]. Additional studies are required to confirm an association of apoptosis with reovirus-induced disease. However, it appears that the role of reovirus receptors in disease pathogenesis is more complex than simply mediating the virus-docking event.

Tropism of reovirus in the host may also be influenced by postattachment entry steps. All available evidence suggests that reovirus virions are internalized by clathrin-mediated endocytosis. However, inhibition of clathrin-mediated uptake by treatment of cells with hypertonic sucrose or dominant-negative Eps15 has only a modest effect on virus entry [56]. This observation suggests that reovirus is capable of using more than a single entry pathway, a situation observed for other viruses. Influenza virus utilizes both clathrin-mediated and clathrin- and caveolin-independent uptake pathways [94, 124, 129], and human papillomaviruses use different pathways of entry depending on the viral type [19]. Additional studies of reovirus entry pathways are required to dissect the functional mechanisms used by reovirus to internalize into cells. If cell-specific entry pathways are elucidated, then the type of uptake mechanism may influence target cell selection in the host.

Tissue-specific expression of endocytic proteases might serve as an additional determinant of reovirus tropism. Cathepsin B and cathepsin L are required for reovirus uncoating in fibroblasts [50], whereas cathepsin S is required in macrophage-like P388D cells [68]. Interestingly, not all reovirus strains infect P388D cells [68], suggesting that different strains use different enzymes for uncoating in different cell types. While cathepsins B and L are ubiquitously expressed, cathepsin S displays a more restricted and regulated expression pattern with increased levels in tissues and cells of the immune system (reviewed in [28]). It is noteworthy that influenza virus [76, 77] and rotavirus [40, 57] display tropism partly on the basis of expression of proteases required for viral entry. Studies of reovirus pathogenesis using mice deficient in various proteases should clarify the role of these enzymes in viral tropism and disease.

The role of acidic pH in reovirus disassembly is unclear. Viruses with a His at residue 354 in σ3 can grow in the presence of AC [157]. This finding suggests that the altered conformation of σ3-His354 imparts an increased susceptibility to cleavage, allowing proteases enhanced access to internal cleavage sites. Thus, σ3-His354 may mimic a pH-dependent conformational intermediate

in the uncoating pathway. However, cathepsin B and cathepsin L require acidic pH for activity. Therefore, it is possible that the requirement for acidic pH during viral entry and disassembly serves to provide the appropriate conditions for the action of these enzymes. AC does not alter reovirus growth in P388D cells in which disassembly is catalyzed by cathepsin S [68], an enzyme that does not require acidic pH [79]. However, yields of reovirus in P388D cells are substantially less after infection by virions than by ISVPs [68], suggesting that entry into these cells is not optimally efficient. The role of acidic pH in internalization and disassembly may be better understood through studies of AC-resistant viral variants currently ongoing in our laboratory [166].

The massive rearrangements of μ1 during disassembly and membrane penetration are of considerable interest. The trigger for these conformational changes is not known, nor is it understood whether the process is simply dependent on the removal of σ3 or on other factors as yet unidentified. In addition, it is not apparent whether the N-terminal myristoylated fragment of μ1 must be released from the virion to mediate membrane penetration or whether the entire particle in some way contributes to membrane rupture. Ongoing studies in this area will likely contribute general insights into nonenveloped virus penetration and establish how viral assembly is precisely coordinated to prime the particle for the stepwise disassembly process.

Acknowledgements We thank Annie Antar, Jackie Campbell, Kartik Chandran, and Denise Wetzel for review of the manuscript and members of our laboratories for helpful discussions. We acknowledge support from Public Health Service awards T32 GM08554 (K.M.G.), T32 AI07611 (E.M.J.), R01 AI45716 (T.S.), R01 AI38296 (T.S.D.), R01 AI32539 (T.S.D.), and R01 GM67853 (T.S. and T.S.D.) and the Elizabeth B. Lamb Center for Pediatric Research.

References

1. Amerongen HM, Wilson GAR, Fields BN, Neutra MR (1994) Proteolytic processing of reovirus is required for adherence to intestinal M cells. J Virol 68:8428–8432
2. Arrate MP, Rodriguez JM, Tran TM, Brock TA, Cunningham SA (2001) Cloning of human junctional adhesion molecule 3 (JAM3) and its identification as the JAM2 counter-receptor. J Biol Chem 276:45826–45832
3. Baer GS, Dermody TS (1997) Mutations in reovirus outer-capsid protein σ3 selected during persistent infections of L cells confer resistance to protease inhibitor E64. J Virol 71:4921–4928
4. Baer GS, Ebert DH, Chung CJ, Erickson AH, Dermody TS (1999) Mutant cells selected during persistent reovirus infection do not express mature cathepsin L and do not support reovirus disassembly. J Virol 73:9532–9543
5. Balda MS, Matter K (2000) Transmembrane proteins of tight junctions. Semin Cell Dev Biol 11:281–289

6. Barrett AJ, Kembhavi AA, Brown MA, Kirschke H, Knight CG, Tamai M, Hanada K (1982) L-*trans*-Epoxysuccinyl-leucylamido(4-guanidino)butane (E-64) and its analogues as inhibitors of cysteine proteinases including cathepsins B, H and L. Biochem J 201:189–198
7. Barton ES, Connolly JL, Forrest JC, Chappell JD, Dermody TS (2001) Utilization of sialic acid as a coreceptor enhances reovirus attachment by multistep adhesion strengthening. J Biol Chem 276:2200–2211
8. Barton ES, Forrest JC, Connolly JL, Chappell JD, Liu Y, Schnell F, Nusrat A, Parkos CA, Dermody TS (2001) Junction adhesion molecule is a receptor for reovirus. Cell 104:441–451
9. Barton ES, Youree BE, Ebert DH, Forrest JC, Connolly JL, Valyi-Nagy T, Washington K, Wetzel JD, Dermody TS (2003) Utilization of sialic acid as a coreceptor is required for reovirus-induced biliary disease. J Clin Invest 111:1823–1833
10. Bass DM, Bodkin D, Dambrauskas R, Trier JS, Fields BN, Wolf JL (1990) Intraluminal proteolytic activation plays an important role in replication of type 1 reovirus in the intestines of neonatal mice. J Virol 64:1830–1833
11. Bassel-Duby R, Spriggs DR, Tyler KL, Fields BN (1986) Identification of attenuating mutations on the reovirus type 3 S1 double-stranded RNA segment with a rapid sequencing technique. J Virol 60:64–67
12. Bazzoni G, Martinez-Estrada OM, Mueller F, Nelboeck P, Schmid G, Bartfai T, Dejana E, Brockhaus M (2000) Homophilic interaction of junctional adhesion molecule. J Biol Chem 275:30970–30976
13. Bazzoni G, Martinez-Estrada OM, Orsenigo F, Cordenonsi M, Citi S, Dejana E (2000) Interaction of junctional adhesion molecule with the tight junction components ZO-1, cingulin, and occludin. J Biol Chem 275:20520–20526
14. Bergelson JM, Cunningham JA, Droguett G, Kurt-Jones EA, Krithivas A, Hong JS, Horwitz MS, Crowell RL, Finberg RW (1997) Isolation of a common receptor for Coxsackie B viruses and adenoviruses 2 and 5. Science 275:1320–1323
15. Bodkin DK, Nibert ML, Fields BN (1989) Proteolytic digestion of reovirus in the intestinal lumens of neonatal mice. J Virol 63:4676–4681
16. Bond JS, Butler PE (1987) Intracellular proteases. Ann Rev Biochem 56:333–364
17. Borsa J, Morash BD, Sargent MD, Copps TP, Lievaart PA, Szekely JG (1979) Two modes of entry of reovirus particles into L cells. J Gen Virol 45:161–170
18. Borsa J, Sargent MD, Lievaart PA, Copps TP (1981) Reovirus: evidence for a second step in the intracellular uncoating and transcriptase activation process. Virology 111:191–200
19. Bousarghin L, Touze A, Sizaret PY, Coursaget P (2003) Human papillomavirus types 16, 31, and 58 use different endocytosis pathways to enter cells. J Virol 77:3846–3850
20. Bullough PA, Hughson FM, Skehel JJ, Wiley DC (1994) Structure of influenza haemagglutinin at the pH of membrane fusion. Nature 371:37–43
21. Canning WM, Fields BN (1983) Ammonium chloride prevents lytic growth of reovirus and helps to establish persistent infection in mouse L cells. Science 219:987–988
22. Carson M (1987) Ribbon models of macromolecules. J Mol Graph 5:103–106

23. Cera MR, Del Prete A, Vecchi A, Corada M, Martin-Padura I, Motoike T, Tonetti P, Bazzoni G, Vermi W, Gentili F, Bernasconi S, Sato TN, Mantovani A, Dejana E (2004) Increased DC trafficking to lymph nodes and contact hypersensitivity in junctional adhesion molecule-A-deficient mice. J Clin Invest 114:729–738
24. Chandran K, Farsetta DL, Nibert ML (2002) Strategy for nonenveloped virus entry: a hydrophobic conformer of the reovirus membrane penetration protein μ1 mediates membrane disruption. J Virol 76:9920–9933
25. Chandran K, Nibert ML (1998) Protease cleavage of reovirus capsid protein μ1/μ1C is blocked by alkyl sulfate detergents, yielding a new type of infectious subvirion particle. J Virol 762:467–475
26. Chandran K, Parker JS, Ehrlich M, Kirchhausen T, Nibert ML (2003) The delta region of outer-capsid protein μ1 undergoes conformational change and release from reovirus particles during cell entry. J Virol 77:13361–13375
27. Chandran K, Walker SB, Chen Y, Contreras CM, Schiff LA, Baker TS, Nibert ML (1999) In vitro recoating of reovirus cores with baculovirus-expressed outer-capsid proteins μ1 and σ3. J Virol 73:3941–3950
28. Chapman HA, Riese RJ, Shi GP (1997) Emerging roles for cysteine proteases in human biology. Annu Rev Physiol 59:63–88
29. Chappell JD, Duong JL, Wright BW, Dermody TS (2000) Identification of carbohydrate-binding domains in the attachment proteins of type 1 and type 3 reoviruses. J Virol 74:8472–8479
30. Chappell JD, Gunn VL, Wetzel JD, Baer GS, Dermody TS (1997) Mutations in type 3 reovirus that determine binding to sialic acid are contained in the fibrous tail domain of viral attachment protein σ1. J Virol 71:1834–1841
31. Chappell JD, Prota A, Dermody TS, Stehle T (2002) Crystal structure of reovirus attachment protein σ1 reveals evolutionary relationship to adenovirus fiber. EMBO J 21:1–11
32. Clarke P, Meintzer SM, Gibson S, Widmann C, Garrington TP, Johnson GL, Tyler KL (2000) Reovirus-induced apoptosis is mediated by TRAIL. J Virol 74:8135–8139
33. Cohen CJ, Shieh JT, Pickles RJ, Okegawa T, Hsieh JT, Bergelson JM (2001) The coxsackievirus and adenovirus receptor is a transmembrane component of the tight junction. Proc Natl Acad Sci U S A 98:15191–15196
34. Connolly JL, Barton ES, Dermody TS (2001) Reovirus binding to cell surface sialic acid potentiates virus-induced apoptosis. J Virol 75:4029–4039
35. Connolly JL, Dermody TS (2002) Virion disassembly is required for apoptosis induced by reovirus. J Virol 76:1632–1641
36. Connolly JL, Rodgers SE, Clarke P, Ballard DW, Kerr LD, Tyler KL, Dermody TS (2000) Reovirus-induced apoptosis requires activation of transcription factor NF-κB. J Virol 74:2981–2989
37. Cunningham SA, Arrate MP, Rodriguez JM, Bjercke RJ, Vanderslice P, Morris AP, Brock TA (2000) A novel protein with homology to the junctional adhesion molecule. Characterization of leukocyte interactions. J Biol Chem 275:34750–34756
38. DeBiasi R, Edelstein C, Sherry B, Tyler K (2001) Calpain inhibition protects against virus-induced apoptotic myocardial injury. J Virol 75:351–361

39. Del Maschio A, De Luigi A, Martin-Padura I, Brockhaus M, Bartfai T, Fruscella P, Adorini L, Martino G, Furlan R, De Simoni MG, Dejana E (1999) Leukocyte recruitment in the cerebrospinal fluid of mice with experimental meningitis is inhibited by an antibody to junctional adhesion molecule (JAM). J Exp Med 190:1351–1356
40. Denisova E, Dowling W, LaMonica R, Shaw R, Scarlata S, Ruggeri F, Mackow ER (1999) Rotavirus capsid protein VP5* permeabilizes membranes. J Virol 73:3147–3153
41. Dermody TS (1998) Molecular mechanisms of persistent infection by reovirus.In: Tyler KL, Oldstone MBA (eds), Curr Topics Micro Immunol, vol. 233. Reoviruses, II Cytopathogenicity and pathogenesis. Springer-Verlag, Berlin Heidelberg, New York, pp 1–22
42. Dermody TS, Nibert ML, Bassel-Duby R, Fields BN (1990) A σ1 region important for hemagglutination by serotype 3 reovirus strains. J Virol 64:5173–5176
43. Dermody TS, Nibert ML, Bassel-Duby R, Fields BN (1990) Sequence diversity in S1 genes and S1 translation products of 11 serotype 3 reovirus strains. J Virol 64:4842–4850
44. Dermody TS, Nibert ML, Wetzel JD, Tong X, Fields BN (1993) Cells and viruses with mutations affecting viral entry are selected during persistent infections of L cells with mammalian reoviruses. J Virol 67:2055–2063
45. Dichter MA, Weiner HL (1984) Infection of neuronal cell cultures with reovirus mimics in vitro patterns of neurotropism. Ann Neurol 16:603–610
46. Dryden KA, Wang G, Yeager M, Nibert ML, Coombs KM, Furlong DB, Fields BN, Baker TS (1993) Early steps in reovirus infection are associated with dramatic changes in supramolecular structure and protein conformation: analysis of virions and subviral particles by cryoelectron microscopy and image reconstruction. J Cell Biol 122:1023–1041
47. Dryden KA, Farsetta DL, Wang G, Keegan JM, Fields BN, Baker TS, Nibert ML (1998) Internal structures containing transcriptase-related proteins in top component particles of mammalian orthoreovirus. Virology 245:33–46
48. Duncan R, Lee PWK (1994) Localization of two protease-sensitive regions separating distinct domains in the reovirus cell-attachment protein sigma 1. Virology 203:149–152
49. Duncan R, Horne D, Strong JE, Leone G, Pon RT, Yeung MC, Lee PWK (1991) Conformational and functional analysis of the C-terminal globular head of the reovirus cell attachment protein. Virology 182:810–819
50. Ebert DH, Deussing J, Peters C, Dermody TS (2002) Cathepsin L and cathepsin B mediate reovirus disassembly in murine fibroblast cells. J Biol Chem 277:24609–24617
51. Ebert DH, Kopecky-Bromberg SA, Dermody TS (2004) Cathepsin B is inhibited in mutant cells selected during persistent reovirus infection. J Biol Chem 279:3837–3851
52. Ebert DH, Wetzel JD, Brumbaugh DE, Chance SR, Stobie LE, Baer GS, Dermody TS (2001) Adaptation of reovirus to growth in the presence of protease inhibitor E64 segregates with a mutation in the carboxy terminus of viral outer-capsid protein σ3. J Virol 75:3197–3206

53. Ebnet K, Schulz CU, Meyer Zu Brickwedde MK, Pendl GG, Vestweber D (2000) Junctional adhesion molecule interacts with the PDZ domain-containing proteins AF-6 and ZO-1. J Biol Chem 275:27979–27988
54. Ebnet K, Suzuki A, Horikoshi Y, Hirose T, Meyer Zu Brickwedde MK, Ohno S, Vestweber D (2001) The cell polarity protein ASIP/PAR-3 directly associates with junctional adhesion molecule (JAM). EMBO J 20:3738–3748
55. Ebnet K, Suzuki A, Ohno S, Vestweber D (2004) Junctional adhesion molecules (JAMs): more molecules with dual functions? J Cell Sci 117:19–29
56. Ehrlich M, Boll W, Van Oijen A, Hariharan R, Chandran K, Nibert ML, Kirchhausen T (2004) Endocytosis by random initiation and stabilization of clathrin-coated pits. Cell 118:591–605
57. Estes MK, Graham DY, Mason BB (1981) Proteolytic enhancement of rotavirus infectivity: molecular mechanisms. J Virol 39:879–888
58. Fleeton M, Contractor N, Leon F, Wetzel JD, Dermody TS, Kelsall B (2004) Peyer's patch dendritic cells process viral antigen from apoptotic epithelial cells in the intestine of reovirus-infected mice. J Exp Med 200:235–245
59. Forrest JC, Campbell JA, Schelling P, Stehle T, Dermody TS (2003) Structure-function analysis of reovirus binding to junctional adhesion molecule 1. Implications for the mechanism of reovirus attachment. J Biol Chem 278:48434–48444
60. Fraser RDB, Furlong DB, Trus BL, Nibert ML, Fields BN, Steven AC (1990) Molecular structure of the cell-attachment protein of reovirus: correlation of computer-processed electron micrographs with sequence-based predictions. J Virol 64:2990–3000
61. Furlong DB, Nibert ML, Fields BN (1988) Sigma 1 protein of mammalian reoviruses extends from the surfaces of viral particles. J Virol 62:246–256
62. Gal S, Gottesman MM (1986) The major excreted protein (MEP) of transformed mouse cells and cathepsin L have similar protease specificity. Biochem Biophys Res Commun 139:156–162
63. Gal S, Willingham MC, Gottesman MM (1985) Processing and lysosomal localization of a glycoprotein whose secretion is transformation stimulated. J Cell Biol 100:535–544
64. Gentsch JR, Pacitti AF (1985) Effect of neuraminidase treatment of cells and effect of soluble glycoproteins on type 3 reovirus attachment to murine L cells. J Virol 56:356–364
65. Gentsch JR, Pacitti AF (1987) Differential interaction of reovirus type 3 with sialylated receptor components on animal cells. Virology 161:245–248
66. Georgi A, Mottola-Hartshorn C, Warner A, Fields B, Chen LB (1990) Detection of individual fluorescently labeled reovirions in living cells. Proc Natl Acad Sci U S A 87:6579–6583
67. Geraghty RJ, Krummenacher C, Cohen GH, Eisenberg RJ, Spear PG (1998) Entry of alphaherpesviruses mediated by poliovirus receptor-related protein 1 and poliovirus receptor. Science 280:1618–1620
68. Golden JW, Bahe JA, Lucas WT, Nibert ML, Schiff LA (2004) Cathepsin S supports acid-independent infection by some reoviruses. J Biol Chem 279:8547–8557
69. Gottesman MM, Sobel ME (1980) Tumor promoters and Kirsten sarcoma virus increase synthesis of a secreted glycoprotein by regulating levels of translatable mRNA. Cell 19:449–455

70. Hamazaki Y, Itoh M, Sasaki H, Furuse M, Tsukita S (2002) Multi-PDZ domain protein 1 (MUPP1) is concentrated at tight junctions through its possible interaction with claudin-1 and junctional adhesion molecule. J Biol Chem 277:455–461
71. Helander A, Silvey KJ, Mantis NJ, Hutchings AB, Chandran K, Lucas WT, Nibert ML, Neutra MR (2003) The viral sigma1 protein and glycoconjugates containing alpha2–3-linked sialic acid are involved in type 1 reovirus adherence to M cell apical surfaces. J Virol 77:7964–7977
72. Itoh M, Sasaki H, Furuse M, Ozaki H, Kita T, Tsukita S (2001) Junctional adhesion molecule (JAM) binds to PAR-3: a possible mechanism for the recruitment of PAR-3 to tight junctions. J Cell Biol 154:491–497
73. Jané-Valbuena J, Nibert ML, Spencer SM, Walker SB, Baker TS, Chen Y, Centonze VE, Schiff LA (1999) Reovirus virion-like particles obtained by recoating infectious subvirion particles with baculovirus-expressed σ3 protein: an approach for analyzing σ3 functions during virus entry. J Virol 73:2963–2973
74. Jané-Valbuena J, Breun LA, Schiff LA, Nibert ML (2002) Sites and determinants of early cleavages in the proteolytic processing pathway of reovirus surface protein sigma3. J Virol 76:5184–5197
75. Kaye KM, Spriggs DR, Bassel-Duby R, Fields BN, Tyler KL (1986) Genetic basis for altered pathogenesis of an immune-selected antigenic variant of reovirus type 3 Dearing. J Virol 59:90–97
76. Kido H, Towatari T, Niwa Y, Okumura Y, Beppu Y (1996) Cellular proteases involved in the pathogenicity of human immunodeficiency and influenza viruses. Adv Exp Med Biol 389:233–240
77. Kido H, Murakami M, Oba K, Chen Y, Towatari T (1999) Cellular proteinases trigger the infectivity of the influenza A and Sendai viruses. Mol Cells 9:235–244
78. Kirschke H, Langner J, Wiederanders B, Ansorge S, Bohley P (1977) Cathepsin L. A new proteinase from rat-liver lysosomes. Eur J Biochem 74:293–301
79. Kirschke H, Wiederanders B, Bromme D, Rinne A (1989) Cathepsin S from bovine spleen. Purification, distribution, intracellular localization and action on proteins. Biochem J 264:467–473
80. Kostrewa D, Brockhaus M, D'Arcy A, Dale GE, Nelboeck P, Schmid G, Mueller F, Bazzoni G, Dejana E, Bartfai T, Winkler FK, Hennig M (2001) X-ray structure of junctional adhesion molecule: structural basis for homophilic adhesion via a novel dimerization motif. EMBO J 20:4391–4398
81. Kothandaraman S, Hebert MC, Raines RT, Nibert ML (1998) No role for pepstatin-A-sensitive acidic proteinases in reovirus infections of L or MDCK cells. Virology 251:264–272
82. Lechner F, Sahrbacher U, Suter T, Frei K, Brockhaus M, Koedel U, Fontana A (2000) Antibodies to the junctional adhesion molecule cause disruption of endothelial cells and do not prevent leukocyte influx into the meninges after viral or bacterial infection. J Infect Dis 182:978–982
83. Lee PW, Hayes EC, Joklik WK (1981) Protein σ1 is the reovirus cell attachment protein. Virology 108:156–163
84. Leone G, Duncan R, Lee PWK (1991) Trimerization of the reovirus cell attachment protein (σ1) induces conformational changes in σ1 necessary for its cell-binding function. Virology 184:758–761

85. Lerner AM, Cherry JD, Finland M (1963) Haemagglutination with reoviruses. Virology 19:58–65
86. Liemann S, Chandran K, Baker TS, Nibert ML, Harrison SC (2002) Structure of the reovirus membrane-penetration protein, μ1, in a complex with is protector protein, σ3. Cell 108:283–295
87. Liu Y, Nusrat A, Schnell FJ, Reaves TA, Walsh S, Ponchet M, Parkos CA (2000) Human junction adhesion molecule regulates tight junction resealing in epithelia. J Cell Sci 113:2363–2374
88. Mach L, Stuwe K, Hagen A, Ballaun C, Glossl J (1992) Proteolytic processing and glycosylation of cathepsin B. The role of the primary structure of the latent precursor and of the carbohydrate moiety for cell-type-specific molecular forms of the enzyme. Biochem J 282:577–582
89. Mann MA, Knipe DM, Fischbach GD, Fields BN (2002) Type 3 reovirus neuroinvasion after intramuscular inoculation: direct invasion of nerve terminals and age-dependent pathogenesis. Virology 303:222–231
90. Maratos-Flier E, Goodman MJ, Murray AH, Kahn CR (1986) Ammonium inhibits processing and cytotoxicity of reovirus, a nonenveloped virus. J Clin Invest 78:617–625
91. Martinez CG, Guinea R, Benavente J, Carrasco L (1996) The entry of reovirus into L cells is dependent on vacuolar proton-ATPase activity. J Virol 70:576–579
92. Martin-Padura I, Lostaglio S, Schneemann M, Williams L, Romano M, Fruscella P, Panzeri C, Stoppacciaro A, Ruco L, Villa A, Simmons D, Dejana E (1998) Junctional adhesion molecule, a novel member of the immunoglobulin superfamily that distributes at intercellular junctions and modulates monocyte transmigration. J Cell Biol 142:117–127
93. Mason RW (1989) Interaction of lysosomal cysteine proteinases with alpha-2-macroglobulin: conclusive evidence for the endopeptidase activities of cathepsins B and H. Arch Biochem Biophys 273:367–374
94. Matlin KS, Reggio HV, Helenius A, Simons K (1982) Infectious entry pathway of influenza virus in a canine kidney cell line. J Cell Biol 91:601–613
95. Maxfield FR (1982) Weak bases and ionophores rapidly and reversibly raise the pH in endocytic vesicles in cultured mouse fibroblasts. J Cell Biol 95:676–681
96. McCrae MA, Joklik WK (1978) The nature of the polypeptide encoded by each of the ten double-stranded RNA segments of reovirus type 3. Virology 89:578–593
97. Metcalf P, Cyrklaff M, Adrian M (1991) The 3-dimensional structure of reovirus obtained by cryoelectron microscopy. EMBO J 10:3129–3136
98. Mizuochi T, Yee ST, Kasai M, Kakiuchi T, Muno D, Kominami E (1994) Both cathepsin B and cathepsin D are necessary for processing of ovalbumin as well as for degradation of class II MHC invariant chain. Immunol Let 43:189–193
99. Morrison LA, Sidman RL, Fields BN (1991) Direct spread of reovirus from the intestinal lumen to the central nervous system through vagal autonomic nerve fibers. Proc Natl Acad Sci U S A 88:3852–3856
100. Mustoe TA, Ramig RF, Sharpe AH, Fields BN (1978) Genetics of reovirus: identification of the dsRNA segments encoding the polypeptides of the μ and σ size classes. Virology 89:594–604
101. Nakagawa T, Roth W, Wong P, Nelson A, Farr A, Deussing J, Villadangos JA, Ploegh H, Peters C, Rudensky AY (1998) Cathespin L: critical role in Ii degradation and CD4 T cell selection in the thymus. Science 280:450–453

102. Nason E, Wetzel J, Mukherjee S, Barton E, Prasad B, Dermody T (2001) A monoclonal antibody specific for reovirus outer-capsid protein σ3 inhibits σ1-mediated hemagglutination by steric hindrance. J Virol 75:6625–6634
103. Nibert ML, Fields BN (1992) A carboxy-terminal fragment of protein μ1/μ1C is present in infectious subvirion particles of mammalian reoviruses and is proposed to have a role in penetration. J Virol 66:6408–6418
104. Nibert ML, Schiff LA (2001) Reoviruses and their replication. In: Knipe DM, Howley PM (eds) Fields virology, 4th edn. Lippincott Williams Wilkins, Philadelphia, pp 1679–1728
105. Nibert ML, Furlong DB, Fields BN (1991) Mechanisms of viral pathogenesis: distinct forms of reoviruses and their roles during replication in cells and host. J Clin Invest 88:727–734
106. Nibert ML, Schiff LA, Fields BN (1991) Mammalian reoviruses contain a myristoylated structural protein. J Virol 65:1960–1967
107. Nibert ML, Chappell JD, Dermody TS (1995) Infectious subvirion particles of reovirus type 3 Dearing exhibit a loss in infectivity and contain a cleaved σ1 protein. J Virol 69:5057–5067
108. Nibert ML, Odegard AL, Agosto MA, Chandran K, Schiff LA (2005) Putative autocleavage of reovirus mu1 protein in concert with outer-capsid disassembly and activation for membrane permeabilization. J Mol Biol 345:461–474
109. Oberhaus SM, Smith RL, Clayton GH, Dermody TS, Tyler KL (1997) Reovirus infection and tissue injury in the mouse central nervous system are associated with apoptosis. J Virol 71:2100–2106
110. Odegard AL, Chandran K, Zhang X, Parker JS, Baker TS, Nibert ML (2004) Putative autocleavage of outer capsid protein μ1, allowing release of myristoylated peptide μ1N during particle uncoating, is critical for cell entry by reovirus. J Virol 78:8732–8745
111. Ohkuma S, Poole B (1978) Fluorescence probe measurement of the intralysosomal pH in living cells and the perturbation of pH by various agents. Proc Natl Acad Sci U S A 75:3327–3331
112. Olland AM, Jané-Valbuena J, Schiff LA, Nibert ML, Harrison SC (2001) Structure of the reovirus outer capsid and dsRNA-binding protein σ3 at 1.8 Å resolution. EMBO J 20:979–989
113. Ostermann G, Weber KS, Zernecke A, Schroder A, Weber C (2002) JAM-1 is a ligand of the beta(2) integrin LFA-1 involved in transendothelial migration of leukocytes. Nat Immunol 3:151–158
114. Ozaki H, Ishii K, Horiuchi H, Arai H, Kawamoto T, Okawa K, Iwamatsu A, Kita T (1999) Cutting edge: combined treatment of TNF-alpha and IFN-gamma causes redistribution of junctional adhesion molecule in human endothelial cells. J Immunol 163:553–557
115. Paul RW, Lee PWK (1987) Glycophorin is the reovirus receptor on human erythrocytes. Virology 159:94–101
116. Paul RW, Choi AH, Lee PWK (1989) The α-anomeric form of sialic acid is the minimal receptor determinant recognized by reovirus. Virology 172:382–385
117. Prota AE, Campbell JA, Schelling P, Forrest JC, Peters TR, Watson MJ, Aurrand-Lions M, Imhof B, Dermody TS, Stehle T (2003) Crystal structure of human junctional adhesion molecule 1: implications for reovirus binding. Proc Natl Acad Sci U S A 100:5366–5371

118. Riese RJ, Wolf PR, Bromme D, Natkin LR, Villadangos JA, Ploegh HL, Chapman HA (1996) Essential role for cathepsin S in MHC class II-associated invariant chain processing and peptide loading. Immunity 4:357–366
119. Rodgers SE, Barton ES, Oberhaus SM, Pike B, Gibson CA, Tyler KL, Dermody TS (1997) Reovirus-induced apoptosis of MDCK cells is not linked to viral yield and is blocked by Bcl-2. J Virol 71:2540–2546
120. Rosen L (1960) Serologic grouping of reovirus by hemagglutination-inhibition. Am J Hyg 71:242–249
121. Rowan AD, Mason P, Mach L, Mort JS (1992) Rat procathepsin B. Proteolytic processing to the mature form in vitro. J Biol Chem 267:15993–15999
122. Rubin DH, Weiner DB, Dworkin C, Greene MI, Maul GG, Williams WV (1992) Receptor utilization by reovirus type 3: distinct binding sites on thymoma and fibroblast cell lines result in differential compartmentalization of virions. Microb Pathog 12:351–365
123. Rubin DH, Wetzel JD, Williams WV, Cohen JA, Dworkin C, Dermody TS (1992) Binding of type 3 reovirus by a domain of the σ1 protein important for hemagglutination leads to infection of murine erythroleukemia cells. J Clin Invest 90:2536–2542
124. Rust MJ, Lakadamyali M, Zhang F, Zhuang X (2004) Assembly of endocytic machinery around individual influenza viruses during viral entry. Nat Struct Mol Biol 11:567–573
125. Ryan RE, Sloane BF, Sameni M, Wood PL (1995) Microglial cathepsin B: an immunological examination of cellular and secreted species. J Neurochem 65:1035–1045
126. Sabin AB (1959) Reoviruses: a new group of respiratory and enteric viruses formerly classified as ECHO type 10 is described. Science 130:1387–1389
127. Sagik B, Puck T, Levine S (1954) Quantitative aspects of the spontaneous elution of influenza virus from red cells. J Exp Med 99:251–260
128. Salminen A, Gottesman MM (1990) Inhibitor studies indicate that active cathepsin L is probably essential to its own processing in cultured fibroblasts. Biochem J 272:39–44
129. Sieczkarski SB, Whittaker GR (2002) Influenza virus can enter and infect cells in the absence of clathrin-mediated endocytosis. J Virol 76:10455–10464
130. Smith RE, Zweerink HJ, Joklik WK (1969) Polypeptide components of virions, top component and cores of reovirus type 3. Virology 39:791–810
131. Songyang Z, Fanning AS, Fu C, Xu J, Marfatia SM, Chishti AH, Crompton A, Chan AC, Anderson JM, Cantley LC (1997) Recognition of unique carboxyl-terminal motifs by distinct PDZ domains. Science 275:73–77
132. Spear PG (2002) Viral interactions with receptors in cell junctions and effects on junctional stability. Dev Cell 3:462–464
133. Spriggs DR, Fields BN (1982) Attenuated reovirus type 3 strains generated by selection of haemagglutinin antigenic variants. Nature 297:68–70
134. Spriggs DR, Bronson RT, Fields BN (1983) Hemagglutinin variants of reovirus type 3 have altered central nervous system tropism. Science 220:505–507
135. Stehle T, Dermody TS (2003) Structural evidence for common functions and ancestry of the reovirus and adenovirus attachment proteins. Rev Med Virol 13:123–132

136. Stehle T, Dermody TS (2004) Structural similarities in the cellular receptors used by adenovirus and reovirus. Viral Immunol 17:129–143
137. Stiasny K, Allison SL, Marchler-Bauer A, Kunz C, Heinz FX (1996) Structural requirements for low-pH-induced rearrangements in the envelope glycoprotein of tick-borne encephalitis virus. J Virol 70:8142–8147
138. Strong JE, Leone G, Duncan R, Sharma RK, Lee PW (1991) Biochemical and biophysical characterization of the reovirus cell attachment protein sigma 1: evidence that it is a homotrimer. Virology 184:23–32
139. Sturzenbecker LJ, Nibert ML, Furlong DB, Fields BN (1987) Intracellular digestion of reovirus particles requires a low pH and is an essential step in the viral infectious cycle. J Virol 61:2351–2361
140. Takahashi K, Nakanishi H, Miyahara M, Mandai K, Satoh K, Satoh A, Nishioka H, Aoki J, Nomoto A, Mizoguchi A, Takai Y (1999) Nectin/PRR: an immunoglobulin-like cell adhesion molecule recruited to cadherin-based adherens junctions through interaction with Afadin, a PDZ domain-containing protein. J Cell Biol 145:539–549
141. Tardieu M, Weiner HL (1982) Viral receptors on isolated murine and human ependymal cells. Science 215:419–421
142. Tardieu M, Powers ML, Weiner HL (1983) Age-dependent susceptibility to reovirus type 3 encephalitis: role of viral and host factors. Ann Neurol 13:602–607
143. Tosteson MT, Nibert ML, Fields BN (1993) Ion channels induced in lipid bilayers by subvirion particles of the nonenveloped mammalian reoviruses. Proc Natl Acad Sci U S A 90:10549–10552
144. Tsukita S, Furuse M, Itoh M (1999) Structural and signalling molecules come together at tight junctions. Curr Opin Cell Biol 11:628–633
145. Turner DL, Duncan R, Lee PW (1992) Site-directed mutagenesis of the C-terminal portion of reovirus protein σ1: evidence for a conformation-dependent receptor binding domain. Virology 186:219–227
146. Tyler KL (2001) Mammalian reoviruses. In: Knipe DM, Howley PM (eds) Fields virology, 4th edn. Lippincott Williams Wilkins, Philadelphia, pp 1729–1945
147. Tyler KL, McPhee DA, Fields BN (1986) Distinct pathways of viral spread in the host determined by reovirus S1 gene segment. Science 233:770–774
148. Tyler KL, Squier MK, Rodgers SE, Schneider SE, Oberhaus SM, Grdina TA, Cohen JJ, Dermody TS (1995) Differences in the capacity of reovirus strains to induce apoptosis are determined by the viral attachment protein σ1. J Virol 69:6972–6979
149. Ullmer C, Schmuck K, Figge A, Lubbert H (1998) Cloning and characterization of MUPP1, a novel PDZ domain protein. FEBS Lett 424:63–68
150. Van Raaij MJ, Mitraki A, Lavigne G, Cusack S (1999) A triple β-spiral in the adenovirus fibre shaft reveals a new structural motif for a fibrous protein. Nature 401:935–938
151. Virgin HW, Tyler KL, Dermody TS (1997) Reovirus. In: Nathanson N (ed) Viral pathogenesis. Lippincott-Raven, New York, pp 669–699
152. Warner MS, Geraghty RJ, Martinez WM, Montgomery RI, Whitbeck JC, Xu R, Eisenberg RJ, Cohen GH, Spear PG (1998) A cell surface protein with herpesvirus entry activity (HveB) confers susceptibility to infection by mutants of herpes simplex virus type 1, herpes simplex virus type 2, and pseudorabies virus. Virology 246:179–189

153. Weiner HL, Drayna D, Averill DR Jr, Fields BN (1977) Molecular basis of reovirus virulence: role of the S1 gene. Proc Natl Acad Sci U S A 74:5744–5748
154. Weiner HL, Ault KA, Fields BN (1980) Interaction of reovirus with cell surface receptors. I. Murine and human lymphocytes have a receptor for the hemagglutinin of reovirus type 3. J Immunol 124:2143–2148
155. Weiner HL, Powers ML, Fields BN (1980) Absolute linkage of virulence and central nervous system tropism of reoviruses to viral hemagglutinin. J Infect Dis 141:609–616
156. Weis W, Brown JH, Cusack S, Paulson JC, Skehel JJ, Wiley DC (1988) Structure of the influenza virus haemagglutinin complexed with its receptor, sialic acid. Nature 333:426–431
157. Wetzel JD, Wilson GJ, Baer GS, Dunnigan LR, Wright JP, Tang DSH, Dermody TS (1997) Reovirus variants selected during persistent infections of L cells contain mutations in the viral S1 and S4 genes and are altered in viral disassembly. J Virol 71:1362–1369
158. Williams LA, Martin-Padura I, Dejana E, Hogg N, Simmons DL (1999) Identification and characterisation of human junctional adhesion molecule (JAM). Mol Immunol 36:1175–1188
159. Wilson GJ, Wetzel JD, Puryear W, Bassel-Duby R, Dermody TS (1996) Persistent reovirus infections of L cells select mutations in viral attachment protein σ1 that alter oligomer stability. J Virol 70:6598–6606
160. Wilson GJ, Nason EL, Hardy CS, Ebert DH, Wetzel JD, Prasad BVV, Dermody TS (2002) A single mutation in the carboxy terminus of reovirus outer-capsid protein σ3 confers enhanced kinetics of σ3 proteolysis, resistance to inhibitors of viral disassembly, and alterations in σ3 structure. J Virol 76:9832–9843
161. Wilson JH, Luftig RB, Wood WB (1970) Interaction of bacteriophage T4 tail fiber components with a lipopolysaccharide fraction from Escherichia coli. J Mol Biol 51:423–434
162. Wolf JL, Rubin DH, Finberg R, Kaufman RS, Sharpe AH, Trier JS, Fields BN (1981) Intestinal M cells: a pathway of entry of reovirus into the host. Science 212:471–472
163. Yoon M, Spear PG (2002) Disruption of adherens junctions liberates nectin-1 to serve as receptor for herpes simplex virus and pseudorabies virus entry. J Virol 76:7203–7208
164. Zahraoui A, Louvard D, Galli T (2000) Tight junction, a platform for trafficking and signaling protein complexes. J Cell Biol 151:F31–F36
165. Campbell JA, Schelling P, Wetzel JD, Johnson EM, Forrest JC, Wilson GA, Aurrand-Lions M, Imhof BA, Stehle T, Dermody TS (2005) Junctional adhesion molecule a serves as a receptor for prototype and field-isolate strains of mammalian reovirus. J Virol 79:7967–778
166. Clark KM, Wetzel JD, Gu Y, Ebert DH, McAbee SA, Stoneman EK, Baer GS, Zhu Y, Wilson GJ, Prasad BVV, Dermody TS (2006) Reovirus variants selected for resistance to ammonium chloride have mutations in viral outer capsid protein σ3. J Virol 80:671–681

APPENDIX B

THE REOVIRUS σ1 ASPARTIC ACID SANDWICH: A TRIMERIZATION MOTIF POISED FOR CONFORMATIONAL CHANGE

Pierre Schelling*, Kristen M. Guglielmi*, Eva Kirchner*, Bernhard Paetzold, Terence S. Dermody, and Thilo Stehle

Journal of Biological Chemistry. 282(15):11582-11589;2007

*Authors contributed equally to this manuscript

THE JOURNAL OF BIOLOGICAL CHEMISTRY VOL. 282, NO. 15, pp. 11582–11589, April 13, 2007

The Reovirus σ1 Aspartic Acid Sandwich

A TRIMERIZATION MOTIF POISED FOR CONFORMATIONAL CHANGE[*][S]

Received for publication, November 22, 2006, and in revised form, January 18, 2007 Published, JBC Papers in Press, February 15, 2007, DOI 10.1074/jbc.M610805200

Pierre Schelling[‡1,2], **Kristen M. Guglielmi**[§¶1], **Eva Kirchner**[‡1], **Bernhard Paetzold**[‡], **Terence S. Dermody**[§¶‖3], **and Thilo Stehle**[‡¶‖4]

From the [‡]*Interfakultäres Institut für Biochemie, Universität Tübingen, Hoppe-Seyler-Strasse 4, D-72076 Tübingen, Germany and the* [§]*Department of Microbiology and Immunology,* [¶]*Elizabeth B. Lamb Center for Pediatric Research, and* [‖]*Department of Pediatrics, Vanderbilt University School of Medicine, Nashville, Tennessee 37232*

Reovirus attachment protein σ1 mediates engagement of receptors on the surface of target cells and undergoes dramatic conformational rearrangements during viral disassembly in the endocytic pathway. The σ1 protein is a filamentous, trimeric molecule with a globular β-barrel head domain. An unusual cluster of aspartic acid residues sandwiched between hydrophobic tyrosines is located at the σ1 subunit interface. A 1.75-Å structure of the σ1 head domain now reveals two water molecules at the subunit interface that are held strictly in position and interact with neighboring residues. Structural and biochemical analyses of mutants affecting the aspartic acid sandwich indicate that these residues and the corresponding chelated water molecules act as a plug to block the free flow of solvent and stabilize the trimer. This arrangement of residues at the σ1 head trimer interface illustrates a new protein design motif that may confer conformational mobility during cell entry.

Mammalian orthoreoviruses (reoviruses)[5] attach to cells by specific binding to both carbohydrate and proteinaceous receptors. For serotype 3 reoviruses, viral attachment is a multistep process initiated by low affinity binding to sialic acid followed by high affinity binding to junctional adhesion molecule-A (JAM-A) (1, 2). These steps are mediated by discrete receptor-binding domains in the attachment protein, σ1 (3), a fiber-like molecule with head-and-tail morphology (4–6). Strain type 3 Dearing (T3D) σ1 has distinct binding sites for its receptors: the head domain binds to JAM-A with high affinity (2), whereas a region in the tail has been implicated in binding to sialic acid (1, 3, 7).

Viral attachment to the cell surface by σ1 leads to internalization of the virus by receptor-mediated endocytosis that is likely clathrin-dependent (8–10). Within endosomes, virions undergo acid-dependent, proteolytic disassembly to form infectious subvirion particles (8, 11). Infectious subvirion particles penetrate endosomal membranes and release transcriptionally active cores into the cytoplasm (12–14). Accumulating evidence suggests that σ1 undergoes dramatic conformational changes during viral disassembly and that these changes facilitate key steps in the cell entry process (4, 15, 16).

We previously determined the structure of the C-terminal half of σ1, which comprises the head domain plus a short region of the tail (6). This structure provided clues about the interaction of the head domain with its receptor JAM-A and the nature of trimer contacts. The head domain contains a water-filled cavity formed by three eight-stranded β-barrels, one donated by each monomer. The tail region consists of three β-spiral repeats. One of the most remarkable features of the σ1 structure is a cluster of aspartic acid residues at the base of the head domain (6). Molecular dynamics studies suggest that these residues are likely to play a role in mediating conformational changes in σ1 (17). However, at 2.6 Å resolution, the structure did not allow precise placement of water molecules and visualization of contacts between amino acids with sufficient accuracy to explain how such a unique arrangement of amino acids is compatible with a higher order structure.

In this study, we determined a high resolution structure of a fragment of T3D σ1 that comprises the head domain and a single β-spiral repeat of the tail. The structure has been refined to a resolution of 1.75 Å, allowing us to discern with high clarity details of the subunit interface in the vicinity of the aspartic acid cluster. Furthermore, we have analyzed two σ1 mutants with alterations in the vicinity of the subunit interface to determine the effects on receptor binding capacity and trimer stability. Our studies suggest that the aspartic acid cluster serves as a

* This work was supported by the Swiss National Foundation (to P. S.), Public Health Service Awards T32 GM08554 (to K. M. G.) and R01 GM67853 (to T. S. D. and T. S.), and the Elizabeth B. Lamb Center for Pediatric Research. Additional support was provided by Public Health Service Awards CA68485 for the Vanderbilt Cancer Center and DK20593 for the Vanderbilt Diabetes Research and Training Center. The costs of publication of this article were defrayed in part by the payment of page charges. This article must therefore be hereby marked "*advertisement*" in accordance with 18 U.S.C. Section 1734 solely to indicate this fact.

[S] The on-line version of this article (available at http://www.jbc.org) contains supplemental Figs. 1 and 2.

The atomic coordinates and structure factors (code 2OJ5 and 2OJ6) have been deposited in the Protein Data Bank, Research Collaboratory for Structural Bioinformatics, Rutgers University, New Brunswick, NJ (http://www.rcsb.org/).

[1] These authors contributed equally to this manuscript.

[2] Current address: Millipore SAS, EBC, BP116, 67124 Molsheim, France.

[3] To whom correspondence may be addressed: Dept. of Pediatrics, Vanderbilt University School of Medicine, 1161 21st Ave. South, Nashville, TN 37232. Tel.: 615-343-9943; Fax: 615-343-9723; E-mail: terry.dermody@vanderbilt.edu.

[4] To whom correspondence may be addressed: Interfakultäres Institut für Biochemie, Universität Tübingen, Hoppe-Seyler-Str. 4, D-72076 Tübingen, Germany. Tel.: 49-7071-2973043; Fax: 49-7071-295565; E-mail: thilo.stehle@uni-tuebingen.de.

[5] The abbreviations used are: reoviruses, mammalian orthoreoviruses; JAM-A, junctional adhesion molecule-A; T3D, type 3 Dearing; GST, glutathione *S*-transferase; VSV, vesicular stomatitis virus.

molecular switch that, depending on the microenvironment, can stabilize or destabilize the formation of a trimeric structure.

EXPERIMENTAL PROCEDURES

Protein Expression, Purification, and Analysis—A cDNA encoding residues 293–455 of T3D σ1 was amplified by PCR and introduced into pGEX4T-3 (GE Healthcare). Mutations were engineered using site-directed PCR with appropriate mutagenic primers. Expression was induced with 0.2 mM IPTG in *Escherichia coli* strain BL21(DE3) pLys-S cells (Novagen) at 25 °C. Bacteria were centrifuged to form a pellet, solubilized in 50 mM Tris (pH 7.8), 3 mM EDTA, 1% Triton X-100, 2 mM β-mercaptoethanol, 1 mM phenylmethylsulfonyl fluoride, and 100 μg/ml lysozyme, submitted to 50% duty-cycle sonication pulses using a Branson Sonifier 450, and centrifuged at 15,000 × *g*. The soluble fraction was purified using a 5-ml GSTrapFF column (GE Healthcare) and eluted with 30 mM reduced glutathione, 2 mM β-mercaptoethanol, 3 mM EDTA, and 50 mM Tris (pH 8.05). Controlled tryptic protease treatment was performed overnight at 4 °C to remove the glutathione *S*-transferase (GST) tag. The sample was equilibrated using PD-10 desalting columns and purified further using Mono Q anion-exchange chromatography (GE Healthcare) with an increasing gradient of NaCl in 20 mM HEPES (pH 7.1). The σ1-Y313A mutant protein was cleaved with thrombin on-column and further purified by gel filtration using a Superdex 75 column (GE Healthcare). Human JAM-A (hJAM-A), expressed as a GST fusion protein, was purified as described (18). Analytical scale gel filtration was performed using a Superdex 75 column mounted on a SMART system (GE Healthcare) in 20 mM Tris (pH 7.5), 100 mM NaCl.

Protein Crystallization and Data Collection—Purified T3D σ1 head domain was subjected to size-exclusion chromatography in 20 mM Tris (pH 7.5), 100 mM NaCl, and 0.01% sodium azide and concentrated using Millipore 5 MWCO filters to 13.6 mg/ml, as assessed by direct measurement of absorbance at 260 and 280 nm using the relationship: c[mg/ml] = (1.55 × $A_{280\,nm}$) − (0.76 × $A_{260\,nm}$), since the T3D σ1 head domain does not react linearly with either Bradford or Lowry dyes (data not shown). Crystals of native σ1 protein were grown from 10–12% polyethylene glycol 8000, 0.2 M magnesium sulfate, and 0.1 M sodium cacodylate (pH 6.9) by mixing an equal amount of protein and precipitant solution. σ1-D345N was concentrated to 8 mg/ml, and crystals were grown using the same conditions used to cultivate crystals of the wild-type protein but with 20% polyethylene glycol 8000. Crystals were flash-frozen using glycerol as cryoprotectant. Data from wild-type crystals were collected at the Brookhaven National Laboratory Synchrotron (beamline X29 features high flux radiation and ADSC Quantum-315 CCD detector). Data for σ1-D345N crystals were collected at the X6S beamline of the Swiss Light Source (Villigen, Switzerland) using a MarCCD detector. Both data sets were collected from single crystals and processed with HKL2000 (19).

Structure Determination—Crystals of wild-type σ1 belong to space group $P2_1$ (a = 83.93 Å, b = 51.38 Å, c = 108.87 Å, β = 95.66°) and contain six molecules, forming two complete trimers, in the asymmetric unit. The structure was determined by molecular replacement using the trimeric σ1 head domain (6) as a search model in AMoRe (20). Alternating rounds of model building and refinement were performed initially using the programs O (21) and CNS (22), respectively. The programs Coot (23) and Refmac5 (24) were then used to refine the model. σ1-D345N also formed crystals that belong to space group $P2_1$, with very similar unit cell dimensions (Table 1). The structure of this protein was solved and refined to 1.85 Å using Coot and Refmac5. Structure factors and coordinates have been deposited with the Protein Data Bank with accession codes 2OJ5 and 2OJ6 for the wild-type and mutant proteins, respectively.

Surface Plasmon Resonance—A BIAcore CM5 chip (Pharmacia Biosensor AB) was coated with mouse ascites containing monoclonal anti-GST antibody (Sigma) to 10,000 RU protein (~2000 RU antibody) by amine coupling. Purified GST or GST-hJAM-A ectodomain fusion protein at a concentration of 2 μM in HEPES-buffered saline (pH 7.0) were captured by injection across individual flow cells of an antibody-coated CM5 chip for 3 min at 30 μl/min using a BIAcore 2000 (Pharmacia Biosensor AB). Purified T3D σ1 head domain was injected across the conjugated chip surface at 30 μl/min. Following σ1 binding, chip surfaces were regenerated with a 20-μl pulse of 10 mM glycine (pH 2.5). Affinity constants for σ1 binding to hJAM-A were determined using separate k_{on} and k_{off} nonlinear regression with BIAevaluation 3.0 software (Pharmacia Biosensor AB), assuming a 1:1 Langmuir binding model (25).

RESULTS

Purification of the σ1 Head—The previously crystallized T3D σ1 protein (6) contained a flexible linker between the C-terminal two β-spiral repeats of the tail. This flexibility likely contributed to the observed diffraction limit of 2.6 Å for these crystals. To obtain better diffracting crystals of T3D σ1, we designed a modified construct containing the entire head domain and only the C-terminal β-spiral repeat of the tail (residues 293–455). We also tested an additional construct comprising only the head domain (residues 309–455), but it did not yield soluble and trimeric protein, suggesting that the C-terminal β-spiral contributes to trimer formation. The protein was produced with a cleavable N-terminal GST tag and purified via sequential glutathione affinity chromatography and anion exchange chromatography. Subsequent gel filtration showed that the protein elutes at an apparent molecular weight of ~45 kDa, consistent with a trimer (see Fig. 4*A*). N-terminal sequencing confirmed that the product released following protease treatment was the σ1 head domain with two additional amino acids from the protease recognition sequence (data not shown).

Binding of the σ1 Head Domain to JAM-A—To determine whether the purified protein folds natively, we quantitatively assessed the capacity of the σ1 head domain to bind to JAM-A using surface plasmon resonance. The JAM-A ectodomain, expressed and purified as a GST fusion protein (18), was captured on a biosensor surface with a GST-specific antibody. When injected across the biosensor surface, purified σ1 head bound saturably and reversibly to the GST-JAM-A ectodomain but not to GST alone (Fig. 1*A*). Kinetic

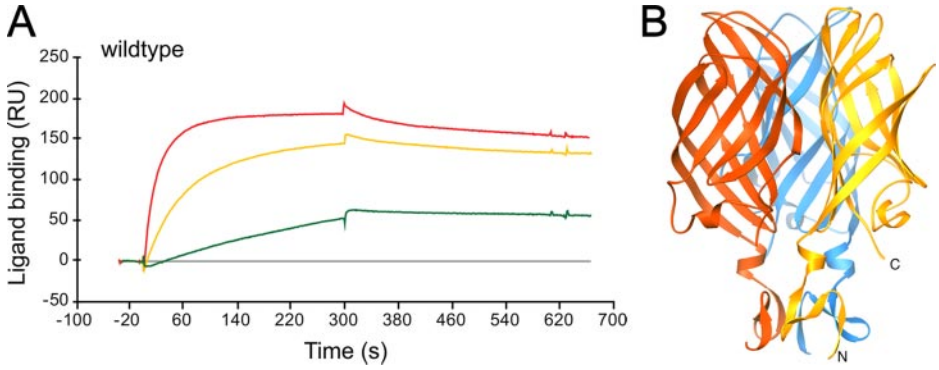

FIGURE 1. **Functional and structural characterization of the σ1 head domain.** *A*, T3D σ1 head binding to the JAM-A ectodomain. Purified σ1 head domain at 300 nM (*red*), 30 nM (*yellow*), and 3 nM (*green*) concentrations was injected over a biosensor surface coated with either GST or GST-JAM-A. Binding of σ1 head domain to GST was set as the base line (*gray*). Binding is measured in resonance units (*RU*). The calculated affinity for binding to GST-JAM-A, expressed as apparent K_D, is approximately 7×10^{-9} M. *B*, high resolution structure of the σ1 head. Shown is a ribbon tracing of the trimer, with the three chains drawn in *red*, *orange*, and *blue*. Termini are labeled in one monomer with N (N terminus) and C (C terminus). *B* was prepared using RIBBONS (36).

TABLE 1

Data collection and refinement statistics for the wild-type σ1 and σ1-D345N crystal structures

Data set	Wild-type σ1	σ1-D345N
Diffraction data[a]		
Space group	$P2_1$	$P2_1$
Unit cell dimensions (Å)	$a = 83.9$	$a = 84.0$
	$b = 51.4$	$b = 51.6$
	$c = 108.9$	$c = 108.9$
Angles (°)	$\beta = 95.7$	$\beta = 95.6$
Resolution range (Å)	30-1.75	30-1.85
Completeness (%)	96.7 (86.7)	98.7 (97.9)
Total reflections	300,167	347,405
Redundancy (%)	3.3 (2.6)	4.4 (4.0)
R_{merge} (%)[b]	9.3 (42.7)	9.6 (41.6)
$I/\sigma I$	15.7 (2.3)	6.5 (1.4)
Refinement statistics		
R_{cryst} (%); work set[c]	22.8 (30.3)	17.5 (23.0)
R_{cryst} (%); free set[c]	27.4 (38.1)	22.4 (27.3)
Overall *B*-factor (Å^2)	15.7	17.2
Root mean square deviation bond lengths (Å)	0.008	0.012
Root mean square deviation bond angles (°)	0.963	1.202
Number of water molecules	1166	953
Ramachandran plot:[d]		
Most favorable regions	88.5%	87.9%
Additional allowed regions	10.0%	10.5%
Generously allowed regions	1.0%	1.5%
Disallowed regions	0.5%	0.0%

[a] Data sets were collected at 100 K and a wavelength of 1.1 Å (wild-type) and 1.0 Å (D345N). Values in parentheses refer to the outermost resolution shell (1.75–1.81 Å for wild-type σ1 and 1.85–1.92 Å for D345N).

[b] $R_{merge} = \sum_{hkl}|I - \langle I\rangle|/\sum_{hkl} I$, where I is the intensity of a reflection *hkl*, and $\langle I\rangle$ is the average over symmetry-related observations of *hkl*.

[c] $R_{cryst} = \sum_{hkl}|F_{obs} - F_{calc}|/\sum_{hkl}F_{obs}$, where F_{obs} and F_{calc} are observed and calculated structure factors, respectively. Free set (38) contains 10% of the data.

[d] Calculated with PROCHECK (24).

analysis of the σ1-GST-JAM-A interaction using BIAevaluation 3.0 software indicated a K_D of $\sim 7 \times 10^{-9}$ M, a value that approximates the K_D determined for a larger fragment of σ1 (2). These results indicate that the purified σ1 head domain is functional and that the JAM-A-binding domain of σ1 lies within residues 293–455.

Overall Structure of the σ1 Head Domain at 1.75 Å Resolution—Diffraction data were collected at the National Synchrotron Light Source (Brookhaven National Laboratory) using crystals of the purified σ1 head domain. The structure was solved by molecular replacement using the previously determined lower resolution structure of a C-terminal fragment of σ1 (6) and refined to 1.75 Å (Table 1). An omit map for a portion of the refined structure calculated without model bias (supplemental Fig. 1) demonstrates that the model is accurate. Concordantly, both working and free *R*-factors (38) are very low (Table 1), indicating that the structure is well refined and of high quality. A total of six monomers, arranged into two almost identical trimers, are present in the asymmetric unit of the crystals. A ribbon tracing of one trimer is shown in Fig. 1*B*. Each σ1 monomer is composed of an eight-stranded β-barrel. The overall conformation of the monomers is very similar, with the exception of two longer and presumably flexible loops: the G-H loop at the top of each monomer and the D-E loop at its base. With the exception of His-388, all σ1 residues occupy allowed regions in the Ramachandran diagram (24). However, since the density corresponding to His-388 is unambiguous, it appears that a salt bridge to Glu-348 fixes its side chain in its observed conformation. Asp-345 is located in the generously allowed region of the Ramachandran diagram; it forms, together with Asp-346, a β-hairpin between β-strands B and C (supplemental Fig. 1). The dihedral angles classify this region as a type II′ β-hairpin (26).

Contacts in the σ1 Trimer—Trimer formation buries from solvent an area of 2292 Å^2 per monomer. Residues in the tail account for about 25% of this area, primarily through hydrophobic interactions between the strands of the β-spiral. The three β-barrel domains that form the head engage in a more complex pattern of interactions. Multiple contacts between the subunits at the outer edges of each monomer result in binding surfaces that extend from the base of the head to its top (Fig. 2*A*). However, a large cavity exists at the center of the trimer, and this cavity is surrounded by smaller regions that lack intersubunit contacts (Fig. 2*A*). The central cavity measures ~15 Å in height and ~10 Å in width and contains a large number of ordered water molecules that are connected to the exterior surface through channels at the top of the trimer (Fig. 2*B*). The cavity probably also contains many less well ordered water molecules, which are not visible in our electron density maps. Dimensions of the channels leading toward the cavity suggest that water molecules can flow freely to the top of the trimer. In contrast, the bottom of the cavity is sealed by the three Tyr-347 side chains.

The Aspartic Acid Sandwich—An unusual cluster of aspartic acid residues lies just below the water-filled cavity. Each monomer contributes two aspartic acid residues, Asp-345 and Asp-346, to this cluster, giving rise to a total of six aspartic acid side chains that are arranged in close proximity. Asp-345 and Asp-346 are located at the very tip of a β-hairpin between β-strands B and C (Fig. 3, *A* and *B*). β-Hairpins are small structural motifs stabilized by a defined backbone hydrogen bond pattern (27).

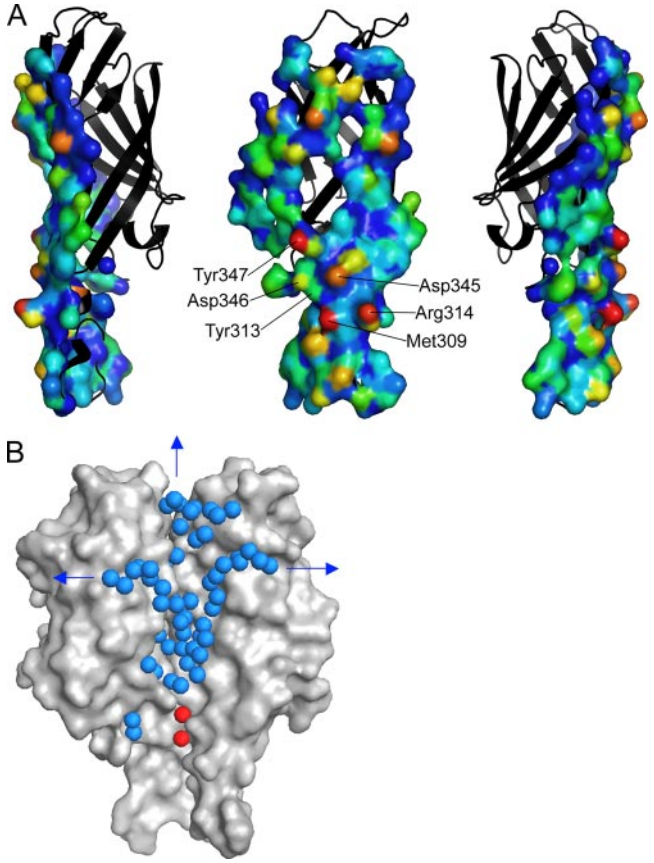

FIGURE 2. **Architecture of the σ1 head subunit interface.** *A*, contacts between subunits in the T3D σ1 trimer. Three views, each differing by 90°, are shown. One monomer is shown as a *black ribbon*, and its contact area with the other two monomers is represented as a molecular surface. Residues discussed in the text are labeled. The contact area was calculated using AREAIMOL (24) as the solvent-accessible area difference between the trimeric and monomeric forms of the molecule. The difference values range from 1 Å^2 (*dark blue*) to 52 Å^2 (*red*). Regions with a high area difference have low solvent accessibility in the trimer and thus represent areas with high affinity intersubunit contacts. Surfaces with an area difference of less than 1 Å^2 are not shown. Calculations were performed using a point density/Å^2 of 1 and a solvent molecule radius of 1.4 Å. *B*, solvent structure at the σ1 head interface. Two monomers are shown as a surface representation; the third monomer has been removed to allow a view into the trimer interface. Ordered water molecules at the interface are represented with *spheres*. The waters shown in *blue* fill most of the central cavity between the monomers and can leave the cavity via channels leading to the top and the sides of the trimer (*arrows*). The two water molecules shown in *red* are located near the Asp-345 side chains. These waters are solvent-inaccessible. This figure was generated using PyMOL (37).

The hairpins of the three monomers face each other, with the side chains of Asp-345 making key contacts. The aspartic acids are partitioned between two layers that each contain three tyrosine residues, Tyr-347 at the top and Tyr-313 at the bottom (Fig. 3, *C* and *D*).

Each Asp-346 side chain forms a salt bridge with Arg-314 from a neighboring monomer, but the Asp-345 side chains are not engaged in any ionic interactions (with other residues or with cations) that would negate their negative charges. The accumulation of three negative charges in such a hydrophobic environment would be highly unfavorable. Although hydrogen atoms cannot be seen in our electron density maps even at the high resolution obtained (1.75 Å), the location and orientation of the carboxyl groups strongly suggests that they are protonated. A protonated state of Asp-345 is also suggested by molecular dynamics studies of σ1 (17). Each protonated carboxylate forms two hydrogen bonds. One of these involves the hydrogen atom of the Asp-345 carboxyl group and the carbonyl oxygen of a neighboring Asp-346 residue; a second is formed between the carbonyl oxygen and the backbone amide group of Asp-346 in a neighboring monomer. Since these two hydrogen bonds occur three times, and since there are few other hydrogen bonds involved in head trimerization, the aspartic acid sandwich likely makes a major contribution to trimer stability.

The cluster of aspartic acids is sandwiched between hydrophobic residues that block access of solvent molecules to the carboxylate groups. One side of this sandwich (the "*top*" in Fig. 3*D*) is formed by Val-344 and Tyr-347, the other (the "*bottom*" in Fig. 3*D*) is formed by Tyr-313 and Met-309. Two well ordered water molecules located directly on the 3-fold axis are also present in this arrangement of amino acids. These water molecules interact with Tyr-313 and Asp-345, respectively, and they are held in place by an extensive hydrogen bond network. Buried water molecules can sometimes be exchanged without major unfolding. However, residues in the immediate vicinity of the two water molecules have temperature factors that are among the lowest of the entire structure (supplemental Fig. 2), suggesting that thermal mobility is low in this area. Thus, it is unlikely that the water molecules can be exchanged.

Purification and Characterization of σ1 Y313A—To explore potential conformational changes of σ1, we generated substitutions of two key residues of the cluster, Tyr-313 (Y313A) and Asp-345 (D345N). The mutant proteins were analyzed for receptor binding properties and the capacity to form trimers. We reasoned that substitution of Tyr-313 with a smaller amino acid might allow influx of water molecules to the aspartic acid cluster, thereby causing the trimer to undergo structural changes triggered by charged Asp-345 side chains. The σ1-Y313A mutant protein was expressed as a GST fusion in bacteria, purified by glutathione affinity, proteolytically cleaved from the GST tag on-column, and further purified using gel filtration. Purified σ1-Y313A is soluble and elutes as a monomer by gel filtration chromatography (Fig. 4*A*). Treatment of σ1-Y313A with each of three different cross-linking reagents of various lengths (11.4 to 16.1 Å) failed to alter the chromatographic mobility of the mutant protein (data not shown). σ1-Y313A was incapable of binding to JAM-A by either gel filtration (data not shown) or surface plasmon resonance (Fig. 4*B*), indicating that a trimeric form of σ1 is required for JAM-A engagement. Circular dichroism spectra of σ1-Y313A show a secondary structure content similar to that of wild-type σ1, suggesting that σ1-Y313A is folded properly (data not shown). Thus, our results indicate that residue Tyr313 is required for trimerization and that the trimeric form of σ1 is essential for receptor binding.

Characterization and Structure Analysis of σ1 D345N—To determine whether structural and functional changes occur upon replacement of Asp-345 with asparagine, we engineered a D345N mutation in the wild-type T3D σ1 head construct. We anticipated that hydrogen bonds might form between the asparagine residues, stabilizing the trimer interface in much the same manner as accomplished by the protonated Asp-345 side chains. The mutant protein was puri-

fied using the strategy employed for purification of the wild-type T3D σ1 head domain. The σ1-D345N mutant forms trimers at neutral pH (Fig. 4*A*) and binds to JAM-A with an affinity similar to that of wild-type σ1 (Fig. 4*B*). Thus, σ1-D345N is biochemically and functionally indistinguishable from the wild-type protein.

To test whether the D345N mutation in the T3D σ1 head domain alters the conformation of the aspartic acid sandwich, we determined the structure of σ1-D345N. The mutant protein was crystallized using conditions similar to those employed to crystallize the wild-type protein. We collected a complete data set from the σ1-D345N crystals to 1.85 Å and solved the structure by molecular replacement using the wildtype protein structure as a model (Table 1). The σ1-D345N mutant crystallized as a trimer with a structure that is nearly identical to that of the wild-type T3D σ1 head domain (Fig. 1*B*). At the subunit interface, the two water molecules observed just above and below residues 345 are at almost exactly the same position in σ1-D345N (Fig. 5). The amino groups of Asn-345 form the same hydrogen bond pattern as the hydroxyl group of protonated Asp-345. Thus, the mutant structure provides evidence that in trimeric, wild-type σ1 all Asp-345 residues must be protonated.

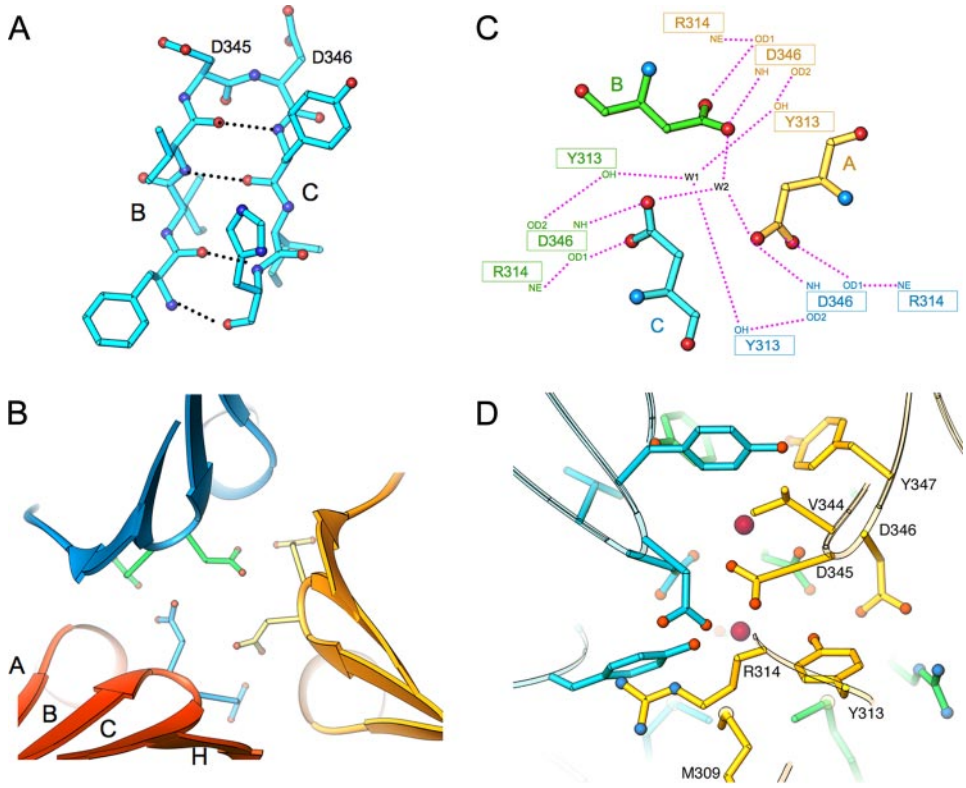

FIGURE 3. **An aspartic acid sandwich at the σ1 head trimer interface.** *A*, *ball-and-stick* view of the type II′ β-hairpin on which Asp-345 is located. Residues 342–349 are shown. Oxygen atoms are shown in *red*, and nitrogen atoms are shown in *blue*. Main-chain hydrogen bonds are represented with *black dotted lines*. *Letters B* and *C* refer to β-strands in the σ1 head. *B*, arrangement of β-hairpins and the aspartic acid cluster as seen from the top of the molecule. The view is along the 3-fold axis. The β-strands are depicted as *arrows*, and β-strands of one monomer are labeled. Side chains of Asp-345 and Asp-346 are shown in *ball-and-stick* representation. *C*, schematic view of the aspartic acid cluster, shown in the same orientation as that in *B*. Residues that interact with Asp-345 are shown in *orange* (monomer A), *green* (monomer B), and *blue* (monomer C). Hydrogen bonds are shown as *dotted lines*. *W1* and *W2* represent the two water molecules trapped inside the cluster. *D*, *ball-and-stick* representation of the aspartic acid cluster and surrounding residues. The view is perpendicular to the 3-fold axis. Residues discussed in the text are labeled in one monomer. The two trapped water molecules are represented with *red spheres*. The color code is the same as that used in *C*. This figure was prepared using RIBBONS (36).

DISCUSSION

Formation of σ1 Trimers—Although a C-terminal fragment of σ1 has been crystallized (6), further characterization at an atomic level of resolution has enhanced an understanding of its trimeric nature. Interactions that form the trimer are highly complex. The base of the trimer is held firmly together by hydrophobic interactions, a standard means of inducing the formation of oligomeric structures. In contrast, contacts at the center and top of the trimer involve interrupted surfaces, cavities filled with water molecules, trapped individual water molecules, very few hydrophobic contacts, and protonated side chains that form hydrogen bonds. These types of interactions are unusual for protein-protein contacts. We think that the σ1 head is designed to exist as both monomeric and trimeric species. In fact, the mutation of only one residue, Y313A, results in soluble, folded protein that is entirely monomeric. A single substitution at the base of the trimer therefore suffices to completely abolish trimer formation, indicating that the lower affinity contacts at the center and top of the σ1 head are not sufficient for stabilization of the trimer.

Comparison of deduced amino acid sequences of σ1 proteins from prototype and field-isolate reovirus strains reveals that Asp-345 and Asp-346 are highly conserved (6, 28). Additionally, hydrophobic residues that form the top and bottom of the aspartic acid sandwich show a high degree of conservation. Phenyl ring-containing side chains are found at positions 313 and 347 in a σ1 sequence alignment. For example, strain type 1 Lang contains phenylalanine and tryptophan residues, and strain type 2 Jones contains tyrosine and tryptophan residues at positions corresponding to Tyr-313 and Tyr-347 in T3D σ1. Furthermore, a hydrophobic residue (isoleucine, leucine, methionine, or valine) is found at position 309, and a valine is absolutely conserved at position 344. The striking level of sequence conservation at these positions suggests that the aspartic acid sandwich serves an essential function in reovirus replication.

Engagement of JAM-A—Our analysis shows that the σ1-Y313A mutant is soluble and monomeric. Furthermore, since its CD spectrum is similar to that of wild-type σ1, σ1-Y313A appears to be properly folded. However, the mutant

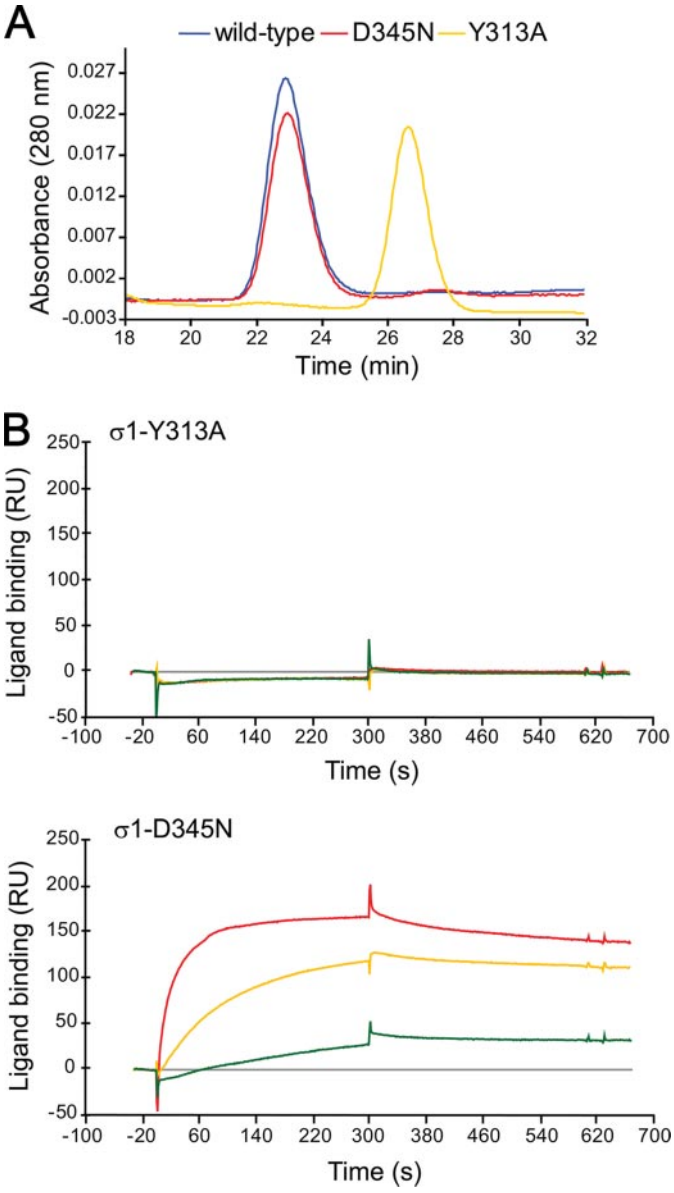

FIGURE 4. **Functional analysis of σ1 mutants.** *A*, gel filtration of T3D σ1 head mutants. Purified wild-type T3D σ1 head (*blue*), σ1-D345N (*red*), and σ1-Y313A (*yellow*) constructs were applied to a Superdex 75 gel filtration column (GE Healthcare) in 20 mM Tris (pH 7.5), 100 mM NaCl. The D345N mutant elutes at the same time as the wild-type protein, indicating that it forms a trimer, whereas the Y313A mutant shows a significantly smaller molecular weight that corresponds to monomeric protein. *B*, binding of T3D σ1 head mutants to the JAM-A ectodomain. Purified point mutants of the σ1 head domain at 300 nM (*red*), 30 nM (*yellow*), and 3 nM (*green*) concentrations were injected across a biosensor surface coated with either GST or GST-JAM-A. Binding of σ1 head point mutants to GST was set as the base line (*gray line*). Binding is measured in resonance units (*RU*). The identity of the mutants is indicated. The calculated affinity for binding of σ1-D345N to GST-JAM-A, expressed as apparent K_D, is approximately 1×10^{-8} M.

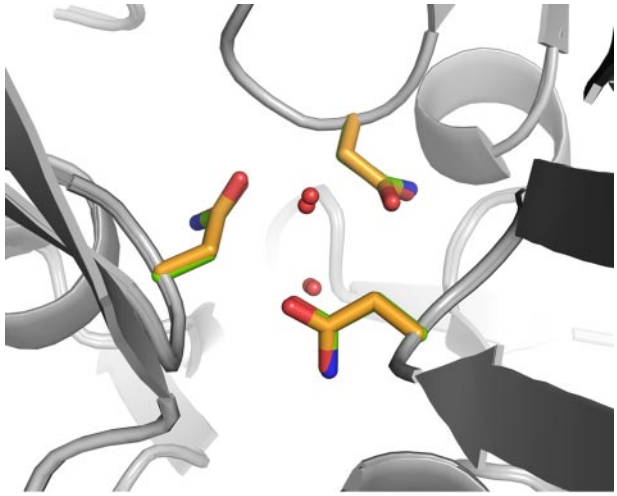

FIGURE 5. **Structure of σ1-D345N.** Superposition of wild-type T3D σ1 and σ1-D345N at the aspartic acid cluster. *Ribbon drawings* of the wild-type and σ1-D345N backbones are shown in *gray*, oxygen atoms are shown in *red*, and nitrogen atoms are shown in *blue*. The Asn-345 side chains of σ1-D345N (*green*) show the same conformation as those of wild-type σ1 (*yellow*). The water molecules above and below the cluster also occupy virtually identical positions in both molecules. This figure was generated using PyMOL (37).

protein does not bind to JAM-A. The most likely interpretation of these findings is that a trimeric form of σ1 is required for engagement of JAM-A. We envision two possible explanations for these results. First, the JAM-A binding site may extend across more than one monomer. Second, the surface structure of the JAM-A-binding region may be stable only in the context of a trimer. We think it unlikely that JAM-A makes a direct contact with Tyr-313 or with residues in close proximity. Tyr-313 is not exposed to solvent in the trimeric wild-type protein and would be unlikely to encounter JAM-A at its position in the head trimer interior.

The structure of σ1 is closely related to that of the adenovirus attachment protein, fiber (6). Moreover, the receptors for reovirus and adenovirus, JAM-A and coxsackievirus and adenovirus receptor, respectively, also share significant structural and functional homology and may engage their viral ligands in a similar manner (29). We note that the adenovirus fiber knob binds to its receptor coxsackievirus and adenovirus receptor via contacts between two knob subunits and a single receptor molecule. If this mode of binding is conserved in σ1, it would be affected by alterations at the trimer interface.

We observed a single magnesium ion adjacent to residues Asp-365 and Glu-419 at the center of the concave surface of the σ1 head (data not shown). This surface of σ1 mimics the JAM-A dimer interface and has been proposed to participate in interactions with JAM-A (29, 30). The side chains of Asp-365 and Glu-419 are exposed to solvent and exist in close spatial proximity to side chains of Arg-427 and Arg-429. These residues would be positioned to engage in salt-bridge interactions with charged residues in the receptor. In support of this idea, our preliminary analysis of point mutants of JAM-A suggests that acidic and basic residues in the JAM-A dimer interface are required for high-affinity interactions with σ1.[6]

A Unique Cluster of Aspartic Acid Residues at the Head Trimer Interface—The structure of σ1 reveals a unique cluster of solvent-inaccessible, conserved aspartic acid residues at the head trimer interface. A key aspect of these residues is that they are located at the very tip of a β-hairpin. As judged by its temperature factors (supplemental Fig. 2), the β-hairpin is rigid and possesses limited mobility. Three lines of evidence support the conclusion that the side chains of Asp-345 must be protonated

[6] K. M. Guglielmi and T. S. Dermody, unpublished observations.

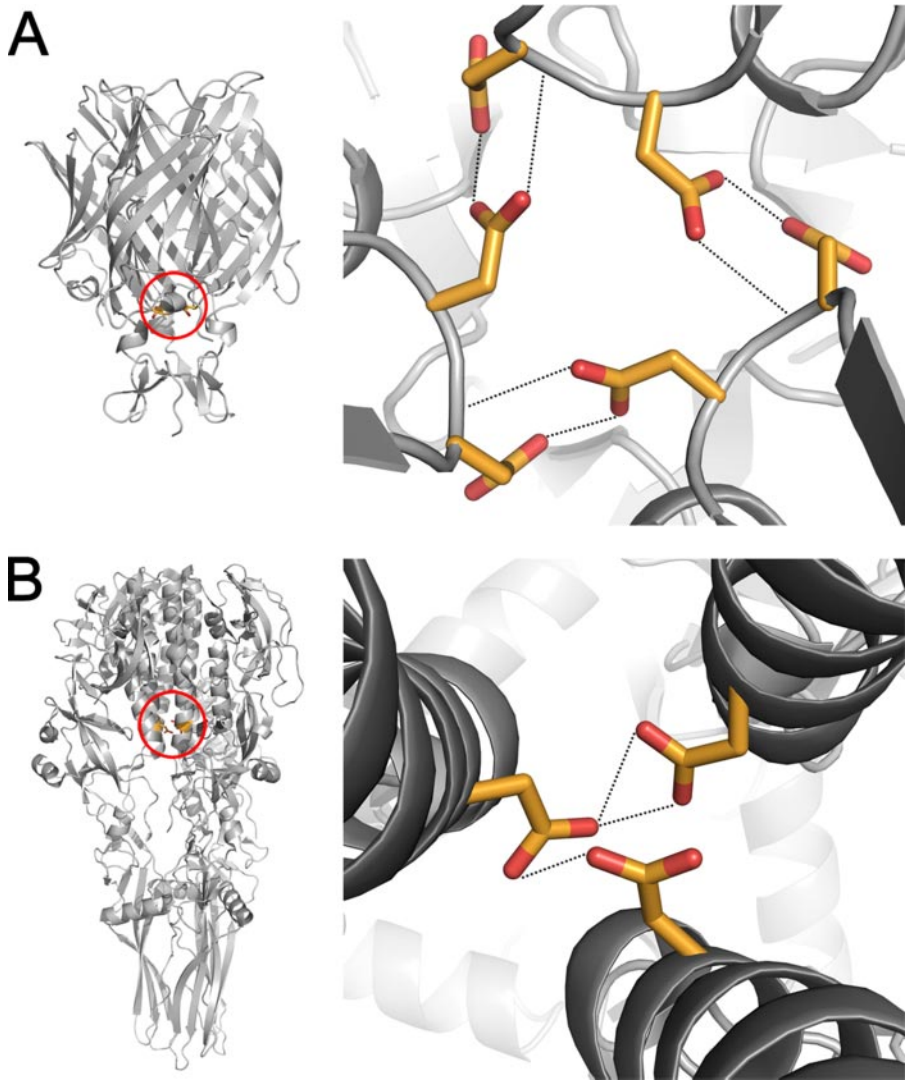

FIGURE 6. **Comparison of aspartic acid clusters in reovirus σ1 and VSV G.** Views into the aspartic acid clusters of σ1 (*A*) and VSV G (*B*). In both cases, the view is along the 3-fold axis. *Ribbon drawings* of the complete trimers are shown on the *left* in each case to depict the location of the clusters (*red circles*). *Ribbon tracings* of the backbones are shown in *gray*, carbon atoms of aspartic acid residues Asp-268 (VSV G) and Asp-345 and Asp-346 (σ1) are shown in *orange*, and oxygen atoms are shown in *red*. Hydrogen bonds are represented with *dotted lines*. This figure was generated using PyMOL (37).

to allow formation of the trimer. First, molecular dynamics studies show that the introduction of negative charges at the Asp-345 side chains destabilizes the trimer, causing partial separation of the three chains at the base of the σ1 head (17). Second, the mutant σ1-D345N protein assembles into a trimeric structure that is indistinguishable from that of the wild-type protein. Remarkably, the arrangement of water molecules in the vicinity of residue 345 in both the wild-type and mutant structures is identical. Since the asparagine side chain is an excellent mimic for a protonated aspartic acid but not for a charged aspartate, the structural similarities between the two proteins argue strongly that the wild-type protein contains protonated Asp-345 residues. Third, substitution of a residue that shields Asp-345 from solvent, Y313A, results in monomeric protein. It is likely that mutation of Tyr-313 renders Asp-345 solvent-accessible, causing it to lose its proton at neutral pH.

We performed gel-filtration experiments using purified σ1 head domain under conditions of low, neutral, and high pH (data not shown). The σ1 head eluted as a trimer under all conditions tested. These results provide additional evidence that the aspartic acids are protonated and inaccessible to solvent in the assembled trimer.

The hypothesis that Asp-345 in σ1 is protonated is also supported by the finding of a similar cluster of aspartic acids in the G protein of vesicular stomatitis virus (VSV) (31). Although the global architecture of VSV G differs substantially from reovirus σ1, VSV G also forms a trimer that features three aspartic acids that face each other at the trimer interface. The location and orientation of the aspartic acid clusters in VSV G and σ1 are in fact surprisingly similar (Fig. 6). In both cases, hydrogen bonds are thought to mediate interactions between protonated aspartic acid side chains. These hydrogen bonds lie in a plane that is perpendicular to the trimer axes, and deprotonation would lead to destabilization of the trimer. In both molecules, the aspartic acids emanate from well ordered backbone structures with low mobility (an α-helix in VSV G and a β-hairpin in σ1). Most interestingly, both clusters contain trapped water molecules that form hydrogen bonds with the protonated carboxylate groups.

What are the implications of the aspartic acid cluster for σ1 function in viral attachment and cell entry? Both VSV and reovirus enter cells via the endosomal pathway and thus encounter a low pH environment during the entry process. The VSV G structure has been interpreted as a low-pH conformer of the molecule (31). In keeping with this conclusion, it is possible that the σ1 structure reported here also represents a form of the protein found at low pH. Both VSV G and reovirus σ1 were crystallized at close-to-neutral pH, but the conditions used for crystallization are far from physiologic in both cases and may easily create an environment that favors protonated aspartic acids. Thus, the aspartic acid cluster may act as a molecular switch that disfavors trimerization when charged but favors trimerization when the protein encounters a low pH environment that allows it to be protonated. Because the aspartic acids project from rigid structural motifs, they may prevent trimerization in environments that favor deprotonation.

Conformational changes of viral proteins in response to ligand binding or exposure to acidic pH are well documented

(32–34). These changes allow viruses to expose previously hidden epitopes for ligand binding and membrane penetration. For example, the influenza virus hemagglutinin undergoes a massive rearrangement upon exposure to acidic pH. This conformational change is enabled by prior proteolytic cleavage and leads to the formation of α-helical coiled-coil structures that expose a hydrophobic fusion peptide. Importantly, the hemagglutinin structure at neutral pH represents a metastable form of the protein, as the low pH conformer, once formed, is stable even at neutral pH (35). The conspicuous location of Asp-345 at the σ1 trimer interface suggests that the aspartic acid cluster serves a similar function to mediate a structural transition between a form of the protein that is at least partially detrimerized in the head region and a fully trimerized molecule (as seen in the crystal structure here). Based on our current data, it appears that the fully trimerized protein is the energetically favored form. Placed in the context of the entire virion, such a conformational change might facilitate events during reovirus entry subsequent to viral attachment, such as internalization into the endocytic pathway and proteolytic disassembly to form infectious subvirion particles.

Acknowledgments—We thank the members of our laboratories for many useful discussions while conducting this research.

REFERENCES

1. Barton, E. S., Connolly, J. L., Forrest, J. C., Chappell, J. D., and Dermody, T. S. (2001) *J. Biol. Chem.* **276,** 2200–2211
2. Barton, E. S., Forrest, J. C., Connolly, J. L., Chappell, J. D., Liu, Y., Schnell, F., Nusrat, A., Parkos, C. A., and Dermody, T. S. (2001) *Cell* **104,** 441–451
3. Chappell, J. D., Duong, J. L., Wright, B. W., and Dermody, T. S. (2000) *J. Virol.* **74,** 8472–8479
4. Furlong, D. B., Nibert, M. L., and Fields, B. N. (1988) *J. Virol.* **62,** 246–256
5. Fraser, R. D. B., Furlong, D. B., Trus, B. L., Nibert, M. L., Fields, B. N., and Steven, A. C. (1990) *J. Virol.* **64,** 2990–3000
6. Chappell, J. D., Prota, A., Dermody, T. S., and Stehle, T. (2002) *EMBO J.* **21,** 1–11
7. Chappell, J. D., Gunn, V. L., Wetzel, J. D., Baer, G. S., and Dermody, T. S. (1997) *J. Virol.* **71,** 1834–1841
8. Sturzenbecker, L. J., Nibert, M. L., Furlong, D. B., and Fields, B. N. (1987) *J. Virol.* **61,** 2351–2361
9. Baer, G. S., Ebert, D. H., Chung, C. J., Erickson, A. H., and Dermody, T. S. (1999) *J. Virol.* **73,** 9532–9543
10. Ehrlich, M., Boll, W., Van Oijen, A., Hariharan, R., Chandran, K., Nibert, M. L., and Kirchhausen, T. (2004) *Cell* **118,** 591–605
11. Baer, G. S., and Dermody, T. S. (1997) *J. Virol.* **71,** 4921–4928
12. Chandran, K., Farsetta, D. L., and Nibert, M. L. (2002) *J. Virol.* **76,** 9920–9933
13. Chandran, K., Parker, J. S., Ehrlich, M., Kirchhausen, T., and Nibert, M. L. (2003) *J. Virol.* **77,** 13361–13375
14. Odegard, A. L., Chandran, K., Zhang, X., Parker, J. S., Baker, T. S., and Nibert, M. L. (2004) *J. Virol.* **78,** 8732–8745
15. Dryden, K. A., Wang, G., Yeager, M., Nibert, M. L., Coombs, K. M., Furlong, D. B., Fields, B. N., and Baker, T. S. (1993) *J. Cell Biol.* **122,** 1023–1041
16. Nibert, M. L., Chappell, J. D., and Dermody, T. S. (1995) *J. Virol.* **69,** 5057–5067
17. Cavalli, A., Prota, A. E., Stehle, T., Dermody, T. S., Recanatini, M., Folkers, G., and Scapozza, L. (2004) *Biophys. J.* **86,** 3423–3431
18. Prota, A. E., Campbell, J. A., Schelling, P., Forrest, J. C., Peters, T. R., Watson, M. J., Aurrand-Lions, M., Imhof, B., Dermody, T. S., and Stehle, T. (2003) *Proc. Natl. Acad. Sci. U. S. A.* **100,** 5366–5371
19. Otwinowski, Z., and Minor, W. (1997) *Methods Enzymol.* **276,** 307–326
20. Navaza, J. (1994) *Acta Crystallogr. Sect. A* **50,** 157–163
21. Jones, T. A., Zhou, J. Y., Cowan, S. W., and Kjeldgaard, M. (1991) *Acta Crystallogr. Sect. A* **47,** 110–119
22. Brünger, A. T., Adams, P. D., Clore, G. M., DeLano, W. L., Gros, P., Grosse-Kunstleve, R. W., Jiang, J. S., Kuszewski, J., Nilges, M., Pannu, N. S., Read, R. J., Rice, L. M., Simonson, T., and Warren, G. L. (1998) *Acta Crystallogr. Sect. D Biol. Crystallogr.* **54,** 905–921
23. Emsley, P., and Cowtan, K. (2004) *Acta Crystallogr. Sect. D Biol. Crystallogr.* **60,** 2126–2132
24. Collaborative Computational Project, Number 4 (1994) *Acta Crystallogr. Sect. D Biol. Crystallogr.* **50,** 760–763
25. Karlsson, R., and Falt, A. (1997) *J. Immunol. Methods* **200,** 121–133
26. Sibanda, B. L., and Thornton, J. M. (1991) *Methods Enzymol.* **202,** 59–82
27. Blanco, F., Ramírez-Alvarado, M., and Serrano, L. (1998) *Curr. Opin. Struct. Biol.* **8,** 107–111
28. Campbell, J. A., Shelling, P., Wetzel, J. D., Johnson, E. M., Wilson, G. A. R., Forrest, J. C., Aurrand-Lions, M., Imhof, B., Stehle, T., and Dermody, T. S. (2005) *J. Virol.* **79,** 7967–7978
29. Stehle, T., and Dermody, T. S. (2004) *Viral Immunol.* **17,** 129–143
30. Forrest, J. C., Campbell, J. A., Schelling, P., Stehle, T., and Dermody, T. S. (2003) *J. Biol. Chem.* **278,** 48434–48444
31. Roche, S., Bressanelli, S., Rey, F. A., and Gaudin, Y. (2006) *Science* **313,** 187–191
32. Bullough, P. A., Hughson, F. M., Skehel, J. J., and Wiley, D. C. (1994) *Nature* **371,** 37–43
33. Kwong, P. D., Wyatt, R., Robinson, J., Sweet, R. W., Sodroski, J., and Hendrickson, W. A. (1998) *Nature* **393,** 648–659
34. Chen, B., Vogan, E. M., Gong, H., Skehel, J. J., Wiley, D. C., and Harrison, S. C. (2005) *Nature* **433,** 834–841
35. Chen, J., Wharton, S. A., Weissenhorn, W., Calder, L. J., Hughson, F. M., Skehel, J. J., and Wiley, D. C. (1995) *Proc. Natl. Acad. Sci. U. S. A.* **92,** 12205–12209
36. Carson, M. (1987) *J. Mol. Graph.* **5,** 103–106
37. DeLano, W. L. (2002) *The PyMOL Molecular Graphics System*, DeLano Scientific, San Carlos, CA
38. Brünger, A. T. (1992) *Nature* **355,** 472–475

APPENDIX C

REOVIRUS BINDING DETERMINANTS IN JUNCTIONAL ADHESION MOLECULE-A

Kristen M. Guglielmi, Eva Kirchner, Geoffrey H. Holm, Thilo Stehle, and Terence S. Dermody

Journal of Biological Chemistry. 282(24):17930-17940;2007

THE JOURNAL OF BIOLOGICAL CHEMISTRY VOL. 282, NO. 24, pp. 17930–17940, June 15, 2007

Reovirus Binding Determinants in Junctional Adhesion Molecule-A*[S]

Received for publication, March 13, 2007, and in revised form, April 23, 2007 Published, JBC Papers in Press, April 23, 2007, DOI 10.1074/jbc.M702180200

Kristen M. Guglielmi[‡§], Eva Kirchner[¶], Geoffrey H. Holm[§‖], Thilo Stehle[§¶‖], and Terence S. Dermody[‡§‖1]

From the Departments of [‡]Microbiology and Immunology, [‖]Pediatrics, and the [§]Elizabeth B. Lamb Center for Pediatric Research, Vanderbilt University School of Medicine, Nashville, Tennessee 37232 and the [¶]Interfakultäres Institut für Biochemie, Universität Tübingen, Hoppe-Seyler-Strasse 4, D-72076 Tübingen, Germany

Junctional adhesion molecule-A (JAM-A) serves as a serotype-independent receptor for mammalian orthoreoviruses (reoviruses). The membrane-distal immunoglobulin-like D1 domain of JAM-A is required for homodimerization and binding to reovirus attachment protein σ1. We employed a structure-guided mutational analysis of the JAM-A dimer interface to identify determinants of reovirus binding. We purified mutant JAM-A ectodomains for solution-phase and surface plasmon resonance binding studies and expressed mutant forms of full-length JAM-A in Chinese hamster ovary cells to assess reovirus binding and infectivity. Mutation of residues in the JAM-A dimer interface that participate in salt-bridge or hydrogen-bond interactions with apposing JAM-A monomers abolishes the capacity of JAM-A to form dimers. JAM-A mutants incapable of dimer formation form complexes with the σ1 head that are indistinguishable from wild-type JAM-A-σ1 head complexes, indicating that σ1 binds to JAM-A monomers. Residues Glu^{61} and Lys^{63} of β-strand C and Leu^{72} of β-strand C′ in the dimer interface are required for efficient JAM-A engagement of strain type 3 Dearing σ1. Mutation of neighboring residues alters the kinetics of the σ1-JAM-A binding interaction. Prototype reovirus strains type 1 Lang and type 2 Jones share similar, although not identical, binding requirements with type 3 Dearing. These results indicate that reovirus engages JAM-A monomers via residues found mainly on β-strands C and C′ of the dimer interface and raise the possibility that the distinct disease phenotypes produced in mice following infection with different strains of reovirus are in part attributable to differences in contacts with JAM-A.

Mammalian orthoreoviruses (reoviruses)[2] are nonenveloped, icosahedral viruses that contain a genome of 10 double-stranded RNA gene segments encapsulated within two concentric protein shells (1). Reoviruses infect a broad range of mammalian hosts, including humans, but cause disease primarily in the very young (2). The three reovirus serotypes, each represented by a prototype strain, type 1 Lang (T1L), type 2 Jones (T2J), and type 3 Dearing (T3D), differ mainly in the sequence of the viral attachment protein, σ1 (3, 4). Following oral or intramuscular inoculation of newborn mice, strains T1L and T3D invade the central nervous system, yet these viruses use different routes and produce distinct pathologic consequences. T1L spreads to the central nervous system hematogenously and infects ependymal cells (5, 6), resulting in hydrocephalus (7). In contrast, T3D reovirus spreads to the central nervous system by neural routes and infects neurons (5, 6, 8), causing lethal encephalitis (7, 9). Pathways of viral spread (5) and tropism for neural tissues (6, 10) segregate with the viral S1 gene, which encodes the σ1 protein (11, 12). Collectively, these studies suggest that the σ1 protein determines the central nervous system cell types that serve as targets for reovirus infection, presumably through specific receptor binding.

Reovirus attachment protein σ1 is a filamentous, trimeric molecule ~480 Å in length with distinct head-and-tail morphology (13, 14). Reovirus σ1 shares striking structural similarities with the adenovirus attachment protein, fiber (15). Each is a trimer with a tail that partially inserts into the virion at the icosahedral vertices and a head that projects away from the virion surface. Both σ1 and fiber possess an uncommon triple β-spiral fold in the tail and an 8-stranded β-barrel structure that composes the head. Discrete regions of reovirus σ1 mediate binding to cell-surface receptors. Sequences in the N-terminal tail bind carbohydrate (16–18), whereas the C-terminal head binds junctional adhesion molecule-A (JAM-A) (19, 20).

JAM-A is a member of the immunoglobulin (Ig) superfamily postulated to regulate formation of intercellular tight junctions (21–23). JAM-A contains two extracellular Ig-like domains, a short transmembrane region, and a cytoplasmic tail possessing a PDZ domain-binding motif (21, 22). Crystal structures of the extracellular region of human (h) JAM-A (24) and murine (m) JAM-A (25) reveal two concatenated Ig-like domains (D1 and D2) (Fig. 1*A*). Two monomers form a symmetrical dimer with a

* This work was supported by United States Public Health Service Awards T32 GM08554 (to K. M. G.), R37 AI38296 (to T. S. D.), R01 GM67853 (to T. S. D. and T. S.), and the Elizabeth B. Lamb Center for Pediatric Research. Additional support was provided by the Vanderbilt-Ingram Cancer Center and the Vanderbilt Diabetes Research and Training Center. The costs of publication of this article were defrayed in part by the payment of page charges. This article must therefore be hereby marked "*advertisement*" in accordance with 18 U.S.C. Section 1734 solely to indicate this fact.

[S] The on-line version of this article (available at http://www.jbc.org) contains supplemental Table S1.

[1] To whom correspondence should be addressed: Lamb Center for Pediatric Research, D7235 MCN, 1161 21st Ave. S., Nashville, TN 37232-2581. Tel.: 615-343-8911; Fax: 615-343-9723; E-mail: terry.dermody@vanderbilt.edu.

[2] The abbreviations used are: reoviruses, mammalian orthoreoviruses; T1L, type 1 Lang; T2J, type 2 Jones; T3D, type 3 Dearing; JAM-A, junctional adhesion molecule-A; Ig, immunoglobulin; hJAM-A, human JAM-A; mJAM-A, murine JAM-A; CAR, coxsackievirus and adenovirus receptor; CHO, Chinese hamster ovary; GST, glutathione *S*-transferase; PBS, phosphate-buffered saline; SPR, surface plasmon resonance; GST-JAM-A, NH_2-terminal glutathione *S*-transferase fusion with the extracellular region of JAM-A; HIV, human immunodeficiency virus.

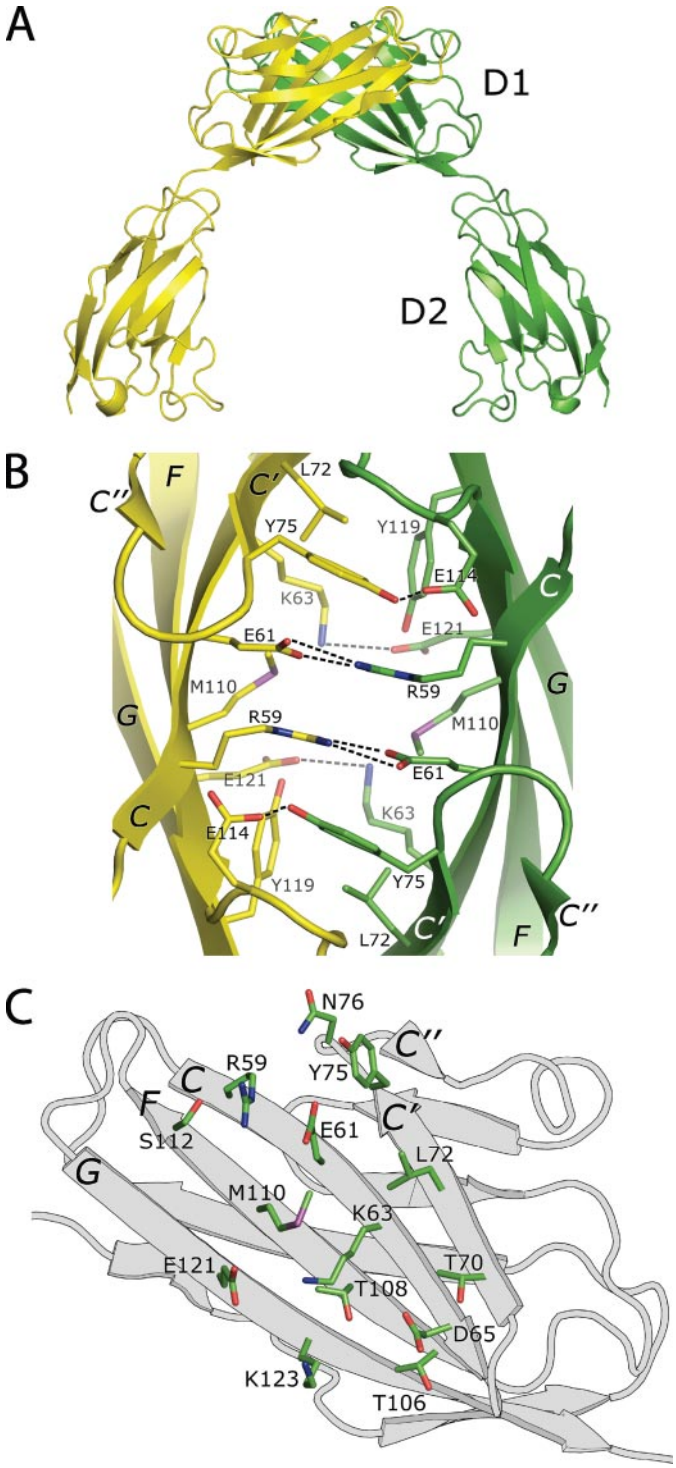

FIGURE 1. **Structure and location of residues in the JAM-A D1 domain.** *A*, ribbon drawing of the hJAM-A dimer, with one monomer shown in *yellow* and the other in *green*. *B*, view of the interface between two hJAM-A monomers. The interface is formed by residues on the GFCC′ faces of two D1 domains. The view is along a crystallographic dyad. Oxygen atoms are shown in *red*, nitrogen in *blue*, and sulfur in *purple*. Hydrogen bonds and salt-bridges are represented by *dashed lines*. Amino acids are labeled in single-letter code. *C*, view of the GFCC′ β-sheet that composes the dimer interface of one JAM-A monomer, labeled as in *B*. Side chains are shown for residues that were altered in this study. This figure was generated using PyMOL (54).

large interface between apposing D1 domains. The JAM-A dimer interface is concave and primarily composed of four β-strands (C′, C, F, and G). The intermolecular interface is stabilized by four pairs of salt-bridges as well as hydrophobic interactions and two hydrogen bonds (Fig. 1*B*). Remarkably, JAM-A serves as a receptor for prototype and field-isolate strains of all three reovirus serotypes (19, 26).

JAM-A belongs to a structurally related family of cell-adhesion molecules. The most closely related of these proteins to JAM-A are JAM-B and JAM-C (27–29), neither of which serves as a receptor for reovirus (24, 26). Although structural information is not available for JAM-B and JAM-C, sequence analysis suggests that homophilic contacts are conserved between JAM family members (24). The coxsackievirus and adenovirus receptor (CAR) also contains two extracellular Ig-like domains that form similar dimers via the GFCC′ interface. Moreover, intermolecular interactions in CAR also include some contacts between charged residues (30, 31).

Chinese hamster ovary (CHO) cells transfected with plasmids encoding chimeric CAR-JAM-A receptor constructs or JAM-A domain-deletion mutants provide evidence that the N-terminal D1 domain of JAM-A is required for reovirus attachment and infection (32). Reovirus binding to JAM-A occurs more rapidly than homotypic JAM-A association and is competed by excess JAM-A *in vitro* and on cells (32). Chemical cross-linking of JAM-A diminishes the capacity of reovirus to bind JAM-A *in vitro* and on cells and negates the competitive effects of soluble JAM-A on reovirus attachment (32). These findings suggest that reovirus binds to monomeric JAM-A by engaging the dimer interface to effect stable cell attachment. However, the precise nature of σ1-JAM-A interactions is not understood. Moreover, as all reovirus serotypes bind to JAM-A, it is not apparent how JAM-A binding contributes to the serotype-dependent differences in reovirus tropism in the murine central nervous system.

In this study, we performed a systematic mutagenic analysis of the dimer interface of the D1 domain of JAM-A. We engineered point mutations in the dimer-contributing surface of the extracellular domain of JAM-A, purified the resultant mutants, and characterized effects of the mutations on JAM-A homodimerization and binding to the purified σ1 head domain. In complementary experiments, we tested the capacity of CHO cells expressing full-length JAM-A point mutants to support binding and infection by prototype strains from each of the three reovirus serotypes. Our results indicate that reovirus T3D σ1 engages JAM-A via residues in β-strands C and C′ within the dimer interface and that JAM-A binding requirements differ significantly among the reovirus serotypes. These findings enhance an understanding of reovirus-receptor interactions and suggest that the nature of JAM-A contacts contributes to differences in pathogenesis among reovirus serotypes.

EXPERIMENTAL PROCEDURES

Cells, Viruses, and Antibodies—Spinner-adapted murine L929 cells were cultured as described (33). CHO cells were maintained in Ham's F-12 medium supplemented to contain 10% fetal bovine serum, 2 mM L-glutamine, 100 units/ml penicillin, and 100 μg/ml streptomycin. Reovirus strains T1L, T2J, and T3D are laboratory stocks. Strain T3SA− is a reassortant strain containing the S1 gene of T3C44, which does not bind sialic acid (17, 34), and the remaining nine genes of T1L (33).

Reoviruses were purified by cesium chloride gradient centrifugation from infected L929 cells as described (13). Particle concentrations were determined by spectrophotometry at 260 nm using a conversion factor of 2.1×10^{12} particles/ml/A_{260}. hJAM-A-specific monoclonal antibody J10.4 was provided by Dr. Charles Parkos (Emory University).

Protein Expression and Purification—The C-terminal head domain of T3D σ1 was purified as described (20). Soluble ectodomains of wild-type and point mutant hJAM-A constructs were fused to an amino-terminal GST affinity tag via a thrombin cleavage site and purified as described (24). Nucleotide sequences corresponding to residues 27–233 of wild-type hJAM-A were cloned by PCR, digested with BamHI and XhoI, and ligated into pGEX-4T-3 (GE Healthcare) for bacterial transformation. Point mutants of hJAM-A were engineered using the QuikChange Site-directed Mutagenesis Kit (Stratagene), as per the manufacturer's instructions. Sequences of primers used to engineer point mutations in hJAM-A are listed in supplemental Table 1. A GST fusion with the D1 domain of hJAM-A was engineered by inserting a XhoI or BamHI restriction site into the D1/D2 linker of hJAM-A in pGEX-4T-3 using site-directed PCR mutagenesis. Digestion with XhoI or BamHI followed by ligation eliminated the D2 domain (residues 131–233) or D1 domain (residues 27–131), respectively, and fused the remaining domain to GST. Bacteria transformed with plasmids encoding GST-JAM-A constructs were cultured in Luria-Bertani broth at 37 °C with shaking, and protein expression was induced with 0.2 mM isopropyl β-D-thiogalactoside (GE Healthcare) at 25 °C. Bacteria were harvested by centrifugation, solubilized in phosphate-buffered saline (PBS) plus 1% Triton X-100, 2 mM β-mercaptoethanol, 1 mM phenylmethylsulfonyl fluoride, and 100 μg/ml lysozyme, and lysed by sonication. GST-hJAM-A proteins were purified from bacterial lysates by glutathione affinity chromatography. Soluble wild-type and point-mutant hJAM-A ectodomains were liberated from the glutathione resin by incubation with 20 units/ml thrombin (Sigma) at room temperature overnight.

Gel Filtration Chromatography—Gel filtration of purified hJAM-A extracellular domains was performed by loading ~0.5 mg of each protein onto a Superdex 75 column mounted on a BioLogic HR Work station (Bio-Rad). Proteins were resolved in 20 mM Tris (pH 7.5), 100 mM NaCl, 0.01% sodium azide. Gel filtration of the hJAM-A extracellular domain and the σ1 head domain was performed using a Superdex 75 column mounted on a SMART analytical chromatography system (GE Healthcare). The σ1 head (10 μg) in 20 mM HEPES (pH 7.1) and wild-type or mutant forms of the hJAM-A extracellular domain (12.74 μg) in PBS were mixed and incubated at 0 °C for 40 min prior to gel filtration. Mixtures of proteins or individual proteins were resolved in 20 mM Tris (pH 7.5), 100 mM NaCl.

GST Capture Assays—Swelled, washed, glutathione-coated beads (Sigma) were incubated with 20 μg of purified GST or GST-hJAM-A fusion proteins and diluted in 200 μl of PBS plus 1% Tween 20 at 4 °C for 1 h. Glutathione beads with captured GST fusion proteins were washed twice with PBS plus 1% Tween 20 and incubated with 10 μg of purified T3D σ1 head domain in 200 μl of PBS plus 1% Tween 20 at 4 °C for 1 h, followed by two additional washes. After the final wash, buffer was aspirated carefully, and beads with bound proteins were resuspended in 30 μl of sample buffer (313 mM Tris (pH 6.8), 4% SDS, 10% β-mercaptoethanol, 20% glycerol, 0.01% bromphenol blue). Samples (15 μl/lane) were loaded into wells of a SDS 4–20% continuous gradient polyacrylamide gel and electrophoresed at 120 V until the dye front reached the bottom of the gel. Proteins were visualized by staining with Coomassie Brilliant Blue.

Assessment of σ1-JAM-A Interactions Using Surface Plasmon Resonance (SPR)—A BIAcore CM5 chip (Pharmacia Biosensor AB) was coated with mouse ascites containing monoclonal GST-specific antibody (Sigma) to ~1800 resonance units of IgG by amine coupling. Purified GST or wild-type or mutant GST-hJAM-A ectodomain fusion proteins at a concentration of 2 μM in HEPES-buffered saline (pH 7.0) were captured by injection across individual flow cells of an antibody-coated chip for 3 min at 30 μl/min using a BIAcore 2000 (GE Healthcare). Purified T3D σ1 head domain was injected across the conjugated chip surface at 30 μl/min. Following σ1 binding, chip surfaces were regenerated with a 20-μl pulse of 10 mM glycine (pH 2.5). Affinity constants for σ1 binding to hJAM-A were determined using separate k_{on} and k_{off} nonlinear regression with BIAevaluation 3.0 software (GE Healthcare), assuming a 1:1 Langmuir binding model (35). Molar concentrations of σ1 constructs were calculated based on σ1 forming a homotrimer (20, 36).

Flow Cytometric Analysis of Receptor Expression and Virus Binding—CHO cells (10^6) were transiently transfected with receptor-encoding plasmids using Lipofectamine and PLUS reagent (Invitrogen) according to the manufacturer's instructions and incubated for 24 h to allow receptor expression. Cells were detached from plates by incubation with 20 mM EDTA in PBS and incubated with hJAM-A-specific monoclonal antibody J10.4 at 10 μg/ml or incubated with reovirus T1L, T2J, or T3SA− (10^5 particles/cell) on ice for 1 h. Virus-adsorbed cells were washed with PBS containing 0.1% bovine serum albumin and incubated with clarified, combined T1L/T3D antiserum (37) at 1:1000 dilution on ice for 1 h. Samples were washed with PBS containing 0.1% bovine serum albumin and incubated with Alexa 488-conjugated goat anti-rabbit or goat anti-mouse IgG (Invitrogen) at a 1:1000 dilution on ice for 1 h. Cells were washed twice with PBS containing 0.1% bovine serum albumin and fixed with 4% paraformaldehyde in PBS. Cells were analyzed for antibody or virus binding using a FACSCalibur flow cytometer (BD Biosciences).

Transient Transfection and Infection of CHO Cells—Point mutations were engineered into full-length hJAM-A in pcDNA3.1 (24) using the QuikChange Site-directed Mutagenesis Kit (Stratagene) and the same primers used to engineer mutations in the hJAM-A extracellular domain in pGEX-4T-3 (supplemental Table 1). CHO cells (2×10^5) were transiently transfected with receptor-encoding plasmids using Lipofectamine and PLUS reagent (Invitrogen) and incubated for 24 h to allow receptor expression. Cells were infected with reovirus at multiplicities of infection of 1 (T1L), 5 (T2J), and 10 (T3SA−) plaque forming units/cell and incubated at 37 °C for 18–20 h. Infected cells were processed for indirect immunofluorescence as described (33). Images were captured at ×200 magnification using a Zeiss Axiovert 200 microscope. For each experiment, three fields of view were scored from three inde-

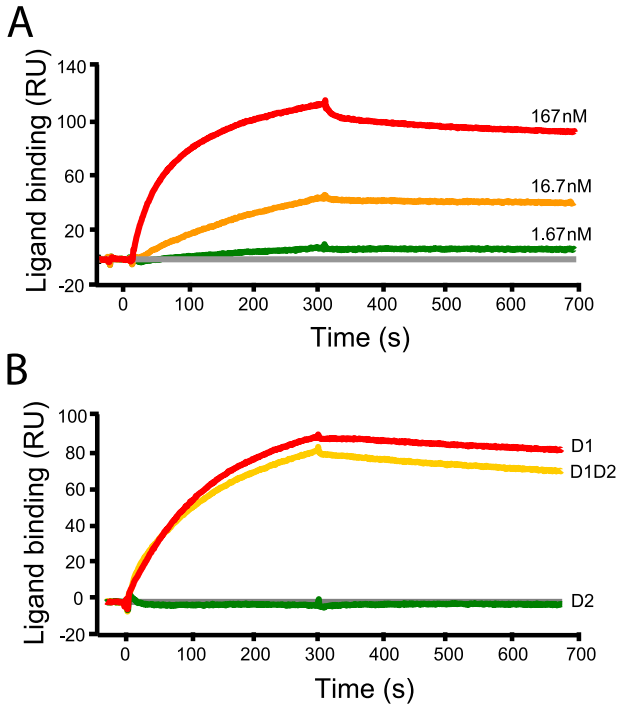

FIGURE 2. **Characterization of the σ1 head domain binding to GST-JAM-A.** *A*, binding of the σ1 head domain to GST-JAM-A. Purified σ1 head domain, at concentrations of 167 (*red*), 16.7 (*yellow*), or 1.67 nM (*green*), was injected for 5 min across a biosensor surface on which GST fused to the JAM-A ectodomain previously had been captured. Buffer alone was injected for 6.7 min. The baseline is 167 nM σ1 head domain binding to GST (*gray*). The K_D of σ1 head binding to GST-JAM-A is $\sim 2.4 \times 10^{-9}$ M. *B*, binding of the σ1 head domain to GST-JAM-A Ig-like domains. Purified σ1 head domain, at a concentration of 167 nM, was injected for 5 min across a biosensor surface on which GST-JAM-A fusion proteins previously had been captured. Buffer alone was injected for 6.7 min. The resultant traces show binding to GST-JAM-A (*yellow*), GST-D1 (*red*), and GST-D2 (*green*). The baseline is 167 nM σ1 head domain binding to GST (*gray*). Binding is expressed in resonance units (*RU*).

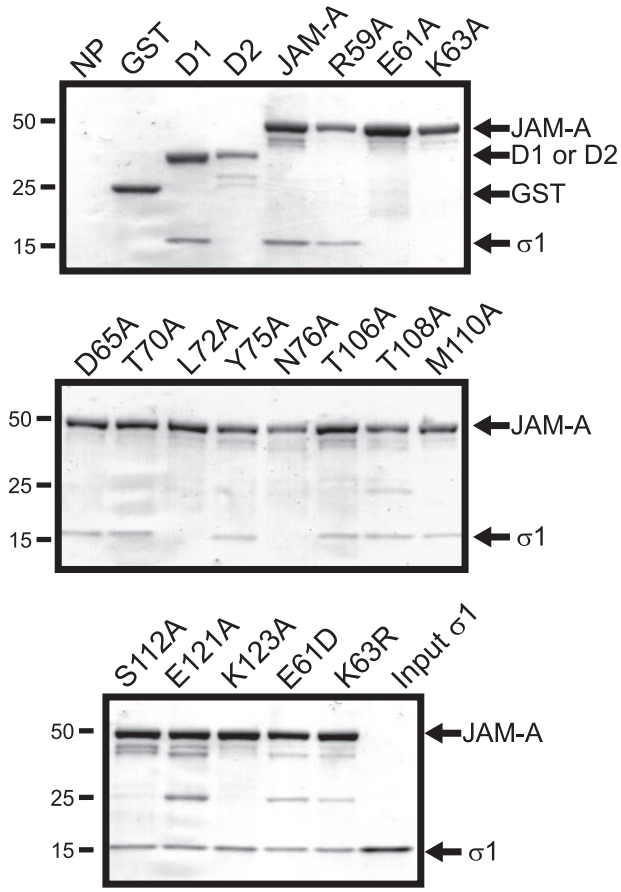

FIGURE 3. **Precipitation of the σ1 head domain with purified GST-JAM-A point mutants.** Glutathione-agarose was incubated with buffer alone (*NP*), GST, or GST fused to the JAM-A D1, D2, entire extracellular domain (JAM-A), or point mutants shown at 4 °C for 1 h. The glutathione-agarose was pelleted, washed, and incubated with purified T3D σ1 head at 4 °C for an additional 1 h. The glutathione-agarose was washed, pelleted, resuspended in SDS sample buffer, and boiled. Samples were resolved by SDS-PAGE and stained with Coomassie Brilliant Blue to visualize captured proteins. Input T3D σ1 head also was resolved following boiling in SDS sample buffer. Molecular masses of protein standards in kDa are indicated on the *left*. Proteins are labeled on the *right*.

pendently transfected wells. Mean values from three independent experiments were compared using the unpaired Student's *t* test as applied using Microsoft Excel. *p* values of less than 0.05 were considered statistically significant.

RESULTS

Analysis of σ1 Head Binding to GST-JAM-A—For studies of σ1-JAM-A interactions, we purified an N-terminal GST fusion with the extracellular region of JAM-A (GST-JAM-A) (24). Bacteria were transfected with plasmids encoding GST-JAM-A, harvested by centrifugation, and lysed by sonication. GST-JAM-A constructs were purified from bacterial lysates using glutathione affinity chromatography (32). To determine whether GST-JAM-A is capable of binding σ1, we captured GST-JAM-A on the surface of a biosensor chip via a covalently linked GST-specific antibody. We then injected a purified C-terminal fragment of T3D σ1 at three different concentrations and detected association with GST-JAM-A by SPR (Fig. 2*A*). The injected fragment of σ1 incorporates residues 293 to 455, which comprise the globular β-barrel head domain and one β-spiral repeat of the tail and is referred to as the σ1 head (20). The σ1 head did not show any specific binding to the GST-specific antibody or to GST captured on the biosensor surface (data not shown). However, the σ1 head bound GST-JAM-A with an affinity of $\sim 2.4 \times 10^{-9}$ M, which approximates previous calculations of σ1 affinity for JAM-A (19, 20). To determine whether the isolated D1 Ig-like domain of JAM-A is capable of σ1 engagement, we expressed and purified only the D1 or D2 Ig-like domains of JAM-A with an N-terminal GST tag. We assessed the capacity of the fusion proteins to bind the σ1 head using the SPR strategy employed for GST-JAM-A. Whereas the σ1 head bound GST-D1 with an affinity similar to GST-JAM-A, GST-D2 was incapable of capturing the σ1 head (Fig. 2*B* and data not shown). In accordance with data obtained using chimeric receptor molecules (32), these data indicate that the membrane distal D1 domain of JAM-A is sufficient for high affinity interactions with σ1.

Generation and Characterization of JAM-A Dimer Interface Point Mutants—To identify specific residues in the D1 domain required for σ1 binding, we generated individual alanine substitutions of residues with surface-exposed side chains in the JAM-A dimer interface (Fig. 1*C*). Two groups of residues were targeted for mutagenesis: (i) those that form direct protein-protein intersubunit contacts: Arg^{59}, Glu^{61}, Lys^{63}, Leu^{72}, Tyr^{75}, Met^{110}, and Glu^{121}, and (ii) those that make indirect contacts: Asp^{65}, Thr^{70}, Asn^{76},

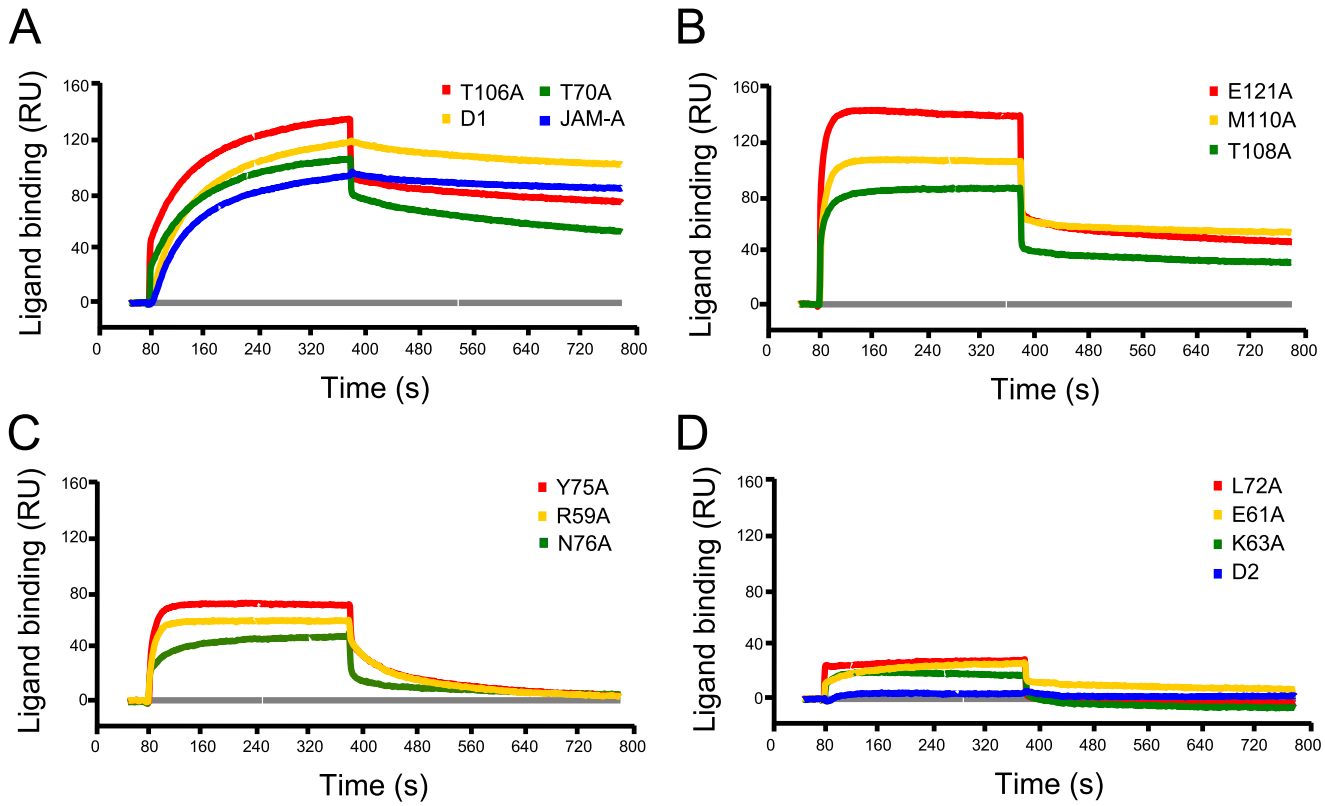

FIGURE 4. **Binding of the σ1 head to GST-JAM-A point mutants.** Purified σ1 head domain, at a concentration of 167 nM, was injected for 5 min across a biosensor surface on which GST-JAM-A fusion proteins, as indicated, had been captured. Buffer alone was injected for 6.7 min. The resultant traces show binding to GST-JAM-A and GST-JAM-A point mutants, as indicated. The resultant sensograms are grouped based on binding kinetics: *A*, k_{on} and k_{off} similar to wild-type JAM-A; *B*, faster k_{on} than wild-type JAM-A; *C*, faster k_{on} and k_{off} than wild-type; and *D*, no specific binding. The baseline is 167 nM σ1 head domain binding to GST (*gray*). Binding is expressed in resonance units (*RU*).

Thr[106], Thr[108], Ser[112], and Lys[123]. GST-JAM-A point mutants were purified by glutathione affinity chromatography and used in GST precipitation assays to identify mutations that ablate σ1 binding. In these experiments, glutathione-coated beads bound GST fusion proteins, which in turn were used to capture the σ1 head domain. As anticipated, the σ1 head was bound efficiently by GST-JAM-A and GST-D1 but not detectably by beads alone, GST, or GST-D2 (Fig. 3). The majority of JAM-A dimer interface point mutants were capable of binding the σ1 head. However, mutants E61A, K63A, L72A, and N76A were incapable of binding the σ1 head as detected by Coomassie Blue staining or immunoblotting, despite similar capture of the GST-JAM-A mutants on the beads (Fig. 3 and data not shown). Residues Leu[72] and Asn[76] are located on β-strand C′ and the C′C″ loop, respectively (Fig. 1*C*). Leu[72] participates in a hydrophobic interaction with Tyr[119] on an apposing JAM-A monomer. Residues Glu[61] and Lys[63] are located on β-strand C and participate in salt-bridge interactions that stabilize JAM-A dimers. These data suggest that the σ1 head engages JAM-A via residues near the top of (as oriented in Fig. 1*C*) and within the dimer interface.

Kinetics of σ1 Head Binding to GST-JAM-A Dimer Interface Point Mutants—To quantitatively assess the effects of mutations in the JAM-A dimer interface on interactions with σ1, GST-JAM-A point mutants were captured on a biosensor surface and tested for σ1 binding by SPR. Based on the kinetics and affinity of the interaction with σ1, the majority of JAM-A mutants clustered into one of four groups. The first group (I) includes point mutants that display binding kinetics similar to wild-type (Fig. 4*A* and Table 1). Group I includes mutants of Thr[70] in β-strand C′ and nearby residue Thr[106] in β-strand F, which do not contribute to intersubunit interactions at the JAM-A dimer interface. The second group of GST-JAM-A mutants (II) exhibited faster association kinetics than wild-type JAM-A by ~5–10-fold, resulting in higher calculated affinities for σ1 than wild-type JAM-A (Fig. 4*B* and Table 1). Initially upon injection of wash buffer, much of the σ1 was removed from these mutants. However, specifically bound σ1 protein exhibited a similar off-rate to wild-type GST-JAM-A. Group II includes mutants T108A, M110A, and E121A. Thr[108], Met[110],

TABLE 1
Kinetics of purified σ1 head binding to GST-JAM-A point mutants
Association and dissociation rates and dissociation constants were calculated using BIAevaluation 3.0 software. Mutants are grouped as in Fig. 4. Group IV mutants did not display specific binding.

Group	JAM-A mutant	Association rate	Dissociation rate	Dissociation constant
		1/ms	*1/s*	*M*
I	Wild-type	8.9×10^{4}	2.5×10^{-4}	2.8×10^{-9}
	D1	8.9×10^{4}	3.1×10^{-4}	3.5×10^{-9}
	T70A	7.1×10^{4}	9.9×10^{-4}	1.4×10^{-8}
	T106A	7.8×10^{4}	4.5×10^{-4}	5.8×10^{-9}
II	T108A	4.1×10^{5}	6.1×10^{-4}	1.5×10^{-9}
	M110A	6.5×10^{5}	3.5×10^{-4}	5.4×10^{-10}
	E121A	5.7×10^{5}	8.5×10^{-4}	1.5×10^{-9}
III	R59A	3.8×10^{5}	8.4×10^{-3}	2.2×10^{-8}
	Y75A	5.0×10^{5}	7.0×10^{-3}	1.4×10^{-8}
	N76A	7.3×10^{4}	3.5×10^{-3}	4.7×10^{-8}

and Glu[121] all are located within the dimer interface in proximity to one another on β-strands F and G (Fig. 1*C*). Glu[121] participates in salt-bridge interactions that stabilize the dimer interface (24). Met[110] participates in a hydrophobic interaction with Met[110] on an apposing JAM-A monomer. The third group (III) includes GST-JAM-A mutants R59A, Y75A, and N76A (Fig. 4*C*), which exhibited a faster σ1 on-rate than wild-type JAM-A but also a faster off-rate, resulting in affinities similar to wild-type. The N76A mutant exhibited a slower on-rate and a lower level of σ1 binding, relative to the other mutants in this group, and binding returned to baseline levels over several minutes of wash buffer injection. This result agrees with results obtained in the GST precipitation assay, in which the N76A mutant of JAM-A was incapable of capturing the σ1 head domain (Fig. 3). Arg[59], Tyr[75], and Asn[76] are located on β-strands C and C′ in the dimer interface (Fig. 1*C*). The final group of JAM-A point mutants includes E61A, K63A, and L72A (Fig. 4*D*), which showed very low levels of σ1 binding above background. Upon injection of wash buffer, the binding signal returned to baseline levels immediately, indicating that the observed binding was not specific. We were unable to find suitable binding models for the interaction of these mutants with the σ1 head using BIAevaluation software (data not shown). These results also are in accord with results obtained in the GST precipitation assay (Fig. 3), in which no σ1 head was bound detectably by the E61A, K63A, or L72A GST-JAM-A point mutants. These data reinforce the importance of Glu[61], Lys[63], and Leu[72] as mediators of σ1-JAM-A interactions and suggest that these residues serve as contact points for the σ1 head.

TABLE 2

Characterization of selected point mutants of the JAM-A dimer interface by gel filtration

Apparent molecular masses were calculated by graphing $V_e - V_o$ against the $\log_{10} M_r$ of protein standards, performing linear regression, and back-calculating, based on elution time.

JAM-A mutant	Apparent molecular mass	Apparent oligomeric state	σ1 Binding
	kDa		
Wild-type	46.1	Dimeric	+
R59A	32.5	Monomeric	+
E61A	32.5	Monomeric	−
K63A	33.8	Monomeric	−
Y75A	27.8	Monomeric	+
S112A	49.8	Dimeric	+
E121A	30.0	Monomeric	+
K123A	46.1	Dimeric	+

Oligomeric State of JAM-A Point Mutants—Because two residues that participate in salt-bridge interactions at the JAM-A dimer interface are required for efficient σ1 binding, we asked whether mutation of these residues or other residues in the dimer interface alters the capacity of JAM-A to form dimers. To answer this question, the extracellular domains of wild-type and selected JAM-A point mutants were released from the immobilized GST tag by thrombin cleavage and further purified using gel filtration. The extracellular domain of wild-type JAM-A eluted as a single peak, with an apparent molecular mass of ~48 kDa, indicating that it forms a dimer (Table 2 and data not shown) (24). Likewise, alanine substitutions of Ser[112] and Lys[123], which participate in indirect contacts at the intersubunit interface, do not alter the oligomeric state of JAM-A (Table 2). In sharp contrast, JAM-A extracellular domains with alanine substitutions of Arg[59], Glu[61], Lys[63], or Glu[121], which form salt-bridges across the dimer interface, or position Tyr[75], which forms a hydrogen bond with Glu[114] from an apposing monomer, eluted from the column as a single species with an apparent molecular mass of ~30 kDa. This elution peak likely represents solely monomeric JAM-A. These data indicate that each salt-bridge pair and Tyr[75] individually is required for stabilization of JAM-A dimers.

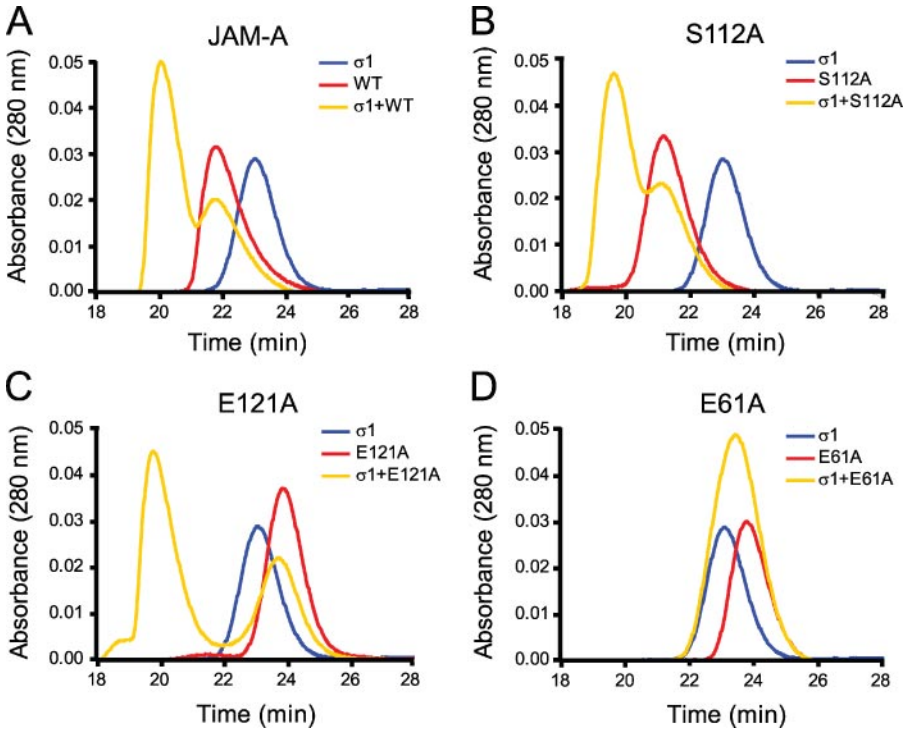

FIGURE 5. **Characterization of σ1 head/JAM-A extracellular domain mixtures using gel filtration chromatography.** Purified T3D σ1 head and wild-type JAM-A (*A*) or JAM-A point mutants S112A (*B*), E121A (*C*), and E61A (*D*) were mixed in a 3:1 molar ratio and incubated on ice for 40 min. The mixtures (*yellow*) or individual purified proteins (*red* and *blue*) were applied to a Superdex 75 gel-filtration column, and proteins in the column fractions were detected by A_{280}. Dimeric forms of wild-type JAM-A and S112A elute earlier than monomeric forms E121A and E61A. Wild-type JAM-A, S112A, and E121A each form a complex with σ1 that elutes from the column at approximately the same time, thus with similar apparent molecular weight, for each protein mixture.

To determine whether σ1 engages monomeric or dimeric forms of the JAM-A extracellular domain, we assessed binding of the σ1 head to the JAM-A extracellular domain in solution using gel-filtration chromatography. Incubation of purified wild-type JAM-A and the σ1 head in a 3:1 molar ratio (three JAM-A monomers to one σ1 trimer), results in formation of a higher molecular weight complex that contains both JAM-A and the σ1 head (Fig. 5*A* and data not

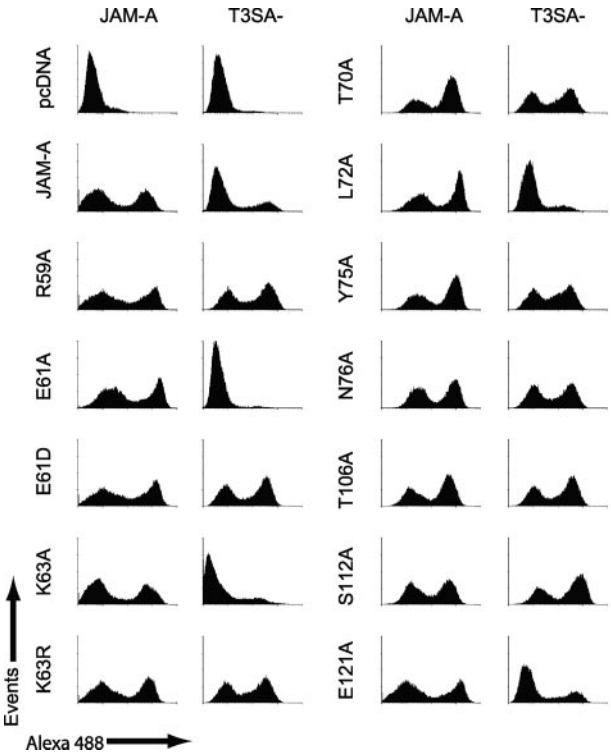

FIGURE 6. **Reovirus T3SA− binding to CHO cells expressing JAM-A mutants.** CHO cells (10^6) were transiently transfected with plasmids encoding the indicated receptor constructs. Following incubation for 24 h to permit receptor expression, cells were lifted from plates using EDTA and stained with hJAM-A-specific monoclonal antibody J10.4 or adsorbed with reovirus T3SA− (10^5 particles/cell). Cell-surface expression of receptor constructs and virus binding was assessed by flow cytometry.

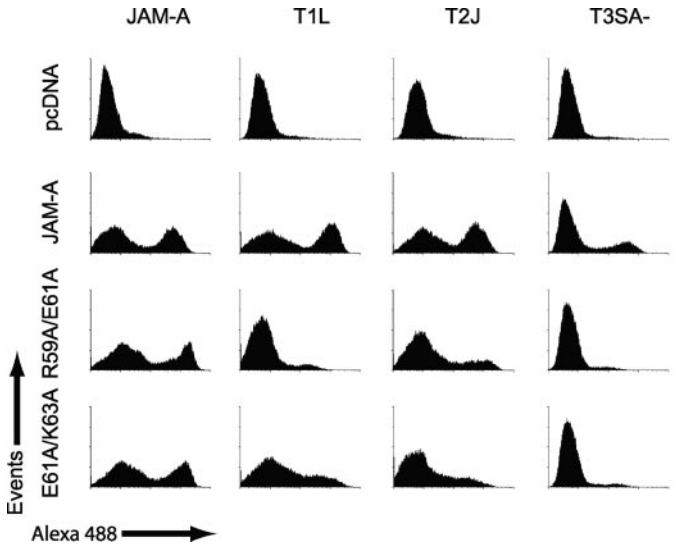

FIGURE 7. **Reovirus T1L, T2J, and T3SA− binding to CHO cells expressing JAM-A mutants.** CHO cells (10^6) were transiently transfected with plasmids encoding the indicated receptor constructs. Following incubation for 24 h to permit receptor expression, cells were lifted from plates using EDTA and stained with hJAM-A-specific monoclonal antibody J10.4 or adsorbed with reovirus T1L, T2J, or T3SA− (10^5 particles/cell). Cell-surface expression of receptor constructs and virus binding was assessed by flow cytometry.

shown). Similar findings were made following incubation of the extracellular domain of dimeric JAM-A mutant S112A or the monomeric mutant E121A with the σ1 head (Fig. 5, *A*–*C*). In both cases, a complex was formed that eluted from the size-exclusion column at the same volume as the complex observed following incubation of wild-type JAM-A with the σ1 head. As expected, monomeric JAM-A point mutant E61A does not form a detectable complex when incubated with the σ1 head (Fig. 5*D*). Because mutant forms of JAM-A that are incapable of forming dimers retain the capacity to interact with σ1, we conclude that the σ1 head can engage monomeric forms of JAM-A.

Reovirus Binding and Infectivity of CHO Cells Expressing Mutant Forms of JAM-A—To determine the capacity of reovirus to bind JAM-A mutants in cell culture, we transiently transfected CHO cells, which are poorly permissive for reovirus infection (26, 32), with plasmids encoding wild-type (24) or mutant forms of full-length JAM-A. Transfected cells were incubated for 24 h to allow receptor expression and adsorbed with reovirus virions. Surface expression of JAM-A and reovirus binding were assessed by flow cytometry (Fig. 6). Wild-type JAM-A and each of the JAM-A mutants were expressed at the surface of transfected cells at approximately equivalent levels, providing confidence that the mutant constructs are properly folded. Virions of T3SA−, a non-sialic acid-binding reovirus strain with a serotype 3 σ1 identical in sequence to T3D in the σ1 head domain (33), bound poorly to vector-transfected CHO cells, whereas specific binding to CHO cells expressing wild-type JAM-A was observed. We used T3SA− rather than T3D in these studies to diminish background binding to cells due to interactions with carbohydrate. T3SA− binding approximated JAM-A expression at the surface of CHO cells expressing the majority of the point mutants. However, T3SA− binding to cells expressing the K63A or L72A mutants was diminished, and no binding above background was observed with cells expressing the E61A mutant form of JAM-A. These results closely mimic the binding of the T3D σ1 head to JAM-A mutants in the GST precipitation and SPR assays (Figs. 2 and 3). Interestingly, mutation of Glu^{61} to aspartate or Lys^{63} to arginine was not associated with the binding defects observed for the E61A and K63A mutants (Fig. 6), indicating that the acidic or basic properties of these residues are important for reovirus engagement.

To compare JAM-A binding determinants for reoviruses of the three serotypes, we assessed binding of virions of strains T1L and T2J to CHO cells expressing wild-type and mutant forms of JAM-A by flow cytometry. Because no serotype 1 or 2 reoviruses incapable of binding carbohydrate have been isolated, we used prototype strains T1L and T2J to represent serotypes 1 and 2. Similar to T3SA−, each virus bound poorly to vector-transfected cells, whereas T1L and T2J binding to cells expressing wild-type JAM-A approximated JAM-A expression (Fig. 7). In contrast to T3SA−, T1L and T2J showed approximately wild-type binding to CHO cells expressing each of the JAM-A point mutants (data not shown). To determine whether T1L and T2J might share similar binding determinants with T3D and T3SA− but with less stringency, we constructed double point mutants R59A/E61A and E61A/K63A. As anticipated, T3SA− showed no specific binding to CHO cells expressing either of the JAM-A double point mutants (Fig. 7). Although not with the same magnitude as T3SA−, both T1L and T2J showed diminished binding to CHO cells expressing the double

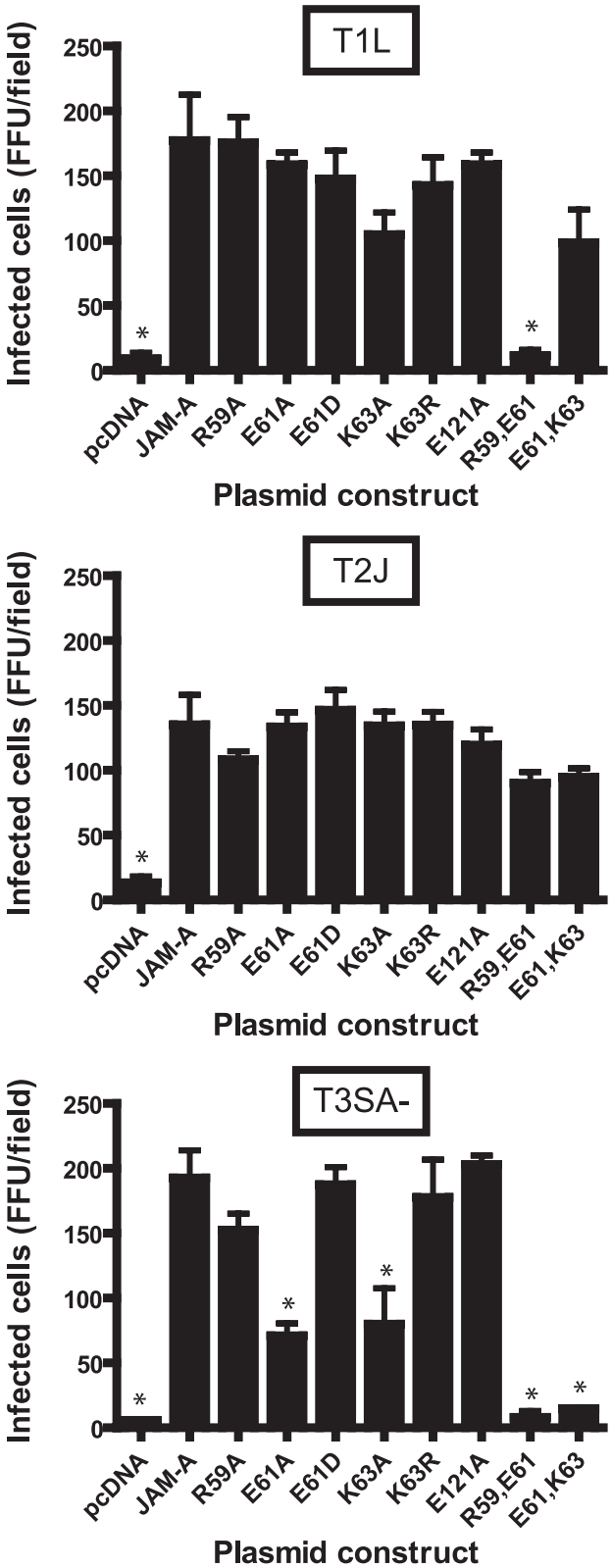

FIGURE 8. **Reovirus infection of CHO cells expressing JAM-A mutants.** CHO cells (2×10^5) were transiently transfected with empty vector (pcDNA) or plasmids encoding mutant forms of JAM-A. Following incubation for 24 h to permit receptor expression, cells were adsorbed with reovirus at a multiplicity of infection of 1 (*T1L*), 5 (*T2J*), or 10 (*T3SA−*) plaque-forming units/cell at room temperature for 1 h. Cells were washed with PBS, incubated in complete medium at 37 °C for 20 h, and stained for reovirus antigen. Infected cells were identified by indirect immunofluorescence and quantified by counting cells exhibiting cytoplasmic staining in three confluent fields of view per experiment. The results are expressed as the mean fluorescent focus units (*FFU*) per field of view for triplicate experiments. *Error bars* indicate S.D. *, $p < 0.05$ in comparison to cells expressing wild-type JAM-A.

point mutants, with T1L exhibiting highly impaired binding to CHO cells expressing the R59A/E61A JAM-A mutant.

To assess the functional significance of mutations in JAM-A that alter reovirus binding, we quantified infectivity of T1L, T2J, and T3SA− following adsorption to CHO cells expressing full-length wild-type or mutant forms of JAM-A by indirect immunofluorescence (33). Infectivity of T3SA− was significantly decreased (~50%) following infection of CHO cells expressing the E61A and K63A mutants in comparison to cells expressing wild-type JAM-A (Fig. 8). Consistent with the flow cytometry experiments (Fig. 7), conservation of charge at residues Glu^{61} and Lys^{63} by substituting aspartate and arginine, respectively, rescued the infectivity defect. T3SA− infectivity was decreased almost to the level of background following adsorption to CHO cells expressing the double point mutants R59A/E61A and E61A/K63A. As predicted by the binding results, T1L also showed a striking loss of infectivity in cells expressing the R59A/E61A JAM-A mutant and a slight decrease in infectivity in cells expressing the K63A or E61A/K63A mutants. T2J showed only a very modest decrease in infectivity, less than 25%, in CHO cells expressing the R59A mutant or either of the two double point mutants, in accordance with the flow cytometry results. Taken together, these data reinforce the validity of results obtained from binding assays using the T3D σ1 head domain and suggest that T1L, T2J, and T3SA− engage JAM-A using non-identical residues.

DISCUSSION

The goal of this study was to identify reovirus binding determinants in JAM-A. We generated alanine substitutions of residues with solvent-exposed side chains in the JAM-A dimer interface in the context of a GST-JAM-A fusion. Analysis of the point mutants using GST precipitation assays and SPR experiments led to the identification of Glu^{61}, Lys^{63}, and Leu^{72} that individually are required for efficient binding of the T3D σ1 head. Glu^{61} and Lys^{63} have charged side chains and participate in salt-bridge contacts that stabilize the JAM-A dimer interface (24). Leu^{72} is located in proximity to Glu^{61} and Lys^{63} and participates in hydrophobic interactions with Tyr^{119} from the apposing JAM-A monomer (24). SPR findings were concordant with these results and indicate that mutation of specific residues in the JAM-A dimer interface can enhance or diminish the rate of association and dissociation of the T3D σ1 head. Specifically, T108A, M110A, and E121A mutations enhanced association of σ1, leading to higher calculated binding affinities in comparison to wild-type JAM-A. On the other hand, R59A and Y75A displayed faster association with the σ1 head but also faster dissociation. The same charged residues required for JAM-A-σ1 interactions in biochemical assays, Glu^{61} and Lys^{63}, also are required for serotype 3 σ1 interactions with JAM-A in cultured cells.

Gel-filtration chromatography of purified, mutant JAM-A extracellular domains revealed that mutation to alanine of any residue in the JAM-A dimer interface that contributes to salt-

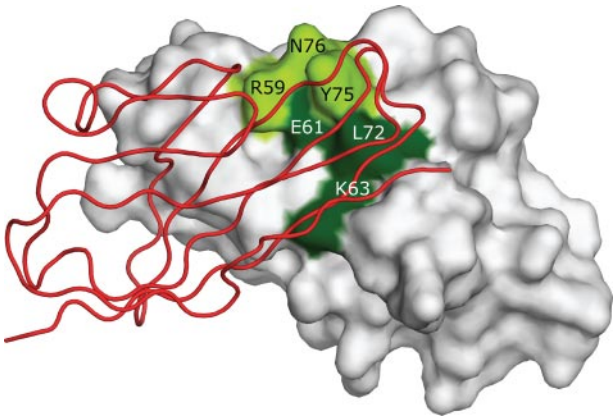

FIGURE 9. **Predicted serotype 3 reovirus binding region in JAM-A.** View of the JAM-A D1 domain dimer. One monomer is oriented as in Fig. 1*C* and is shown as a space-filling representation. The apposing monomer is shown as a *red ribbon* drawing. Residues Glu^{61}, Lys^{63}, and Leu^{72} (*dark green*) are required for efficient serotype 3 reovirus engagement of JAM-A and are proposed to serve as critical contacts for T3D σ1. Residues Arg^{59}, Tyr^{75}, and Asn^{76} (*light green*) are proposed to serve as additional contacts. This figure was generated using PyMOL (54).

bridge interactions as well as one residue, Tyr^{75}, which makes a hydrogen-bond contact with Glu^{114} (24), abolishes the capacity of JAM-A to form dimers in solution at neutral pH. These data indicate that each salt-bridge interaction and the Tyr^{75}–Glu^{114} hydrogen-bond interaction are essential mediators of JAM-A dimer stabilization. Both monomeric and dimeric point mutants of JAM-A are capable of binding the σ1 head. Because residues required for σ1 head binding are found within the dimer interface, we hypothesize that a monomeric form of JAM-A is the relevant σ1 binding partner. Based on elution profiles, it is formally possible that the σ1-JAM-A complex contains dimeric JAM-A and monomeric σ1. However, we think it unlikely that dimeric JAM-A is in the complexes, because the monomeric E121A mutant of JAM-A forms complexes with σ1 that are indistinguishable by gel filtration from wild-type JAM-A-σ1 complexes. It also is unlikely that monomeric σ1 interacts with JAM-A, as a σ1 point mutant that is incapable of trimer formation is incapable of binding JAM-A (20).

Our data support a model of reovirus-JAM-A interactions in which the T3D σ1 head domain directly engages the dimer interface of JAM-A via critical contacts with Glu^{61} and Lys^{63} in β-strand C and Leu^{72} in β-strand C′ and additional, less-critical contacts with nearby residues Arg^{59}, Tyr^{75}, and Asn^{76} (Figs. 1*C* and 9). In this model, σ1 is anticipated to bind with high affinity only to JAM-A monomers. Comparisons of the hJAM-A and mJAM-A crystal structures suggest that small movements of one JAM-A monomer with respect to the apposing monomer can occur in a physiologic context (24). We envision two possible scenarios to explain how σ1 accesses monomeric forms of JAM-A. In the first, small movements of JAM-A monomers with respect to one another might provide σ1 the opportunity to interact weakly with residues closer to the solvent-exposed regions of the JAM-A dimer interface, such as Arg^{59}, Tyr^{75}, and Asn^{76}, as the dimer shifts slightly to a more open conformation. This interaction could potentially orient σ1 to access the dimer interface, where interactions that lead to high-affinity binding occur. In support of this model, mutation of Arg^{59}, Tyr^{75}, or Asn^{76} to alanine leads to reduced levels of binding and faster association and dissociation kinetics between JAM-A and the σ1 head, whereas mutation of Glu^{61}, Lys^{63}, or Leu^{72} to alanine ablates σ1 binding altogether. In the second, reovirus might exploit an equilibrium between monomeric and dimeric forms of JAM-A at the cell surface to engage the dimer interface of JAM-A monomers.

Our binding and infectivity data from CHO cells transfected with JAM-A mutants highlight differences in JAM-A engagement among the reovirus serotypes. Residues Arg^{59} and Glu^{61} are required for efficient T1L binding and infectivity, but only when both residues are altered simultaneously, whereas a small infectivity diminishment is observed when Lys^{63} is altered. In contrast, binding and infectivity of JAM-A-expressing CHO cells by reovirus strain T3SA− requires residues Glu^{61} or Lys^{63}, with some additional contribution from Arg^{59}. In a previous study, T1L virions showed diminished binding to JAM-A mutants S57K and Y75A in a plate-based binding assay (32). These two residues are located in proximity to Glu^{61}, with Ser^{57} residing at the NH_2 terminus of β-strand C (24). Thus, it appears that T1L utilizes a binding site that overlaps with, but is not identical to, the serotype 3 binding site. Based on our binding and infectivity studies with CHO cells, it does not appear that T2J shares contact points with serotype 1 or 3 reoviruses. T2J showed a slight decrease in binding to CHO cells transfected with JAM-A double point mutants R59A/E61A and E61A/K63A, but infectivity was not significantly diminished in these cells. These findings constitute the first evidence that different serotypes of reovirus engage JAM-A at distinct sites or via different contact residues and, therefore, potentially with different specificities and affinities. Of note, differences in affinity for the primary cellular receptor α-dystroglycan have been shown to mediate strain-specific differences in tropism for lymphocytic choriomeningitis virus (38). It is possible that a similar mechanism contributes to serotype-dependent differences in reovirus pathogenesis. For example, a reovirus serotype that has a higher affinity for JAM-A might be capable of infecting cells that express JAM-A at a low level, whereas a reovirus serotype with a lower affinity for the receptor may not. Instead, the tropism of a reovirus with a lower affinity for JAM-A might be more dependent on the carbohydrate binding specificity of the virus or engagement of unidentified receptors on cells expressing low levels of JAM-A.

Although our data suggest non-identical binding sites in JAM-A for different serotypes or strains of reovirus, we find it noteworthy that both T1L and T2J are capable of agglutinating human erythrocytes (39), presumably via carbohydrate engagement, whereas T3SA− is unable to bind sialic acid or agglutinate mammalian erythrocytes (33, 34). Reovirus utilizes an adhesion-strengthening mechanism of attachment to host cells, in which initial low affinity interactions with carbohydrate are thought to tether the virus to the cell surface where it can diffuse laterally until it encounters and engages JAM-A in a high affinity interaction (19, 33). Therefore, it is possible that engagement of carbohydrates on the surface of CHO cells by T1L and T2J reovirus provides an advantage in the capacity of these viruses to encounter JAM-A mutants. The proximity to JAM-A afforded by carbohydrate binding, combined with avid-

ity effects, might lead to detectable binding by T1L and T2J but undetectable binding by T3SA− to some JAM-A mutants expressed at the cell surface.

Whereas the precise nature of σ1-JAM-A interactions will not be known until the structure of the attachment protein bound to the receptor is available, data generated in this study allow some speculation about the nature of these interactions. Because JAM-A serves as a receptor for all serotypes of reovirus (19, 26), we previously hypothesized that conserved residues in σ1 might contribute to σ1-JAM-A interactions (26, 36). While possible, our data suggest that different serotypes of reovirus engage JAM-A via distinct but perhaps overlapping residues, a result that has led us to extend our search for the JAM-A binding site in σ1. Residues at positions 61 and 63 of JAM-A are critical mediators of efficient interactions with σ1. However, efficient binding and infectivity of CHO cells expressing mutant forms of JAM-A is achieved whether there is an aspartate or glutamate at position 61 or an arginine or lysine at position 63. These results demonstrate that the side chain charge of residues at positions 61 and 63 is important for σ1 binding, whereas the length of the side chain is not. Because the charged residues required for efficient σ1 binding participate in salt-bridge interactions that stabilize the dimer interface, we think that charged residues in σ1 form similar salt-bridge interactions with JAM-A, mimicking the dimer interface. There are several clusters of solvent-exposed charged residues in σ1. Furthermore, β-sheet BADG in σ1 can be superimposed onto JAM-A β-sheet GFCC′ with low root mean square deviations (31). Using a newly developed plasmid-based reverse genetics system for reovirus (40), we can make directed mutations in the JAM-A binding region of σ1 to directly test this hypothesis. Non-JAM-A-binding reoviruses might prove invaluable as tools to define the independent contributions of JAM-A and carbohydrate co-receptors to tropism *in vivo*.

In this study, we identified reovirus binding determinants in the most membrane-distal Ig-like domain of JAM-A. We also provided the first evidence that reoviruses of different serotypes engage JAM-A via distinct contact residues. It is interesting that so many viruses have adapted to utilize Ig superfamily members as attachment moieties (19, 41–50). Even more intriguing is the observation that viruses as evolutionarily diverse as adenovirus, HIV, and reovirus bind the same structural regions of Ig superfamily molecules (51, 52). Perhaps this family of molecules, which mediate diverse protein-protein recognition functions such as cell-cell adhesion and high affinity antigen binding, are well suited to serve as virus receptors due to the adhesive nature of their D1 domains (53). Future studies with reovirus and other viruses may serve to enhance an understanding of the co-evolution of cell-adhesion molecules, viral attachment proteins, and immune recognition.

Acknowledgments—We acknowledge Annukkah Antar, Jim Chappell, Takeshi Kobayashi, Sameep Naik, and Bernhard Paetzhold for helpful discussions and ideas. We thank Hannah Fish and the technicians at the Veterans Affairs Flow Cytometry Resource Center for expert technical assistance.

REFERENCES

1. Nibert, M. L., and Schiff, L. A. (2001) in *Fields Virology* (Knipe, D. M., and Howley, P. M., eds) 4th Ed., pp. 1679–1728, Lippincott Williams & Wilkins, Philadelphia
2. Tyler, K. L. (2001) in *Fields Virology* (Knipe, D. M., and Howley, P. M., eds) 4th Ed., pp. 1729–1745, Lippincott Williams & Wilkins, Philadelphia
3. Duncan, R., Horne, D., Cashdollar, L. W., Joklik, W. K., and Lee, P. W. K. (1990) *Virology* **174,** 399–409
4. Nibert, M. L., Dermody, T. S., and Fields, B. N. (1990) *J. Virol.* **64,** 2976–2989
5. Tyler, K. L., McPhee, D. A., and Fields, B. N. (1986) *Science* **233,** 770–774
6. Weiner, H. L., Powers, M. L., and Fields, B. N. (1980) *J. Infect. Dis.* **141,** 609–616
7. Weiner, H. L., Drayna, D., Averill, D. R., Jr., and Fields, B. N. (1977) *Proc. Natl. Acad. Sci. U. S. A.* **74,** 5744–5748
8. Morrison, L. A., Sidman, R. L., and Fields, B. N. (1991) *Proc. Natl. Acad. Sci. U. S. A.* **88,** 3852–3856
9. Tardieu, M., Powers, M. L., and Weiner, H. L. (1983) *Ann. Neurol.* **13,** 602–607
10. Dichter, M. A., and Weiner, H. L. (1984) *Ann. Neurol.* **16,** 603–610
11. Weiner, H. L., Ault, K. A., and Fields, B. N. (1980) *J. Immunol.* **124,** 2143–2148
12. Lee, P. W., Hayes, E. C., and Joklik, W. K. (1981) *Virology* **108,** 156–163
13. Furlong, D. B., Nibert, M. L., and Fields, B. N. (1988) *J. Virol.* **62,** 246–256
14. Fraser, R. D. B., Furlong, D. B., Trus, B. L., Nibert, M. L., Fields, B. N., and Steven, A. C. (1990) *J. Virol.* **64,** 2990–3000
15. Stehle, T., and Dermody, T. S. (2003) *Rev. Med. Virol.* **13,** 123–132
16. Dermody, T. S., Nibert, M. L., Bassel-Duby, R., and Fields, B. N. (1990) *J. Virol.* **64,** 4842–4850
17. Chappell, J. D., Gunn, V. L., Wetzel, J. D., Baer, G. S., and Dermody, T. S. (1997) *J. Virol.* **71,** 1834–1841
18. Chappell, J. D., Duong, J. L., Wright, B. W., and Dermody, T. S. (2000) *J. Virol.* **74,** 8472–8479
19. Barton, E. S., Forrest, J. C., Connolly, J. L., Chappell, J. D., Liu, Y., Schnell, F., Nusrat, A., Parkos, C. A., and Dermody, T. S. (2001) *Cell* **104,** 441–451
20. Schelling, P., Guglielmi, K. M., Kirchner, E., Paetzold, B., Dermody, T. S., and Stehle, T. (2007) *J. Biol. Chem.* **282,** 11582–11589
21. Martin-Padura, I., Lostaglio, S., Schneemann, M., Williams, L., Romano, M., Fruscella, P., Panzeri, C., Stoppacciaro, A., Ruco, L., Villa, A., Simmons, D., and Dejana, E. (1998) *J. Cell Biol.* **142,** 117–127
22. Williams, L. A., Martin-Padura, I., Dejana, E., Hogg, N., and Simmons, D. L. (1999) *Mol. Immunol.* **36,** 1175–1188
23. Liu, Y., Nusrat, A., Schnell, F. J., Reaves, T. A., Walsh, S., Ponchet, M., and Parkos, C. A. (2000) *J. Cell Sci.* **113,** 2363–2374
24. Prota, A. E., Campbell, J. A., Schelling, P., Forrest, J. C., Peters, T. R., Watson, M. J., Aurrand-Lions, M., Imhof, B., Dermody, T. S., and Stehle, T. (2003) *Proc. Natl. Acad. Sci. U. S. A.* **100,** 5366–5371
25. Kostrewa, D., Brockhaus, M., D'Arcy, A., Dale, G. E., Nelboeck, P., Schmid, G., Mueller, F., Bazzoni, G., Dejana, E., Bartfai, T., Winkler, F. K., and Hennig, M. (2001) *EMBO J.* **20,** 4391–4398
26. Campbell, J. A., Schelling, P., Wetzel, J. D., Johnson, E. M., Wilson, G. A. R., Forrest, J. C., Aurrand-Lions, M., Imhof, B., Stehle, T., and Dermody, T. S. (2005) *J. Virol.* **79,** 7967–7978
27. Ebnet, K., Suzuki, A., Ohno, S., and Vestweber, D. (2004) *J. Cell Sci.* **117,** 19–29
28. Cunningham, S. A., Arrate, M. P., Rodriguez, J. M., Bjercke, R. J., Vanderslice, P., Morris, A. P., and Brock, T. A. (2000) *J. Biol. Chem.* **275,** 34750–34756
29. Arrate, M. P., Rodriguez, J. M., Tran, T. M., Brock, T. A., and Cunningham, S. A. (2001) *J. Biol. Chem.* **276,** 45826–45832
30. van Raaij, M. J., Chouin, E., van der Zandt, H., Bergelson, J. M., and Cusack, S. (2000) *Structure* **8,** 1147–1155
31. Stehle, T., and Dermody, T. S. (2004) *Viral Immunol.* **17,** 129–143
32. Forrest, J. C., Campbell, J. A., Schelling, P., Stehle, T., and Dermody, T. S. (2003) *J. Biol. Chem.* **278,** 48434–48444
33. Barton, E. S., Connolly, J. L., Forrest, J. C., Chappell, J. D., and Dermody, T. S. (2001) *J. Biol. Chem.* **276,** 2200–2211

34. Dermody, T. S., Nibert, M. L., Bassel-Duby, R., and Fields, B. N. (1990) *J. Virol.* **64,** 5173–5176
35. Karlsson, R., and Falt, A. (1997) *J. Immunol. Methods* **200,** 121–133
36. Chappell, J. D., Prota, A., Dermody, T. S., and Stehle, T. (2002) *EMBO J.* **21,** 1–11
37. Becker, M. M., Goral, M. I., Hazelton, P. R., Baer, G. S., Rodgers, S. E., Brown, E. G., Coombs, K. M., and Dermody, T. S. (2001) *J. Virol.* **75,** 1459–1475
38. Smelt, S. C., Borrow, P., Kunz, S., Cao, W., Tishon, A., Lewicki, H., Campbell, K. P., and Oldstone, M. B. (2001) *J. Virol.* **75,** 448–457
39. Lerner, A. M., Cherry, J. D., and Finland, M. (1963) *Virology* **19,** 58–65
40. Kobayashi, T., Antar, A. A. R., Boehme, K. W., Danthi, P., Eby, E. A., Guglielmi, K. M., Holm, G. H., Johnson, E. M., Maginnis, M. S., Naik, S., Skelton, W. B., Wetzel, J. D., Wilson, G. J., Chappell, J. D., and Dermody, T. S. (2007) *Cell Host and Microbe* **1,** 147–157
41. Geraghty, R. J., Krummenacher, C., Cohen, G. H., Eisenberg, R. J., and Spear, P. G. (1998) *Science* **280,** 1618–1620
42. Warner, M. S., Geraghty, R. J., Martinez, W. M., Montgomery, R. I., Whitbeck, J. C., Xu, R., Eisenberg, R. J., Cohen, G. H., and Spear, P. G. (1998) *Virology* **246,** 179–189
43. Bergelson, J. M., Cunningham, J. A., Droguett, G., Kurt-Jones, E. A., Krithivas, A., Hong, J. S., Horwitz, M. S., Crowell, R. L., and Finberg, R. W. (1997) *Science* **275,** 1320–1323
44. Tomko, R. P., Xu, R., and Philipson, L. (1997) *Proc. Natl. Acad. Sci. U. S. A.* **94,** 3352–3356
45. Dalgleish, A. G., Beverley, P. C. L., Clapham, P. R., Crawford, D. H., Greaves, M. F., and Weiss, R. A. (1984) *Nature* **312,** 763–767
46. Maddon, P. J., Dalgleish, A. G., McDougal, J. S., Clapham, P. R., Weiss, R. A., and Axel, R. (1986) *Cell* **47,** 333–348
47. Tatsuo, H., Ono, N., Tanaka, K., and Yanagi, Y. (2000) *Nature* **406,** 893–897
48. Greve, J. M., Davis, G., Meyer, A. M., Forte, C. P., Yost, S. C., Marlor, C. W., Kamarck, M. E., and McClelland, A. (1989) *Cell* **56,** 839–847
49. Staunton, D. E., Merluzzi, V. J., Rothlein, R., Barton, R., Marlin, S. D., and Springer, T. A. (1989) *Cell* **56,** 849–853
50. Tomassini, J. E., Graham, D., DeWitt, C. M., Lineberger, D. W., Rodkiey, J. A., and Colonno, R. J. (1989) *Proc. Natl. Acad. Sci. U. S. A.* **86,** 4907–4911
51. Bewley, M. C., Springer, K., Zhang, Y. B., Freimuth, P., and Flanagan, J. M. (1999) *Science* **286,** 1579–1583
52. Kwong, P. D., Wyatt, R., Robinson, J., Sweet, R. W., Sodroski, J., and Hendrickson, W. A. (1998) *Nature* **393,** 648–659
53. Du Pasquier, L., Zucchetti, I., and De Santis, R. (2004) *Immunol. Rev.* **198,** 233–248
54. DeLano, W. L. (2002) *PyMOL*, DeLano Scientific, San Carlos, CA

APPENDIX D

A PLASMID-BASED REVERSE GENETICS SYSTEM FOR ANIMAL DOUBLE-STRANDED RNA VIRUSES

Takeshi Kobayashi, Annukka A. R. Antar, Karl W. Boehme, Pranav Danthi, Elizabeth A. Eby, Kristen M. Guglielmi, Geoffrey H. Holm, Elizabeth M. Johnson, Melissa S. Maginnis, Sam Naik, Wesley B. Skelton, J. Denise Wetzel, Gregory J. Wilson, James D. Chappell, and Terence S. Dermody

Cell Host & Microbe. 1(2):147-157;2007

Cell Host & Microbe
Resource

A Plasmid-Based Reverse Genetics System for Animal Double-Stranded RNA Viruses

Takeshi Kobayashi,[1,2] Annukka A.R. Antar,[2,3,5] Karl W. Boehme,[1,2,5] Pranav Danthi,[1,2,5] Elizabeth A. Eby,[2,3,5] Kristen M. Guglielmi,[2,3,5] Geoffrey H. Holm,[1,2,5] Elizabeth M. Johnson,[2,3,5] Melissa S. Maginnis,[2,3,5] Sam Naik,[2,4,5] Wesley B. Skelton,[1,2,5] J. Denise Wetzel,[1,2,5] Gregory J. Wilson,[1,2,5] James D. Chappell,[1,2,4,*] and Terence S. Dermody[1,2,3,*]
[1] Department of Pediatrics
[2] Elizabeth B. Lamb Center for Pediatric Research
[3] Department of Microbiology and Immunology
[4] Department of Pathology
Vanderbilt University School of Medicine, Nashville, TN 37232, USA
[5] These authors contributed equally to this work.
*Correspondence: jim.chappell@vanderbilt.edu (J.D.C.), terry.dermody@vanderbilt.edu (T.S.D.)
DOI 10.1016/j.chom.2007.03.003

SUMMARY

Mammalian orthoreoviruses (reoviruses) are highly tractable experimental models for studies of double-stranded (ds) RNA virus replication and pathogenesis. Reoviruses infect respiratory and intestinal epithelium and disseminate systemically in newborn animals. Until now, a strategy to rescue infectious virus from cloned cDNA has not been available for any member of the *Reoviridae* family of dsRNA viruses. We report the generation of viable reovirus following plasmid transfection of murine L929 (L) cells using a strategy free of helper virus and independent of selection. We used the reovirus reverse genetics system to introduce mutations into viral capsid proteins σ1 and σ3 and to rescue a virus that expresses a green fluorescent protein (GFP) transgene, thus demonstrating the tractability of this technology. The plasmid-based reverse genetics approach described here can be exploited for studies of reovirus replication and pathogenesis and used to develop reovirus as a vaccine vector.

INTRODUCTION

Reoviruses are members of the *Reoviridae* family, which includes several genera that cause disease in humans and animals. Chief among these are the rotaviruses, which are the most common cause of viral gastroenteritis in human infants (Kapikian et al., 2001). Reoviruses infect the respiratory and gastrointestinal tracts of virtually all mammals, including humans (Tyler, 2001). However, disease associated with reovirus infection occurs primarily in the very young (Tyler et al., 2004). Reoviruses are highly virulent in newborn mice, the preferred experimental system for studies of reovirus pathogenesis, and produce injury to a variety of host tissues, including the central nervous system (CNS), heart, and liver (Tyler, 2001).

Reoviruses contain a genome of 10 dsRNA gene segments enclosed in two concentric protein shells, termed *outer capsid* and *core*. Reovirus infection is initiated by viral attachment to host cells via the filamentous attachment protein σ1 (Furlong et al., 1988). The σ1 protein engages cell-surface carbohydrate (Chappell et al., 1997, 2000) and junctional adhesion molecule-A (JAM-A) (Barton et al., 2001b; Campbell et al., 2005), an integral component of intercellular tight junctions (Martin-Padura et al., 1998). Following attachment to the cell surface, reovirus internalization is mediated by β1 integrins (Maginnis et al., 2006), most likely via clathrin-dependent endocytosis (Ehrlich et al., 2004). In the endocytic compartment, viral outer-capsid proteins σ3 and μ1/μ1C are cleaved by acid-dependent cysteine proteases (Baer and Dermody, 1997; Ebert et al., 2002), resulting in generation of infectious subvirion particles (ISVPs) (Borsa et al., 1981). During ISVP formation, σ3 is removed and a hydrophobic conformer of μ1/μ1C is exposed, facilitating endosomal membrane penetration and delivery of transcriptionally active reovirus core particles into the cytoplasm (Chandran et al., 2002; Odegard et al., 2004), where the remainder of the replication cycle occurs.

With the exception of dsRNA viruses, a plasmid-based reverse genetics system exists for all major groups of animal RNA viruses, including bornaviruses, bunyaviruses, coronaviruses, flaviviruses, orthomyxoviruses, paramyxoviruses, picornaviruses, and rhabdoviruses (Table S1 in the Supplemental Data available with this article online). Despite extensive efforts in several laboratories, generation of an animal dsRNA virus entirely from cloned cDNAs has not been achieved. This critical technological gap is perhaps the single most important limitation to studies of these viruses. Previous efforts on reovirus and rotavirus reverse genetics have resulted in entirely RNA-based (Roner et al., 1997) or partially plasmid-based (Komoto et al., 2006) systems that permit replacement of one or two viral genes. These approaches have been used to

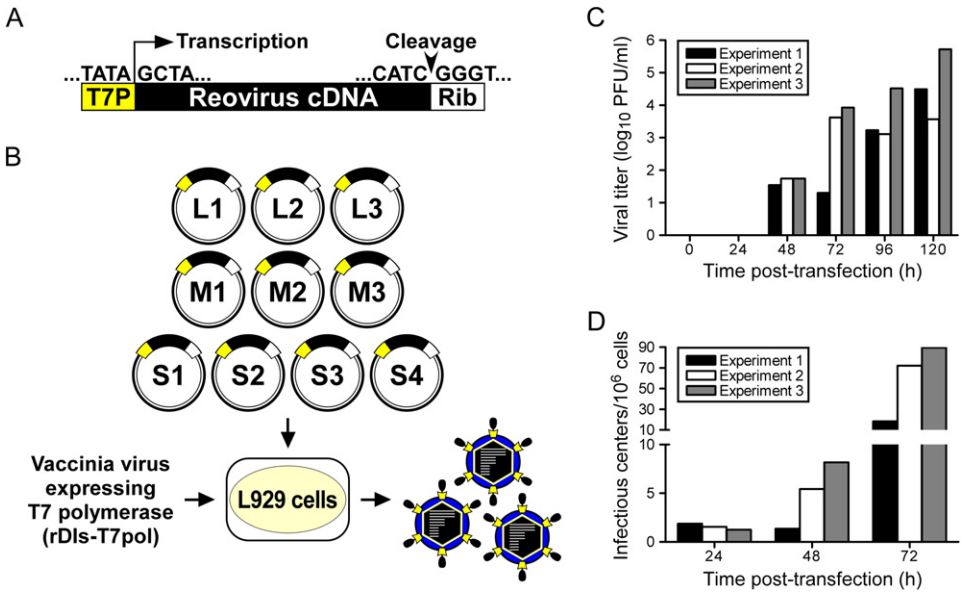

Figure 1. Experimental Strategy to Generate Reovirus from Cloned cDNA

(A) Prototype reovirus gene segment cDNA in plasmid. Cloned cDNAs representing each of the ten full-length reovirus RNA gene segments are flanked by the bacteriophage T7 RNA polymerase promoter (T7P) and the antigenomic hepatitis delta virus (HDV) ribozyme (Rib).

(B) Schematic of approach. The ten reovirus cDNA constructs are transfected into murine L cells expressing T7 RNA polymerase from recombinant vaccinia virus strain rDIs-T7pol, which is replication defective. Nascent transcripts correspond to viral mRNAs containing the native 5′ end. Self cleavage by the HDV ribozyme generates the native viral 3′ end. Following 5 days of incubation, transfected cells are lysed by freeze-thaw, and viable viruses rescued from cloned cDNAs are isolated by plaque assay using L cells.

(C) Kinetics of virus production following plasmid transfection of L cells. Cells were transfected with plasmid DNA according to the protocol in (B) and lysed at the intervals shown. Viral titers in cell lysates were determined by plaque assay.

(D) Infectious center assay following plasmid transfection of L cells. Cells were transfected with plasmid DNA, trypsinized at the intervals shown post-transfection, washed, counted, diluted, and applied directly to monolayers of untreated L cells. The number of the infectious centers was determined by plaque assay.

rescue temperature-sensitive reovirus strains (Roner et al., 1997), define packaging signals in reovirus RNAs (Roner and Steele, 2007), and isolate rotaviruses containing engineered changes in the viral attachment protein (Komoto et al., 2006). However, neither the reovirus nor rotavirus reverse genetics systems in their current configurations permit selective introduction and recovery of desired mutations in each viral gene segment.

We report the development of an entirely plasmid-based reverse genetics system for mammalian reovirus in which viable viruses are generated from cloned cDNAs. Neither helper virus nor coexpression of viral replication proteins is required for recovery of wild-type (WT) virus or engineered viral mutants. Point mutations introduced into viral capsid proteins σ1 and σ3 were used to define sequences that govern susceptibility to cleavage by intestinal proteases. We also recovered a recombinant virus that expresses green fluorescent protein (GFP) by replacement of the σ3 open reading frame (ORF) with GFP. The establishment of plasmid-based reverse genetics for reovirus will allow heretofore technically unapproachable problems in dsRNA virus biology to be studied, provide a platform for development of analogous marker rescue systems for other segmented dsRNA viruses, and foster exploration of reovirus as a vaccine vector to elicit protective immunity against a variety of mucosal pathogens.

RESULTS

Generation of Viable Reovirus from Cloned cDNA

To generate recombinant reovirus from cloned cDNAs, plasmids encoding each of the ten viral gene segments were engineered to facilitate transcription of full-length viral mRNAs under control of the bacteriophage T7 RNA polymerase promoter, which directs transcription initiation preferentially from a juxtaposed guanosine residue (Milligan et al., 1987). As all reovirus (+)-sense RNAs are terminated with a 5′ guanosine (Furuichi et al., 1975a, 1975b), plasmid-generated transcripts are anticipated to possess native 5′ ends (Roner and Joklik, 2001) (Figure 1A). Murine L929 fibroblast (L) cells, which efficiently support reovirus replication (Barton et al., 2001a), were infected with the attenuated, T7 RNA polymerase-expressing vaccinia virus strain rDIs-T7pol 1 hr prior to transfection with the ten reovirus cDNA plasmids (Figure 1B). Nascent transcripts were synthesized with the hepatitis delta virus (HDV) ribozyme fused to the 3′ terminus, which is expected to generate a native 3′ end upon autocatalytic removal (Roner and Joklik, 2001) (Figure 1A). Thus, this

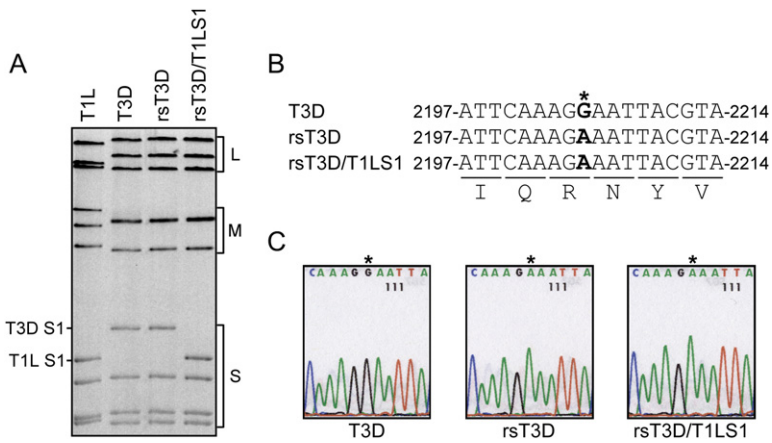

Figure 2. Rescue of rsT3D and rsT3D/T1LS1

(A) Electropherotypes of T1L, T3D, rsT3D, and rsT3D/T1LS1. Viral dsRNA was extracted from purified virions and electrophoresed in an SDS-polyacrylamide gel, followed by ethidium bromide staining to visualize viral gene segments. Size classes of gene segments (L, M, S) are indicated.

(B) Recombinant viruses contain a novel mutation in the L1 gene. The single nucleotide difference in L1 unique to rsT3D and rsT3D/T1LS1 is shown in the alignment as an asterisk. The G→A substitution at position 2205 is a signature change engineered into the cloned T3D L1 cDNA used for marker rescue.

(C) Sequence analysis of L1 gene RT-PCR products from rescued reoviruses. A fragment of the L1 gene was amplified by one-step RT-PCR performed using viral dsRNA extracted from purified virions of T3D, rsT3D, and rsT3D/T1LS1. Products were subjected to direct sequence analysis and compared to the L1 sequence of T3D. Shown are sequence chromatograms demonstrating G→A substitution at position 2205 of the rsT3D and rsT3D/T1LS1 L1 genes.

expression strategy should yield ten unique reovirus mRNA species competent to complete all steps in the viral RNA life cycle. Accordingly, rescued viruses were recovered from cell-culture supernatants by plaque assay on L cell monolayers (Figure 1C).

To ensure that viruses isolated following plasmid transfection represented single clones, and to preclude contamination of reovirus stocks by rDIs-T7pol, all viruses were isolated by plaque purification using L cell monolayers. rDIs-T7pol is replication defective and produces no detectable growth in mammalian cells (Ishii et al., 2002). Concordantly, no viral plaques arose on L cell monolayers when the cotransfections were prepared with nine of the ten reovirus marker-rescue plasmids (data not shown). Furthermore, vaccinia virus proteins were not detected by immunoblot analysis of second-passage stocks of plaque-purified reoviruses (data not shown).

Infectious center assays were performed to assess the efficiency of reovirus infection in plasmid-transfected L cells. At 24–48 hr posttransfection, times corresponding to the primary round of infection, eight or fewer infectious centers per 10^6 cells were detected (Figure 1D). The number of infectious centers increased substantially between 48 and 72 hr posttransfection to 18 to 90 per 10^6 cells, suggesting that a secondary round of infection had ensued by the 72 hr time point. Viral titer in transfection lysates was below the limit of detection (~10 PFU/ml) at 24 hr but was detectable at 48 hr and increased logarithmically at time points thereafter (Figure 1C). The ratio of viral PFU in transfection lysates to infectious centers was ~10 to 100 at 48 and 72 hr. These results indicate that initiation of productive reovirus replication from transfected plasmids is inefficient, with approximately 1 cell per 10^5 to 10^6 cells giving rise to, on average, 10 to 100 viable virus particles that establish infection of the culture. In our experiments, yields of WT virus 5 days after plasmid transfection are regularly in the range of 10^4–10^6 PFU/ml (Figure 1C).

Separation of reovirus genomic dsRNA using SDS-PAGE produces unique electrophoretic patterns that can be used to discriminate different viral strains (Barton et al., 2001a). To confirm that viruses isolated using the plasmid-based rescue procedure contained the expected combination of gene segments, genomic dsRNA isolated from recombinant strain (rs) T3D and rsT3D/T1LS1 was resolved in SDS-polyacrylamide gels and visualized by ethidium bromide staining (Figure 2A). The electropherotype of rsT3D was indistinguishable from that of strain T3D, the origin of the cloned cDNA sequences used to generate rsT3D. Likewise, rsT3D/T1LS1 displayed an electropherotype consistent with nine cloned gene segments derived from T3D and a single cloned gene segment, S1, derived from strain T1L. To exclude the possibility of contamination, a silent point mutation, G to A at nucleotide 2205, was introduced into the L1 gene of all virus strains generated from cloned cDNAs (Figure 2B). This change has not been observed in any reported T3D L1 sequence (Wiener and Joklik, 1989) and serves as a signature for viruses derived through plasmid-based rescue. As anticipated, sequence analysis of rsT3D and rsT3D/T1LS1 revealed the expected G to A substitution (Figure 2C), confirming the plasmid origins of these isolates.

Characterization of Reoviruses Generated by Plasmid Transfection

Reoviruses replicate and assemble within cytoplasmic inclusions in infected cells (Fields, 1971). Viral inclusions contain dsRNA (Silverstein and Schur, 1970), viral proteins (Fields, 1971), and both complete and incomplete viral particles (Fields, 1971). Reovirus strain T3D forms large globular inclusions that localize to the perinuclear space (Parker et al., 2002). To determine whether rsT3D forms viral inclusions in a manner similar to native T3D, cells were infected with T3D and rsT3D and processed 18 hr postinfection for image analysis by confocal microscopy (Figure 3A). Both T3D and rsT3D formed morphologically indistinguishable large globular inclusions that were

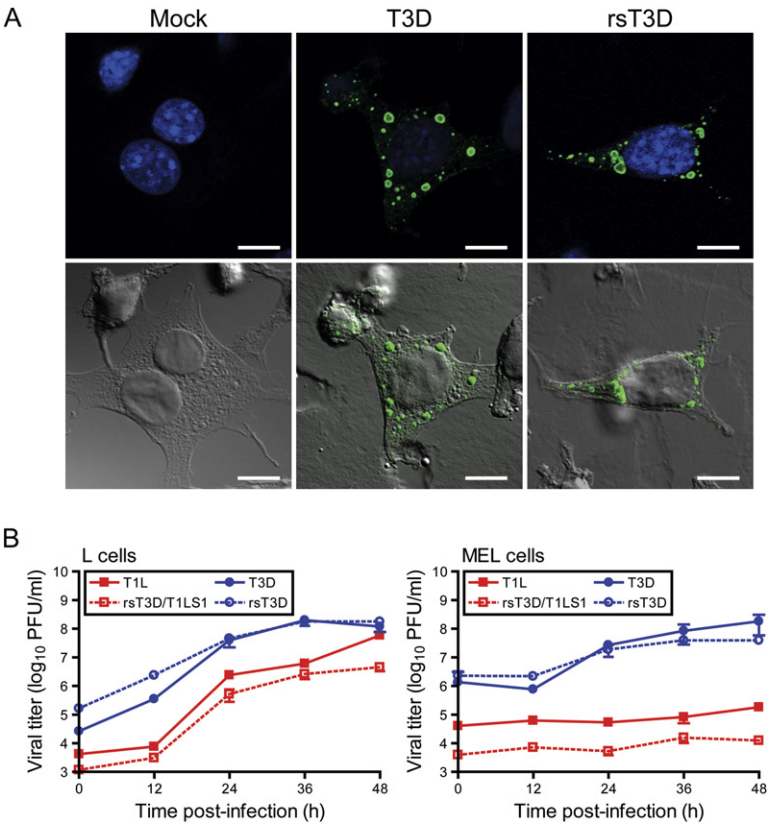

Figure 3. Infectivity of Native and Recombinant Reoviruses

(A) Immunofluorescence of cells infected with T3D and rsT3D. L cells were mock infected or infected with either T3D or rsT3D, stained at 18 hr postinfection with anti-μNS antiserum to visualize reovirus inclusions (green) and TO-PRO3 to visualize nuclei (blue), and imaged by confocal laser scanning microscopy. Representative digital fluorescence (top panel) and DIC images (bottom panel) for mock-, T3D-, and rsT3D-infected cells are shown. Scale bar, 10 μM.

(B) One-step growth curve for T1L, T3D, rsT3D, and rsT3D/T1LS1 in L cells (left) and MEL cells (right). Cells were infected with virus, incubated for the intervals shown, and lysed by freeze-thaw. Viral titers in cell lysates were determined by plaque assay. The results are presented as the mean viral titers for triplicate experiments. Error bars indicate SD.

localized to the perinuclear compartment. We conclude that recombinant rsT3D recapitulates a hallmark of native T3D infection in cultured cells.

To confirm that the recombinant viruses exhibit replication kinetics similar to the native strains, T1L, T3D, rsT3D, and rsT3D/T1LS1 were tested for infection of L cells and MEL cells (Figure 3B). L cells support replication of all reovirus strains tested in our laboratory. In contrast, MEL cells support replication of only sialic acid-binding reovirus strains (Rubin et al., 1992; Chappell et al., 1997). T1L, rsT3D/T1LS1, T3D, and rsT3D produced ~1000-fold yields of viral progeny in L cells. However, only sialic acid-binding strains T3D and rsT3D were capable of efficiently infecting MEL cells, producing yields in each case of ~100-fold, whereas strains T1L and rsT3D/T1LS1 produced minimal yields of viral progeny in these cells (<10-fold). Together, these data indicate that recombinant reoviruses display replication characteristics indistinguishable from native strains.

Susceptibility of Attachment Protein σ1 to Proteolytic Cleavage Attenuates Reovirus Intestinal Infection and Systemic Spread

The σ1 protein exhibits strain-specific differences in susceptibility to cleavage following in vitro treatment with intestinal proteases to generate ISVPs (Nibert et al., 1995; Chappell et al., 1998). This difference in cleavage susceptibility segregates with a single amino acid polymorphism in the tail domain of σ1 (Figure 4A). Strains with a threonine at residue 249 in σ1 are susceptible to cleavage by trypsin after Arg245, whereas those with an isoleucine at residue 249 are resistant to cleavage (Chappell et al., 1998). The importance of sequence polymorphism at residue 249 has been confirmed in studies using expressed protein (Chappell et al., 1998) and recoated core particles (Chandran et al., 2001) but not with intact virions.

To determine whether the single Thr-Ile polymorphism at residue 249 in σ1 protein is sufficient to alter σ1 cleavage susceptibility during treatment of virions with intestinal proteases to generate ISVPs, we used plasmid-based rescue to generate rsT3D-σ1T249I, which differs from rsT3D by the presence of an isoleucine in σ1 at residue 249 (Table S2). Purified virions of rsT3D and rsT3D-σ1T249I were treated with trypsin and analyzed by SDS-PAGE. As expected, a digestion pattern consistent with formation of ISVPs (loss of σ3 protein and generation of the δ fragment of μ1C protein) was observed for both viruses (Figure 4B). However, the stability of rsT3D and rsT3D-σ1T249I σ1 proteins differed. The band corresponding to rsT3D σ1 diminished in intensity immediately after trypsin addition until it was eventually undetectable (Figure 4B). However, the rsT3D-σ1T249I σ1 band was intact even after 60 min of digestion. Thus, the T249I polymorphism is an independent determinant of σ1 cleavage susceptibility.

Proteolytic cleavage of σ1 at a site adjacent to Thr249 releases the JAM-A-binding σ1 head domain, leading to

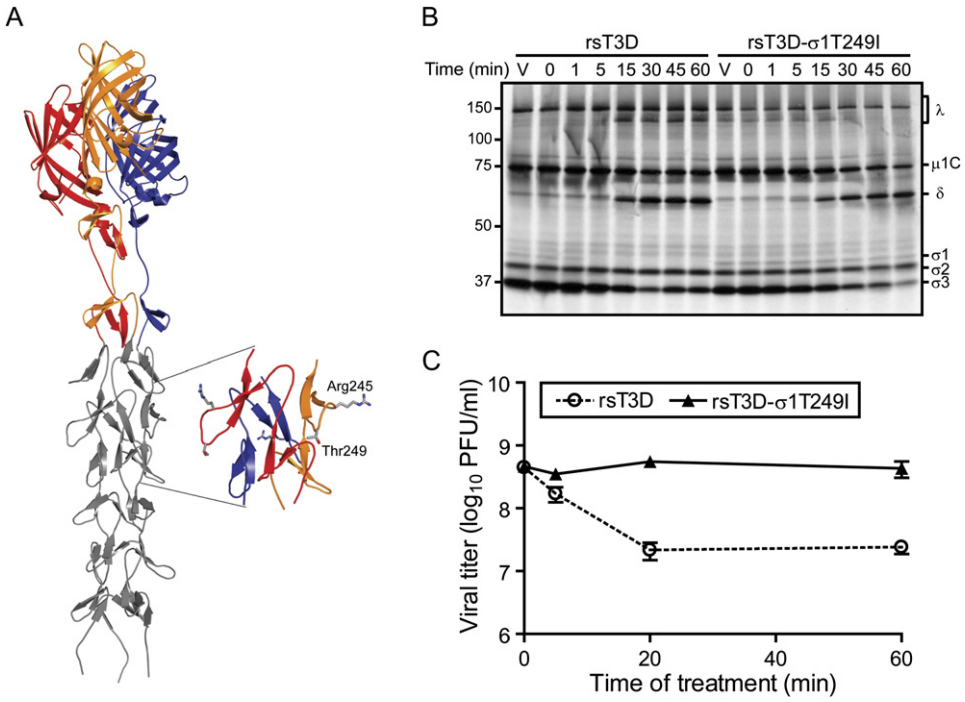

Figure 4. The σ1 Protein of rsT3D-σ1T249I Is Resistant to Trypsin

(A) Model of σ1 generated by adding five β spiral repeats to the N terminus of the crystallized fragment of σ1 (Chappell et al., 2002). The three monomers in the crystallized fragment are shown in red, yellow, and blue; the model is shown in gray. The inset shows an enlarged view of the β spiral region in σ1 that influences susceptibility of the molecule to cleavage by intestinal proteases (Chappell et al., 1998). Side chains of Arg245 and Thr249 are depicted in ball-and-stick representation.

(B) Electrophoretic analysis of viral structural proteins of rsT3D and rsT3D-σ1T249I during treatment with trypsin to generate ISVPs. Purified ^{35}S-methionine-labeled virions were treated with trypsin for the indicated intervals and loaded into wells of a 4%–20% polyacrylamide gradient gel. After electrophoresis, the gel was prepared for fluorography and exposed to film. Samples of untreated virions appear in the lanes labeled "V." Viral proteins are labeled. Positions of molecular weight standards (in kDa) are indicated. The experiments shown are representative of two performed for each virus.

(C) Infectivity of rsT3D and rsT3D-σ1T249I during treatment with trypsin to generate ISVPs. Purified virions were treated with trypsin at 37°C for the intervals shown. Titers of virus in the treatment mixtures were determined by plaque assay. The results are presented as the mean viral titers for triplicate experiments. Error bars indicate SD.

diminished viral infectivity (Nibert et al., 1995). To test whether rsT3D and rsT3D-σ1T249I differ in infectivity after protease treatment to generate ISVPs, purified virions of each strain were exposed to trypsin for various intervals, and titers of infectious virus in the treatment mixtures were determined by plaque assay (Figure 4C). As observed with WT T3D in previous experiments (Nibert et al., 1995), rsT3D lost infectious titer rapidly after protease treatment. In contrast, titers of rsT3D-σ1T249I remained relatively stable throughout the assay time course. Loss of infectivity of rsT3D correlated with kinetics of σ1 cleavage (compare Figures 4B and 4C), indicating that changes in viral infectivity after trypsin treatment are governed by the cleavage state of σ1. Furthermore, both phenotypes are linked to a single σ1 polymorphism at amino acid 249.

Reovirus strains T1L and T3D differ in the capacity to infect the murine intestine after peroral (PO) inoculation (Bodkin et al., 1989), a property that segregates with the viral S1 (encoding σ1 and σ1s) and L2 (encoding λ2) genes (Bodkin and Fields, 1989). Exposure of T3D to an intestinal wash results in σ1 cleavage (Chappell et al., 1998), raising the possibility that failure of T3D to infect the intestine is in part attributable to σ1 cleavage susceptibility. To test whether susceptibility of σ1 to proteolytic cleavage is associated with diminished T3D growth in animals, we assessed the capacity of rsT3D and rsT3D-σ1T249I to infect the intestine and disseminate systemically following PO inoculation (Figure 5A). Newborn mice were inoculated perorally with each strain, and viral titers in the intestine and brain were determined at 4, 8, and 12 days after inoculation. At all time points tested, titers of rsT3D-σ1T249I in the intestine were greater than those produced by rsT3D. Furthermore, rsT3D-σ1T249I produced greater titers in the brain at days 8 and 12 than did rsT3D. However, when inoculated by the intracranial (IC) route, rsT3D and rsT3D-σ1T249I produced equivalent titers (Figure 5B), although rsT3D reached peak titers at earlier time points than did rsT3D-σ1T249I. These findings indicate that a Thr-Ile polymorphism at amino acid 249 in T3D σ1 controls viral growth in the murine intestine and systemic spread to the CNS.

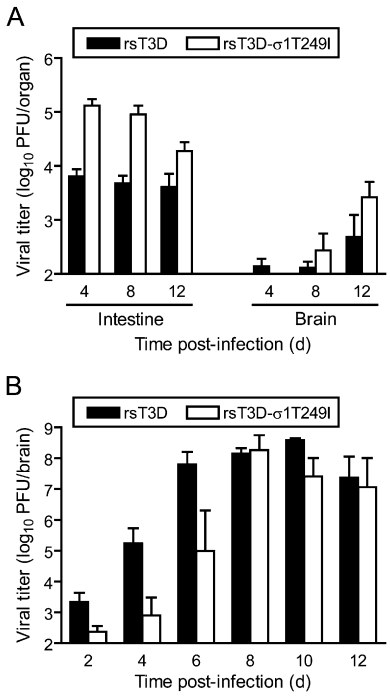

Figure 5. rsT3D-σ1T249I Infects the Murine Intestine and Disseminates to the CNS

Titers of rsT3D and rsT3D-σ1T249I after either PO (A) or IC (B) inoculation. Mice were inoculated with virus and euthanized at the indicated times postinoculation. Viral titers in organ homogenates were determined by plaque assay. The limit of detection was 100 PFU/ml of organ homogenate. Each data point represents the average viral titer from 3 to 12 mice. Error bars indicate SD.

Regulation of Reovirus Disassembly by a Single Polymorphism in Outer-Capsid Protein σ3

Previous studies identified a tyrosine-to-histidine substitution at amino acid 354 in T3D σ3 as a key regulator of the kinetics of virion-to-ISVP conversion in vitro (Wetzel et al., 1997) and viral resistance to growth inhibition by the cysteine protease inhibitor E64 (Baer and Dermody, 1997; Ebert et al., 2001). Tyr354 is located in the virion-distal lobe of σ3 adjacent to sites in the protein that are cleaved during formation of ISVPs (Ebert et al., 2002) (Figure 6A). The importance of this residue in viral replication has been deduced by analysis of reassortant viruses containing WT and mutant σ3 proteins (Wetzel et al., 1997; Ebert et al., 2001; Clark et al., 2006) and analysis of ISVPs recoated with WT and mutant forms of σ3 (Wilson et al., 2002; Clark et al., 2006).

To determine whether the Y354H mutation in σ3 is sufficient to confer enhanced virion-to-ISVP conversion and resistance to E64, we generated rsT3D-σ3Y354H (Table S2) and compared this virus to rsT3D for kinetics of σ3 proteolysis following protease treatment in vitro. Virions of each strain were treated with chymotrypsin for various intervals and processed for analysis of viral structural proteins by SDS-PAGE (Figure 6B). Treatment of rsT3D and rsT3D-σ3Y354H virions with chymotrypsin resulted in degradation of σ3 and cleavage of μ1C to form δ, indicative of ISVP formation. Proteolysis of rsT3D-σ3Y354H σ3 during chymotrypsin treatment occurred with substantially faster kinetics than that of rsT3D σ3. This result indicates that amino acid 354 in σ3 protein is an independent determinant of virion susceptibility to proteolytic digestion and likely functions as an autonomous regulator of viral disassembly in cellular endosomes.

The role of σ3 mutation Y354H in virion disassembly in cyto was investigated by quantifying yields of rsT3D and rsT3D-σ3Y354H after 24 hr of growth in L cells treated with 0–200 μM E64 (Figure 6C). Both strains produced yields of ~1000 fold following growth in untreated cells. However, yields of rsT3D-σ3Y354H were ~100-fold greater than those of rsT3D following growth in cells treated with 200 μM E64 (the highest concentration tested). Therefore, a single mutation in σ3, Y354H, regulates resistance of reovirus to an inhibitor of cysteine proteases within cellular endosomes.

Transduction of GFP by a Recombinant Reovirus

To determine whether reoviruses capable of expressing a foreign gene can be recovered following plasmid transfection, we introduced sequences encoding GFP into the σ3 ORF of the T3D S4 plasmid (Figure 7A). In this configuration, GFP is expressed as a fusion protein incorporating amino acids 1–39 of σ3 protein at the N terminus. Recombinant virus rsT3D/S4-GFP was recovered following plasmid transfection of L cells stably expressing WT σ3 protein, which is required for propagation of this strain (Figure S1). RT-PCR analysis using primers specific for T3D S4 and GFP confirmed incorporation of a recombinant S4-GFP gene segment into rsT3D/S4-GFP (Figure 7B). Infection of L cells with rsT3D/S4-GFP resulted in expression of GFP and viral inclusion-forming proteins μNS and σNS but not σ3 (Figures 7C and 7D). The capacity of rsT3D/S4-GFP to express GFP was not altered through four passages (data not shown). These results demonstrate that reovirus can be engineered to express foreign genes.

DISCUSSION

The absence of DNA intermediates in the life cycle of RNA viruses poses a technical challenge to genetic analysis of viral phenotypes. Prior to the development of reverse genetics, or "marker rescue," for RNA viruses of animals, in which plasmid-borne cDNAs of viral genomes initiate synthesis of replication-competent RNAs, classical Darwinian methods were used to select viral mutants that could be subjected to correlative genetic studies—so-called "forward genetics." However, reverse genetics technology permits testing of tightly focused, rational hypotheses about complex questions of virus structure, virus-cell interactions, and viral pathogenesis through direct engineering of the viral genome without a need to devise complicated selection strategies for isolation of viral mutants. Furthermore, reverse genetics of RNA viruses has supported rapid generation of vaccines against these and other infectious agents and propelled their use as gene

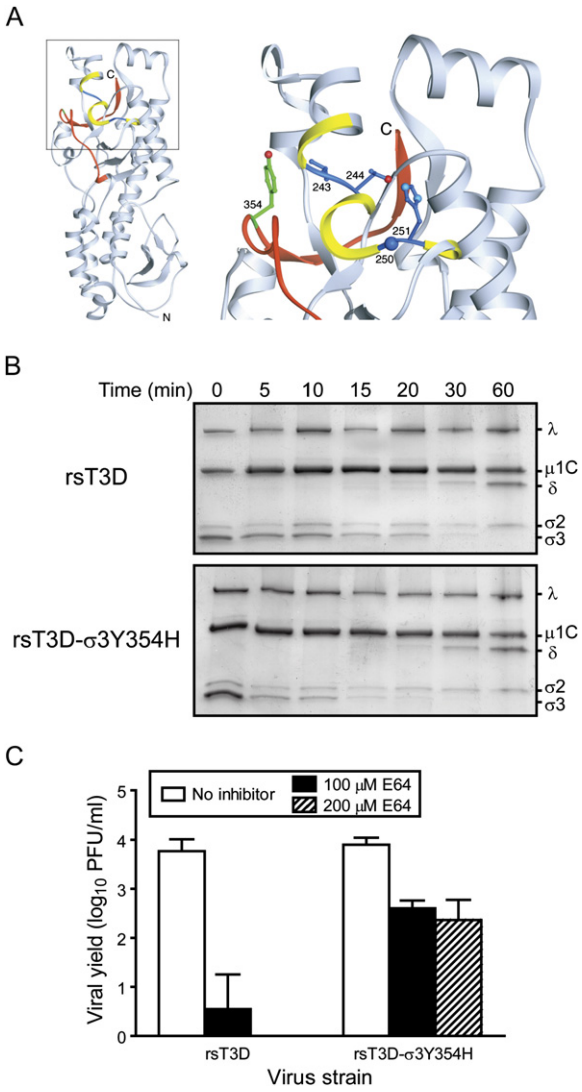

Figure 6. A Single Mutation in Outer-Capsid Protein σ3 Accelerates Proteolytic Disassembly of Reovirus

(A) Crystal structure of T3D σ3 (Olland et al., 2001), in which cathepsin L cleavage sites are depicted in blue between amino acids 243 and 244 and between 250 and 251 (Ebert et al., 2002). Surrounding residues, from amino acids 241 to 253, are shown in yellow. The C-terminal residues of σ3, from amino acids 340–365, are colored red. Tyr354, which is altered in several PI (Wetzel et al., 1997), D-EA (Ebert et al., 2001), and ACA-D viruses (Clark et al., 2006), is shown in green. The virion-distal end of σ3 is at the top of the figure, and the virion-proximal end and N terminus are at the bottom. The inset shows an enlarged view of the boxed region of σ3 using the same color scheme. Side chains of amino acids 243, 244, 250, 251, and 354 are depicted in ball-and-stick representation.

(B) Chymotrypsin treatment of rsT3D and rsT3D-σ3Y354H. Purified virions were treated with chymotrypsin for the indicated intervals and loaded into wells of 10% polyacrylamide gels. After electrophoresis, the gels were stained with Coomassie blue. Viral proteins are labeled. The experiments shown are representative of two performed for each virus.

(C) Growth of rsT3D and rsT3D-σ3Y354H in L cells treated with E64. L cells were preincubated in medium with or without E64 at the concentrations shown. The medium was removed, cells were adsorbed with virus for 1 hr, and fresh medium with or without E64 was added. After 24 hr incubation, viral titers in cell lysates were determined by plaque assay. The results are presented as the mean viral yields, calculated by dividing titer at 24 hr by titer at 0 hr for each concentration of E64, for triplicate experiments. Error bars indicate SD.

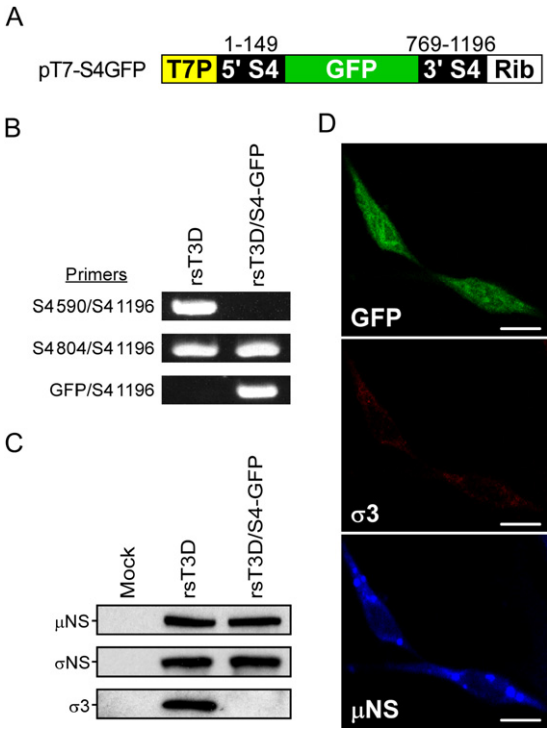

Figure 7. Expression of GFP by rsT3D/S4-GFP

(A) Schematic of pT7-S4GFP. The GFP ORF is flanked by S4 gene nucleotides 1–149 and 769–1196.

(B) RT-PCR analysis of rsT3D and rsT3D/S4-GFP. Viral dsRNA was extracted from purified virions and subjected to RT-PCR using primers specific for T3D S4 and GFP sequences. Numbers delineate the S4 RNA nucleotide position corresponding to the 5′ end of S4-specific primers.

(C) Viral protein expression in cells infected with rsT3D/S4-GFP. L cells were infected with rsT3D or rsT3D/S4-GFP at an MOI of 1 PFU per cell and incubated for 24 hr. Cell lysates were analyzed by immunoblotting using antibodies specific for μNS, σNS, and σ3 proteins.

(D) Image analysis of cells infected with rsT3D/S4-GFP. L cells were infected with rsT3D/S4-GFP, stained with antibodies specific for μNS (blue) and σ3 (red) proteins at 24 hr postinfection, and imaged by confocal laser scanning microscopy. Scale bar, 10 μM.

delivery vehicles (Blaney et al., 2006; Horimoto and Kawaoka, 2006; Riezebos-Brilman et al., 2006).

We developed a fully plasmid-based reverse genetics technology for mammalian reoviruses. This system permits selective introduction of desired mutations into cloned cDNAs encoding each of the ten viral gene segments, followed by isolation of mutant viruses from cells transfected with the plasmid constructs. Moreover, gene segment cDNAs can be manipulated to facilitate expression of a transgene. Importantly, recombinant viruses are generated without a requirement for helper virus and free of any selection. Thus, this new technology provides

a means to directly and precisely engineer the viral genome in the context of infectious virus.

We used the newly developed plasmid-based reovirus reverse genetics system to engineer mutations in the σ1 and σ3 proteins. These proteins form part of the viral outer capsid, which is responsible for numerous major events in reovirus interaction with the cell and host, including attachment, disassembly within endosomes, penetration of cell membranes, induction of apoptosis, growth in the intestine, pathways of spread, neurovirulence, and tropism within the CNS (for reviews, see Chandran and Nibert, 2003; O'Donnell et al., 2003; Guglielmi et al., 2006). Therefore, we initially applied reverse genetics technology to the study of outer-capsid proteins to better understand how these proteins mediate critical steps in reovirus replication and disease.

The infectivity of ISVPs of reovirus strain T1L in L cells is approximately 10-fold greater than that of T3D ISVPs (Nibert et al., 1995). This difference in infectivity is hypothesized to be a direct result of σ1 cleavage (Nibert et al., 1995; Chappell et al., 1998), presumably due to removal of the JAM-A-binding region of the molecule. Although the T249I substitution in expressed T3D σ1 renders it resistant to cleavage by trypsin (Chappell et al., 1998), until now it has not been possible to define the role of σ1 cleavage in T3D infectivity for lack of means to generate a mutant T3D virus with the T249I change. This virus has been generated using reverse genetics, and our findings indicate that cleavage susceptibility of viral attachment protein σ1 due to a single polymorphism at amino acid position 249 is the basis for reduced infectivity of T3D ISVPs relative to virions (Figure 4C) and contributes to diminished growth of T3D in the murine intestine following PO inoculation (Figure 5A).

Previous studies of T3D-derived reovirus strains with altered disassembly kinetics point to a critical role for sequences in the virion-distal, C-terminal lobe of σ3 in susceptibility to acid-dependent proteolysis. A C-terminal Y354H mutation in σ3 protein of strain T3D was selected during persistent infection of L cells (PI viruses) (Wetzel et al., 1997) and by serial passage of virus in L cells treated with either E64 (D-EA viruses) (Ebert et al., 2001) or ammonium chloride (ACA-D viruses) (Clark et al., 2006). Using reovirus reverse genetics, the Y354H substitution was introduced into a WT T3D genetic background, and the resultant virus, rsT3D-σ3Y354H, demonstrated accelerated kinetics of σ3 cleavage (Figure 6B) and diminished sensitivity to the growth-inhibitory effects of E64 (Figure 6C). Residue 354 is located in a position thought to be important for controlling access to protease-hypersensitive regions in σ3, residues 208–214 and 238–242, thereby influencing σ3 cleavage kinetics (Jané-Valbuena et al., 2002). Therefore, it appears that residue 354 in σ3 is a gatekeeper for the viral outer capsid, serving to regulate the balance between viral stability and an irreversible, proteolytically triggered disassembly cascade committing the virion particle to either replication or inactivation.

We exploited the reovirus reverse genetics system to develop a gene-delivery vehicle by replacing the σ3 ORF in the S4 plasmid with a GFP-encoding cDNA (Figure 7). The resultant virus, rsT3D/S4-GFP, expresses GFP through successive passages in cell culture. These results reveal the potential for exploitation of reovirus as a gene-transduction vector with application in the development of new mucosal vaccines, more effective oncolytic agents (Coffey et al., 1998), and high-level expression of foreign genes in animal cells. Ideal reovirus vectors will contain stable σ1 proteins and combine excellent extracellular stability with highly efficient intracellular disassembly. We find that each of these parameters can be independently adjusted through strategic alterations in outer-capsid proteins. Manipulation of inner-capsid proteins and the genomic RNA itself should allow construction of viruses able to circumvent other aspects of virus-cell and virus-host interactions that pose potential barriers to antigen and gene delivery by reovirus.

Our results indicate that productive viral infection is established in a small fraction of L cells, approximately 1 in 10^5–10^6 cells, transfected with plasmids encoding the ten reovirus gene segments (Figure 1D). Thus, the reovirus plasmid-based marker rescue system is suited to the isolation of viable viral clones by plaque assay, followed by expansion in cell culture to attain quantities of virus sufficient for phenotypic analyses. Manipulations that severely cripple viral replication or particle assembly are more challenging to study because these changes may prohibit virus isolation. However, recovery of a GFP-expressing virus, rsT3D/S4-GFP, demonstrates that marker rescue of lethal mutations is possible by transcomplementation (in this case with WT σ3 protein) (Figure 7 and Figure S1). This result also agrees with our previous finding that inhibition of reovirus replication by RNAi-mediated reduction of viral protein synthesis is reversible by transcomplementation with ectopically expressed WT protein (Kobayashi et al., 2006). Furthermore, transcomplementation allows precise definition through systematic mutational analysis of functional domains in reovirus proteins that are essential for viral replication (Kobayashi et al., 2006). It should be possible to apply this technique to the new marker rescue system for delineation of structure-function relationships in reovirus proteins and RNA.

Quantitative success of plasmid-initiated reovirus infection in this reverse genetics system probably is not limited by the amount of template or transfection efficiency, since the molar ratio of plasmid to target cell is approximately 5×10^4, and increasing the amount of plasmid does not effect higher viral yields from cotransfection lysates (data not shown). Furthermore, it does not appear that infection efficiency is limited by the absence of viral replication proteins during early steps of replication because high-level expression of the replication proteins μ2, μNS, and σNS, which collaborate to form viral inclusions in infected cells (Mbisa et al., 2000; Broering et al., 2002; Becker et al., 2003; Miller et al., 2003), did not enhance viral recovery (data not shown). Perhaps the presence of other viral or cellular factors associated with natural infection by intact virion particles is required for maximal reovirus infectivity.

Presently, no entirely plasmid-based reverse genetics system has been described for any other dsRNA virus of animals. Although each genus within this constellation of viruses bears unique biologic characteristics and physiochemical properties, there are nonetheless numerous unifying features of virion particle structure and replication mechanisms that should allow principles and techniques established in this study to be applied broadly across the group. We expect that new insights into mammalian reovirus replication learned with the use of this reverse genetics system will be quickly extrapolated to other *Reoviridae* family members, leading to accelerated development of analogous marker-rescue technologies for those viruses.

EXPERIMENTAL PROCEDURES

Cells and Viruses

L cells and HeLa cells were maintained as described (Barton et al., 2001a). Reovirus strains T1L and T3D are laboratory stocks originally obtained from Dr. Bernard Fields. Virus was purified after growth in L cells by CsCl-gradient centrifugation (Furlong et al., 1988). Purified ^{35}S-methionine-labeled virions were prepared as described (Nibert et al., 1995). Attenuated vaccinia virus strain rDIs-T7pol expressing T7 RNA polymerase was propagated in chick embryo fibroblasts as described (Ishii et al., 2002).

Plasmid Construction

Full-length reovirus cDNAs were amplified by RT-PCR using viral dsRNA extracted from purified virions as template. Amplified cDNAs were initially cloned into pBluescript II SK (−) (Stratagene) for the T3D L1, L2, and L3 genes or pCR 2.1 (Invitrogen) for the T3D M1, M2, M3, S1, S2, S3, and S4 genes and the T1L S1 gene (Table S3). To generate pT7-L1T3D, pT7-L2T3D, pT7-L3T3D, pT7-M1T3D, pT7-M2T3D, pT7-M3T3D, pT7-S2T3D, pT7-S3T3D, and pT7-S4T3D, viral cDNA-containing fragments were subcloned into p3E5EGFP (Watanabe et al., 2004). Viral cDNAs fused at their native 5′ termini to the phage T7 RNA polymerase promoter were inserted into p3E5EGFP by partial or complete replacement of plasmid sequences encoding GFP and the Ebola virus leader and trailer, resulting in ligation of native 3′ termini to the HDV ribozyme sequence. To generate pBacT7-S1T3D and pBacT7-S1T1L, encoding the T3D S1 and T1L S1 genes, respectively, S1 cDNAs fused to the T7 promoter and a portion of the HDV ribozyme were first cloned into the BseRI site of p3E5EGFP, and fragments containing the S1 gene flanked 5′ by the T7 promoter and 3′ by the HDV ribozyme and T7 terminator sequences were subcloned into the XbaI site of pBacPAK8 (Clontech). pBacT7-S1T3D and pT7-S4T3D were used as templates to generate mutant constructs pBacT7-S1T3DT249I and pT7-S4T3DY354H, respectively, by introduction of specific nucleotide substitutions using the QuickChange site-directed mutagenesis kit (Stratagene) (Table S4). To generate pT7-S4GFP, S4 nucleotide sequences 150–768 within pT7-S4T3D were replaced with the GFP ORF. Nucleotide sequences of recombinant plasmids were confirmed by DNA sequencing. Detailed description of cloning strategies is provided in the Supplemental Data.

Plasmid Transfection and Recovery of Recombinant Virus

Monolayers of L cells at approximately 90% confluence (3×10^6 cells) in 60 mm dishes (Costar) were infected with rDIs-T7pol at an MOI of ~0.5 $TCID_{50}$. At 1 hr postinfection, cells were cotransfected with ten plasmid constructs representing the cloned T3D genome—pT7-L1T3D (2 μg), pT7-L2T3D (2 μg), pT7-L3T3D (2 μg), pT7-M1T3D (1.75 μg), pT7-M2T3D (1.75 μg), pT7-M3T3D (1.75 μg), pBacT7-S1T3D (2 μg), pT7-S2T3D (1.5 μg), pT7-S3T3D (1.5 μg), and pT7-S4T3D (1.5 μg)—using 3 μl of TransIT-LT1 transfection reagent (Mirus) per microgram of plasmid DNA. Following 0–5 days of incubation, recombinant virus was isolated from transfected cells by plaque purification on monolayers of L cells (Virgin et al., 1988). Electrophoretic analysis of viral dsRNA was performed as described (Wilson et al., 1996). Confirmation of mutations in the S1, S4, and L1 genes of recombinant viruses was performed using the Onestep RT-PCR kit (Qiagen), gene-specific primer sets, and viral dsRNA extracted from purified virions as template. PCR products were analyzed following electrophoresis in Tris-borate-EDTA agarose gels or purified and subjected directly to sequence analysis.

Infectious Center and Viral Yield Assays

L cells were cotransfected with ten plasmids corresponding to the T3D genome as described. For infectious center assays, transfected cells were released from plates by trypsin treatment at various intervals posttransfection, washed, counted, diluted, and applied directly to monolayers of untreated L cells (Dermody et al., 1995), which were processed for plaque assay (Virgin et al., 1988). For viral yield assays, transfected L cells were lysed by freezing and thawing, and viral titers in cell lysates were determined by plaque assay (Virgin et al., 1988).

Immunofluorescence Detection of Reovirus Infection

Parental L cells or L cell transfectants selected for stable expression of σ3 protein (5×10^4) were plated on glass coverslips in 24-well plates (Costar) and infected at an MOI of 10,000 (T3D and rsT3D) or 20,000 (rsT3D/S4-GFP) particles per cell. Following incubation at 37°C for various intervals, cells were fixed and stained for μNS and σ3 proteins as described (Maginnis et al., 2006). Images were acquired using a Zeiss LSM 510 META inverted confocal system (Carl Zeiss) with a Zeiss inverted Axiovert 200M microscope and a Plan-APOCHROMAT 63×/1.4 NA oil immersion DIC objective. Images were processed using MetaMorph image analysis software (Molecular Devices).

Infectivity of Recombinant Viruses

Monolayers of L or L-σ3 cells (2.5 to 5×10^5) in 24-well plates or suspension cultures of MEL cells (5×10^5 cells/ml) were infected with virus at an MOI of 1–2 PFU/cell. After 1 hr adsorption at room temperature, the inoculum was removed, cells were washed twice with PBS, and fresh medium was added. Cells were incubated at 37°C for various intervals, and viral titers in cell lysates were determined by plaque assay (Virgin et al., 1988).

Analysis of Viral Capsid Proteins after Protease Treatment

Purified virions at a concentration of either 2×10^{12} particles/ml (trypsin) or 9×10^{12} particles/ml (chymotrypsin) were digested with either 50 μg/ml of N α-p-tosyl-L-sulfonyl phenylalanyl chloromethyl ketone-treated bovine trypsin (Sigma) or 200 μg/ml of *Nα-p*-tosyl-L-lysine chloromethyl ketone-treated bovine α-chymotrypsin (Sigma) for various intervals at either 25°C (trypsin) or 8°C (chymotrypsin) as described (Nibert et al., 1995; Wetzel et al., 1997). Protease digestion was stopped by adding either 0.5 mg/ml soybean trypsin inhibitor (trypsin) (Sigma) or 5 mM phenylmethyl-sulfonyl fluoride (chymotrypsin) (Sigma) to the treatment mixtures and cooling at 0°C. Viral proteins were resolved by SDS-PAGE and visualized by either autoradiography (Nibert et al., 1995) or staining with Coomassie blue (Wetzel et al., 1997).

Infection of Mice

Newborn C57/BL6 mice weighing 2.0–2.5 grams (2–4 days old) were inoculated perorally or intracranially with 10^3 or 10^2 PFU, respectively, of purified reovirus virions diluted in PBS. PO inoculations (50 μl) were delivered intragastrically as described (Rubin and Fields, 1980). IC inoculations (5 μl) were delivered to the left cerebral hemisphere using a Hamilton syringe and 30-gauge needle (Tyler et al., 1985). At various intervals following inoculation, mice were euthanized, and organs were harvested into 1 ml of PBS and homogenized by freezing, thawing, and sonication. Viral titers in organ homogenates were determined by plaque assay (Virgin et al., 1988). Animal husbandry and experimental procedures were performed in accordance with Public Health Service policy and approved by the Vanderbilt University School of Medicine Institutional Animal Care and Use Committee.

Growth of Virus in Cells Treated with E64

Monolayers of L cells (2×10^5) in 24-well plates were preincubated in medium supplemented with 0–200 μM E64 (Sigma) for 4 hr. The medium was removed, and cells were adsorbed with virus at an MOI of 2 PFU/cell. After incubation at 4°C for 1 hr, the inoculum was removed, cells were washed with PBS, and 1 ml of fresh medium supplemented with 0 to 200 μM E64 was added. Cells were incubated at 37°C for 24 hr and frozen and thawed twice. Viral titers in cell lysates were determined by plaque assay (Virgin et al., 1988).

Generation of σ3-Expressing Cells

L cells stably expressing σ3 protein (L-σ3 cells) were selected by transfection of cells with pCXN-S4T3D, which encodes the entire T3D σ3 ORF, and incubation in the presence of 1 mg/ml of geneticin (Invitrogen).

Supplemental Data

The Supplemental Data include Supplemental Experimental Procedures, four supplemental tables, and one supplemental figure and can be found with this article online at http://www.cellhostandmicrobe.com/cgi/content/full/1/2/147/DC1/.

ACKNOWLEDGMENTS

We thank Erik Barton, Craig Forrest, and Tim Peters for review of the manuscript and Dirk Reiter, Johannes Schilling, and Thilo Stehle for assistance in preparation of the figures. We thank Yoshihiro Kawaoka for plasmid p3E5EGFP and Tatsuo Miyamura and Koji Ishii for vaccinia virus rDIs-T7pol. This research was supported by a fellowship from the Naito Foundation (T.K.), Public Health Service awards T32 GM07347 (A.A.R.A. and E.A.E.), T32 CA09385 (K.W.B.), T32 GM08554 (K.M.G.), T32 AI49824 and F32 AI71440 (G.H.H.), T32 AI07611 (E.M.J.), T32 AI07281 (M.S.M.), K08 AI62862 (J.D.C.), R01 AI32539, and R37 AI38296, and the Elizabeth B. Lamb Center for Pediatric Research. Additional support was provided by Public Health Service awards P30 CA68485 for the Vanderbilt-Ingram Cancer Center and P60 DK20593 for the Vanderbilt Diabetes Research and Training Center.

Received: December 29, 2006
Revised: February 16, 2007
Accepted: March 19, 2007
Published: April 18, 2007

REFERENCES

Baer, G.S., and Dermody, T.S. (1997). Mutations in reovirus outercapsid protein σ3 selected during persistent infections of L cells confer resistance to protease inhibitor E64. J. Virol. *71*, 4921–4928.

Barton, E.S., Connolly, J.L., Forrest, J.C., Chappell, J.D., and Dermody, T.S. (2001a). Utilization of sialic acid as a coreceptor enhances reovirus attachment by multistep adhesion strengthening. J. Biol. Chem. *276*, 2200–2211.

Barton, E.S., Forrest, J.C., Connolly, J.L., Chappell, J.D., Liu, Y., Schnell, F., Nusrat, A., Parkos, C.A., and Dermody, T.S. (2001b). Junction adhesion molecule is a receptor for reovirus. Cell *104*, 441–451.

Becker, M.M., Peters, T.R., and Dermody, T.S. (2003). Reovirus σNS and μNS proteins form cytoplasmic inclusion structures in the absence of viral infection. J. Virol. *77*, 5948–5963.

Blaney, J.E., Jr., Durbin, A.P., Murphy, B.R., and Whitehead, S.S. (2006). Development of a live attenuated dengue virus vaccine using reverse genetics. Viral Immunol. *19*, 10–32.

Bodkin, D.K., and Fields, B.N. (1989). Growth and survival of reovirus in intestinal tissue: Role of the L2 and S1 genes. J. Virol. *63*, 1188–1193.

Bodkin, D.K., Nibert, M.L., and Fields, B.N. (1989). Proteolytic digestion of reovirus in the intestinal lumens of neonatal mice. J. Virol. *63*, 4676–4681.

Borsa, J., Sargent, M.D., Lievaart, P.A., and Copps, T.P. (1981). Reovirus: Evidence for a second step in the intracellular uncoating and transcriptase activation process. Virology *111*, 191–200.

Broering, T.J., Parker, J.S., Joyce, P.L., Kim, J., and Nibert, M.L. (2002). Mammalian reovirus nonstructural protein μNS forms large inclusions and colocalizes with reovirus microtubule-associated protein μ2 in transfected cells. J. Virol. *76*, 8285–8297.

Campbell, J.A., Shelling, P., Wetzel, J.D., Johnson, E.M., Wilson, G.A.R., Forrest, J.C., Aurrand-Lions, M., Imhof, B., Stehle, T., and Dermody, T.S. (2005). Junctional adhesion molecule-A serves as a receptor for prototype and field-isolate strains of mammalian reovirus. J. Virol. *79*, 7967–7978.

Chandran, K., and Nibert, M.L. (2003). Animal cell invasion by a large nonenveloped virus: Reovirus delivers the goods. Trends Microbiol. *11*, 374–382.

Chandran, K., Zhang, X., Olson, N.H., Walker, S.B., Chappell, J.D., Dermody, T.S., Baker, T.S., and Nibert, M.L. (2001). Complete in vitro assembly of the reovirus outer capsid produces highly infectious particles suitable for genetic studies of the receptor-binding protein. J. Virol. *75*, 5335–5342.

Chandran, K., Farsetta, D.L., and Nibert, M.L. (2002). Strategy for nonenveloped virus entry: A hydrophobic conformer of the reovirus membrane penetration protein μ1 mediates membrane disruption. J. Virol. *76*, 9920–9933.

Chappell, J.D., Gunn, V.L., Wetzel, J.D., Baer, G.S., and Dermody, T.S. (1997). Mutations in type 3 reovirus that determine binding to sialic acid are contained in the fibrous tail domain of viral attachment protein σ1. J. Virol. *71*, 1834–1841.

Chappell, J.D., Barton, E.S., Smith, T.H., Baer, G.S., Duong, D.T., Nibert, M.L., and Dermody, T.S. (1998). Cleavage susceptibility of reovirus attachment protein σ1 during proteolytic disassembly of virions is determined by a sequence polymorphism in the σ1 neck. J. Virol. *72*, 8205–8213.

Chappell, J.D., Duong, J.L., Wright, B.W., and Dermody, T.S. (2000). Identification of carbohydrate-binding domains in the attachment proteins of type 1 and type 3 reoviruses. J. Virol. *74*, 8472–8479.

Chappell, J.D., Prota, A., Dermody, T.S., and Stehle, T. (2002). Crystal structure of reovirus attachment protein σ1 reveals evolutionary relationship to adenovirus fiber. EMBO J. *21*, 1–11.

Clark, K.M., Wetzel, J.D., Bayley, J., Ebert, D.H., McAbee, S.A., Stoneman, E.K., Baer, G.S., Zhu, Y., Wilson, G.J., Prasad, B.V.V., and Dermody, T.S. (2006). Reovirus variants selected for resistance to ammonium chloride have mutations in viral outer-capsid protein σ3. J. Virol. *80*, 671–681.

Coffey, M.C., Strong, J.E., Forsyth, P.A., and Lee, P.W. (1998). Reovirus therapy of tumors with activated Ras pathway. Science *282*, 1332–1334.

Dermody, T.S., Chappell, J.D., Hofler, J.G., Kramp, W., and Tyler, K.L. (1995). Eradication of persistent reovirus infection from a B-cell hybridoma. Virology *212*, 272–276.

Ebert, D.H., Wetzel, J.D., Brumbaugh, D.E., Chance, S.R., Stobie, L.E., Baer, G.S., and Dermody, T.S. (2001). Adaptation of reovirus to growth in the presence of protease inhibitor E64 segregates with a mutation in the carboxy terminus of viral outer-capsid protein σ3. J. Virol. *75*, 3197–3206.

Ebert, D.H., Deussing, J., Peters, C., and Dermody, T.S. (2002). Cathepsin L and cathepsin B mediate reovirus disassembly in murine fibroblast cells. J. Biol. Chem. *277*, 24609–24617.

Ehrlich, M., Boll, W., Van Oijen, A., Hariharan, R., Chandran, K., Nibert, M.L., and Kirchhausen, T. (2004). Endocytosis by random initiation and stabilization of clathrin-coated pits. Cell *118*, 591–605.

Fields, B.N. (1971). Temperature-sensitive mutants of reovirus type 3 features of genetic recombination. Virology *46*, 142–148.

Furlong, D.B., Nibert, M.L., and Fields, B.N. (1988). Sigma 1 protein of mammalian reoviruses extends from the surfaces of viral particles. J. Virol. *62*, 246–256.

Furuichi, Y., Morgan, M., Muthukrishnan, S., and Shatkin, A.J. (1975a). Reovirus messenger RNA contains a methylated blocked 5′-terminal structure M7G(5′)ppp(5′)GmpCp-. Proc. Natl. Acad. Sci. USA *72*, 362–366.

Furuichi, Y., Muthukrishnan, S., and Shatkin, A.J. (1975b). 5′-Terminal $M^7G(5')ppp(5')G^mp$ in vivo: Identification in reovirus genome RNA. Proc. Natl. Acad. Sci. USA *72*, 742–745.

Guglielmi, K.M., Johnson, E.M., Stehle, T., and Dermody, T.S. (2006). Attachment and cell entry of mammalian orthoreovirus. Curr. Top. Microbiol. Immunol. *309*, 1–38.

Horimoto, T., and Kawaoka, Y. (2006). Strategies for developing vaccines against H5N1 influenza A viruses. Trends Mol. Med. *12*, 506–514.

Ishii, K., Ueda, Y., Matsuo, K., Matsuura, Y., Kitamura, T., Kato, K., Izumi, Y., Someya, K., Ohsu, T., Honda, M., and Miyamura, T. (2002). Structural analysis of vaccinia virus DIs strain: Application as a new replication-deficient viral vector. Virology *302*, 433–444.

Jané-Valbuena, J., Breun, L.A., Schiff, L.A., and Nibert, M.L. (2002). Sites and determinants of early cleavages in the proteolytic processing pathway of reovirus surface protein σ3. J. Virol. *76*, 5184–5197.

Kapikian, A., Hoshino, Y., and Chanock, R. (2001). Rotaviruses. In Fields Virology, D.M. Knipe and P.M. Howley, eds. (Philadelphia: Lippincott-Raven), pp. 1787–1833.

Kobayashi, T., Chappell, J.D., Danthi, P., and Dermody, T.S. (2006). Gene-specific inhibition of reovirus replication by RNA interference. J. Virol. *80*, 9053–9063.

Komoto, S., Sasaki, J., and Taniguchi, K. (2006). Reverse genetics system for introduction of site-specific mutations into the double-stranded RNA genome of infectious rotavirus. Proc. Natl. Acad. Sci. USA *103*, 4646–4651.

Maginnis, M.S., Forrest, J.C., Kopecky-Bromberg, S.A., Dickeson, S.K., Santoro, S.A., Zutter, M.M., Nemerow, G.R., Bergelson, J.M., and Dermody, T.S. (2006). β1 integrin mediates internalization of mammalian reovirus. J. Virol. *80*, 2760–2770.

Martin-Padura, I., Lostaglio, S., Schneemann, M., Williams, L., Romano, M., Fruscella, P., Panzeri, C., Stoppacciaro, A., Ruco, L., Villa, A., et al. (1998). Junctional adhesion molecule, a novel member of the immunoglobulin superfamily that distributes at intercellular junctions and modulates monocyte transmigration. J. Cell Biol. *142*, 117–127.

Mbisa, J.L., Becker, M.M., Zou, S., Dermody, T.S., and Brown, E.G. (2000). Reovirus μ2 protein determines strain-specific differences in the rate of viral inclusion formation in L929 cells. Virology *272*, 16–26.

Miller, C.L., Broering, T.J., Parker, J.S., Arnold, M.M., and Nibert, M.L. (2003). Reovirus σNS protein localizes to inclusions through an association requiring the μNS amino terminus. J. Virol. *77*, 4566–4576.

Milligan, J.F., Groebe, D.R., Witherell, G.W., and Uhlenbeck, O.C. (1987). Oligoribonucleotide synthesis using T7 RNA polymerase and synthetic DNA templates. Nucleic Acids Res. *15*, 8783–8798.

Nibert, M.L., Chappell, J.D., and Dermody, T.S. (1995). Infectious subvirion particles of reovirus type 3 Dearing exhibit a loss in infectivity and contain a cleaved σ1 protein. J. Virol. *69*, 5057–5067.

Odegard, A.L., Chandran, K., Zhang, X., Parker, J.S., Baker, T.S., and Nibert, M.L. (2004). Putative autocleavage of outer capsid protein μ1, allowing release of myristoylated peptide μ1N during particle uncoating, is critical for cell entry by reovirus. J. Virol. *78*, 8732–8745.

O'Donnell, S.M., Hansberger, M.W., and Dermody, T.S. (2003). Viral and cellular determinants of apoptosis induced by mammalian reovirus. Int. Rev. Immunol. *22*, 477–503.

Olland, A.M., Jané-Valbuena, J., Schiff, L.A., Nibert, M.L., and Harrison, S.C. (2001). Structure of the reovirus outer capsid and dsRNA-binding protein σ3 at 1.8 Å resolution. EMBO J. *20*, 979–989.

Parker, J.S., Broering, T.J., Kim, J., Higgins, D.E., and Nibert, M.L. (2002). Reovirus core protein μ2 determines the filamentous morphology of viral inclusion bodies by interacting with and stabilizing microtubules. J. Virol. *76*, 4483–4496.

Riezebos-Brilman, A., de Mare, A., Bungener, L., Huckriede, A., Wilschut, J., and Daemen, T. (2006). Recombinant alphaviruses as vectors for anti-tumour and anti-microbial immunotherapy. J. Clin. Virol. *35*, 233–243.

Roner, M.R., and Joklik, W.K. (2001). Reovirus reverse genetics: Incorporation of the CAT gene into the reovirus genome. Proc. Natl. Acad. Sci. USA *98*, 8036–8041.

Roner, M.R., and Steele, B.G. (2007). Localizing the reovirus packaging signals using an engineered m1 and s2 ssRNA. Virology *358*, 89–97.

Roner, M.R., Nepliouev, I., Sherry, B., and Joklik, W.K. (1997). Construction and characterization of a reovirus double temperature-sensitive mutant. Proc. Natl. Acad. Sci. USA *94*, 6826–6830.

Rubin, D.H., and Fields, B.N. (1980). Molecular basis of reovirus virulence: Role of the M2 gene. J. Exp. Med. *152*, 853–868.

Rubin, D.H., Wetzel, J.D., Williams, W.V., Cohen, J.A., Dworkin, C., and Dermody, T.S. (1992). Binding of type 3 reovirus by a domain of the σ1 protein important for hemagglutination leads to infection of murine erythroleukemia cells. J. Clin. Invest. *90*, 2536–2542.

Silverstein, S.C., and Schur, P.H. (1970). Immunofluorescent localization of double-stranded RNA in reovirus-infected cells. Virology *41*, 564–566.

Tyler, K.L. (2001). Mammalian reoviruses. In Fields Virology, D.M. Knipe and P.M. Howley, eds. (Philadelphia: Lippincott Williams & Wilkins), pp. 1729–1745.

Tyler, K.L., Bronson, R.T., Byers, K.B., and Fields, B.N. (1985). Molecular basis of viral neurotropism: Experimental reovirus infection. Neurology *35*, 88–92.

Tyler, K.L., Barton, E.S., Ibach, M.L., Robinson, C., Valyi-Nagy, T., Campbell, J.A., Clarke, P., O'Donnell, S.M., Wetzel, J.D., and Dermody, T.S. (2004). Isolation and molecular characterization of a novel type 3 reovirus from a child with meningitis. J. Infect. Dis. *189*, 1664–1675.

Virgin, H.W., IV, Bassel-Duby, R., Fields, B.N., and Tyler, K.L. (1988). Antibody protects against lethal infection with the neurally spreading reovirus type 3 (Dearing). J. Virol. *62*, 4594–4604.

Watanabe, S., Watanabe, T., Noda, T., Takada, A., Feldmann, H., Jasenosky, L.D., and Kawaoka, Y. (2004). Production of novel Ebola virus-like particles from cDNAs: An alternative to Ebola virus generation by reverse genetics. J. Virol. *78*, 999–1005.

Wetzel, J.D., Wilson, G.J., Baer, G.S., Dunnigan, L.R., Wright, J.P., Tang, D.S.H., and Dermody, T.S. (1997). Reovirus variants selected during persistent infections of L cells contain mutations in the viral S1 and S4 genes and are altered in viral disassembly. J. Virol. *71*, 1362–1369.

Wiener, J.R., and Joklik, W.K. (1989). The sequences of the reovirus serotype *1*, 2, and 3 L1 genome segments and analysis of the mode of divergence of the reovirus serotypes. Virology *169*, 194–203.

Wilson, G.J., Wetzel, J.D., Puryear, W., Bassel-Duby, R., and Dermody, T.S. (1996). Persistent reovirus infections of L cells select mutations in viral attachment protein σ1 that alter oligomer stability. J. Virol. *70*, 6598–6606.

Wilson, G.J., Nason, E.L., Hardy, C.S., Ebert, D.H., Wetzel, J.D., Prasad, B.V.V., and Dermody, T.S. (2002). A single mutation in the carboxy terminus of reovirus outer-capsid protein σ3 confers enhanced kinetics of σ3 proteolysis, resistance to inhibitors of viral disassembly, and alterations in σ3 structure. J. Virol. *76*, 9832–9843.

Accession Numbers

GenBank accession numbers for cDNAs corresponding to the T3D L1, L2, L3, M1, M2, M3, S1, S2, S3, and S4 genes and the T1L S1 gene are provided in Table S3.

REFERENCES

1. **Arrate, M. P., J. M. Rodriguez, T. M. Tran, T. A. Brock, and S. A. Cunningham.** 2001. Cloning of human junctional adhesion molecule 3 (JAM3) and its identification as the JAM2 counter-receptor. The Journal of Biological Chemistry **276:**45826-45832.

2. **Aurrand-Lions, M., L. Duncan, C. Ballestrem, and B. A. Imhof.** 2001. JAM-2, a novel immunoglobulin superfamily molecule, expressed by endothelial and lymphatic cells. The Journal of Biological Chemistry **276:**2733-2741.

3. **Baer, G. S., and T. S. Dermody.** 1997. Mutations in reovirus outer-capsid protein σ3 selected during persistent infections of L cells confer resistance to protease inhibitor E64. Journal of Virology **71:**4921-4928.

4. **Baer, G. S., D. H. Ebert, C. J. Chung, A. H. Erickson, and T. S. Dermody.** 1999. Mutant cells selected during persistent reovirus infection do not express mature cathepsin L and do not support reovirus disassembly. Journal of Virology **73:**9532-9543.

5. **Barton, E. S., J. L. Connolly, J. C. Forrest, J. D. Chappell, and T. S. Dermody.** 2001. Utilization of sialic acid as a coreceptor enhances reovirus attachment by multistep adhesion strengthening. The Journal of Biological Chemistry **276:**2200-2211.

6. **Barton, E. S., J. C. Forrest, J. L. Connolly, J. D. Chappell, Y. Liu, F. Schnell, A. Nusrat, C. A. Parkos, and T. S. Dermody.** 2001. Junction adhesion molecule is a receptor for reovirus. Cell **104:**441-451.

7. **Barton, E. S., B. E. Youree, D. H. Ebert, J. C. Forrest, J. L. Connolly, T. Valyi-Nagy, K. Washington, J. D. Wetzel, and T. S. Dermody.** 2003. Utilization of sialic acid as a coreceptor is required for reovirus-induced biliary disease. The Journal of Clinical Investigation **111:**1823-1833.

8. **Bassel-Duby, R., D. R. Spriggs, K. L. Tyler, and B. N. Fields.** 1986. Identification of attenuating mutations on the reovirus type 3 S1 double-stranded RNA segment with a rapid sequencing technique. Journal of Virology **60:**64-67.

9. **Bazzoni, G., O. M. Martinez-Estrada, F. Mueller, P. Nelboeck, G. Schmid, T. Bartfai, E. Dejana, and M. Brockhaus.** 2000. Homophilic interaction of junctional adhesion molecule. The Journal of Biological Chemistry **275:**30970-30976.

10. **Bazzoni, G., O. M. Martinez-Estrada, F. Orsenigo, M. Cordenonsi, S. Citi, and E. Dejana.** 2000. Interaction of junctional adhesion molecule with the tight

junction components ZO-1, cingulin, and occludin. The Journal of Biological Chemistry **275:**20520-20526.

11. **Becker, M. M., M. I. Goral, P. R. Hazelton, G. S. Baer, S. E. Rodgers, E. G. Brown, K. M. Coombs, and T. S. Dermody.** 2001. Reovirus σNS protein is required for nucleation of viral assembly complexes and formation of viral inclusions. Journal of Virology **75:**1459-1475.

12. **Bergelson, J. M., J. A. Cunningham, G. Droguett, E. A. Kurt-Jones, A. Krithivas, J. S. Hong, M. S. Horwitz, R. L. Crowell, and R. W. Finberg.** 1997. Isolation of a common receptor for Coxsackie B viruses and adenoviruses 2 and 5. Science **275:**1320-1323.

13. **Bewley, M. C., K. Springer, Y. B. Zhang, P. Freimuth, and J. M. Flanagan.** 1999. Structural analysis of the mechanism of adenovirus binding to its human cellular receptor, CAR. Science **286:**1579-1583.

14. **Bhat, T. N.** 1988. Calculation of an OMIT map. Journal of Applied Crystallography **21:**279-281.

15. **Blanco, F., M. Ramírez-Alvarado, and L. Serrano.** 1998. Formation and stability of b-hairpin structures in polypeptides. Current Opinion in Structural Biology **8:**107-111.

16. **Blixt, O., S. Head, T. Mondala, C. Scanlan, M. E. Huflejt, R. Alvarez, M. C. Bryan, F. Fazio, D. Calarese, J. Stevens, N. Razi, D. J. Stevens, J. J. Skehel, I. van Die, D. R. Burton, I. A. Wilson, R. Cummings, N. Bovin, C. H. Wong, and J. C. Paulson.** 2004. Printed covalent glycan array for ligand profiling of diverse glycan binding proteins. Proceedings of the National Academy of Sciences USA **101:**17033-17038.

17. **Brünger, A. T.** 1992. Free *R* value: a novel statistical quantity for assessing the accuracy of crystal structures. Nature **355:**472-475.

18. **Brünger, A. T., P. D. Adams, G. M. Clore, W. L. DeLano, P. Gros, R. W. Grosse-Kunstleve, J. S. Jiang, J. Kuszewski, M. Nilges, N. S. Pannu, R. J. Read, L. M. Rice, T. Simonson, and G. L. Warren.** 1998. Crystallography & NMR system: A new software suite for macromolecular structure determination. Acta Crystallographica **D 54:**905-921.

19. **Bullough, P. A., F. M. Hughson, J. J. Skehel, and D. C. Wiley.** 1994. Structure of influenza haemagglutinin at the pH of membrane fusion. Nature **371:**37-43.

20. **Campbell, J. A., P. Shelling, J. D. Wetzel, E. M. Johnson, G. A. R. Wilson, J. C. Forrest, M. Aurrand-Lions, B. Imhof, T. Stehle, and T. S. Dermody.** 2005.

Junctional adhesion molecule-A serves as a receptor for prototype and field-isolate strains of mammalian reovirus. Journal of Virology **79:**7967-7978.

21. **Carson, M.** 1987. Ribbon models of macromolecules. Journal of Molecular Graphics and Modelling **5:**103-106.

22. **Cavalli, A., A. E. Prota, T. Stehle, T. S. Dermody, M. Recanatini, G. Folkers, and L. Scapozza.** 2004. A molecular dynamics study of reovirus attachment protein σ1 reveals conformational changes in σ1 structure. Biophysical Journal **86:**3423-3431.

23. **CCP4.** 1994. The CCP4 suite: programs for protein crystallography. Acta Crystallographica **D 50:**760-763.

24. **Cera, M. R., A. Del Prete, A. Vecchi, M. Corada, I. Martin-Padura, T. Motoike, P. Tonetti, G. Bazzoni, W. Vermi, F. Gentili, S. Bernasconi, T. N. Sato, A. Mantovani, and E. Dejana.** 2004. Increased DC trafficking to lymph nodes and contact hypersensitivity in junctional adhesion molecule-A-deficient mice. The Journal of Clinical Investigation **114:**729-738.

25. **Chandran, K., D. L. Farsetta, and M. L. Nibert.** 2002. Strategy for nonenveloped virus entry: a hydrophobic conformer of the reovirus membrane penetration protein μ1 mediates membrane disruption. Journal of Virology **76:**9920-9933.

26. **Chandran, K., J. S. Parker, M. Ehrlich, T. Kirchhausen, and M. L. Nibert.** 2003. The delta region of outer-capsid protein μ1 undergoes conformational change and release from reovirus particles during cell entry. Journal of Virology **77:**13361-13375.

27. **Chandran, K., X. Zhang, N. H. Olson, S. B. Walker, J. D. Chappell, T. S. Dermody, T. S. Baker, and M. L. Nibert.** 2001. Complete in vitro assembly of the reovirus outer capsid produces highly infectious particles suitable for genetic studies of the receptor-binding protein. Journal of Virology **75:**5335-5342.

28. **Chappell, J. D., J. L. Duong, B. W. Wright, and T. S. Dermody.** 2000. Identification of carbohydrate-binding domains in the attachment proteins of type 1 and type 3 reoviruses. Journal of Virology **74:**8472-8479.

29. **Chappell, J. D., V. L. Gunn, J. D. Wetzel, G. S. Baer, and T. S. Dermody.** 1997. Mutations in type 3 reovirus that determine binding to sialic acid are contained in the fibrous tail domain of viral attachment protein σ1. Journal of Virology **71:**1834-1841.

30. **Chappell, J. D., A. Prota, T. S. Dermody, and T. Stehle.** 2002. Crystal structure of reovirus attachment protein σ1 reveals evolutionary relationship to adenovirus fiber. EMBO Journal **21:**1-11.

31. **Chen, B., E. M. Vogan, H. Gong, J. J. Skehel, D. C. Wiley, and S. C. Harrison.** 2005. Structure of an unliganded simian immunodeficiency virus gp120 core. Nature **433:**834-841.

32. **Chen, J., S. A. Wharton, W. Weissenhorn, L. J. Calder, F. M. Hughson, J. J. Skehel, and D. C. Wiley.** 1995. A soluble domain of the membrane-anchoring chain of influenza virus hemagglutinin (HA2) folds in Escherichia coli into the low-pH-induced conformation. Proceedings of the National Academy of Sciences USA **92:**12205-12209.

33. **Chiu, C. Y., P. Mathias, G. R. Nemerow, and P. L. Stewart.** 1999. Structure of adenovirus complexed with its internalization receptor, avb5 integrin. Journal of Virology **73:**6759-6768.

34. **Corada, M., S. Chimenti, M. R. Cera, M. Vinci, M. Salio, F. Fiordaliso, N. De Angelis, A. Villa, M. Bossi, L. I. Staszewsky, A. Vecchi, D. Parazzoli, T. Motoike, R. Latini, and E. Dejana.** 2005. Junctional adhesion molecule-A-deficient polymorphonuclear cells show reduced diapedesis in peritonitis and heart ischemia-reperfusion injury. Proceedings of the National Academy of Sciences USA **102:**10634-10639.

35. **Cunningham, S. A., M. P. Arrate, J. M. Rodriguez, R. J. Bjercke, P. Vanderslice, A. P. Morris, and T. A. Brock.** 2000. A novel protein with homology to the junctional adhesion molecule. Characterization of leukocyte interactions. The Journal of Biological Chemistry **275:**34750-34756.

36. **Dalgleish, A. G., P. C. L. Beverley, P. R. Clapham, D. H. Crawford, M. F. Greaves, and R. A. Weiss.** 1984. The CD4 (T4) antigen is an essential component of the receptor for the AIDS retrovirus. Nature **312:**763-767.

37. **Del Maschio, A., A. De Luigi, I. Martin-Padura, M. Brockhaus, T. Bartfai, P. Fruscella, L. Adorini, G. Martino, R. Furlan, M. G. De Simoni, and E. Dejana.** 1999. Leukocyte recruitment in the cerebrospinal fluid of mice with experimental meningitis is inhibited by an antibody to junctional adhesion molecule (JAM). Journal of Experimental Medicine **190:**1351-1356.

38. **DeLano, W. L.** 2002. The PyMOL Molecular Graphics System. DeLano Scientific, San Carlos, USA.

39. **Dermody, T. S., M. L. Nibert, R. Bassel-Duby, and B. N. Fields.** 1990. A sigma 1 region important for hemagglutination by serotype 3 reovirus strains. Journal of Virology **64:**5173-5176.

40. **Dermody, T. S., M. L. Nibert, R. Bassel-Duby, and B. N. Fields.** 1990. Sequence diversity in S1 genes and S1 translation products of 11 serotype 3 reovirus strains. Journal of Virology **64:**4842-4850.

41. **Dichter, M. A., and H. L. Weiner.** 1984. Infection of neuronal cell cultures with reovirus mimics in vitro patterns of neurotropism. Annals of Neurology **16:**603-610.

42. **Dryden, K. A., D. L. Farsetta, G. Wang, J. M. Keegan, B. N. Fields, T. S. Baker, and M. L. Nibert.** 1998. Internal structures containing transcriptase-related proteins in top component particles of mammalian orthoreovirus. Virology **245:**33-46.

43. **Dryden, K. A., G. Wang, M. Yeager, M. L. Nibert, K. M. Coombs, D. B. Furlong, B. N. Fields, and T. S. Baker.** 1993. Early steps in reovirus infection are associated with dramatic changes in supramolecular structure and protein conformation: analysis of virions and subviral particles by cryoelectron microscopy and image reconstruction. The Journal of Cell Biology **122:**1023-1041.

44. **Duncan, R., D. Horne, J. E. Strong, G. Leone, R. T. Pon, M. C. Yeung, and P. W. K. Lee.** 1991. Conformational and functional analysis of the C-terminal globular head of the reovirus cell attachment protein. Virology **182:**810-819.

45. **Duncan, R., and P. W. K. Lee.** 1994. Localization of two protease-sensitive regions separating distinct domains in the reovirus cell-attachment protein sigma 1. Virology **203:**149-152.

46. **Ebert, D. H., S. A. Kopecky-Bromberg, and T. S. Dermody.** 2004. Cathepsin B is inhibited in mutant cells selected during persistent reovirus infection. The Journal of Biological Chemistry **279:**3837-3851.

47. **Ebnet, K., C. U. Schulz, M. K. Meyer Zu Brickwedde, G. G. Pendl, and D. Vestweber.** 2000. Junctional adhesion molecule interacts with the PDZ domain-containing proteins AF-6 and ZO-1. The Journal of Biological Chemistry **275:**27979-27988.

48. **Ebnet, K., A. Suzuki, Y. Horikoshi, T. Hirose, M. K. Meyer Zu Brickwedde, S. Ohno, and D. Vestweber.** 2001. The cell polarity protein ASIP/PAR-3 directly associates with junctional adhesion molecule (JAM). EMBO Journal **20:**3738-3748.

49. **Ebnet, K., A. Suzuki, S. Ohno, and D. Vestweber.** 2004. Junctional adhesion molecules (JAMs): more molecules with dual functions? Journal of Cell Science **117:**19-29.

50. **Ehrlich, M., W. Boll, A. Van Oijen, R. Hariharan, K. Chandran, M. L. Nibert, and T. Kirchhausen.** 2004. Endocytosis by random initiation and stabilization of clathrin-coated pits. Cell **118:**591-605.

51. **Emsley, P., and K. Cowtan.** 2004. Coot: model building tools for molecular graphics. Acta Crystallographica **D 60:**2126-2132.

52. **Forrest, J. C., J. A. Campbell, P. Schelling, T. Stehle, and T. S. Dermody.** 2003. Structure-function analysis of reovirus binding to junctional adhesion molecule 1. Implications for the mechanism of reovirus attachment. The Journal of Biological Chemistry **278:**48434-48444.

53. **Forsyth, P., G. Roldan, D. George, C. Wallace, C. A. Palmer, D. Morris, G. Cairncross, M. V. Matthews, J. Markert, Y. Gillespie, M. Coffey, B. Thompson, and M. Hamilton.** 2008. A phase I trial of intratumoral administration of reovirus in patients with histologically confirmed recurrent malignant gliomas. Molecular Therapy.

54. **Fraser, R. D. B., D. B. Furlong, B. L. Trus, M. L. Nibert, B. N. Fields, and A. C. Steven.** 1990. Molecular structure of the cell-attachment protein of reovirus: correlation of computer-processed electron micrographs with sequence-based predictions. Journal of Virology **64:**2990-3000.

55. **Furlong, D. B., M. L. Nibert, and B. N. Fields.** 1988. Sigma 1 protein of mammalian reoviruses extends from the surfaces of viral particles. Journal of Virology **62:**246-256.

56. **Gamblin, S. J., D. W. Rodgers, and T. Stehle.** 1996. Improving electron density maps calculated from weak or anisotropic data, p. 160-163, Proceedings of the CCP4 Study Weekend. Daresbury Laboratory, Daresbury, UK.

57. **Gentsch, J. R., and A. F. Pacitti.** 1987. Differential interaction of reovirus type 3 with sialylated receptor components on animal cells. Virology **161:**245-248.

58. **Gentsch, J. R., and A. F. Pacitti.** 1985. Effect of neuraminidase treatment of cells and effect of soluble glycoproteins on type 3 reovirus attachment to murine L cells. Journal of Virology **56:**356-364.

59. **Geraghty, R. J., C. Krummenacher, G. H. Cohen, R. J. Eisenberg, and P. G. Spear.** 1998. Entry of alphaherpesviruses mediated by poliovirus receptor-related protein 1 and poliovirus receptor. Science **280:**1618-1620.

60. **Greber, U. F., M. Willetts, P. Webster, and A. Helenius.** 1993. Stepwise dismantling of adenovirus 2 during entry into cells. Cell **75:**477-486.

61. **Greve, J. M., G. Davis, A. M. Meyer, C. P. Forte, S. C. Yost, C. W. Marlor, M. E. Kamarck, and A. McClelland.** 1989. The major human rhinovirus receptor is ICAM-1. Cell **56:**839-847.

62. **Gu, W., A. Ogose, H. Kawashima, M. Ito, T. Ito, A. Matsuba, H. Kitahara, T. Hotta, K. Tokunaga, H. Hatano, T. Morita, S. Urakawa, T. Yoshizawa, R. Kuwano, and N. Endo.** 2004. High-level expression of the coxsackievirus and adenovirus receptor messenger RNA in osteosarcoma, Ewing's sarcoma, and benign neurogenic tumors among musculoskeletal tumors. Clinical Cancer Research **10:**3831-3838.

63. **Guardado, C. P., G. C. Fox, X. L. Hermo Parrado, A. L. Llamas-Saiz, C. Costas, J. Martinez-Costas, J. Benavente, and M. J. van Raaij.** 2005. Structure of the carboxy-terminal receptor-binding domain of avian reovirus fibre sigmaC. Journal of Molecular Biology **354:**137-149.

64. **Guglielmi, K. M., E. M. Johnson, T. Stehle, and T. S. Dermody.** 2006. Attachment and cell entry of mammalian orthoreovirus. Current Topics in Microbiology and Immunology **309:**1-38.

65. **Guglielmi, K. M., E. Kirchner, G. H. Holm, T. Stehle, and T. S. Dermody.** 2007. Reovirus binding determinants in junctional adhesion molecule-A. The Journal of Biological Chemistry **282:**17930-17940.

66. **Hamazaki, Y., M. Itoh, H. Sasaki, M. Furuse, and S. Tsukita.** 2002. Multi-PDZ domain protein 1 (MUPP1) is concentrated at tight junctions through its possible interaction with claudin-1 and junctional adhesion molecule. The Journal of Biological Chemistry **277:**455-461.

67. **Helander, A., K. J. Silvey, N. J. Mantis, A. B. Hutchings, K. Chandran, W. T. Lucas, M. L. Nibert, and M. R. Neutra.** 2003. The viral σ1 protein and glycoconjugates containing α2-3-linked sialic acid are involved in type 1 reovirus adherence to M cell apical surfaces. Journal of Virology **77:**7964-7977.

68. **Hsu, K. H., K. Lonberg-Holm, B. Alstein, and R. L. Crowell.** 1988. A monoclonal antibody specific for the cellular receptor for the group B coxsackieviruses. Journal of Virology **62:**1647-52.

69. **Ishii, K., Y. Ueda, K. Matsuo, Y. Matsuura, T. Kitamura, K. Kato, Y. Izumi, K. Someya, T. Ohsu, M. Honda, and T. Miyamura.** 2002. Structural analysis of vaccinia virus DIs strain: application as a new replication-deficient viral vector. Virology **302:**433-444.

70. **Itoh, M., H. Sasaki, M. Furuse, H. Ozaki, T. Kita, and S. Tsukita.** 2001. Junctional adhesion molecule (JAM) binds to PAR-3: a possible mechanism for

the recruitment of PAR-3 to tight junctions. The Journal of Cell Biology **154:**491-497.

71. **Janin, J., S. Miller, and C. Chothia.** 1988. Surface, subunit interfaces and interior of oligomeric proteins. Journal of Molecular Biology **204:**155-164.

72. **Jones, S., and J. M. Thornton.** 1996. Principles of protein-protein interactions. Proceedings of the National Academy of Sciences USA **93:**13-20.

73. **Jones, T. A., J. Y. Zhou, S. W. Cowan, and M. Kjeldgaard.** 1991. Improved methods for building protein models in electron density maps and the location of errors in these models. Acta Crystallographica **A 47:**110-119.

74. **Karlsson, R., and A. Falt.** 1997. Experimental design for kinetic analysis of protein-protein interactions with surface plasmon resonance biosensors. Journal of Immunological Methods **200:**121-133.

75. **Kawashima, H., A. Ogose, T. Yoshizawa, R. Kuwano, Y. Hotta, T. Hotta, H. Hatano, and N. Endo.** 2003. Expression of the coxsackievirus and adenovirus receptor in musculoskeletal tumors and mesenchymal tissues: efficacy of adenoviral gene therapy for osteosarcoma. Cancer Science **94:**70-75.

76. **Kaye, K. M., D. R. Spriggs, R. Bassel-Duby, B. N. Fields, and K. L. Tyler.** 1986. Genetic basis for altered pathogenesis of an immune-selected antigenic variant of reovirus type 3 Dearing. Journal of Virology **59:**90-97.

77. **Kleywegt, G. J., and T. A. Jones.** 1994. Halloween - masks and bones, p. 59-66. *In* S. Bailey, R. Hubbard, and D. Waller (ed.), From first map to final model. SERC Daresbury Laboratory, Warrington (UK).

78. **Kobayashi, T., A. A. R. Antar, K. W. Boehme, P. Danthi, E. A. Eby, K. M. Guglielmi, G. H. Holm, E. M. Johnson, M. S. Maginnis, S. Naik, W. B. Skelton, J. D. Wetzel, G. J. Wilson, J. D. Chappell, and T. S. Dermody.** 2007. A plasmid-based reverse genetics system for animal double-stranded RNA viruses. Cell Host and Microbe **1:**147-157.

79. **Kostrewa, D., M. Brockhaus, A. D'Arcy, G. E. Dale, P. Nelboeck, G. Schmid, F. Mueller, G. Bazzoni, E. Dejana, T. Bartfai, F. K. Winkler, and M. Hennig.** 2001. X-ray structure of junctional adhesion molecule: structural basis for homophilic adhesion via a novel dimerization motif. EMBO Journal **20:**4391-4398.

80. **Kundin, W. D., C. Liu, and J. Gigstad.** 1966. Reovirus infection in suckling mice: immunofluorescent and infectivity studies. The Journal of Immunology **97:**393-401.

81. **Kwong, P. D., R. Wyatt, J. Robinson, R. W. Sweet, J. Sodroski, and W. A. Hendrickson.** 1998. Structure of an HIV gp120 envelope glycoprotein in complex with the CD4 receptor and a neutralizing antibody. Nature **393:**648-659.

82. **Landau, N. R., M. Warton, and D. R. Littman.** 1988. The envelope glycoprotein of the human immunodeficiency virus binds to the immunoglobulin-like domain of CD4. Nature **334:**159-162.

83. **Laskowski, R. A., M. W. MacArthur, D. S. Moss, and J. M. Thornton.** 1993. PROCHECK: A program to check the stereochemical quality of protein structures. Journal of Applied Crystallography **26:**283-291.

84. **Laukoetter, M. G., P. Nava, W. Y. Lee, E. A. Severson, C. T. Capaldo, B. A. Babbin, I. R. Williams, M. Koval, E. Peatman, J. A. Campbell, T. S. Dermody, A. Nusrat, and C. A. Parkos.** 2007. JAM-A regulates permeability and inflammation in the intestine in vivo. The Journal of Experimental Medicine **204:**3067-3076.

85. **Lechner, F., U. Sahrbacher, T. Suter, K. Frei, M. Brockhaus, U. Koedel, and A. Fontana.** 2000. Antibodies to the junctional adhesion molecule cause disruption of endothelial cells and do not prevent leukocyte influx into the meninges after viral or bacterial infection. The Journal of Infectious Diseases **182:**978-982.

86. **Lee, P. W. K., E. C. Hayes, and W. K. Joklik.** 1981. Protein σ1 is the reovirus cell attachment protein. Virology **108:**156-163.

87. **Leone, G., R. Duncan, D. C. Mah, A. Price, L. W. Cashdollar, and P. W. K. Lee.** 1991. The animo-terminal heptad repeat region of reovirus cell attachment protein σ1 is responsible for σ1 oligomer stability and possesses intrinsic oligomerization function. Virology **182:**336-345.

88. **Lerner, A. M., J. D. Cherry, and M. Finland.** 1963. Haemagglutination with reoviruses. Virology **19:**58-65.

89. **Lerner, M. G., and H. A. Carlson.** 2006. APBS plugin for PyMOL.

90. **Liang, T. W., H. H. Chiu, A. Gurney, A. Sidle, D. B. Tumas, P. Schow, J. Foster, T. Klassen, K. Dennis, R. A. DeMarco, T. Pham, G. Frantz, and S. Fong.** 2002. Vascular endothelial-junctional adhesion molecule (VE-JAM)/JAM 2 interacts with T, NK, and dendritic cells through JAM 3. Journal of Immunology **168:**1618-26.

91. **Liemann, S., K. Chandran, T. S. Baker, M. L. Nibert, and S. C. Harrison.** 2002. Structure of the reovirus membrane-penetration protein, μ1, in a complex with its protector protein, σ3. Cell **108:**283-295.

92. **Liu, T. C., and D. Kirn.** 2007. Systemic efficacy with oncolytic virus therapeutics: clinical proof-of-concept and future directions. Cancer Research **67:**429-432.

93. **Liu, Y., A. Nusrat, F. J. Schnell, T. A. Reaves, S. Walsh, M. Ponchet, and C. A. Parkos.** 2000. Human junction adhesion molecule regulates tight junction resealing in epithelia. Journal of Cell Science **113:**2363-2374.

94. **Maddon, P. J., A. G. Dalgleish, J. S. McDougal, P. R. Clapham, R. A. Weiss, and R. Axel.** 1986. The T4 gene encodes the AIDS virus receptor and is expressed in the immune system and the brain. Cell **47:**333-348.

95. **Maginnis, M. S., J. C. Forrest, S. A. Kopecky-Bromberg, S. K. Dickeson, S. A. Santoro, M. M. Zutter, G. R. Nemerow, J. M. Bergelson, and T. S. Dermody.** 2006. β1 integrin mediates internalization of mammalian reovirus. Journal of Virology **80:**2760-2770.

96. **Makino, A., M. Shimojima, T. Miyazawa, K. Kato, Y. Tohya, and H. Akashi.** 2006. Junctional adhesion molecule 1 is a functional receptor for feline calicivirus. Journal of Virology **80:**4482-4490.

97. **Mann, M. A., D. M. Knipe, G. D. Fischbach, and B. N. Fields.** 2002. Type 3 reovirus neuroinvasion after intramuscular inoculation: direct invasion of nerve terminals and age-dependent pathogenesis. Virology **303:**222-231.

98. **Martin-Padura, I., S. Lostaglio, M. Schneemann, L. Williams, M. Romano, P. Fruscella, C. Panzeri, A. Stoppacciaro, L. Ruco, A. Villa, D. Simmons, and E. Dejana.** 1998. Junctional adhesion molecule, a novel member of the immunoglobulin superfamily that distributes at intercellular junctions and modulates monocyte transmigration. The Journal of Cell Biology **142:**117-127.

99. **Matthews, B. W.** 1968. Solvent content of protein crystals. Journal of Molecular Biology **33:**491-497.

100. **Mercier, G. T., J. A. Campbell, J. D. Chappell, T. Stehle, T. S. Dermody, and M. A. Barry.** 2004. A chimeric adenovirus vector encoding reovirus attachment protein σ1 targets cells expressing junctional adhesion molecule 1. Proceedings of the National Academy of Sciences USA **101:**6188-6193.

101. **Merckel, M. C., J. T. Huiskonen, D. H. Bamford, A. Goldman, and R. Tuma.** 2005. The structure of the bacteriophage PRD1 spike sheds light on the evolution of viral capsid architecture. Molecular Cell **18:**161-170.

102. **Metcalf, P., M. Cyrklaff, and M. Adrian.** 1991. The 3-dimensional structure of reovirus obtained by cryoelectron microscopy. EMBO Journal **10:**3129-3136.

103. **Morrison, L. A., R. L. Sidman, and B. N. Fields.** 1991. Direct spread of reovirus from the intestinal lumen to the central nervous system through vagal autonomic nerve fibers. Proceedings of the National Academy of Sciences USA **88:**3852-3856.

104. **Nam, H. J., B. Gurda-Whitaker, W. Y. Gan, S. Ilaria, R. McKenna, P. Mehta, R. A. Alvarez, and M. Agbandje-McKenna.** 2006. Identification of the sialic acid structures recognized by minute virus of mice and the role of binding affinity in virulence adaptation. The Journal of Biological Chemistry **281:**25670-25677.

105. **Nason, E. L., J. D. Wetzel, S. K. Mukherjee, E. S. Barton, B. V. V. Prasad, and T. S. Dermody.** 2001. A monoclonal antibody specific for reovirus outer-capsid protein σ3 inhibits σ1-mediated hemagglutination by steric hindrance. Journal of Virology **75:**6625-6634.

106. **Navaza, J.** 1994. AMoRe: an automated package for molecular replacement. Acta Crystallographica **A 50:**157-163.

107. **Nibert, M. L., J. D. Chappell, and T. S. Dermody.** 1995. Infectious subvirion particles of reovirus type 3 Dearing exhibit a loss in infectivity and contain a cleaved σ1 protein. Journal of Virology **69:**5057-5067.

108. **Nibert, M. L., T. S. Dermody, and B. N. Fields.** 1990. Structure of the reovirus cell-attachment protein: a model for the domain organization of σ1. Journal of Virology **64:**2976-2989.

109. **Nibert, M. L., and L. A. Schiff.** 2001. Reoviruses and their replication, p. 1679-1728. *In* D. M. Knipe and P. M. Howley (ed.), Fields Virology, Fourth ed. Lippincott Williams & Wilkins, Philadelphia.

110. **Nicholls, A., K. A. Sharp, and B. Honig.** 1991. Protein folding and association: insights from the interfacial and thermodynamic properties of hydrocarbons. Proteins **11:**281-296.

111. **Niwa, H., K. Yamamura, and J. Miyazaki.** 1991. Efficient selection for high-expression transfectants with a novel eukaryotic vector. Gene **108:**193-199.

112. **O'Donnell, S. M., M. W. Hansberger, J. L. Connolly, J. D. Chappell, M. J. Watson, J. M. Pierce, J. D. Wetzel, W. Han, E. S. Barton, J. C. Forrest, T. Valyi-Nagy, F. E. Yull, T. S. Blackwell, J. N. Rottman, B. Sherry, and T. S. Dermody.** 2005. Organ-specific roles for transcription factor NF-κB in reovirus-induced apoptosis and disease. The Journal of Clinical Investigation **115:**2341-2350.

113. **Odegard, A. L., K. Chandran, X. Zhang, J. S. Parker, T. S. Baker, and M. L. Nibert.** 2004. Putative autocleavage of outer capsid protein μ1, allowing release of myristoylated peptide μ1N during particle uncoating, is critical for cell entry by reovirus. Journal of Virology **78:**8732-8745.

114. **Ossiboff, R. J., and J. S. Parker.** 2007. Identification of regions and residues in feline junctional adhesion molecule required for feline calicivirus binding and infection. Journal of Virology **81:**13608-13621.

115. **Ostermann, G., K. S. Weber, A. Zernecke, A. Schroder, and C. Weber.** 2002. JAM-1 is a ligand of the beta(2) integrin LFA-1 involved in transendothelial migration of leukocytes. Nature Immunology **3:**151-158.

116. **Otwinowski, Z., and W. Minor.** 1997. Processing of X-ray diffraction data collected in oscillation mode. Methods in Enzymology **276:**307-326.

117. **Ozaki, H., K. Ishii, H. Arai, H. Horiuchi, T. Kawamoto, H. Suzuki, and T. Kita.** 2000. Junctional adhesion molecule (JAM) is phosphorylated by protein kinase C upon platelet activation. Biochemical and Biophysical Research Communications **276:**873-8.

118. **Ozaki, H., K. Ishii, H. Horiuchi, H. Arai, T. Kawamoto, K. Okawa, A. Iwamatsu, and T. Kita.** 1999. Cutting edge: combined treatment of TNF-alpha and IFN-gamma causes redistribution of junctional adhesion molecule in human endothelial cells. Journal of Immunology **163:**553-557.

119. **Parato, K. A., D. Senger, P. A. Forsyth, and J. C. Bell.** 2005. Recent progress in the battle between oncolytic viruses and tumours. Nature Reviews Cancer **5:**965-976.

120. **Paul, R. W., A. H. Choi, and P. W. K. Lee.** 1989. The α-anomeric form of sialic acid is the minimal receptor determinant recognized by reovirus. Virology **172:**382-385.

121. **Paul, R. W., and P. W. K. Lee.** 1987. Glycophorin is the reovirus receptor on human erythrocytes. Virology **159:**94-101.

122. **Prota, A. E., J. A. Campbell, P. Schelling, J. C. Forrest, T. R. Peters, M. J. Watson, M. Aurrand-Lions, B. Imhof, T. S. Dermody, and T. Stehle.** 2003. Crystal structure of human junctional adhesion molecule 1: implications for reovirus binding. Proceedings of the National Academy of Sciences USA **100:**5366-5371.

123. **Richardson-Burns, S. M., D. J. Kominsky, and K. L. Tyler.** 2002. Reovirus-induced neuronal apoptosis is mediated by caspase 3 and is associated with the activation of death receptors. Journal of Neurovirology **8:**365-380.

124. **Roche, S., S. Bressanelli, F. A. Rey, and Y. Gaudin.** 2006. Crystal structure of the low-pH form of the vesicular stomatitis virus glycoprotein G. Science **313:**187-191.

125. **Rodgers, D. W.** 1994. Cryocrystallography. Structure **2:**1135-1140.

126. **Rosen, L.** 1960. Serologic grouping of reovirus by hemagglutination-inhibition. American Journal of Hygiene **71:**242-249.

127. **Rubin, D. H., D. B. Weiner, C. Dworkin, M. I. Greene, G. G. Maul, and W. V. Williams.** 1992. Receptor utilization by reovirus type 3: distinct binding sites on thymoma and fibroblast cell lines result in differential compartmentalization of virions. Microbial Pathogenesis **12:**351-365.

128. **Rubin, D. H., J. D. Wetzel, W. V. Williams, J. A. Cohen, C. Dworkin, and T. S. Dermody.** 1992. Binding of type 3 reovirus by a domain of the s1 protein important for hemagglutination leads to infection of murine erythroleukemia cells. The Journal of Clinical Investigation **90:**2536-2542.

129. **Sabin, A. B.** 1959. Reoviruses: a new group of respiratory and enteric viruses formerly classified as ECHO type 10 is described. Science **130:**1387-1389.

130. **Sagik, B., T. Puck, and S. Levine.** 1954. Quantitative aspects of the spontaneous elution of influenza virus from red cells. The Journal of Experimental Medicine **99:**251-260.

131. **Schelling, P., K. M. Guglielmi, E. Kirchner, B. Paetzold, T. S. Dermody, and T. Stehle.** 2007. The reovirus s1 aspartic acid sandwich: a trimerization motif poised for conformational change. The Journal of Biological Chemistry **282:**11582-11589.

132. **Sebestyen, Z., J. de Vrij, M. Magnusson, R. Debets, and R. Willemsen.** 2007. An oncolytic adenovirus redirected with a tumor-specific T-cell receptor. Cancer Research **67:**11309-11316.

133. **Seiradake, E., H. Lortat-Jacob, O. Billet, E. J. Kremer, and S. Cusack.** 2006. Structural and mutational analysis of human Ad37 and canine adenovirus 2 fiber heads in complex with the D1 domain of coxsackie and adenovirus receptor. The Journal of Biological Chemistry **281:**33704-33716.

134. **Sibanda, B. L., and J. M. Thornton.** 1991. Conformation of beta hairpins in protein structures: classification and diversity in homologous structures. Methods in Enzymology **202:**59-82.

135. **Smelt, S. C., P. Borrow, S. Kunz, W. Cao, A. Tishon, H. Lewicki, K. P. Campbell, and M. B. Oldstone.** 2001. Differences in affinity of binding of lymphocytic choriomeningitis virus strains to the cellular receptor α-dystroglycan correlate with viral tropism and disease kinetics. Journal of Virology **75:**448-457.

136. **Sobocka, M. B., T. Sobocki, P. Banerjee, C. Weiss, J. I. Rushbrook, A. J. Norin, J. Hartwig, M. O. Salifu, M. S. Markell, A. Babinska, Y. H. Ehrlich, and E. Kornecki.** 2000. Cloning of the human platelet F11 receptor: a cell adhesion molecule member of the immunoglobulin superfamily involved in platelet aggregation. Blood **95:**2600-9.

137. **Spriggs, D. R., R. T. Bronson, and B. N. Fields.** 1983. Hemagglutinin variants of reovirus type 3 have altered central nervous system tropism. Science **220:**505-507.

138. **Spriggs, D. R., and B. N. Fields.** 1982. Attenuated reovirus type 3 strains generated by selection of haemagglutinin antigenic variants. Nature **297:**68-70.

139. **Staunton, D. E., V. J. Merluzzi, R. Rothlein, R. Barton, S. D. Marlin, and T. A. Springer.** 1989. A cell adhesion molecule, ICAM-1, is the major surface receptor for rhinoviruses. Cell **56:**849-853.

140. **Stehle, T., and T. S. Dermody.** 2003. Structural evidence for common functions and ancestry of the reovirus and adenovirus attachment proteins. Reviews in Medical Virology **13:**123-132.

141. **Stehle, T., and T. S. Dermody.** 2004. Structural similarities in the cellular receptors used by adenovirus and reovirus. Viral Immunology **17:**129-143.

142. **Stevens, J., O. Blixt, L. Glaser, J. K. Taubenberger, P. Palese, J. C. Paulson, and I. A. Wilson.** 2006. Glycan microarray analysis of the hemagglutinins from modern and pandemic influenza viruses reveals different receptor specificities. Journal of Molecular Biology **355:**1143-1155.

143. **Stevens, J., O. Blixt, T. M. Tumpey, J. K. Taubenberger, J. C. Paulson, and I. A. Wilson.** 2006. Structure and receptor specificity of the hemagglutinin from an H5N1 influenza virus. Science **312:**404-410.

144. **Stiasny, K., S. L. Allison, A. Marchler-Bauer, C. Kunz, and F. X. Heinz.** 1996. Structural requirements for low-pH-induced rearrangements in the envelope glycoprotein of tick-borne encephalitis virus. Journal of Virology **70:**8142-8147.

145. **Strong, J. E., G. Leone, R. Duncan, R. K. Sharma, and P. W. Lee.** 1991. Biochemical and biophysical characterization of the reovirus cell attachment protein sigma 1: evidence that it is a homotrimer. Virology **184:**23-32.

146. **Sturzenbecker, L. J., M. L. Nibert, D. B. Furlong, and B. N. Fields.** 1987. Intracellular digestion of reovirus particles requires a low pH and is an essential step in the viral infectious cycle. Journal of Virology **61:**2351-2361.

147. **Tardieu, M., M. L. Powers, and H. L. Weiner.** 1983. Age-dependent susceptibility to reovirus type 3 encephalitis: role of viral and host factors. Annals of Neurology **13:**602-607.

148. **Tardieu, M., and H. L. Weiner.** 1982. Viral receptors on isolated murine and human ependymal cells. Science **215:**419-421.

149. **Tatsuo, H., N. Ono, K. Tanaka, and Y. Yanagi.** 2000. SLAM (CDw150) is a cellular receptor for measles virus. Nature **406:**893-897.

150. **Tomassini, J. E., D. Graham, C. M. DeWitt, D. W. Lineberger, J. A. Rodkiey, and R. J. Colonno.** 1989. cDNA cloning reveals that the major group rhinovirus receptor on HeLa cells is intercellular adhesion molecule 1. Proceedings of the National Academy of Sciences USA **86:**4907-4911.

151. **Tomko, R. P., R. Xu, and L. Philipson.** 1997. HCAR and MCAR: the human and mouse cellular receptors for subgroup C adenoviruses and group B coxsackieviruses. Proceedings of the National Academy of Sciences USA **94:**3352-6.

152. **Turner, D. L., R. Duncan, and P. W. Lee.** 1992. Site-directed mutagenesis of the C-terminal portion of reovirus protein σ1: evidence for a conformation-dependent receptor binding domain. Virology **186:**219-227.

153. **Twigger, K., L. Vidal, C. L. White, J. S. De Bono, S. Bhide, M. Coffey, B. Thompson, R. G. Vile, L. Heinemann, H. S. Pandha, F. Errington, A. A. Melcher, and K. J. Harrington.** 2008. Enhanced in vitro and in vivo cytotoxicity of combined reovirus and radiotherapy. Clinical Cancer Research **14:**912-923.

154. **Tyler, K. L.** 2001. Mammalian reoviruses, p. 1729-1745. *In* D. M. Knipe and P. M. Howley (ed.), Fields Virology, Fourth ed. Lippincott Williams & Wilkins, Philadelphia.

155. **Tyler, K. L., D. A. McPhee, and B. N. Fields.** 1986. Distinct pathways of viral spread in the host determined by reovirus S1 gene segment. Science **233:**770-774.

156. **Ullmer, C., K. Schmuck, A. Figge, and H. Lubbert.** 1998. Cloning and characterization of MUPP1, a novel PDZ domain protein. FEBS letters **424:**63-68.

157. **van Raaij, M. J., E. Chouin, H. van der Zandt, J. M. Bergelson, and S. Cusack.** 2000. Dimeric structure of the coxsackievirus and adenovirus receptor D1 domain at 1.7 A resolution. Structure **8:**1147-55.

158. **van Raaij, M. J., A. Mitraki, G. Lavigne, and S. Cusack.** 1999. A triple β-spiral in the adenovirus fibre shaft reveals a new structural motif for a fibrous protein. Nature **401:**935-938.

159. **Virgin, H. W., IV, R. Bassel-Duby, B. N. Fields, and K. L. Tyler.** 1988. Antibody protects against lethal infection with the neurally spreading reovirus type 3 (Dearing). Journal of Virology **62:**4594-4604.

160. **Virgin, H. W., K. L. Tyler, and T. S. Dermody.** 1997. Reovirus, p. 669-699. *In* N. Nathanson (ed.), Viral Pathogenesis. Lippincott-Raven, New York.

161. **Warner, M. S., R. J. Geraghty, W. M. Martinez, R. I. Montgomery, J. C. Whitbeck, R. Xu, R. J. Eisenberg, G. H. Cohen, and P. G. Spear.** 1998. A cell surface protein with herpesvirus entry activity (HveB) confers susceptibility to infection by mutants of herpes simplex virus type 1, herpes simplex virus type 2, and pseudorabies virus. Virology **246:**179-189.

162. **Weber, C., L. Fraemohs, and E. Dejana.** 2007. The role of junctional adhesion molecules in vascular inflammation. Nature Reviews Immunology **7:**467-477.

163. **Weiner, H. L., K. A. Ault, and B. N. Fields.** 1980. Interaction of reovirus with cell surface receptors. I. Murine and human lymphocytes have a receptor for the hemagglutinin of reovirus type 3. Journal of Immunology **124:**2143-2148.

164. **Weiner, H. L., D. Drayna, D. R. Averill, Jr, and B. N. Fields.** 1977. Molecular basis of reovirus virulence: role of the S1 gene. Proceedings of the National Academy of Sciences USA **74:**5744-5748.

165. **Weiner, H. L., M. L. Powers, and B. N. Fields.** 1980. Absolute linkage of virulence and central nervous system tropism of reoviruses to viral hemagglutinin. The Journal of Infectious Diseases **141:**609-616.

166. **Weis, W., J. H. Brown, S. Cusack, J. C. Paulson, J. J. Skehel, and D. C. Wiley.** 1988. Structure of the influenza virus haemagglutinin complexed with its receptor, sialic acid. Nature **333:**426-431.

167. **Wetzel, J. D., J. D. Chappell, A. B. Fogo, and T. S. Dermody.** 1997. Efficiency of viral entry determines the capacity of murine erythroleukemia cells to support persistent infections by mammalian reoviruses. Journal of Virology **71:**299-306.

168. **Wickham, T. J., P. Mathias, D. A. Cheresh, and G. R. Nemerow.** 1993. Integrins $\alpha_v\beta_3$ and $\alpha_v\beta_5$ promote adenovirus internalization but not virus attachment. Cell **73:**309-319.

169. **Williams, L. A., I. Martin-Padura, E. Dejana, N. Hogg, and D. L. Simmons.** 1999. Identification and characterisation of human junctional adhesion molecule (JAM). Molecular Immunology **36:**1175-1188.

170. **Wilson, G. J., J. D. Wetzel, W. Puryear, R. Bassel-Duby, and T. S. Dermody.** 1996. Persistent reovirus infections of L cells select mutations in viral attachment protein σ1 that alter oligomer stability. Journal of Virology **70:**6598-6606.

171. **Wilson, J. H., R. B. Luftig, and W. B. Wood.** 1970. Interaction of bacteriophage T4 tail fiber components with a lipopolysaccharide fraction from Escherichia coli. Journal of Molecular Biology **51:**423-434.

172. **Woodfin, A., C. A. Reichel, A. Khandoga, M. Corada, M. B. Voisin, C. Scheiermann, D. O. Haskard, E. Dejana, F. Krombach, and S. Nourshargh.** 2007. JAM-A mediates neutrophil transmigration in a stimulus-specific manner in vivo: evidence for sequential roles for JAM-A and PECAM-1 in neutrophil transmigration. Blood.

173. **Wu, E., L. Pache, D. J. Von Seggern, T. M. Mullen, Y. Mikyas, P. L. Stewart, and G. R. Nemerow.** 2003. Flexibility of the adenovirus fiber is required for efficient receptor interaction. Journal of Virology **77:**7225-35.